Gold(I)-Catalyzed Enantioselective Hydroamination of Unactivated Alkenes

by

Seong Du Lee

Department of Chemistry
Duke University

Date:_____

Approved:

_____
Ross A. Widenhoefer, Supervisor

_____
Jiyong Hong

_____
Katherine J. Franz

_____
Qiu Wang

Dissertation submitted in partial fulfillment of
the requirements for the degree of Doctor
of Philosophy in the Department of
Chemistry in the Graduate School
of Duke University

2012

ABSTRACT

Gold(I)-Catalyzed Enantioselective Hydroamination of Unactivated Alkenes

by

Seong Du Lee

Department of Chemistry
Duke University

Date:_____

Approved:

_____
Ross A. Widenhoefer, Supervisor

_____
Jiyong Hong

_____
Katherine J. Franz

_____
Qiu Wang

An abstract of a dissertation submitted in partial fulfillment of the requirements for the degree of Doctor of Philosophy in the Department of Chemistry in the Graduate School of Duke University

2012

Copyright by
Seong Du Lee
2012

Abstract

Numerous methodologies for efficient formation of carbon-nitrogen bonds have been developed over the decades due to the widespread importance of nitrogen containing compounds in pharmaceuticals and bulk commercial chemicals. Among many methods, hydroamination, in particular, has attracted considerable attention owing to its high atom economy and use of simple C-C substrates. As a result, numerous methods for hydroamination have been reported which employ a range of metal catalysts. However, the hydroamination of unactivated alkenes remains an unsolved challenge owing to the low reactivity of the C=C double bond. The recent development of gold(I) as an effective π-activation catalyst prompted us to develop efficient gold (I)-catalyzed methods for enatioselective intra- and intermolecular hydroamination of unactivated alkenes.

A gold(I)-catalyzed method for the enantioselective intramolecular hydroamination of unactivated alkenes has been developed. Various gold(I) catalysts have been synthesized to examine their reactivity and enantioselectivity in asymmetric intramolecular hydroamination. Among the catalysts, bis(gold) complexes containing an axially chiral bis(phosphine) ligand catalyze the enantioselective intramolecular hydroamination of unactivated alkenes with carboxamide derivatives most effectively. The method was effective for both carbamate and urea nucleophiles to form pyrrolidine derivatives with up to 85 % ee.

The first enantioselective intermolecular hydroamination of unactivated alkenes was realized by a gold(I)-catalyzed method. The gold(I) catalyst system adds cyclic ureas to unactivated 1-alkenes to produce corresponding enantiomerically enriched hydroamination product in good yield with enantioselectivity up to 78 % ee.

Polymer-embedded ligands have been synthesized to demonstrate proof of concept for fluxional mechanocatalysis; the outcome of a catalytic reaction is influenced by the stress state of the catalyst. Polystyrene (PS) or styrene acrylonitrile (SAN) was introduced into a chiral bis(phosphine) ligand to generate polymer-embedded ligands. The catalytic reactivity of the synthesized PS and SAN-embedded ligands was examined in palladium catalyzed asymmetric allylic alkylation (AAA) and showed good enantioselectivity of 89 % and 92 % ee, respectively. However, the enantioselectivity of AAA under a shear stress in a bob rheometer displayed no changes compared with the enantioselctivity of AAA observed in the absence of a shear stress.

Dedicated to my wife, Boyoung Yoon, and my parents, Jungho Lee and Backhapja Lee .

Contents

Abstract iv

List of Tables x

List of Figures xi

Acknowledgements xvii

Chapter 1 1

Room Temperature Gold(I)-Catalyzed Enantioselective Intramolecular Hydroamination of Unactivated Alkenes 1

1.0 Background 2

1.1 Introduction 3

1.1.1 Metal catalyzed Enantioselective Intramolecular Hydroamination of Unactivated Alkenes 3

1.1.1.1 Enantioselective Hydroamination Catalyzed by Rare-Earth Metal Complexes 3

1.1.1.2 Enantioselective Hydroamination Using Group 4 Metal Catalysts 10

1.1.1.3 Enantioselective Alkene Hydroamination Catalyzed by Late Transition Metal Complexes 15

1.1.2 Special Characteristics of Gold(I) in Homogeneous Catalysis 17

1.1.3 Project Motivation 18

1.2 Results and Discussion 20

1.2.1 Optimization and Substrate Scope 20

1.2.2 Mechanism 28

1.2.3. Summary 31

1.3 Experimental Section 32

1.3.1 General Methods 32

1.3.2 Synthesis of Alkenyl Carbamate Substrates 33

1.3.3 Synthesis of Alkenyl Urea Substrates 36

1.3.4 Synthesis of *N*-(2-allylphenyl)acetamide (28) 39

1.3.5 Gold(I)-Catalyzed Enantioselective Intramolecular Hydroamination of Alkenyl Carbamates 40

1.3.5 Gold(I)-Catalyzed Enantioselective Intramolecular Hydroamination of Alkenyl Ureas 45

1.3.6 Gold(I)-Catalyzed Enantioselective Intramolecular Hydroamination of N-(2-allylphenyl)acetamide (28) 48

1.3.7 Catalyst Synthesis 50

Chapter 2 122

Gold(I)-Catalyzed Enantioselective 122

Intermolecular Hydroamination of Unactivated 122

Alkenes 122

2.1 Introduction 123

2.2 Results and Discussion 128

1.2.1 Optimization and Substrate Scope 128

2.2.2 Mechanism 137

2.3 Experimental Section 138

2.3.1 General Methods 138

2.3.2 Gold(I)-Catalyzed Enantioselective Intermolecular Hydroamination of 1-Alkenes. 139

2.3.3 Control Reactions 142

Chapter 3 146

Synthesis and Application of Polymer Embedded 146

Bis(phosphine) Ligands for Mechanocatalysis 146

3.1 Introduction 147

3.1.1 Mechanocatalysis 147

3.1.2 Asymmetric Allylic Alkylation and Dihedral Angle Effect 149

3.1.3 Project Goals 153

3.2 Results and Discussion 155

3.2.1 Synthesis of Polymer-Embedded Ligands for Fluxional Mechanocatalysis 155

3.2.2 Pd-Catalyzed Asymmetric Allylic Alkylation under a Shear Force 160

3.2.3 Future Directions. 166

3.3 Experimental Section 167

3.3.1 General Methods 167

3.3.2 Ligand Synthesis 168

3.3.3 Asymmetric Allylic Alkylation 175

3.3.3.1 Asymmetric Allylic Alkylation using (*S*)-MeO-BIPHEP 175

3.3.3.2 Asymmetric Allylic Alkylation using Polymer-Embedded Ligands 176

References 190

Biography 196

List of Tables

Table 1. Effect of ligand on the enantioselectivity of the gold(I)-catalyzed intramolecular hydroamination of γ-alkenyl carboxamide and sulfonamides. 22

Table 2. Effect of the solvent and silver salt on the gold-catalyzed enantioselelctive intramolecular hydroamination of 1a and 1b. 24

Table 3. Enantioselective intramolecular hydroamination of alkenyl amines catalyzed by a mixture of [(*S*)-L8](AuCl)$_2$ (2.5 mol %) and $AgBF_4$ (5 mol %) in methanol. 26

Table 4. Effect of silver salt and solvent on the gold(I)-catalyzed enantioselective hydroamination of 1-Octene with 7. 130

Table 5. Effect of ligand and solvent on the gold(I)-catalyzed enantioselective hydroamination of 1-octene with 7. 133

Table 7. Effect of ligand dihedral angle on the yield and enantioselectivity the palladium-catalyzed AAA reaction of 1,3-diphenylpropenyl acetate with dimethyl malonate to form (*E*)-dimethyl 2-(1,3-diphenylallyl)malonate employing Cn-Tunephos ligands. 153

Table 8. Effect of reaction conditions on the AAA reaction 1,3-diphenylpropenyl acetate with dimethyl malonate employing (*S*)-MeO-BIPHEP as the ligand. 161

Table 9. AAA reactions under shear stress. 165

List of Figures

Figure 1. Chiral cyclopentadienyl lanthanocene complexes employed as precatalysts for the intramolecular enantioselective hydroamination of γ-alkenyl amines. 5

Figure 2. Substrates that showed poor reactivity or failed to undergo gold-catalyzed enantioselective intramolecular hydroamination. 28

Figure 3. Chiral HPLC traces (85:15 hexanes/isopropanol, 0.5 mL/min) of racemic (left trace) and enantiomerically enriched (right trace, 72% ee) benzyl 2-methyl-4,4-diphenylpyrrolidine-1-carboxylate (6). 64

Figure 4. Chiral HPLC traces (90:10 hexanes/isopropanol, 0.5 mL/min) of racemic (left trace) and enantiomerically enriched (right trace, 78% ee) (9H-fluoren-9-yl)methyl 2-methyl-4,4-diphenylpyrrolidine-1-carboxylate (2b). 65

Figure 5. Chiral HPLC traces (90:10 hexanes/isopropanol, 0.5 mL/min) of racemic (left trace) and enantiomerically enriched (right trace, 84% ee) (9H-fluoren-9-yl)methyl 2-methyl-4,4-diphenylpyrrolidine-1-carboxylate (2c). 66

Figure 6. Chiral HPLC traces (90:10 hexanes/isopropanol, 0.5 mL/min) of racemic (left trace) and enantiomerically enriched (right trace, 76% ee) 2-methyl-*N*,4,4-triphenylpyrrolidine-1-carboxamide (8). 67

Figure 7. Chiral HPLC traces (90:10 hexanes/isopropanol, 0.5 mL/min) of racemic (left trace) and enantiomerically enriched (right trace, 82% ee) 2-methyl-*N*,4,4-triphenylpyrrolidine-1-carboxamide (8b). 68

Figure 8. Chiral HPLC traces (90:10 hexanes/isopropanol, 0.5 mL/min) of racemic (left trace) and enantiomerically enriched (right trace, 77% ee) propyl 2-methyl-4,4-diphenylpyrrolidine-1-carboxylate (10). 69

Figure 9. Chiral HPLC traces (90:10 hexanes/isopropanol, 0.5 mL/min) of racemic (left trace) and enantiomerically enriched (right trace, 75% ee) 2-(benzyloxy)ethyl 2-methyl-4,4-diphenylpyrrolidine-1-carboxylate (12). 70

Figure 10. Chiral HPLC traces (95:5 hexanes/isopropanol, 0.5 mL/min) of racemic (left trace) and enantiomerically enriched (right trace, 48% ee) 2,2,2-trichloroethyl 2-methyl-4,4-diphenylpyrrolidine-1-carboxylate (14). 71

Figure 11. Chiral HPLC traces (99:1 hexanes/isopropanol, 0.5 mL/min) of racemic (left trace) and enantiomerically enriched (right trace, 55% ee) 9-fluorenylmethyl 2-methyl-4-cyclohexylpyrrolidine-1-carboxylate (16). 72

Figure 12. Chiral HPLC traces (85:15 hexanes/isopropanol, 0.5 mL/min) of racemic (left trace) and enantiomerically enriched (right trace, 85% ee) *N*-methyl-2-methyl-4,4-diphenylpyrrolidine-1-carboxamide (27). 73

Figure 13. Chiral HPLC traces (92:8 hexanes/isopropanol, 0.5 mL/min) of racemic (left trace) and enantiomerically enriched (right trace, 58 % ee) phenyl 2-methyl-4,4-diphenyl-pyrrolidine-1-carboxamide (19). 74

Figure 14. Chiral HPLC traces (80:20 hexanes/isopropanol, 0.5 mL/min) of racemic (left trace) and enantiomerically enriched (right trace, 58% ee) *N*-(4-iodophenyl)-2-methyl-4,4-diphenylpyrrolidine-1-carboxamide (21). 75

Figure 15. Chiral HPLC traces (80:20 hexanes/isopropanol, 0.5 mL/min) of racemic (left trace) and enantiomerically enriched (right trace, 76% ee) 2-methyl-*N*-(4-nitrophenyl)-4,4-diphenylpyrrolidine-1-carboxamide (23). 76

Figure 16. Chiral HPLC traces (85:15 hexanes/isopropanol, 0.5 mL/min) of racemic (left trace) and enantiomerically enriched (right trace, 72% ee) *N*-benzyl-2-methyl-4,4-diphenylpyrrolidine-1-carboxamide (2a). 77

Figure 17. Chiral HPLC traces (85:15 hexanes/isopropanol, 0.5 mL/min) of racemic (left trace) and enantiomerically enriched (right trace, 81% ee) *N*-butyl-2-methyl-4,4-diphenylpyrrolidine-1-carboxamide (25). 78

Figure 18. Chiral HPLC traces (85:15 hexanes/isopropanol, 0.5 mL/min) of racemic (left trace) and enantiomerically enriched (right trace, 38% ee) 1-(2-methylindolin-1-yl)ethanone (29). 79

Figure 19. ^{1}H NMR spectrum of 5 in $CDCl_3$ 80

Figure 20. $^{13}C\{^{1}H\}$ NMR spectrum of 5 in $CDCl_3$. 81

Figure 21. ^{1}H NMR spectrum of 1b in $CDCl_3$. 82

Figure 22. $^{13}C\{^{1}H\}$ NMR spectrum of 1b in $CDCl_3$. 83

Figure 23. ^{1}H NMR spectrum of 7 in $CDCl_3$. 84

Figure 24. $^{13}C\{^{1}H\}$ NMR spectrum of 7 in $CDCl_3$. 85

Figure 25. ^{1}H NMR spectrum of 9 in $CDCl_3$. 86

Figure 26. $^{13}C\{^{1}H\}$ NMR spectrum of 9 in $CDCl_3$. 87

Figure 27. ^{1}H NMR spectrum of 11 in $CDCl_3$. 88

Figure 28. $^{13}C\{^{1}H\}$ NMR spectrum of 11 in $CDCl_3$. 89

Figure 29. ^{1}H NMR spectrum of 13 in $CDCl_3$. 90

Figure 30. $^{13}C\{^{1}H\}$ NMR spectrum of 13 in $CDCl_3$. 91

Figure 31. ^{1}H NMR spectrum of 15 in $CDCl_3$. 92

Figure 32. $^{13}C\{^{1}H\}$ NMR spectrum of 15 in $CDCl_3$. 93

Figure 33. ^{1}H NMR spectrum of 28 in $CDCl_3$. 94

Figure 34. ^{1}H NMR spectrum of 6 in $CDCl_3$. 95

Figure 35. $^{13}C\{^{1}H\}$ NMR spectrum of 6 in $CDCl_3$. 96

Figure 36. ^{1}H NMR spectrum of 2b in $CDCl_3$. 97

Figure 37. $^{13}C\{^{1}H\}$ NMR spectrum of 2b in $CDCl_3$. 98

Figure 38. ^{1}H NMR spectrum of 8 in $CDCl_3$. 99

Figure 39. $^{13}C\{^{1}H\}$ NMR spectrum of 8 in $CDCl_3$. 100

Figure 40. ^{1}H NMR spectrum of 10 in CD_2Cl_2. 101

Figure 41. $^{13}C\{^{1}H\}$ NMR spectrum of 10 in $CDCl_3$. 102

Figure 42. ^{1}H NMR spectrum of 12 in CD_2Cl_2. 103

Figure 43. $^{13}C\{^{1}H\}$ NMR spectrum of 12 in $CDCl_2$. 104

Figure 44. ^{1}H NMR spectrum of 14 in $CDCl_3$. 105

Figure 45. $^{13}C\{^{1}H\}$ NMR spectrum of 14 in $CDCl_3$. 106

Figure 46. ^{1}H NMR spectrum of 16 in $CDCl_3$. 107

Figure 47. $^{13}C\{^{1}H\}$ NMR spectrum of 16 in $CDCl_3$. 108

Figure 48. ^{1}H NMR spectrum of 27 in $CDCl_3$. 109

Figure 49. $^{13}C\{^{1}H\}$ NMR spectrum of 27 in $CDCl_3$. 110

Figure 50. ^{1}H NMR spectrum of 19 in CD_2Cl_2. 111

Figure 51. $^{13}C\{^{1}H\}$ NMR spectrum of 19 in CD_2Cl_2. 112

Figure 52. ^{1}H NMR spectrum of 21 in CD_2Cl_2. 113

Figure 53. $^{13}C\{^{1}H\}$ NMR spectrum of 21 in $(CD_3)_2CO$ 114

Figure 54. ^{1}H NMR spectrum of 23 in CD_2Cl_2. 115

Figure 55. $^{13}C\{^{1}H\}$ NMR spectrum of 23 in $(CD_3)_2CO$ 116

Figure 56. ^{1}H NMR spectrum of 2a in CD_2Cl_2. 117

Figure 57. $^{13}C\{^{1}H\}$ NMR spectrum of 2a in CD_2Cl_2. 118

Figure 58. ^{1}H NMR spectrum of 25 in CD_2Cl_2. 119

Figure 59. $^{13}C\{^{1}H\}$ NMR spectrum of 25 in CD_2Cl_2. 120

Figure 60. 1H NMR spectrum of 28 in $CDCl_3$ 121

Figure 61. Chiral bisphosphine ligands utilized for the gold-catalyzed intermolecular enantioselective hydroamination of 1-alkenes. 132

Figure 63. Substrate combinations that failed to undergo gold-catalyzed enantioslective intermolecular hydroamination under our optimized conditions. 136

Figure 64. Chiral HPLC traces of racemic (left trace) and enantiomerically enriched (right trace, 76 % ee) methyl-3-(octan-2-yl)imidazolidin-2-one (9). 143

Figure 65. Chiral HPLC traces of racemic (left trace) and enantiomerically enriched (right trace, 71 % ee) 1-(octan-2-yl)-3-phenylimidazolidin-2-one (14). 143

Figure 66. Chiral HPLC traces of racemic (left trace) and enantiomerically enriched (right trace, 74 % ee) 1-(4-fluorophenyl)-3-(octan-2-yl)imidazolidin-2-one (15). 144

Figure 67. Chiral HPLC traces of racemic (left trace) and enantiomerically enriched (right trace, 78 % ee) 1-tert-butyl-3-(octan-2-yl)imidazolidin-2-one (16). 144

Figure 68. Chiral HPLC traces of racemic (left trace) and enantiomerically enriched (right trace, 73 % ee) 1-(decan-2-yl)-3-methylimidazolidin-2-one (17). 145

Figure 69. Chiral HPLC traces of racemic (left trace) and enantiomerically enriched (right trace, 75 % ee) 1-(dodecan-2-yl)-3-methylimidazolidin-2-one (18). 145

Figure 70. Examples of mechanocatalysis. 148

Figure 71. Schematic representation of MeO-BIPHEP for quadrants rule and relationship between dihedral and bite angle. 151

Figure 72. Dihedral angle of axially chiral bisphosphine ligands. 152

Figure 73. Schematic representation of fluxional mechanocatalysis. 155

Figure 74. Illustration of applied steady shear flow to a sample of polymer in the 0.25 mm gap (left) and a cup and bob rheometer (right). 163

Figure 75. Chiral HPLC traces (98:2 hexanes/isopropanol, 1.0 mL/min) of racemic dimethyl 2-(1,3-diphenylallyl)malonate. 178

Figure 76. Chiral HPLC traces (98:2 hexanes/isopropanol, 1.0 mL/min) of enatiomerically enriched dimethyl 2-(1,3-diphenylallyl)malonate (eq 3.1), 57 % ee 179

Figure 77. Chiral HPLC traces (98:2 hexanes/isopropanol, 1.0 mL/min) of enatiomerically enriched dimethyl 2-(1,3-diphenylallyl)malonate (Table 8, entry 1), 92 % ee 180

Figure 78. Chiral HPLC traces (98:2 hexanes/isopropanol, 1.0 mL/min) of enatiomerically enriched dimethyl 2-(1,3-diphenylallyl)malonate (Table 8, entry 2), 92 % ee 181

Figure 79. Chiral HPLC traces (98:2 hexanes/isopropanol, 1.0 mL/min) of enatiomerically enriched dimethyl 2-(1,3-diphenylallyl)malonate (Table 8, entry 3), 89 % ee. 182

Figure 80. Chiral HPLC traces (98:2 hexanes/isopropanol, 1.0 mL/min) of enatiomerically enriched dimethyl 2-(1,3-diphenylallyl)malonate (Table 8, entry 4), 91 % ee. 183

Figure 81. Chiral HPLC traces (98:2 hexanes/isopropanol, 1.0 mL/min) of enatiomerically enriched dimethyl 2-(1,3-diphenylallyl)malonate (Table 8, entry 5), 92 % ee. 184

Figure 82. Chiral HPLC traces (98:2 hexanes/isopropanol, 1.0 mL/min) of enatiomerically enriched dimethyl 2-(1,3-diphenylallyl)malonate (Table 8, entry 6), 92 % ee. 185

Figure 83. Chiral HPLC traces (98:2 hexanes/isopropanol, 1.0 mL/min) of enatiomerically enriched dimethyl 2-(1,3-diphenylallyl)malonate (Table 8, entry 7), 92 % ee. 186

Figure 84. Chiral HPLC traces (98:2 hexanes/isopropanol, 1.0 mL/min) of enatiomerically enriched dimethyl 2-(1,3-diphenylallyl)malonate (Table 8, entry 8), 89 % ee. 187

Figure 85. Chiral HPLC traces (98:2 hexanes/isopropanol, 1.0 mL/min) of enatiomerically enriched dimethyl 2-(1,3-diphenylallyl)malonate (Table 8, entry 9), 89 % ee. 188

Figure 86. Chiral HPLC traces (98:2 hexanes/isopropanol, 1.0 mL/min) of enatiomerically enriched dimethyl 2-(1,3-diphenylallyl)malonate (Table 8, entry 10), 89 % ee. 189

Acknowledgements

I would like to express my gratitude to all individuals who have offered me personal and scientific support during my doctoral course at Duke University.

First and foremost, I would like to thank my research advisor, Professor Ross A. Widenhoefer, for his guidance and encouragement over the past five years. I have learnt a great deal of invaluable science from him, and I am really grateful that he always waited for me with patience and encouragement, especially, when things were not going well.

I would like to extend my gratitude to dissertation committee, Professor Jiyong Hong, Professor Katherine J. Franz, and Professor Qui Wang for the support and guidance. I would also like to thank Professor Stephen L. Craig for offering me a chance to extend my knowledge and giving me great advice.

I would like to give special thank to present Widenhoefer group members, Rachel Brooner, and Robert Harris for supporting and helping me in various ways. I am grateful to former Widenhoefer group members, Hao Li, Rachel Witek, Zhibin Zhang, Timothy Brown, Kristina Butler, Paramita Mukherjee for their support. Also, I would like to thanks Zachary Kean for running a great project together and sharing valuable ideas.

Finally, I must thank my wife, Boyoung Yoon, for unconditional love, support, and encouragement, and for bringing me lovely sons, Juneseo and Yoonseo. I am also grateful to my parents and parents-in-law for their support and encouragement throughout

my doctoral career. Likewise, I would like to thank my brother, Seongwon Lee, for advice and encouragement.

Chapter 1

Room Temperature Gold(I)-Catalyzed Enantioselective Intramolecular Hydroamination of Unactivated Alkenes

1.0 Background

The synthesis of amines has attracted considerable interest for decades due to the importance of amines in pharmaceuticals and commercial chemicals. Among the various synthetic approaches to amines, hydroamination, the direct formation of a C-N bond by addition of an amine to an unsaturated C=C or C≡C bond, represents a particularly expedient and atom-economical route to amines from readily available and inexpensive starting materials.[1] With these advantages, catalytic hydroamination has attracted considerable attention over the past ~30 years. Many examples of hydroamination have been reported employing either early transition metals or late transition metal complexes as catalysts.[2] While many reports document the facile hydroamination of alkynes[3-19] and allenes,[20-41] the hydroamination of unactivated alkenes remains a challenge owing to the stability of the C=C double bond and its low inherent reactivity toward nucleophiles. In this respect, the enantioselective hydroamination of alkenes is particularly challenging because the reaction often requires low temperature to achieve higher enantioselectivity, resulting in low conversion and low reaction rates. For this reason, extant reports of enantioselective alkene hydroamination typically employ activated C=C double bond such as vinylarenes,[42-44] strained olefins,[45,46] and 1,3-dienes.[47,48] Nevertheless, a number of methods for the enantioselective hydroamination of unactivated alkenes have been described employing rare-earth metals, early transition metals (groups 3-5), or late transition metals (groups 8-10).

1.1 Introduction

1.1.1 Metal catalyzed Enantioselective Intramolecular Hydroamination of Unactivated Alkenes

1.1.1.1 Enantioselective Hydroamination Catalyzed by Rare-Earth Metal Complexes

Since Marks reported the first examples of enantioselective hydroamination catalyzed by chiral *ansa*-lanthanocene complexes in 1992,[49] use of rare-earth metal catalysts for enantioselective hydroamination has progressed significantly. The proposed mechanism[50,51] for the hydroamination of 4-pentenylamine catalyzed by a rare-earth metallocene complex is initiated by activation of the precatalyst through formation of a metal-amido species (**I**) by protonolysis of the M–N or M–C bond of a metal-amido or metal-alkyl precatalyst, respectively (Scheme 1). Insertion of the pendant C=C double bond into the M–N bond of **I** via a chair-like transition state produces metal-alkyl complex (**II**), and fast protonolysis of the M–C bond of **II** with the N–H bond of another alkenylamine molecule releases the pyrrolidine product and regenerates the active metal-amido complex (**I**).

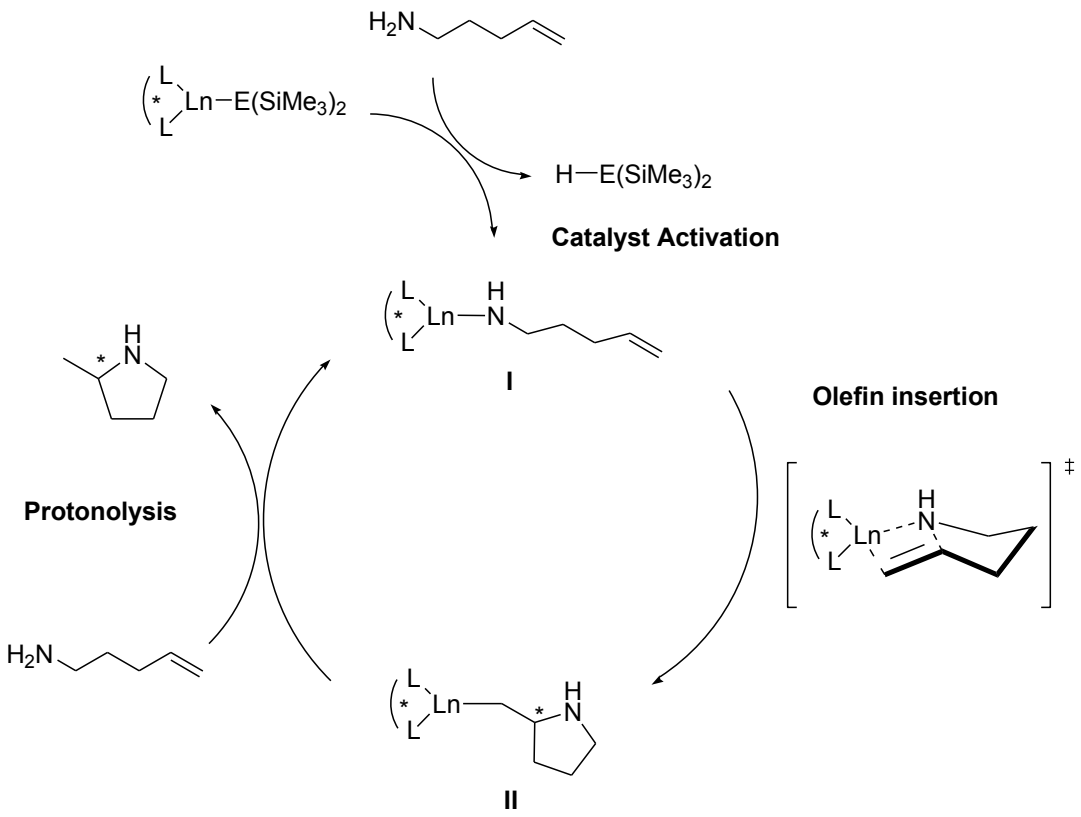

Scheme 1.1. Proposed mechanism of the intramolecular hydroamination of 4-pentcnylamine catalyzed by a rare-earth metallocene complex.

1.1.1.1.1 Cyclopentadienyl Catalysts

Various cyclopentadienyl *ansa*-lanthanocene catalysts for the enantioselective intramolecular hydroamination of alkenylamines were developed by Marks and coworkers.[47,52,53] The catalysts possessed a chiral substituent such as a phenylmenthyl, (–)-mentyl, or (+)-neomentyl group appended to one of the cyclopentadienyl rings of the *ansa*-metallocene ligand generating diastereomeric catalysts (Figure 1). Cyclization of 4-pentenylamines employing these *ansa*-lanthanocene precatalysts typically occurred with

poor to modes enantioselectivity.[47,50] For example, treatment of 2,2-dimethyl-4-penten-1-amine (**1**) with a samarocene amido complex at –30 °C led to formation of 2,4,4-trimethylpyrrolidine (**2**) in 100 % conversion with 74 % ee (eq 1.1).

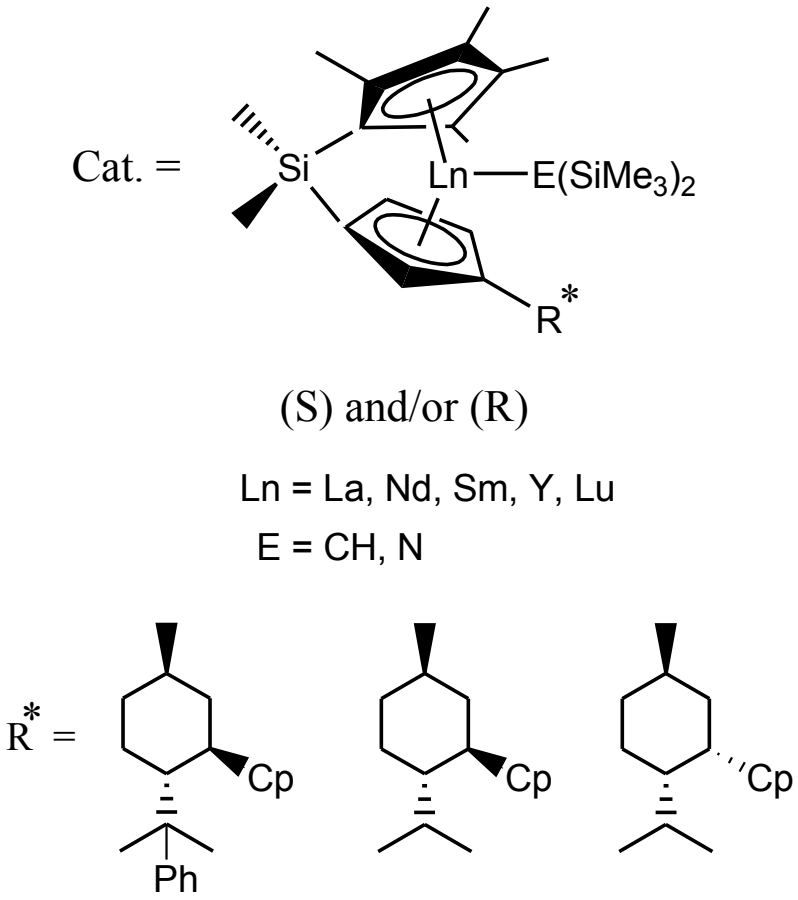

Figure 1. Chiral cyclopentadienyl lanthanocene complexes employed as precatalysts for the intramolecular enantioselective hydroamination of γ-alkenyl amines.

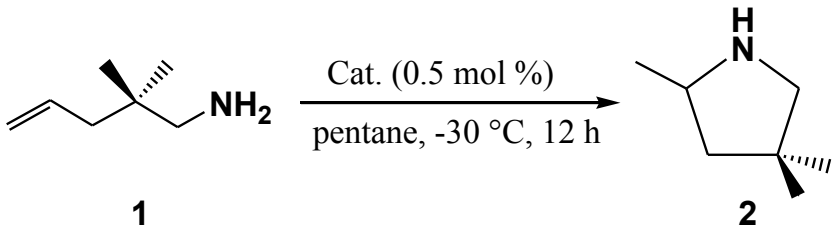

1 2 (eq 1.1)

100 % conv.
74 % ee

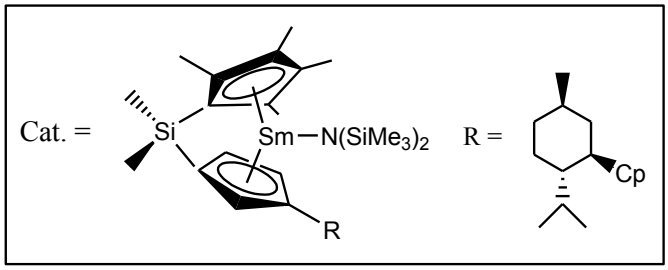

1.1.1.1.2 Non-Cyclopentadienyl Catalysts

Significant progress in enantioselective hydroamination has been made through employment of non-cyclopentadienyl rare-earth metal complexes including lanthanide ate-complexes, aminothiophenolate complexes, binaphtholate aryl complexes, and bisoxazoline complexes as catalysts.[1,2] Lanthanide ate-complexes displayed moderate to good activity and enantioselectivity of up to 87 % ee as catalysts for the cyclization of *gem*-dialkyl substituted amino alkenes.[54] For example, cyclization of (1-allylcyclohexyl)methanamine catalyzed by ytterbium ate-complex formed 3-methyl-2-azaspiro[4.5]decane in 90 % conversion with 87 % ee (eq 1.2).

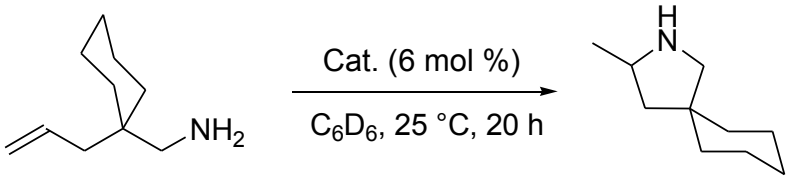

(eq 1.2)

90 % conv.

87 % ee

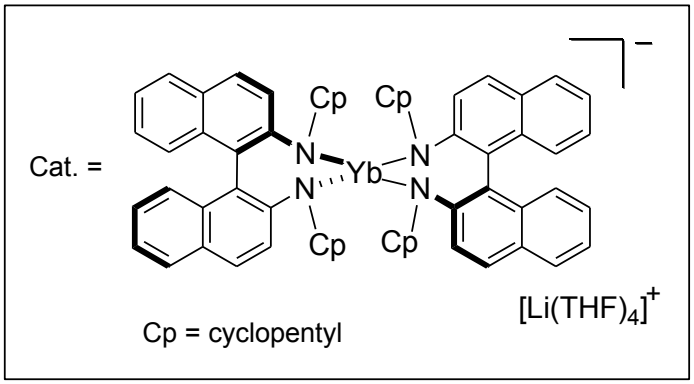

Aminothiophenolate complexes catalyzed the intermolecular enantioselective hydroamination of γ- and δ-alkenylamines that contained internal C=C bond or a secondary amine moiety to form the corresponding pyrrolidines or piperidines with moderate to good enantioselectivity. While good enantioselectivity could be realized employing this catalyst system, the reactions were prohibitively sluggish. For example, treatment of 4-pentenylamine with an yttrium aminothiophenolate complex at 30 °C for 552 h formed 2-methylpyrrolidine in >95% conversion and with 89% ee (eq 1.3).[55]

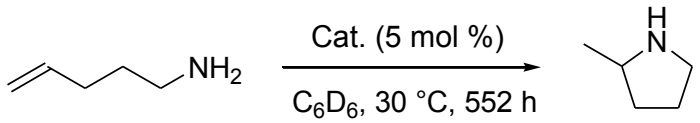

(eq 1.3)

>95 % conv.
89 % ee

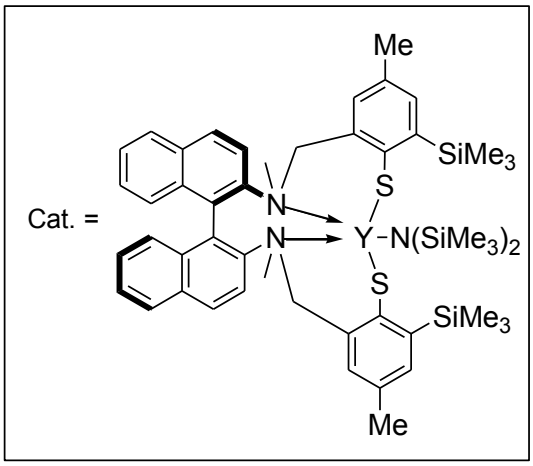

Rare earth binaphtholate aryl complexes with sterically encumbered tris(aryl)silyl substituents showed high reactivity and excellent enantioselectivity for the intramolecular hydroamination of unfunctionalized amino alkenes at room temperature (eq 1.4).[56] While the more sterically demanding binaphtholate complex achieved better enantioselectivity with sterically less demanding aminoalkenes, a less sterically demanding binaphtholate complex was more effective for cyclization of more sterically hindered *gem*-diphenyl or *gem*-cyclohexyl substituted alkenyamines. Despite the great success of binaphtholate complexes, an organophosphine oxide substituted binaphtholate complex was significantly less active and enantioselective in catalyzing the hydroamination. (eq 1.5).[57]

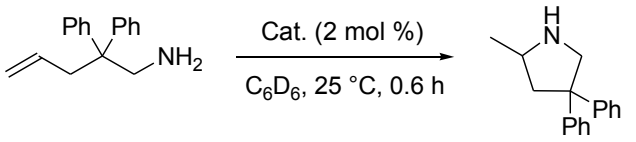

(eq 1.4)

94 % conv.
95 % ee

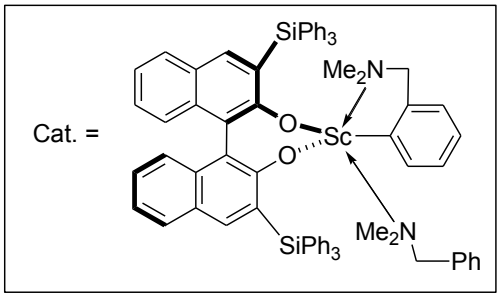

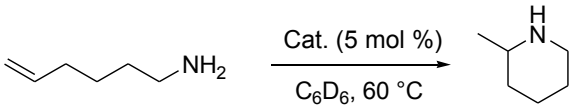

(eq 1.5)

30 % conv.
24 % ee

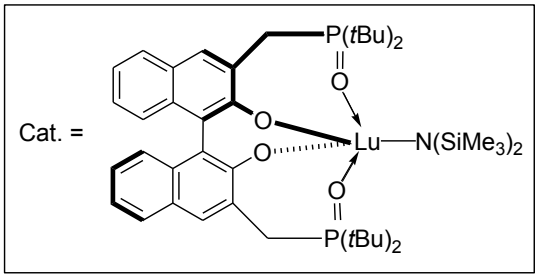

Successful application of bisoxazoline complexes in many enantioselective organic transformations[58,59] has led to the application of these to enantioselective alkene hydroamination. However, even with extensive modification of the bisoxazoline ligands, intramolecular hydroamination of alkenyl amines catalyzed by rare earth bisoxazoline

complexes displayed low to moderate enantioselectivity. For example, treatment of 2,2-dimethyl-4-pentenylamine with a lanthanide bisoxazoline complex led to intramolecular hydroamination to form 2,4,4-trimethylpyrrolidine in high conversion with 67% ee (eq 1.6).[60]

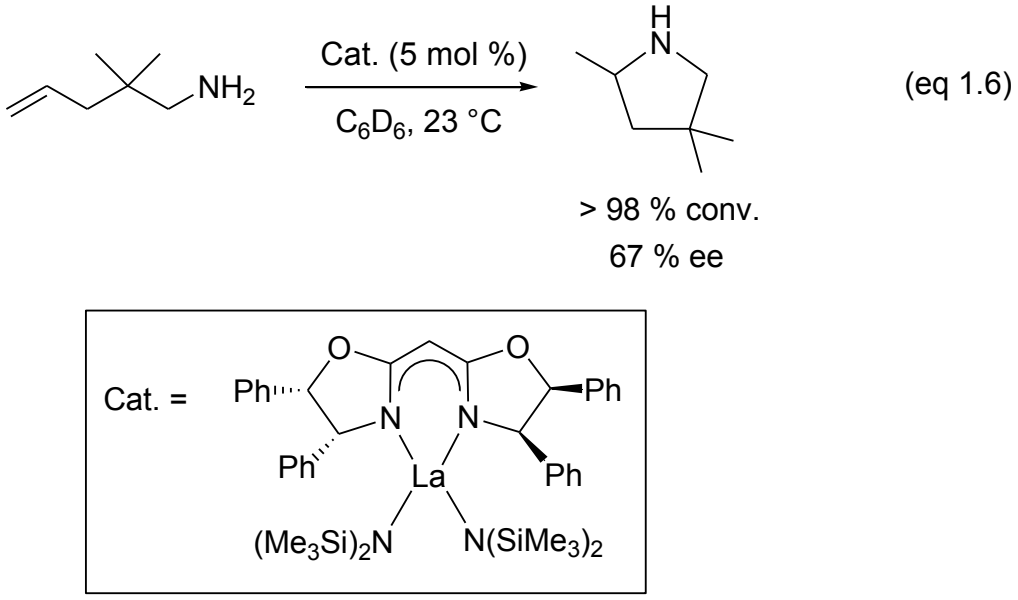

1.1.1.2 Enantioselective Hydroamination Using Group 4 Metal Catalysts

The first example of the enantioselective hydroamination of an unactivated alkene by a group 4 metal complex, was described by Scott in 2004 employing a cationic zirconium aminophenolate complex.[61] This catalyst system was effective for the cyclization of secondary aminoalkenes with up to 82 % ee. For example, cyclization of *N*-2,2-trimethylhex-5-en-1-amine catalyzed by a cationic zirconium aminophenolate

complex formed 1,2,5,5-tetramethylpiperidine with 100% conversion and with 82 % ee (eq 1.7). The proposed mechanism for the intramolecular hydroamination of a secondary 4-pentenylamine catalyzed by a group 4 complex involves initial generation of an active cationic zirconium amido complex (**III**),[1] followed by insertion of the pendant C=C bond into the Zr–N bond to generate the zirconium-alkyl species (**IV**). Protonolysis of the Zr–C bond of **IV** forms the pyrrolidine product with regeneration of the active catalyst (Scheme 1.2). Owing to facile deprotonation of the cationic zirconium amido complex generated from a primary aminoalkene to generate the inactive zirconium imido complex (**V**), these zirconium complexes were not effective for the intramolecular hydroamination of the primary 4-pentenylamines.

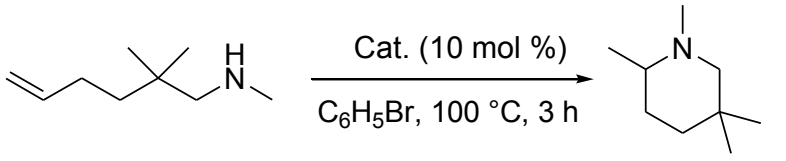

(eq 1.7)

100 % conv.
82 % ee

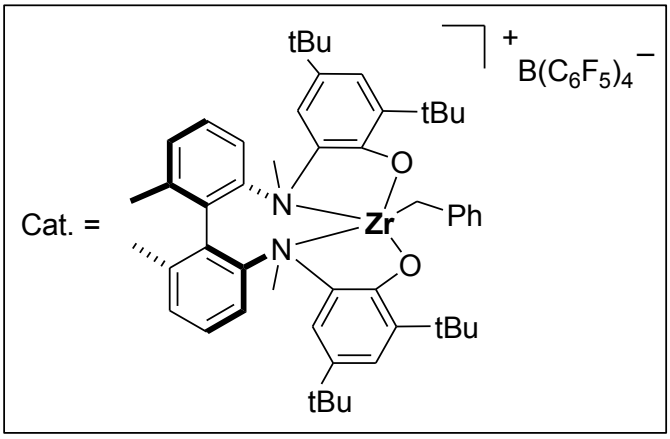

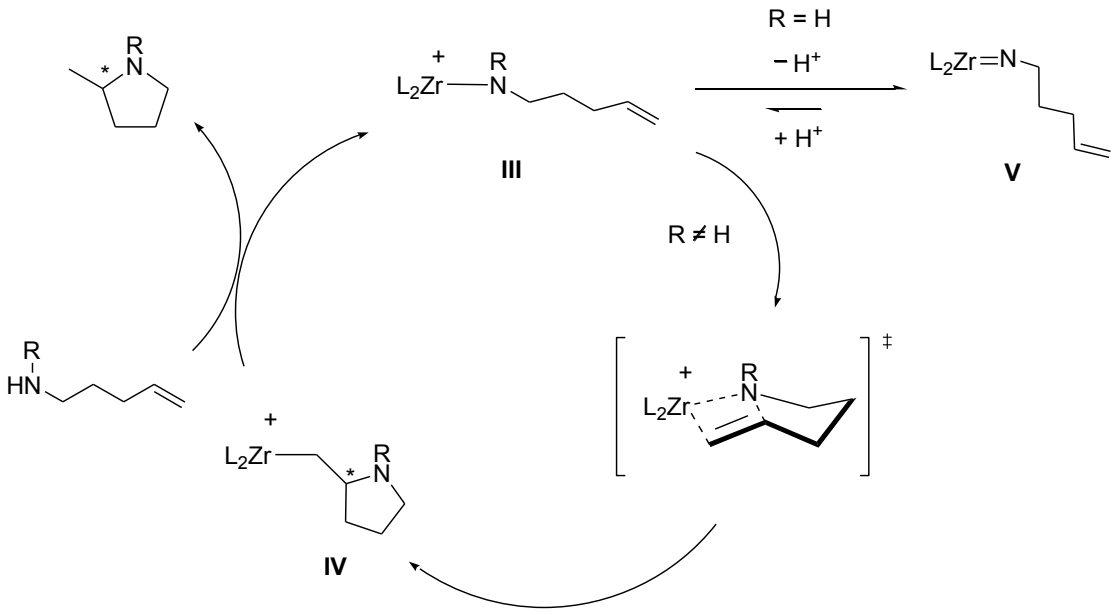

Scheme 1.2 Proposed mechanism for the intramolecular hydroamination of a secondary 4-pentenylamine catalyzed by a cationic zirconium aminophenolate complex.

Neutral zirconium complexes were effective for the intramolecular enantioselective hydroamination of primary aminoalkenes with modest activities but with good to excellent enantioselectivities.[62] For example, treatment of 2,2-dimethylpent-4-en-1-amine with a catalytic amount of a chiral bis(phosphinic amido) zirconium complex led to isolation of 2,4,4-trimethylpyrrolidine in 91% yield with 80% ee (eq 1.8). Schafer and coworkers have screened a range of neutral zirconium catalysts, and found a chiral bis(amidate) zirconium complex to be the most effective catalyst in terms of reactivity and enantioselectivity.[63] For example, treatment of 2,2-dimethylpent-4-en-1-amine with a

catalytic amount of the enantiomerically enriched zirconium bis(amidate) complex formed 2,4,4-trimethylpyrrolidine in 80 % yield with 93 % ee (eq 1.9).

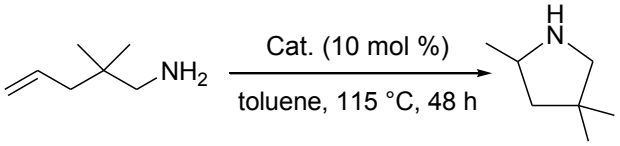

(eq 1.8)

91 % yield
80 % ee

Cat. =

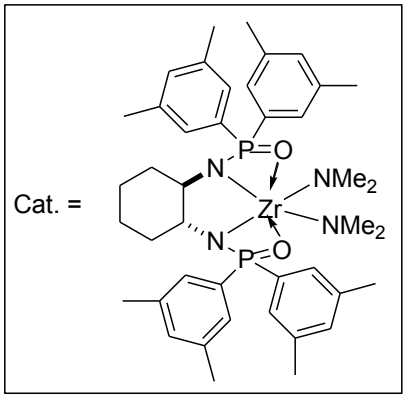

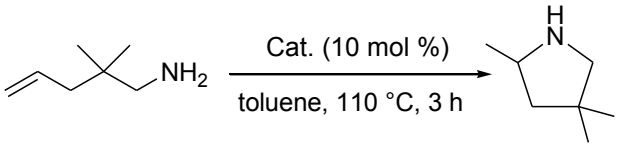

(eq 1.9)

80 % yield
93 % ee

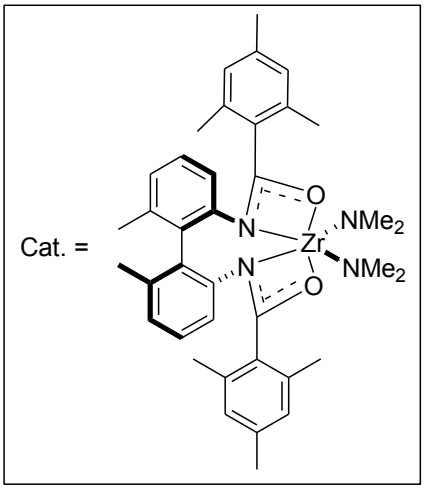

The mechanism of the intramolecular hydroamination of a γ-alkenyl amine catalyzed by a neutral zirconium complex is believed to proceed via formation of the imidozirconium intermediate (**VI**) through protonolysis of both Zr–N bonds of the zirconium bis(amido) precursor by the primary amine group. Subsequent [2+2] cycloaddition of the pendant C=C bond with the Zr=N bond of **VI** generates the azametallocyclobutane **VII**. Subsequent protonolysis of the Zr–N and Zr–C bonds of **VII** with a second molecular of amino alkene releases the pyrrolidine with regeneration of the active catalyst **VI**.[64]

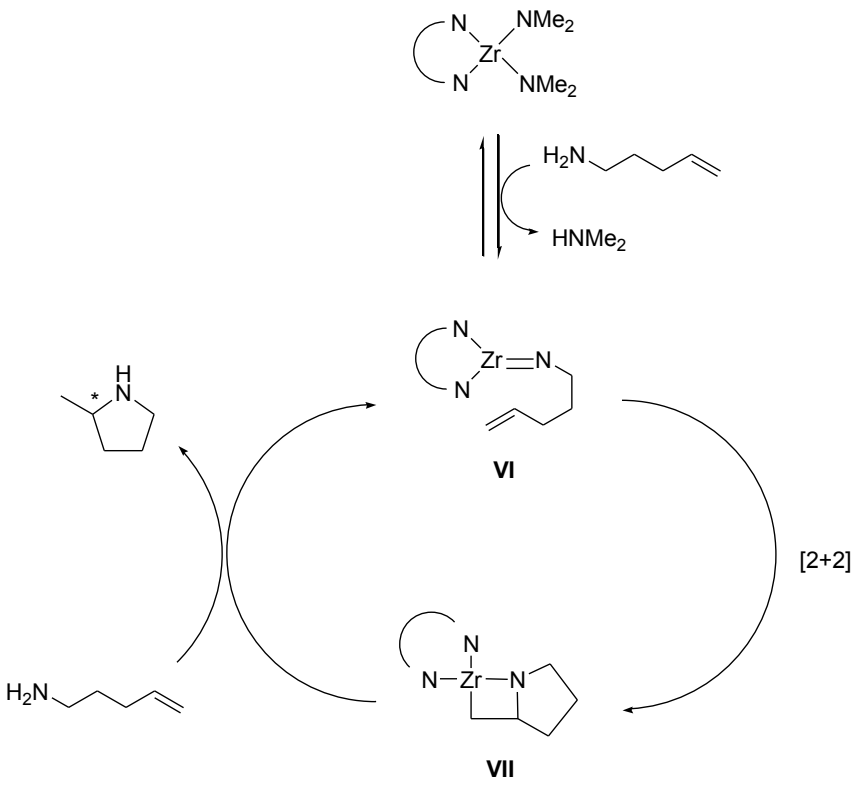

Scheme 1.3 Proposed mechanism for the intramolecular hydroamination of 4-pentenylamine catalyzed by a neutral zirconium complex.

1.1.1.3 Enantioselective Alkene Hydroamination Catalyzed by Late Transition Metal Complexes.

Late transition metal complexes typically display lower air and moisture sensitivity and better functional group tolerance than do rare-earth metal or group 4 transition metal complexes.[2] Despite these favorable traits, only two examples of enantioselective intramolecular hydroamination of unactivated alkenes catalyzed by late transition metals have been reported. The first example of late transition metal catalyzed

enantioselective intramolecular hydroamination of unactivated alkenes was achieved by Buchwald group using $[Rh(cod)_2]BF_4$ and a dialkylbiaryl phosphine ligand.[65] The rhodium-catalyzed method was effective for the enantioselective intramolecular hydroamination of a range of amino alkenes with up to 91% ee. For example, treatment of *N*-2-methylbenzyl-2-phenyl-4-pentenamine with a 1:1 mixture of $[Rh(cod)_2]BF_4$ and a bis(cyclohexyl) *o*-binapthyl ligand led to formation of a 1.1:1 of *cis*- and *trans*- 2-methyl-1-(2-methylbenzyl)-4-phenylpyrrolidine in 80% combined yield with 87% and 91% ee, respectively (eq 1.10).

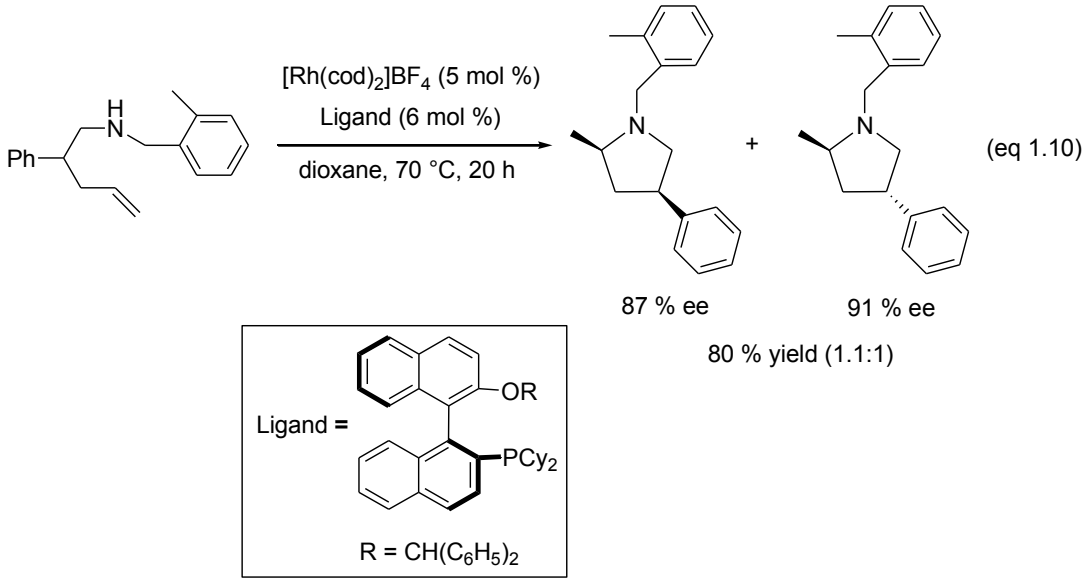

The second example of the enantioselective intramolecular hydroamination of an unactivated alkene was reported by Mikami utilizing diastereomerically pure gold(I) complexes with a chiral phosphoric acid co-catalyst (Eq 1.1).[66] The authors believed that

both the reactivity and selectivity of the intramolecular hydroamination of *N*-alkenyl ureas was enhanced by the dinuclear gold complex, which provided proximal and bimetallic activation of both the alkene and urea, although no experimental evidence supported these claims. Furthermore, the authors reported the enantioselective intramolecular hydroamination of only one substrate – *N*-(2,2-diphenylpent-4-en-1-yl)benzamide – and with only 48% ee (eq 1.11).

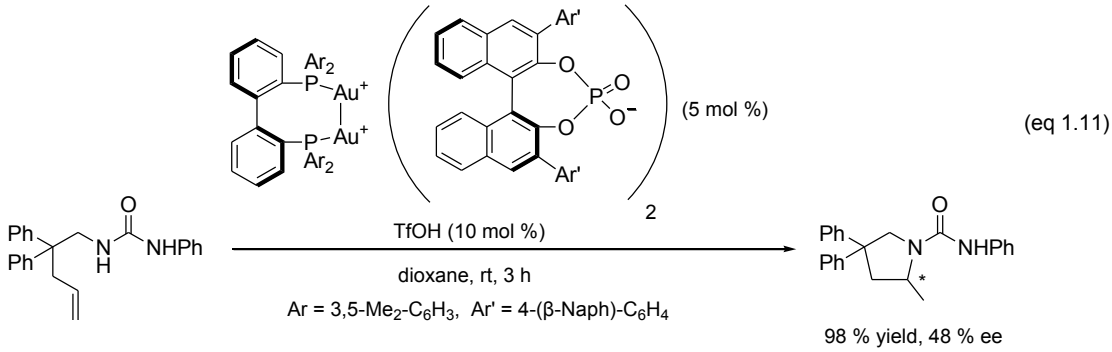

(eq 1.11)

1.1.2 Special Characteristics of Gold(I) in Homogeneous Catalysis

Numerous publications dealing with homogeneous transition metal catalysis utilizing gold(I) complexes have emerged over the past decade.[67-73] Many of these reports describe carbon-carbon and carbon-heteroatom bond formation through the addition of nucleophiles to C–C multiple bonds in the presence of cationic gold(I) complexes. The impressive results of Au(I) catalysis can be attributed in part to the relativistic contraction of the valence s and p shells and relativistic expansion of the valence d and f shells of gold. The relativistic contraction of the valence 6*s* orbitals of

gold are responsible for the enhanced Lewis acidity and high electronegativity of Au(I) species compared to similar transition metals.[74] In conjunction with phosphine ligands, cationic phosphine-Au(I) complexes behave as a 'soft' Lewis acids, as cationic Au(I) is a large, diffuse cation sharing positive charge with the phosphine ligand, and serve to activate 'soft' electrophiles such as carbon-carbon π-bonds toward nucleophilic attack.[71] Also, the pronounced redox stability of Au(I) complexes under ambient conditions can be explained by the relativistic expansion of the Au(I) 5*d* orbitals. With the expansion of the 5*d* orbitals, there should be less electron-electron repulsion and the Au(I) 5*d* electrons are held with greater energy. This produces a less nucleophilic metal species with a low tendency to undergo oxidative addition.

1.1.3 Project Motivation

The most impressive results in the enantioselective intramolecular hydroamination of unactivated alkenes have been achieved using rare-earth and group 4 metal catalysts.[2] However, the high moisture and air sensitivity and low functional group compatibility of the rare-earth and group 4 metal catalyst systems have limited the practical utility of these methods. For these reasons, late transition metal complexes have attracted considerable interest as catalysts for the enantioselective hydroamination of alkenes. However, only two examples of enantioselective intramolecular hydroamination of unactivated alkenes have been reported; one which is catalyzed by a rhodium complex[65] and one of which is catalyzed by a gold(I) complex.[66] The Rh catalyst system

displayed good reactivity and enantioselectivity with a rage of substrates but required elevated temperatures for higher reactivity. The gold system catalyzed hydroamination in good yield at room temperature but with moderate enantioselectivity and limited scope. For this reason, a catalyst system that is active at room temperature yielding both good reactivity and enantioselectivity would be desirable.

Widenhoefer and Bender previously reported the room temperature hydroamination of *N*-alkenyl ureas catalyzed by a gold(I) *N*-heterocyclic carbene complex.[75] As an example, reaction of **3** with a catalytic 1:1 mixture of gold(I) *N*,*N*-diaryl imidazol-2-ylidine complex and AgOTf (5 mol %) in MeOH at room temperature for 22 h led to isolation of pyrrolidine **4** in 98% yield (eq 1.12). This result suggested the possibility of developing a highly active Au(I)-catalyst system for the enantioselective intramolecular hydroamination of unactivated alkenes run at room temperature. Here we describe our efforts directed toward the development of a gold(I)-catalyzed protocol for the room temperature intramolecular hydroamination of unactivated alkenes.

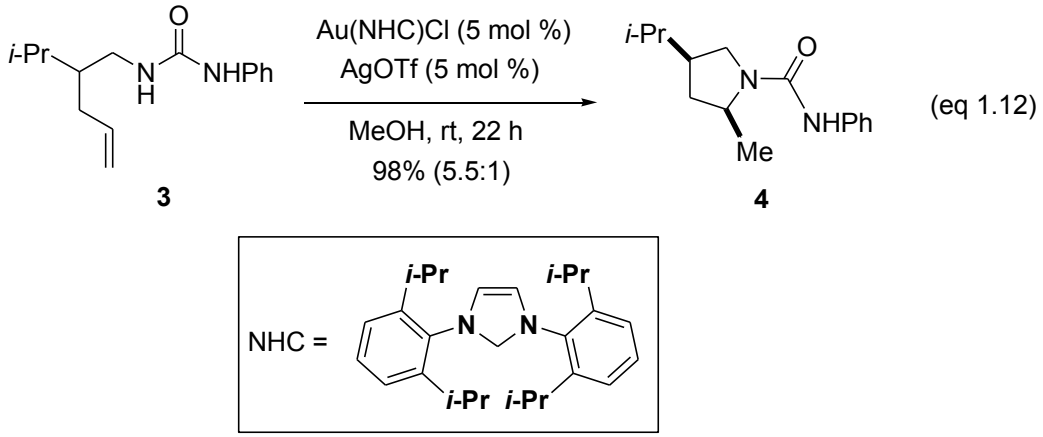

1.2 Results and Discussion

1.2.1 Optimization and Substrate Scope

Initial studies directed toward development of gold(I)-catalyzed intramolecular alkene hydroamination targeted gold complexes containing enantiomerically pure, dialkyl *o*-biphenylphosphine ligands (Table 5, **L1-L3**). This selection was based on previous results showing that gold(I) complexes with electron rich, sterically hindered ligands displayed high reactivity for the intramolecular hydroamination of unactivated alkenes.[74] In accord with our expectations, a catalyst system consisting of a 1:1 mixture of (**L1**)AuCl and $AgBF_4$ (5 mol %) in methanol at room temperature catalyzed the intramolecular hydroamination of 1-benzyl-3-(2,2-diphenylpent-4-enyl)urea (**1a**) to form pyrrolidine **2a**, but with only 15% ee (Table 1, entry 1). Although Au(I) monophosphine biaryl complexes produced high conversion of **1a** to **2a**, increasing or decreasing the size of the *O*-bound substituent on the ligand failed to produce a catalyst that displayed high enantioselectivity (Table 1, entries 2 and 3).

We then targeted bis(gold) complexes containing an axially chiral bis(phosphine) core in combination with P-bound 3,5-di-*tert*-butyl-4-methoxyphenyl (DTBM) groups; similar ligands have been employed in many highly enantioselective transition metal catalyzed transformations.[20,68,76-79] In addition, axially chiral bis(phosphine) ligands with a tunable dihedral angle were of interest; the dihedral angle of ligands can be modified by changing the length of the carbon linker, which can potentially affect their reactivity.[80]

To this end, we synthesized axially chiral bis(phosphine) ligands with P-bound DTBM groups and with a one- (**L4**), three- (**L5**), or five-carbon (**L6**) linker (Table 1). The bis(gold) complexes of these ligands proved only modestly effective as catalysts for the conversion of **1** to **2** and, of these ligands, **L6** provided the better enantioselectivity for the conversion of **1b** to **2b**, but all gave poor conversion (Table 1, entries 4-6).

Table 1. Effect of ligand on the enantioselectivity of the gold(I)-catalyzed intramolecular hydroamination of γ-alkenyl carboxamide and sulfonamides.

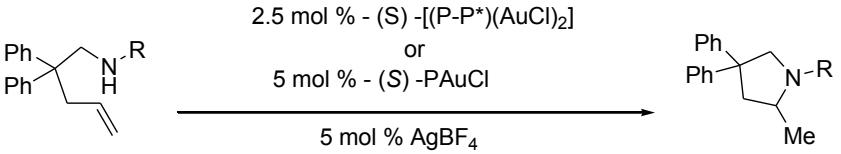

1a : R = CONHBn
1b : R = Fmoc
1c : R = Ts

2a : R = CONHBn
2b : R = Fmoc
2c : R = Ts

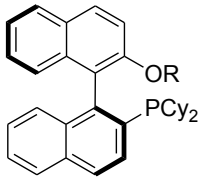

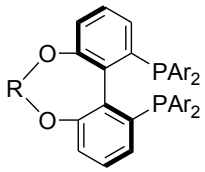

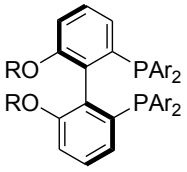

Ar : 3,5-di-tert-butyl-4-methoxyphenyl

P

L1 : R = Me
L2 : R = $CH(C_6H_5)_2$
L3 : R = H

P-P*

L4 : R = CH_2
L5 : R = $(CH_2)_3$
L6 : R = $(CH_2)_5$

L7 : R = H
L8 : R = Me
L9 : R = Et
L10 : R = *i*-Pr
L11 : R = Bn

entry	alkenyl amine	P-P* or P	conv.[%][a]	ee[%][a]
1	**1a**	**L1**	100	15
2	**1a**	**L2**	100	8
3	**1a**	**L3**	96	18
4	**1b**	**L4**	22	14
5	**1b**	**L5**	23	16
6	**1b**	**L6**	26	38
7	**1b**	**L7**	49	47
8	**1b**	**L8**	97	78
9	**1b**	**L9**	34	59
10	**1b**	**L10**	71	21
11	**1b**	**L11**	n.r.	-
12	**1a**	**L8**	100	58
13	**1c**	**L8**	5	36

[a] Conversion and enantiopurity determined by HPLC analysis on a chiral staionary phase. n.r. = no reaction.

Another attempt to achieve both good activity and enantioselectivity for the conversion of **1b** to **2b** was made by modifying the 6,6'-positions of DTBM-MeOBIPHEP ligand (Table 5, **L7-L11**). Among the ligands tested, the parent ligand DTBM-MeOBIPHEP ligand **L8** gave the best combination of reactivity and enantioselectivity. For example, treatment of substrate **1b** with a catalytic mixture of [(*S*)-**L8**](AuCl)$_2$ (2.5 mol %) and $AgBF_4$ (5 mol %) in methanol at room temperature formed pyrrolidine **2b** with 97% conversion and with 78% ee (Table 5, entry 8). Changing the *O*-bound group to hydrogen (**L7**), ethyl (**L9**), isopropyl (**L10**), or benzyl (**L11**) group failed to improve the conversion and/or enantioselectivity (Table 1, entries 7-11). Much to our surprise, even small variation of the *O*-bound substituent at the 6,6'-position, such as changing methyl (**L8**) to ethyl (**L9**), resulted in significant deterioration of the activity and enantioselectivity of the conversion of **1b** to **2b** (Table 1, entries 8 and 9). A 1:2 mixture of bis(gold) complex [(*S*)-**L8**](AuCl)$_2$ and $AgBF_4$ also catalyzed the intramolecular hydroamination of alkenyl urea **1a** with 100 % conversion and 58 % ee, but hydroamination of sulfonamide **1c** catalyzed by [(*S*)-**L8**](AuCl)$_2$ and $AgBF_4$ gave only 5% conversion and 36 % ee (Table 1, entry 13).

Further optimization to examine the effect of counterion and solvent on the yield and enantioselectivity of gold-catalyzed enantioselective intramolecular hydroamination employing the gold complex [(*S*)-**L8**](AuCl)$_2$ revealed that the enantioselectivity depended strongly on solvent and little on counterion (Table 2). For example, running the hydroamination in non polar solvent such as toluene resulted in a significant decrease in enantioselectivity to 2% for the conversion of **1a** to **2a** (Table 2, entry 2). Conversely,

altering the nature of the anion of the silver salt had no significant effect on enantioselectivity for the conversion of **1a** to **2a** (Table 2, entries 6-10).

Table 2. Effect of the solvent and silver salt on the gold-catalyzed enantioselelctive intramolecular hydroamination of **1a** and **1b**.

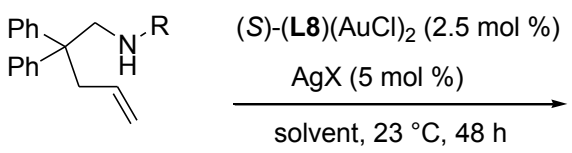

1a : R = CONHBn **2a** : R = CONHBn

1b : R = Fmoc **2b** : R = Fmoc

entry	substrates	X	solvent	conv.(%)[a]	ee(%)[a]
1	**1a**	BF_4	dioxane	100	21
2	**1a**	BF_4	toluene	100	2
3	**1a**	BF_4	Et_2O	100	13
4	**1a**	BF_4	CH_2Cl_2	100	2
5	**1a**	BF_4	*i*-PrOH	100	45
6	**1a**	BF_4	MeOH	100	58
7	**1a**	OTf	MeOH	100	58
8	**1a**	SbF_6	MeOH	100	57
9	**1a**	ClO_4	MeOH	100	53
10	**1a**	OTs	MeOH	100	57
11	**1b**	BF_4	CH_2Cl_2	85	17
12	**1b**	BF_4	dioxane	51	22
13	**1b**	BF_4	toluene	91	18
14	**1b**	BF_4	*i*-PrOH	71	65
15	**1b**	BF_4	CF_3CH_2OH	89	14
16	**1b**	BF_4	MeOH/H_2O(4:1)	7	64
17	**1b**	BF_4	MeOH	97	78

[a] Conversion and enantiopurity determined by HPLC analysis on a chiral stationary phase.

From the experiments outlined in the previous paragraphs, we identified the conditions consisting of **a** 1:2 mixture of [(*S*)-**L8**]$(AuCl)_2$ (2.5 mol %) and $AgBF_4$ (5 mol %) in MeOH at room temperature for the intramolecular enantioselective hydroamination of *N*-γ-alkenyl carbamates and ureas. With these optimized conditions in hand, a variety of *N*-γ-alkenyl carbamates and ureas were cyclized to corresponding pyrrolidines in modest to good yield and enantioselectivity (Table 3). Unfortunately, *gem*-diphenyl groups at the homoallylic position of the *N*-γ-alkenyl carboxamide derivative were required for to realize both good yield and good enatioselectivity in gold-catalyzed intramolecular hydroamination. When the homoallylic position was substituted with a cyclohexyl group (**15**) or was unsubstitued (**17**), the reaction rate and enantioselectivity decreased or no cyclization occurred, respectively (Table 3, entries 9 and 10).

Table 3. Enantioselective intramolecular hydroamination of alkenyl amines catalyzed by a mixture of [(*S*)-**L8**]$(AuCl)_2$ (2.5 mol %) and $AgBF_4$ (5 mol %) in methanol.

Entry	Substrate		Product	*T* [°C]	t [h]	Yield[a] [%]	ee[b] [%]
	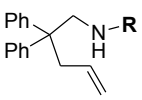		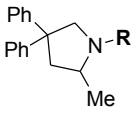				
1	**R =** Cbz	**5**	**6**	23	48	90	72
2	**R =** Fmoc	**1b**	**2b**	23	48	92	78
3[c]	**R** = Fmoc		**2c**	0	70	63	84
4	**R** = CO_2Me	**7**	**8a**	23	48	93	76
5[c]	**R** = CO_2Me		**8b**	0	70	65	82
6	**R** = CO_2Pr	**9**	**10**	23	48	93	77
7	**R** = CO_2EtOBn	**11**	**12**	23	48	85	75
8	**R** = Troc	**13**	**14**	23	48	63	48
	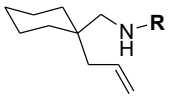		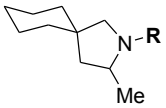				
9	**R** = Fmoc	**15**	**16**	23	48	58	55
10	**R** = Fmoc	**17**		23	48	n.r.	-
	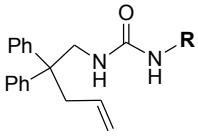		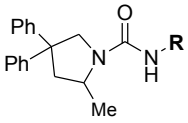				
11	**R** = Ph	**18**	**19**	23	40	92	58
12	**R** = 4-IC_6H_4	**20**	**21**	23	48	70	58
13	**R** = 4-$NO_2C_6H_4$	**22**	**23**	23	48	75	76
14	**R** = Bn	**1a**	**2a**	-20	48	81	71
15	**R** = nBu	**24**	**25**	-20	48	84	81
16	**R** = Me	**26**	**27**	-20	48	88	85
	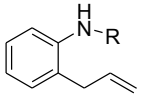		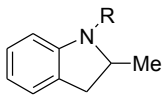				
17[d]	**R** = Ac	**28**	**29**	80	48	96[e]	38

[a] Isolated yield. [b] enantiopurity determined by HPLC analysis on a chiral stationary phase. [c] reaction performed in 0.26 M (entries 1,2,4, 6-10 in 0.13 M, entries 10-16 in 0.4 M, entry 17 in 0.34 M). [d] solvent: dioxane, silver salt: $AgSbF_6$. [e] conversion determined by HPLC analysis. n.r. = no reaction.

The reactivity of the [(*S*)-**L8**]$(AuCl)_2$/$AgBF_4$ catalyst system for the intramolecular hydroamination of unactivated alkenes encouraged us to investigate this transformation at a lower temperature in an attempt to enhance the enantioselectivity. Indeed, the enantioselectivities for the conversion of **1a** to **2a** and for the conversion of **7** to **8** at 0 °C improved from 78% ee to 84% ee (Table 3, entries 2 and 3) and from 76% to 82% ee, respectively, albeit with somewhat reduced yields (Table 3, entries 4 and 5). The gold-catalyzed enantioselective intramolecular hydroamination of *N*-γ-alkenyl ureas possessing a functionalized *N*'-aryl or *N*'-alkyl group was also efficient (Table 3, entries 11-16). Interestingly, *N*-γ-alkenyl ureas possessing a less sterically demanding *N*'-substituent such as a benzyl (**1a**) or *n*-butyl (**24**) or methyl group (**26**) underwent gold-catalyzed intramolecular enantioselective hydroamination at –20 °C with enantioselectivities up to 85% ee in the case of *N'*-methyl of **26** (Table 3, entries 14-16). In addition to these examples, gold-catalyzed hydroamination of *N*-(2-allylphenyl)acetamide (**28**) formed 1-(2-methylindolin-1-yl)ethanone (**29**) in 96% yield, but required 80 °C and displayed poor enantioselectivity (Table 3, entry 17).

Gold-catalyzed intramolecular enantioselective hydroamination to form piperidine rings such as **30** occurred with low conversion and moderate enantioselectivity (Figure 2). Similarly, the *N*-γ-alkenyl acetamide **31**, carbamates **32**-**34**, and carboxamide **35** and the *N*-allyl ureas **36** and **37** failed to undergo gold-catalyzed enantioselective hydroamination.

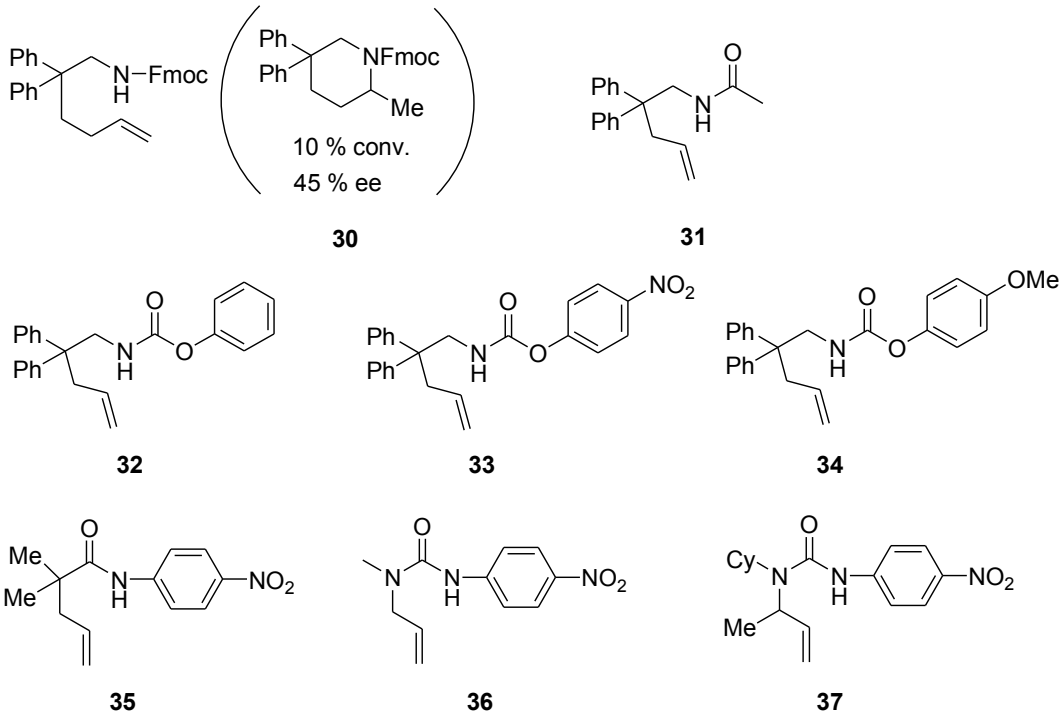

Figure 2. Substrates that showed poor reactivity or failed to undergo gold-catalyzed enantioselective intramolecular hydroamination.

1.2.2 Mechanism

The reaction pathway for the gold(I)-catalyzed hydroamination of alkenes is generally assumed to proceed via π-activation of the C=C bond toward nucleophilic attack,[81-84] and the Widenhoefer group has supported this idea through isolation and study of gold(I) π-alkene complexes.[85,86] In this respect, gold(I)-catalyzed intramolecular hydroamination of alkenes presumably occurs through the outer-sphere addition of the nitrogen nucleophile to the gold-coordinated alkene complex (**VII**) to form a gold alkyl

complex (**VIII**). Protodeauration of **VIII** would then release the pyrrolidine and regenerate the cationic gold catalyst (Scheme 3).

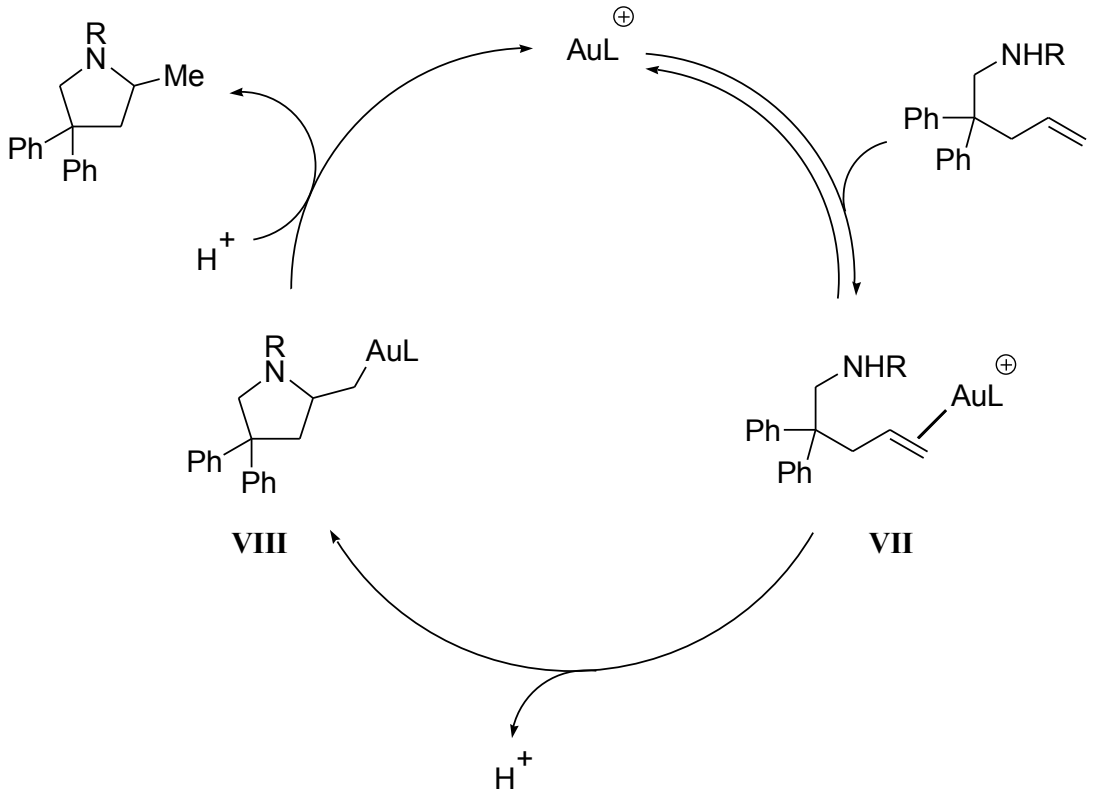

Scheme 3

Along with the mechanism depicted in Scheme 3, the bis(gold) complex employed in our catalyst system was taken into consideration to account for the unusual reactivity and selectivity of this catalyst system. Recently, some groups have posited that bis(gold) complexes show higher reactivity and enantioselectivity relative to mono(gold) complexes because they can coordinate in a bidentate fashion to both an alkene and a

heteroatom.[66,87] This concept can be applied to the [(*S*)-**L8**](AuCl)$_2$ catalyst system to account for observations made in the development of our Au(I) catalyst system. Based on this model, a proposed mechanism is depicted in Scheme 4. The bis(gold) complex may coordinate both the alkene and the urea or carbamate group (**IX**). Outer-sphere addition of the nitrogen nucleophile to the gold-coordinated π-bond followed by loss of a proton generates the gold(I)-alkyl complex (**X**). Protodeauration of **X** forms the pyrrolidine product with regeneration of the gold(I) catalyst.

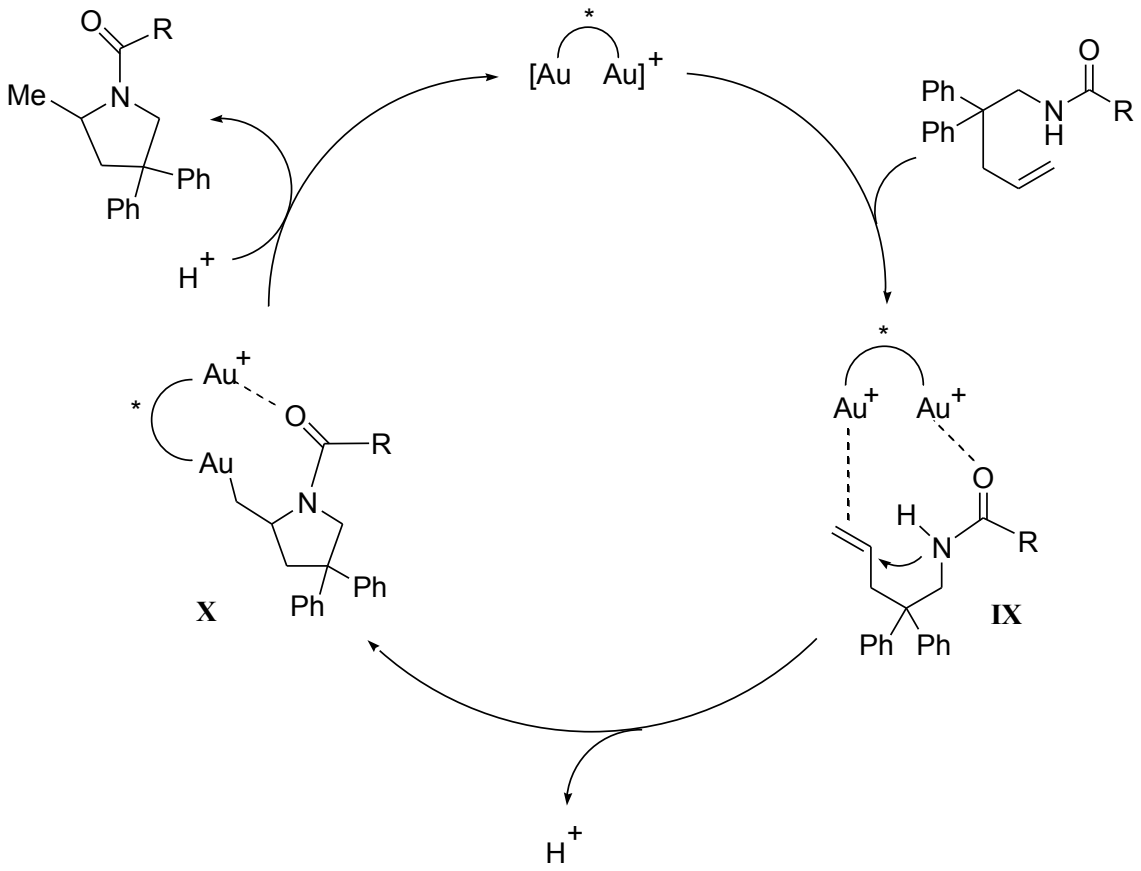

Scheme 4

Bimetallic coordination may create a more enantiodiscriminating environment owing to conformational rigidity. Also, the proximity of the olefin and nucleophile provided by the bimetallic coordination could increase the reaction rate for cyclization. This would explain why bis(gold) complexes display better enantioselectivity than mono(gold) complexes (Table 5). In addition, the failure of the catalyst system to cyclize sterically bulky *N*-γ-alkenyl carbamates is consistent with this model as sterically bulky *N*'-alkyl group would hinder amine coordination, resulting in loss of proximal effect. Likewise, the greater reactivity observed for simple *N*'-alkyl or benzyl ureas over *N*'- aryl ureas is in the agreement with the proposed model where the steric bulk of the *N*'-substituent deteriorates the reactivity of hydroamination by hampering the bimetallic coordination.

1.2.3. Summary

We have developed a gold(I)-catalyzed system for the enantioselective intramolecular hydroamination of unactivated alkenes. This catalyst system was effective for the cyclization of alkenyl carbamates and ureas at or below room temperature with good yield and enantioselectivity up to 85% ee. Also, we proposed a bimetallic activation model that invokes proximal effects and conformational rigidity to account for the high reactivity and enantioselectivity of the Au(I) catalyst system. This gold(I)-catalyzed protocol will offer opportunities to develop more general and enantioselective catalyst systems for enantioselective hydroamination of alkenes.

1.3 Experimental Section

1.3.1 General Methods

Reactions were performed under a nitrogen atmosphere employing standard Schlenk and/or drybox techniques unless specified otherwise. NMR spectra were obtained on Varian spectrometers operating at 500 MHz for ^{1}H NMR and 126 MHz for ^{13}C NMR in $CDCl_3$ at 25 °C unless noted otherwise. IR spectra were obtained on a Nicolet Avatar 360-FT IR spectrometer. Gas chromatography was performed on a Hewlett-Packard 5890 gas chromatography equipped with a 25 m polydimethylsiloxane capillary column and FID detector. Chiral HPLC was performed on a Hewlett-Parkard chromatograph equipped with a 0.46 cm × 25 cm Chiralpak AD-H column. Column chromatography was performed employing 230-400 mesh silica gel (Silicycle). Thin layer chromatography (TLC) was performed on silica gel 60 F_{254} (EMD Chemicals Inc.). Elemental analyses were performed by Complete Analysis Laboratories (Parsippany, NJ). Room temperature is 23 °C. All solvents were purchased from Aldrich or Acros in anhydrous form and used as received. All reagents were purchased from major suppliers and used as received. 2,2-diphenyl-4-pentenylamine (**38**) were synthesized employing a published procedure.[75] Racemic hydroamination products were synthesized employing a published procedure.[75] (*S*)-dicyclohexyl(2'-methoxy-1,1'-binaphthyl-2-yloxy)phosphine (L1), (*S*)-(2-(benzhydryloxy)-1,4'-binaphthyl-3'-yl)dicyclohexylphosphine (L2), (*S*)-3'-

(dicyclohexylphosphino)-1,4'-binaphthyl-2-ol (L3) (Table 1, L1-L3) were synthesized employing known procedure.[88]

1.3.2 Synthesis of Alkenyl Carbamate Substrates

Benzyl 2,2-diphenyl-4-pentenylcarbamate (5). To a suspension of **38** (500 mg, 2.1 mmol) and $NaHCO_3$ (3.2 mmol, 270 mg) in 2:3 mixture of H_2O and EtOH (15 mL) was added benzyl chloroformate (375 mg, 2.2 mmol) dropwise, and the reaction mixture was stirred at room temperature for 2 h. The reaction mixture was extracted with Et_2O (3 × 25 mL) and the organic phase was washed sequentially with H_2O and brine. The combined organic extracts were dried ($MgSO_4$) and concentrated in *vacuo*. The resulting pale yellow oil was chromatographed (hexanes–EtOAc = 5 :1) to give **5** as a colorless oil, 93%. TLC (hexanes–EtOAc = 3:1): R_f = 0.42. ^{1}H NMR (Figure 19): δ 7.38-7.32 (m, 8 H), 7.29-7.24 (m, 3 H), 7.21 (d, J = 7.5 Hz, 4 H), 5.52-5.44 (m, 1 H), 5.10 (s, 2 H), 5.02 (d, J = 12.0 Hz, 2 H), 4.40 (bs, 1 H), 3.98 (d, J = 5.5 Hz, 2 H), 2.91 (d, J = 7.0 Hz, 2 H). ^{13}C{^{1}H} NMR (Figure 20): δ 156.3, 145.3, 136.5, 133.7, 128.6, 128.3, 128.24, 128.20, 128.0, 126.5, 118.7, 66.8, 50.3, 47.7, 41.7. Anal. calcd (found) for $C_{25}H_{25}NO_2$: C, 80.83 (80.82); H, 6.78 (6.69).

(9-Fluorenyl)methyl 2,2-diphenyl-4-pentenylcarbamate **(1b)**, methyl 2,2-diphenylpent-4-enylcarbamate **(7)**, propyl 2,2-diphenyl-4-pentenylcarbamate **(9)**, 2-(benzyloxy)ethyl 2,2-diphenyl-4-pentenylcarbamate **(11)**, and 2,2,2-trichloroethyl 2,2-

diphenyl-4-pentenylcarbamate **(13)** were synthesized employing a procedure similar to that used to synthesize **5**.

(9-Fluorenyl)methyl 2,2-diphenyl-4-pentenylcarbamate (1b). White wax, 81%. TLC (hexanes–EtOAc = 3:1): R_f = 0.45. ^{1}H NMR (Figure 21): δ 7.78 (d, J = 7.0 Hz, 2 H), 7.52 (d, J = 7.5 Hz, 2 H), 7.41 (t, J = 7.5 Hz, 2 H), 7.33-7.29 (m, 6 H), 7.27-7.24 (m, 2 H), 7.20 (d, J = 7.5 Hz, 4 H), 5.51-5.42 (m, 1 H), 5.01 (d, J = 6.5 Hz, 1 H), 4.98 (s, 1 H), 4.36 (d, J = 7.0 Hz, 3 H), 4.19 (t, J = 7.0 Hz, 1 H), 3.95 (d, J = 5.5 Hz, 2 H), 2.86 (d, J = 7.0 Hz, 2 H). ^{13}C{^{1}H} NMR (Figure 22): δ 156.2, 145.2, 143.9, 141.3, 133.7, 130.0, 128.3, 128.0, 127.6, 127.0, 126.5, 125.0, 119.9, 118.6, 66.6, 50.4, 47.6, 47.2, 41.6. Anal. calcd (found) for $C_{32}H_{29}NO_2$: C, 83.63 (83.66); H, 6.36 (6.31).

Methyl 2,2-diphenylpent-4-enylcarbamate (7). Colorless solid, 88%. TLC (hexanes–EtOAc = 3:1): R_f = 0.41. ^{1}H NMR (Figure 23): δ 7.28-7.24 (m, 4 H), 7.21-7.18 (m, 2 H), 7.14 (d, J = 8.0 Hz, 4 H), 5.44-5.36 (m, 1 H), 4.98 (s, 1H), 4.95-4.94 (m, 1 H), 4.23 (br s, 1 H), 3.88 (d, J = 6.0 Hz, 2 H), 3.56 (s, 3 H), 2.84 (d, J = 6.5 Hz, 2 H). ^{13}C{^{1}H} NMR (Figure 24): δ 156.9, 145.2, 133.7, 128.3, 128.0, 126.5, 118.6, 52.1, 50.2, 47.6, 41.6. Anal. calcd (found) for $C_{19}H_{21}NO_2$: C, 77.26 (77.30); H, 7.17 (7.15).

Propyl 2,2-diphenyl-4-pentenylcarbamate (9). Colorless solid, 93%. TLC (hexanes–EtOAc = 3:1): R_f = 0.48. ^{1}H NMR (Figure 25): δ 7.29-7.26 (m, 4 H), 7.21-7.18 (m, 2 H), 7.15 (d, J = 7 Hz, 4 H), 5.51-5.42 (m, 1 H), 5.0-4.95 (m, 2 H), 4.28 (br s, 1 H), 3.93-3.89 (m, 4 H), 2.89 (d, J = 6.5 Hz, 2 H), 1.54 (q, J = 6.5 Hz, 2 H), 0.87 (t, J =

7.5 Hz, 3 H). $^{13}C\{^{1}H\}$ NMR (Figure 26): δ 156.5, 145.5, 134.1, 128.2, 128.0, 126.4, 118.1, 66.3, 50.2, 47.4, 41.4, 22.3, 10.0. Anal. calcd (found) for $C_{21}H_{25}NO_2$: C, 77.98 (77.87); H, 7.79 (7.64).

2-(Benzyloxy)ethyl 2,2-diphenyl-4-pentenylcarbamate (11). Colorless oil, 85%. TLC (hexanes–EtOAc = 3 :1): R_f = 0.19. ^{1}H NMR (Figure 27): δ 7.32-7.24 (m, 9 H), 7.22-7.18 (m, 2 H), 7.15 (d, J = 8.0 Hz, 4 H), 5.48-5.39 (m, 1 H), 4.98-4.92 (m, 2 H), 4.46 (m, 2 H), 4.36 (br s, 1 H), 4.12 (t, J = 5.0 Hz, 2 H), 3.89 (d, J = 6.0 Hz, 2 H), 3.56 (t, J = 4.5 Hz, 2 H), 2.86 (d, J = 6.5 Hz, 2 H). $^{13}C\{^{1}H\}$ NMR (Figure 28): δ 156.2, 145.5, 138.3, 134.1, 128.34, 128.26, 128.0, 127.7, 127.6, 126.4, 118.2, 73.0, 68.6, 64.0, 50.1, 47.5, 41.4, 45.5, 134.1, 128.2, 128.0, 126.4, 118.1, 66.3, 50.2, 47.4, 41.4, 22.3, 10.0. Anal. calcd (found) for $C_{27}H_{29}NO_3$: C, 78.04 (78.13); H, 7.03 (7.11).

2,2,2-Trichloroethyl 2,2-diphenyl-4-pentenylcarbamate (13). Colorless solid, 92%. TLC (hexanes–EtOAc = 3 :1): R_f = 0.65. ^{1}H NMR (Figure 29): δ 7.36–7.33 (m, 4 H), 7.29-7.25 (m, 2 H), 7.21 (d, J = 7.5 Hz, 4 H), 5.49-5.41 (m, 1 H), 5.05-5.01 (m, 2 H), 4.72 (s, 2 H), 4.57 (br m, 1 H), 4.0 (d, J = 6.0 Hz, 2 H), 2.91 (d, J = 7.0 Hz, 2 H). $^{13}C\{^{1}H\}$ NMR (Figure 30): δ 154.5, 145.0, 133.5, 128.3, 127.9, 126.6, 118.8, 74.3, 50.3, 47.8, 41.6. Anal. calcd (found) for $C_{20}H_{20}Cl_3NO_2$: C, 58.20 (58.07); H, 4.88 (4.85).

(9H-Fluoren-9-yl)methyl (1-allylcyclohexyl)methylcarbamate (15). White solid, 63%. TLC (hexanes–EtOAc = 3 :1): R_f = 0.35. ^{1}H NMR (Figure 31): δ 7.76 (d, J = 7.5 Hz, 2 H), δ 7.59 (d, J = 7.5 Hz, 2 H), 7.38 (t, J = 8.0 Hz, 2 H), 7.30 (t, J = 7.5 Hz, 2 H), 5.88-5.79 (m, 1 H), 5.07-5.06 (br m, 1 H), 5.04 (s, 1 H), 4.82 (br s, 1 H), 4.37 (d, J = 6.5

Hz, 2 H), 4.20 (t, J = 6.5 Hz, 1 H), 3.07 (d, J = 6.0 Hz, 2 H), 2.03 (d, J = 7.0 Hz, 2 H), 1.46-1.21 (m, 10 H). $^{13}C\{^{1}H\}$ NMR (Figure 32): δ 156.5, 144.2, 141.3, 134.9, 127.6, 127.0, 125.1, 119.9, 117.1, 66.3, 47.4, 40.4, 37.0, 33.2, 26.2, 21.4. Anal. calcd (found) for $C_{25}H_{29}NO_2$: C, 79.96 (79.88); H, 7.78 (7.71).

1.3.3 Synthesis of Alkenyl Urea Substrates

1-(2,2-Diphenylpent-4-enyl)-3-methylurea (26). Methylisocyanate (110.6 mg, 1.9 mmol) was added to a solution of **38** (0.460 g, 1.9 mmol) in THF (20 mL) at room temperature and the reaction mixture was stirred overnight. The resulting solution was diluted with ether (50 mL), washed sequentially with 1 M HCl (25 mL), saturated $NaHCO_3$ (25 mL), and brine (25 mL). The combined organic extracts were dried ($MgSO_4$) and concentrated in *vacuo*. The resulting white solid was chromatographed (hexanes–EtOAc = 3:1 → 1:1) to give **26** (0.79 g, 80%) as a white solid. TLC (hexanes–EtOAc = 2:1): R_f = 0.15. ^{1}H NMR: δ 7.38-7.24 (m, 10 H), 5.57-5.47 (m, 1 H), 5.08-5.02 (m, 2 H), 4.36 (br d, J = 4.0 Hz, 1 H), 4.06 (br t, J = 5.6 Hz, 1 H), 3.95 (d, J = 5.6 Hz, 2 H), 2.95 (d, J = 6.8 Hz, 2 H), 2.67 (d, J = 4.8 Hz, 3 H). $^{13}C\{^{1}H\}$ NMR: δ 158.9, 145.8, 134.2, 128.4, 128.3, 126.6, 118.6, 50.5, 47.3, 41.9, 27.3. IR (neat, cm^{-1}): 3339, 1619, 1570, 1252, 1069, 699. HRMS calcd (found) for $C_{19}H_{22}N_2O$ (M^+): 294.1732 (294.1736). Anal. calcd (found) for $C_{19}H_{22}N_2O$: C, 77.52 (77.57); H, 7.53 (7.47).

1-(2,2-Diphenylpent-4-enyl)-3-phenylurea (**18**), 1-(2,2-diphenylpent-4-enyl)-3-(4-iodophenyl)urea (**20**), 1-(2,2-diphenylpent-4-enyl)-3-(4-nitrophenyl)urea (**22**), 1-benzyl-3-(2,2-diphenylpent-4-enyl)urea (**1a**), and 1-butyl-3-(2,2-diphenylpent-4-enyl)urea (**24**) were synthesized employing a procedure similar to that used to synthesize **26**.

1-(2,2-Diphenylpent-4-enyl)-3-phenylurea (18). White solid, 80%. TLC (hexane-EtOAc = 3:1): R_f = 0.40. ^{1}H NMR: δ 8.00 (s, 1 H), 7.39-7.15 (m, 14 H), 6.89-6.85 (m, 1 H), 5.58-5.48 (m, 1 H), 5.06 (s, 1 H), 4.99-4.87 (m, 2H), 4.03 (d, J = 6.4 Hz, 2 H), 2.93 (d, J = 8.0 Hz, 2 H). ^{13}C{^{1}H} NMR: δ 155.0, 146.1, 140.6, 134.4, 128.5, 128.0, 127.9, 126.1, 121.3, 117.9, 117.5, 50.2, 46.0, 41.4. IR (neat, cm^{-1}): 3324, 1629, 1568, 1252, 1081, 1037, 698. HRMS calcd (found) for $C_{24}H_{24}N_2O$ (M^+): 356.1889 (356.1887). Anal. calcd (found) for $C_{24}H_{24}N_2O$: C, 80.87 (80.79); H, 6.79 (6.65).

1-(2,2-Diphenylpent-4-enyl)-3-(4-iodophenyl)urea (20). White solid, 85%. TLC (Hexane-EtOAc = 3:1): R_f = 0.45. ^{1}H NMR: δ 8.06 (br s, 1 H), 7.51-7.48 (m, 2 H), 7.31-7.18 (m, 13 H), 5.57-5.47 (m, 1 H), 5.08 (br t, J = 5.6 Hz, 1 H), 4.98-4.87 (m, 2 H), 4.02 (d, J = 5.6 Hz, 2 H), 2.93 (d, J = 7.2 Hz, 2 H). ^{13}C{^{1}H} NMR: δ 154.7, 146.0, 140.7, 137.4, 134.4, 128.0, 128.0, 126.1, 120.0, 117.5, 82.8, 50.2, 46.0, 41.4. IR (neat, cm^{-1}): 3324, 1644, 1602, 1486, 1309. 1231, 698. HRMS calcd (found) for $C_{24}H_{23}IN_2O$ (M^+): 482.0855 (482.0860). Anal. calcd (found) for $C_{22}H_{28}N_2O$: C, 59.76 (59.88); H, 4.81 (4.76).

1-(2,2-Diphenylpent-4-enyl)-3-(4-nitrophenyl)urea (22). Light yellow solid, 78%. TLC (Hexane-EtOAc = 3:1): R_f = 0.30. ^{1}H NMR: δ 8.63 (s, 1 H), 8.11-8.08 (m, 2 H),

7.62-7.60 (m, 2H), 7.32-7.19 (m, 10 H), 5.56-5.46 (m, 1 H), 5.32 (s, 1 H), 5.00-4.89 (m, 2 H), 4.06 (d, J = 6.0 Hz, 2 H), 2.94 (d, J = 7.2 Hz, 2 H). $^{13}C\{^{1}H\}$ NMR: δ 154.3, 146.9, 145.8, 141.3, 134.3, 128.1, 128.0, 126.2, 124.8, 117.7, 117.0, 50.1, 46.0, 41.4. IR (neat, cm^{-1}): 3672, 2985, 2902, 1406, 1229, 1136, 893, 697. HRMS calcd (found) for $C_{24}H_{23}N_3O_3$ (M^+): 401.1739 (401.1746). Anal. calcd (found) for $C_{24}H_{23}N_3O_3$: C, 71.80 (71.94); H, 5.77 (5.74).

1-Benzyl-3-(2,2-diphenylpent-4-enyl)urea (1a). White solid, 89%. TLC (hexane-EtOAc = 3:1): R_f = 0.30. ^{1}H NMR: δ 7.33-7.21 (m, 15 H), 5.99 (br s, 1 H), 5.60-5.51 (m, 1 H), 5.01-4.89 (m, 3 H), 4.39 (d, J = 6.5 Hz, 1 H), 4.29 (d, J = 6.0 Hz, 1 H), 4.02 (d, J = 6 Hz, 2 H), 2.95 (d, J = 7.5 Hz, 2 H). $^{13}C\{^{1}H\}$ NMR: δ 158.2, 145.7, 139.6, 139.1, 134.1, 128.8, 128.7, 128.4, 128.2, 127.5, 127.4, 127.3, 126.6, 118.6, 50.4, 47.2, 44.7, 44.5, 41.9. IR (neat, cm^{-1}): 3324, 1629, 1568, 1252, 1081, 1056, 698. HRMS calcd (found) for $C_{25}H_{26}N_2O$ (M^+): 370.2045 (370.2038). Anal. calcd (found) for $C_{25}H_{26}N_2O$: C, 81.05 (79.95); H, 7.07 (6.98).

1-Butyl-3-(2,2-diphenylpent-4-enyl)urea (24). White solid, 74%. TLC (hexanes–EtOAc = 1:3): R_f = 0.24. ^{1}H NMR: δ 7.29-7.15 (m, 10 H), 5.57-5,47 (m, 2 H), 4.95-4.83 (m, 2 H), 4.65 (br s, 1 H), 3.93 (d, J = 6.4 Hz, 2 H), 3.05-3.00 (m, 2 H), 2.89 (d, J = 7.6 Hz, 2 H), 1.36-1.19(m, 4 H), 0.84 (t, J = 7.6 Hz, 3 H). $^{13}C\{^{1}H\}$ NMR: δ 157.9, 146.3, 134.7, 128.0, 127.9, 125.9, 117.3, 50.3, 46.2, 41.4, 39.3, 32.5, 19.7, 13.2. IR (neat, cm^{-1}): 3341, 1632, 1565, 1253, 1047, 699. HRMS calcd (found) for $C_{22}H_{28}N_2O$ (M^+): 336.2202 (336.2211). Anal. calcd (found) for $C_{22}H_{28}N_2O$: C, 78.53 (78.56); H, 8.39 (8.48).

1.3.4 Synthesis of *N*-(2-allylphenyl)acetamide (28)

To 2-iodobenzenamine (2 g, 9.1 mmol) in acetic anhydride (16 mL) was added three drops of concentrated H_2SO_4. The resulting mixture was stirred at room temperature for 5 min and then quenched with water and extracted with DCM (3 × 30 mL). The combined organic extracts were washed sequentially with H_2O (2 × 40 mL) and brine and then dried ($MgSO_4$). The solvent was removed in *vacuo* and the crude product was crystallized in EtOH to produce *N*-(2-iodophenyl)acetamide (**39**) as a white powder (2.0 g, 85 %). ^{1}H NMR: δ 8.20 (d, *J* = 8.0 Hz, 1 H), 7.80 (d, *J* = 8.0 Hz, 1 H), 7.42 (bs, 1 H), 7.34 (t, *J* = 7.5 Hz, 1 H), 6.84 (t, J = 7.5 Hz, 1 H), 2.24 (s, 3 H).

In a reflux condenser equipped two-necked round-bottomed flask, **39** (778 mg, 3.0 mmol), CsF (904 mg, 6.0 mmol), and $Pd(PPh_3)_4$ (207 mg, 0.18 mmol) in THF (20 mL) was stirred at room temperature for 30 min. A solution of allylboronic acid pinacol ester (1 g, 6.0 mmol) in THF (10 mL) was added to this suspension and the resulting mixture was refluxed at 70 °C for 24 h. After the reaction time, the reaction mixture was washed with water and brine and extracted with DCM (3 × 30 mL). The combined organic extracts was dried ($MgSO_4$) and concentrated in *vacuo*. The resulting mixture was chromatographed (hexanes–EtOAc = 5:1→ 1:1→1:2) to give *N*-(2-allylphenyl)acetamide (**28**) as a white solid (385 mg, 74 %). TLC (hexanes–EtOAc = 1:1): R_f = 0.38. ^{1}H NMR (Figure 33): δ 7.82 (d, *J* = 8.0 Hz, 1 H), 7.32-7.24 (m, 1 H), 7.18 (d, *J* = 6.0 Hz, 1 H),

7.11 (t, J = 7.6 Hz, 1 H), 6.02-5.92 (m, 1 H), 5.23 (dd, J = 1.6, 10.0 Hz, 1 H), 5.10 (dd, J = 1.6, 17.2 Hz, 1 H), 6.84 (t, J = 7.5 Hz, 1 H), 6.77 (d, J = 6.0 Hz, 2 H), 2.15 (s, 3 H).

1.3.5 Gold(I)-Catalyzed Enantioselective Intramolecular Hydroamination of Alkenyl Carbamates

Benzyl 2-methyl-4,4-diphenylpyrrolidine-1-carboxylate (**6**) A suspension of (*S*)-[(**L8**)$(AuCl)_2$] (3.2 mg, 2.0×10^{-3} mmol) and $AgBF_4$ (0.8 mg, 4.0×10^{-3} mmol) in methanol (0.5 mL) was stirred for 15 min. To the reaction mixture was added **5** (30.0 mg, 0.081 mmol), and the reaction mixture was stirred at 23 °C for 48 h. The crude reaction mixture was chromatographed (hexanes–EtOAc = 3:1) on a silica gel column to give benzyl 2-methyl-4,4-diphenylpyrrolidine-1-carboxylate (**6**) (27.1 mg, 90%) as a colorless oil. TLC (hexanes–EtOAc = 3 :1): R_f = 0.50. ^{1}H NMR (Figure 34, 1:1 ratio of rotamers): δ 7.44-7.17 (m, 15 H), [5.33 (d, J = 12.5 Hz), 5.11 (d, J = 12.0 Hz), 1:1, 1 H], [5.20 (abq, J = 13.0 Hz), 1:1, 1 H], [4.76 (dd, J = 2.0, 12.0 Hz), 4.60 (dd, J = 1.5, 12.0 Hz), 1:1, 1 H], 3.84-3.68 (m, 2 H), 2.88-2.83 (m, 1 H), 2.38-2.27 (m, 1 H), [1.38 (d, J = 6.0 Hz), 1.31 (d, J = 6.0 Hz), 1:1, 3 H]. ^{13}C{^{1}H} NMR (Figure 35, 1:1 ratio of rotamers): δ [155.4, 154.6, (1:1)], [145.63, 145.60, (1:1)], [145.0, 144.9, (1:1)], [137.0,136.9, (1:1)], [128.53, 128.51, (1:1)], 128.48, 128.43, 128.39, 127.99, [127.96, 127.75, (1:1)], 127.49, [126.74, 126.72, (1:1)], [126.46, 126.40, (1:1)], 126.33, [126.26, 126.23, (1:1)], [66.7, 66.6, (1:1)], 55.8, [52.78, 52.71, (1:1)], [52.6, 52.2, (1:1)], [46.8, 45.9, (1:1)], [21.1, 20.0, (1:1)]. IR (neat, cm^{-1}): 3061.5, 3029.1, 2960.6, 2928.0, 2979.7, 1700.3, 1597.8, 1498.2, 1447.3, 1410.4, 1367.4, 1324.1, 1261.9, 1261.2, 1163.1, 1133.6, 1095.5, 1021.2, 797.8, 768.4, 752.8,

698.3. HRMS calcd (found) for $C_{25}H_{25}NO_2$ (M^+): 372.1958 (372.1957). Enantiopurity (72% ee) was determined by HPLC analysis (85:15 hexanes/isopropanol, 0.5 mL/min; Figure 6).

All remaining intramolecular hydroamination reactions of alkenyl carbamates were performed employing a procedure analogous to that used to synthesize **6** utilizing the catalyst mixture and conditions outlined in Table 3.

(9H-fluoren-9-yl)methyl 2-methyl-4,4-diphenylpyrrolidine-1-carboxylate (2b and 2c). White solid, 92% (**2b**), 63% (**2c**). TLC (hexanes–EtOAc = 3 :1): R_f = 0.43. ^{1}H NMR (Figure 36, 1:1 ratio of rotamers): δ 7.81 (d, *J* = 7.5 Hz, 1 H), 7.75 (dd, *J* = 3.5, 5.0 Hz, 1 H), [7.65 (d, *J* = 7.5 Hz), 7.62 (d, *J* = 7.0 Hz), 1:1, 1 H], [7.56 (d, *J* = 8.0 Hz), 7.44-7.15 (m), 15 H], [4.71 (dd, *J* = 2, 11.5 Hz), 4.59 (dd, *J* = 6.5, 10.5 Hz), 1:1, 1H], 4.50-4.39 (m, 2 H), [4.32 (t, *J* = 6.0 Hz), 4.27 (t, *J* = 6.5 Hz), 1:1, 1 H], [3.83-3.79 (m), 3.73-3.61 (m), 2H], 2.85 (dd, *J* = 6.5, 12.5 Hz, 1H), 2.32-2.24 (m, 1 H), [1.35 (d, *J* = 6.0 Hz), 1.15 (d, *J* = 6.0 Hz), 1:1, 3 H] ^{13}C{^{1}H} NMR (Figure 37, 1:1 ratio of rotamers): δ [155.6, 154.7, (1:1)], [146.0, 145.9, (1:1)], [145.4, 145.2, (1:1)], [144.5, 144.4, (1:1)], 144.3, [141.64, 141.56, (1:1)], [128.84, 128.81, (1:1)], 128.7, [127.89, 127.86, (1:1)], [127.80, 127.75, (1:1)], 127.33, 127.27, 127.18, 127.0, [126.75, 126.72, (1:1)], 126.63, 126.61, 126.59, 126.55, 125.23, 125.14, 125.09, 120.19, [120.10, 120.08, (1:1)], [67.19, 67.16, (1:1)], 56.1, [53.0, 52.5, (1:1)], [47.65, 47.60, (1:1)], [47.05, 46.19, (1:1)], [21.08, 20.27, (1:1)]. IR (neat, cm^{-1}): 3062.8, 2924.3, 2853.2, 1698.8, 1598.6, 1449.3, 1413.1,

1351.5, 1323.3, 1200.0, 1163.0, 1135.5, 1097.6, 1032.7, 1021.3, 993.8, 740.5, 737.1, 700.3. HRMS calcd (found) for $C_{32}H_{29}NO_2$ (M^+): 460.2271 (460.2268). Anal. calcd (found) for $C_{32}H_{29}NO_2$: C, 83.63 (83.56); H, 6.36 (6.32). Enantiopurity [78% ee (**2b**), 84% ee (**2c**)] was determined by HPLC analysis (90:10 hexanes/isopropanol, 0.5 mL/min; Figure 7 and 8, respectively).

Methyl 2-methyl-4,4-diphenylpyrrolidine-1-carboxylate (8a and 8b). Colorless oil, 93% (**8a**), 65 % (**8b**). TLC (hexanes–EtOAc = 3:1): R_f = 0.45. ^{1}H NMR (Figure 38, 1:1 ratio of rotamers): 7.31-7.15 (m, 10 H), [4.70 (d, J = 11.5 Hz), 4.51(d, J = 12.0 Hz), 1:1, 1 H], 3.76-3.67 (m, 4 H), 2.87-2.81 (m, 1 H), 2.34-2.25 (m, 1 H), [1.34 (d, J = 6.0 Hz), 1.28 (d, J = 6.5 Hz), 1:1, 3 H]. ^{13}C{^{1}H} NMR (Figure 39, 1:1 ratio of rotamers): δ [156.0, 155.2, (1:1)], [145.8, 145.7, (1:1)], [145.3, 145.1, (1:1)], [128.52, 128.46, (1:1)], 126.7, 126.44, 126.41, 126.4, [126.3, 126.2, (1:1)], [55.93, 55.85, (1:1)], [52.7, 52.1, (1:1)], [52.6, 52.5, (1:1)], [52.3, 52.2, (1:1)], [46.8, 46.0, (1:1)], [20.9, 20.0, (1:1)]. IR (neat, cm^{-1}): 3058.2, 3025.6, 2955.8, 2926.9, 2877.7, 1699.1, 1598.1, 1495.2, 1447.2, 1385.7, 1270.8, 1203.6, 1164.0, 1138.8, 1100.7, 1066.4, 1033.8, 771.2, 753.5, 700.1. HRMS calcd (found) for $C_{19}H_{21}NO_2$ (M^+): 296.1645 (296.1639). Anal. calcd (found) for $C_{19}H_{21}NO_2$: C, 77.26 (77.34); H, 7.17 (7.20). Enantiopurity [76% ee (**8a**), 82% ee (**8b**)] was determined by HPLC analysis (90:10 hexanes/isopropanol, 0.5 mL/min; Figure 9 and 10, respectively).

Propyl 2-methyl-4,4-diphenylpyrrolidine-1-carboxylate (10). Colorless oil, 93%. TLC (hexanes–EtOAc = 3:1): R_f = 0.48. ^{1}H NMR (Figure 40, 1:1 ratio of rotamers): δ 7.33-7.14 (m, 10 H), [4.69 (d, J = 11.5 Hz), 4.55 (d, J = 11.5 Hz), 1:1, 1H], 4.11-3.96

(m, 2 H), 3.68-3.59 (m, 2 H), 2.87-2.84 (m, 1 H), 2.31-2.21 (m, 1 H), [1.68 (q, J = 7.5 Hz), 1.60 (q, J = 7.5 Hz), 1:1, 2 H], 1.27 (d, J = 6.0 Hz, 3 H), [0.98 (t, J = 7.5 Hz), 0.89 (t, J = 7.5 Hz), 1:1, 3 H]. $^{13}C\{^{1}H\}$ NMR (Figure 41, 1:1 ratio of rotamers): δ [155.9, 155.1, (1:1)], 146.4, [145.8, 145.7, (1:1)], [128.85,128.80, (1:1)], 127.1, 126.83, 126.76, 126.65, 126.57, [66.9, 66.8, (1:1)], [56.02, 55.96, (1:1)], 53.2, [53.0, 52.5, (1:1)], [47.0, 46.1, (1:1)], [23.0, 22.8, (1:1)], [21.2, 20.2, (1:1)], 10.6. IR (neat, cm^{-1}): 3058.6, 3028.8, 2964.2, 2927.9, 2875.9, 1694.1, 1598.1, 1448.9, 1413.3, 1383.5, 1288.3, 1199.3, 1163.0, 1097.7, 1033.8, 943.0, 771.8, 752.3, 697.8. HRMS calcd (found) for $C_{21}H_{25}NO_2$ (M^+): 324.1958 (324.1955). Anal. calcd (found) for $C_{21}H_{25}NO_2$: C, 77.98 (77.96); H, 7.79 (7.71). Enantiopurity (77% ee) was determined by HPLC analysis (90:10 hexanes/isopropanol, 0.5 mL/min; Figure 11).

2-(Benzyloxy)ethyl 2-methyl-4,4-diphenylpyrrolidine-1-carboxylate (12). Colorless oil, 85%. TLC (hexanes–EtOAc = 3:1): R_f = 0.19. ^{1}H NMR (Figure 42, 1:1 ratio of rotamers): δ 7.38-7.14 (m, 15 H), [4.69 (d, J = 11.5 Hz), 4.59-4.57 (m), 1:1, 1 H], [4.59 (s), 4.48 (s), 1:1, 2 H], 4.33-4.16 (m, 2 H), 3.73-3.62 (m, 4 H), 2.90-2.83 (m, 1 H), 2.31-2.22 (m, 1 H), 1.28 (d, J = 5.5 Hz, 3 H) $^{13}C\{^{1}H\}$ NMR (Figure 43, 1:1 ratio of rotamers): δ [155.5,154.8, (1:1)], [146.4, 146.3, (1:1)], [145.7, 145.6, (1:1)], [138.9, 138.8, (1:1)], 128.9, 128.8, [128.7, 128.6, (1:1)], 128.0, [127.91, 127.81, (1:1)], 127.1, 126.8, 126.7, 126.6, 73.3, [69.11, 69.05, (1:1)], [64.5, 64.4, (1:1)], [56.03, 56.0, (1:1)], [53.2,53.0, (1:1)], [53.1, 52.6, (1:1)], [46.9, 46.1, (1:1)], [21.2, 20.1, (1:1)]. IR (neat, cm^{-1}): 3060.2, 3028.7, 2981.1, 2928.8, 2871.5, 1698.4, 1447.2, 1412.8, 1348.4, 1202.2, 1095.5, 1027.8, 789.4, 750.8, 698.2. HRMS calcd (found) for $C_{27}H_{29}NO_3$ (M^+): 416.222

(416.2215). Anal. calcd (found) for $C_{27}H_{29}NO_3$: C, 78.04 (77.97); H, 7.03 (6.97). Enantiopurity (75% ee) was determined by HPLC analysis (90:10 hexanes/isopropanol, 0.5 mL/min; Figure 12).

2,2,2-Trichloroethyl 2-methyl-4,4-diphenylpyrrolidine-1-carboxylate (14). Colorless oil, 63 %. TLC (hexanes–EtOAc = 3:1): R_f = 0.63. ^{1}H NMR (Figure 44, 1:1 ratio of rotamers): δ 7.34-7.14 (m, 10 H), [5.0 (dd, J = 1.0, 12.0 Hz), 4.60 (dd, J = 1.5, 12.5 Hz), 1:1, 1 H], 4.82-4.69 (m, 2 H), 3.86-3.79 (m, 1 H), [3.77 (d, 12.0 Hz), 3.69 (d, 11.0 Hz), 1:1, 1 H], 2.93-2.87 (m, 1 H), 2.37-2.28 (m, 1 H), [1.40 (d, J = 6.5 Hz), 1.37 (d, 6.0 Hz), 1:1, 3 H]. ^{13}C{^{1}H} NMR (Figure 45, 1:1 ratio of rotamers): δ [153.6, 152.5, (1:1)], 145.4, [144.6, 144.5, (1:1)], 128.6, [128.57, 128.55, (1:1)], [126.72, 126.69, (1:1)], [126.62, 126.59, (1:1)], 126.47, 126.43, [74.8, 74.5, (1:1)], 56.1, 56.8, 53.1, 52.7, [46.7, 45.9, (1:1)], [21.0, 19.7, (1:1)]. IR (neat, cm^{-1}): 3059, 3027, 2980, 2926, 1716, 1496, 1447, 1410, 1351, 1264, 1197, 1134, 1065, 822, 756, 700. HRMS calcd (found) for $C_{19}H_{21}NO_2$ (M^+): 412.0632 (412.0622). Anal. calcd (found) for $C_{19}H_{21}NO_2$: C, 77.26 (77.30); H, 7.17 (7.15). Enantiopurity (48% ee) was determined by HPLC analysis (95:5 hexanes/isopropanol, 0.5 mL/min; Figure 13).

9-Fluorenylmethyl 2-methyl-4-cyclohexylpyrrolidine-1-carboxylate (16). Colorless oil, 58 %. TLC (hexanes–EtOAc = 3:1): R_f = 0.64. ^{1}H NMR (Figure 46, 1:1 ratio of rotamers): δ 7.76 (d, J = 7.5 Hz, 2 H), 7.76-7.59 (m, 2 H), 7.39-7.38 (m, 2 H), 7.33-7.30 (m, 2 H), 4.50-4.25 (m, 3 H), [3.90 (d, J = 7.0 Hz), 3.70 (d, J = 5.5 Hz), 1:1, 1 H], [3.59 (d, J = 10.5 Hz), 3.52 (d, J = 11.0 Hz), 1:1, 1 H], 3.02-2.95 (m, 1 H), 2.05-1.88 (m, 1 H), 1.54-1.22 (m, 11 H), [1.30 (d, J = 6.0 Hz), 1.05 (d, J = 5.5 Hz), 1:1, 3 H].

$^{3}C\{^{1}H\}$ NMR (Figure 47, 1:1 ratio of rotamers): δ [155.5, 155.0, (1:1)], [144.3, 144.2, (1:1)], 141.3, 127.5, 127.0,126.9, 125.1, 124.9,124.8, 119.9, 66.6, [56.7, 56.4, (1:1)], [52.5, 51.9, (1:1)], [47.5, 47.4, (1:1)], [46.4, 45.7, (1:1)], 41.2, 40.9, 36.6, 34.6, 26.1, 24.7, 23.8, 23.3, 22.9, [21.5, 20.7, (1:1)]. IR (neat, cm^{-1}): 2923, 2852, 2781, 1701, 1448, 1408, 1375, 1319, 1261, 1220, 1191, 1137, 1086, 757, 737. Anal. calcd (found) for $C_{25}H_{29}NO_2$: C, 79.96 (79.92); H, 7.78 (7.66). Enantiopurity (55% ee) was determined by HPLC analysis (99:1 hexanes/isopropanol, 0.5 mL/min; Figure 14).

1.3.5 Gold(I)-Catalyzed Enantioselective Intramolecular Hydroamination of Alkenyl Ureas

***N*-Methyl-2-methyl-4,4-diphenylpyrrolidine-1-carboxamide (27).** A suspension of (*S*)-[(**L8**)$(AuCl)_2$] (8.1 mg, 5.0×10^{-3} mmol) and $AgBF_4$ (1.9 mg, 10.0×10^{-3} mmol) in methanol (0.5 mL) was stirred for 15 min. To the reaction mixture was added **S9** (40.0 mg, 0.2 mmol), and the reaction mixture was stirred at – 20 °C for 48 h. The resulting mixture was concentrated and chromatographed (MeOH-CH_2Cl_2 = 20:1 → 10:1) to give N-methyl-2-methyl-4,4-diphenylpyrrolidine-1-carboxamide (**27**) (17.5 mg, 88%) as white microcrystals. TLC (MeOH-CH_2Cl_2 = 1:10): R_f = 0.65. ^{1}H NMR (Figure 48): δ 7.31-7.12 (m, 10 H), 4.50 (d, *J* = 10.4 Hz, 1 H), 4.21 (br s, 1 H), 3.67 (d, *J* = 10.8 Hz, 2 H), 2.85 (s, 3 H), 2.80 (ddd, *J* = 2.0, 6.4, 12.4 Hz, 1 H), 2.34 (dd, *J* = 8.8, 12.0 Hz, 1 H), 1.48-1.40 (m, 2 H), 1.35-1.25 (m, 2 H), 1.29 (d, *J* = 6.0 Hz, 3 H). $^{13}C\{^{1}H\}$ NMR (Figure 49): δ 157.7, 146.0, 145.7, 128.7, 128.6, 127.0, 126.7, 126.5, 56.3, 52.9, 51.9, 47.1, 27.7, 21.1.

IR (neat, cm^{-1}): 3329, 1625, 1537, 1366, 1221, 700. HRMS calcd (found) for $C_{19}H_{23}N_2O$ (MH^+): 295.1810 (295.1813). Anal. calcd (found) for $C_{19}H_{22}N_2O$: C, 77.52 (77.52); H, 7.53 (7.44). Enantiopurity was determined by HPLC analysis (85:15 hexanes/isopropanol, 0.5 mL/min): 85% ee (Figure 15).

All remaining intramolecular hydroamination reactions of alkenyl ureas were performed employing a procedure analogous to that used to synthesize **27** utilizing the catalyst mixture and conditions outlined in Table 3.

Phenyl 2-methyl-4,4-diphenyl-pyrrolidine-1-carboxamide (19). White solid, 92%. TLC (Hexane-EtOAc): R_f = 0.40. ^{1}H NMR (Figure 50): δ 7.41 (d, J = 8.0 Hz, 2 H), 7.32-7.14 (m, 12 H), 7.01 (t, J = 7.0 Hz, 1 H), 6.37 (br s, 1 H), 4.60 (d, J = 11.0 Hz), 3.81-3.75 (m, 2H), 2.89 (ddd, J = 2.0, 7.0, 12.5 Hz, 1 H), 2.36 (dd, J = 9.0, 12.5 Hz, 1 H), 1.33 (d, J = 6.0 Hz, 3 H). ^{13}C{^{1}H} NMR (Figure 51): δ 153.8, 145.8, 145.3, 139.5, 128.8, 128.6, 128.5, 126.8, 126.5, 126.4, 122.7, 119.5, 56.0, 52.9, 52.1, 46.4, 20.6. IR (neat, cm^{-1}): 3324, 1642, 1543, 1484, 1227, 1069, 697. HRMS calcd (found) for $C_{24}H_{25}N_2O$ (MH^+): 357.1967 (357.1972). Anal. calcd (found) for $C_{24}H_{24}N_2O$: C, 80.87 (80.71); H, 6.79 (6.65). Enantiopurity was determined by HPLC analysis (92:8 hexanes/isopropanol, 0.5 mL/min): 58% ee (Figure 16).

***N*-(4-iodophenyl)-2-methyl-4,4-diphenylpyrrolidine-1-carboxamide (21).** White solid, 70%. TLC (hexane-EtOAc = 3:1): R_f = 0.45. ^{1}H NMR (Figure 52): δ 7.56-7.54 (m, 2 H), 7.31-7.14 (m, 12 H), 6.31 (br s, 1 H), 4.56 (d, J = 10.5 Hz, 1 H), 3.79-3.74 (m,

2 H), 2.91 (ddd, J = 1.5, 6.5, 12.0 Hz, 1 H), 2.61 (dd, J = 9.0, 12.0 Hz, 1 H), 1.31 (d, J = 6.5 Hz, 3 H). $^{13}C\{^{1}H\}$ NMR (Figure 53): δ 154.2, 146.6, 146.0, 141.1, 128.6, 128.5, 128.4, 127.0, 126.7, 126.5, 126.4, 121.8, 119.3, 56.3, 53.3, 46.0, 20.2. IR (neat, cm^{-1}): 3325, 1643, 1543, 1485, 1309, 1069, 697. HRMS calcd (found) for $C_{24}H_{24}IN_2O$ (MH^+): 483.0933 (483.0922). Anal. calcd (found) for $C_{24}H_{23}IN_2O$: C, 59.76 (59.68); H, 4.81 (4.67). Enantiopurity was determined by HPLC analysis (80:20 hexanes/isopropanol, 0.5 mL/min): 58 % ee (Figure 17).

2-Methyl-*N*-(4-nitrophenyl)-4,4-diphenylpyrrolidine-1-carboxamide (23). Light yellow solid, 75%, TLC (Hexane-EtOAc = 3:1): R_f = 0.30. ^{1}H NMR (Figure 54): δ 8.12 (d, J = 9.5 Hz, 2 H), 7.60-7.57 (m, 2 H), 7.31-7.13 (m, 10 H), 6.64 (br s, 1 H), 4.58 (br d, J = 8.0 Hz, 1 H), 3.84-3.79 (m, 2 H), 2.94 (dd, J = 6.0, 11.5 Hz, 1 H), 2.37 (dd, J = 9.5, 12.5 Hz, 1 H), 2.03 (d, J = 6.0 Hz, 3 H). $^{13}C\{^{1}H\}$ NMR (Figure 55): δ 153.3, 147.5, 146.3, 145.6, 141.8, 128.7,128.6, 126.9, 126.6, 126.5, 124.8, 118.3, 118.2, 56.3, 53.3, 52.6, 45.7. IR (neat, cm^{-1}): 3355, 2969, 1655, 1499, 1326, 1249, 1111, 852, 751, 699. HRMS calcd (found) for $C_{24}H_{24}N_3O_3$ (MH^+): 402.1818 (402.1818). Anal. calcd (found) for $C_{24}H_{23}N_3O_3$: C, 71.80 (71.85); H, 5.77 (5.82). Enantiopurity was determined by HPLC analysis (80:20 hexanes/isopropanol, 0.5 mL/min): 76% ee (Figure 18).

***N*-benzyl-2-methyl-4,4-diphenylpyrrolidine-1-carboxamide (2a).** White solid, 81%. TLC (hexane-EtOAc = 3:1): R_f = 0.30. ^{1}H NMR (Figure 56): δ 7.33-7.18 (m, 15 H), 4.82 (br t, J = 5.0 Hz, 1 H), 4.59 (d, J = 10.5 Hz, 1 H), 4.42 (d, J = 5.5 Hz, 2 H), 3.69-3.63 (m, 2 H), 2.87 (ddd, J = 2.0, 7.0, 12.5 Hz, 1 H), 2.32 (dd, J = 9.0, 12.0 Hz, 1 H), 1.28 (d, J = 6.0 Hz, 3 H). $^{13}C\{^{1}H\}$ NMR (Figure 57): δ 156.7, 146.0, 145.6, 140.5,

128.6, 128.53, 128.51, 127.3, 127.0, 126.9, 126.6, 126.5, 126.3, 55.9, 53.0, 51.8, 46.7, 44.3, 20.3. IR (neat, cm^{-1}): 3339, 1628, 1528, 1342, 1057, 698. HRMS calcd (found) for $C_{25}H_{27}N_2O$ (MH^+): 371.2123 (371.2117). Anal. calcd (found) for $C_{25}H_{26}N_2O$: C, 81.05 (81.10); H, 7.07 (6.97). Enantiopurity was determined by HPLC analysis (85:15 hexanes/isopropanol, 0.5 mL/min): 71% ee (Figure 19).

***N*-butyl-2-methyl-4,4-diphenylpyrrolidine-1-carboxamide (25).** White solid, 84%. TLC (hexanes–EtOAc = 1:3): R_f = 0.24. ^{1}H NMR (Figure 58): δ 7.30-7.13 (m, 10 H), 4.52 (d, J = 11 Hz, 1 H), 4.35 (br s, 1 H), 3.66-3.56 (m, 2 H), 3.28-3.15 (m, 2 H), 2.82 (ddd, J = 2.0, 6.5, 12 Hz, 1 H), 2.31 (dd, J = 9, 12, Hz, 1 H), 1.48 (quin, J = 6.5 Hz, 2 H), 1.34 (sex, J = 7.5 Hz, 2 H), 1.25 (d, J = 6.5 Hz, 3 H), 0.93 (t, J = 7.5 Hz, 3 H). ^{13}C{^{1}H} NMR (Figure 59): δ 156.9, 146.2, 145.8, 128.5, 126.9, 126.6, 126.5, 126.3, 55.9, 53.0, 51.7, 46.8, 40.3, 32.7, 20.8, 20.2, 13.8. IR (neat, cm^{-1}): 3330, 1622, 1535, 1448, 1390, 1049, 699. HRMS calcd (found) for $C_{22}H_{29}N_2O$ (MH^+): 337.2280 (337.2276). Anal. calcd (found) for $C_{22}H_{29}N_2O$: C, 78.53 (78.44); H, 8.39 (8.53). Enantiopurity was determined by HPLC analysis (85:15 hexanes/isopropanol, 0.5 mL/min): 81 % ee (Figure 20).

1.3.6 Gold(I)-Catalyzed Enantioselective Intramolecular Hydroamination of N-(2-allylphenyl)acetamide (28)

1-(2-methylindolin-1-yl)ethanone (29) A suspension of (*S*)-[(**L8**)$(AuCl)_2$] (6.9 mg, 4.3×10^{-3} mmol) and $AgSbF_6$ (2.9 mg, 8.6×10^{-3} mmol) in dioxane (0.5 mL) was stirred

for 15 min in a heavy-walled pressure tube in a glove box. To the reaction mixture was added **28** (30.0 mg, 0.17 mmol). The pressure tube was caped and took out from a glove box to place in an oil bath. The reaction mixture was stirred at 80 °C for 48 h. The reaction solution was filtered through a silca gel pad eluting with Et_2O/EtOAc (1:1 mixture). The combined solution was evaporated until removing solvents under a reduced pressure to give **29** as a white solid. Conversion (96%) and enantiopurity (38% ee) was determined by HPLC analysis (85:15 hexanes/isopropanol, 0.5 mL/min). ^{1}H NMR (Figure 60): δ 8.15 (d, *J* = 7.2 Hz, 1 H), 7.20 (t, *J* = 8.0 Hz, 2 H), 7.02 (t, *J* = 7.2 Hz, 1 H), 4.47-4.44 (m, 1 H), 3.41 (dd, *J* = 9.2, 16.0 Hz, 1 H), 2.66 (d, *J* = 15.6 Hz, 1 H), 2.28 (s, 3 H), 1.3 (d, *J* = 6 Hz, 3 H).

1.3.7 Catalyst Synthesis

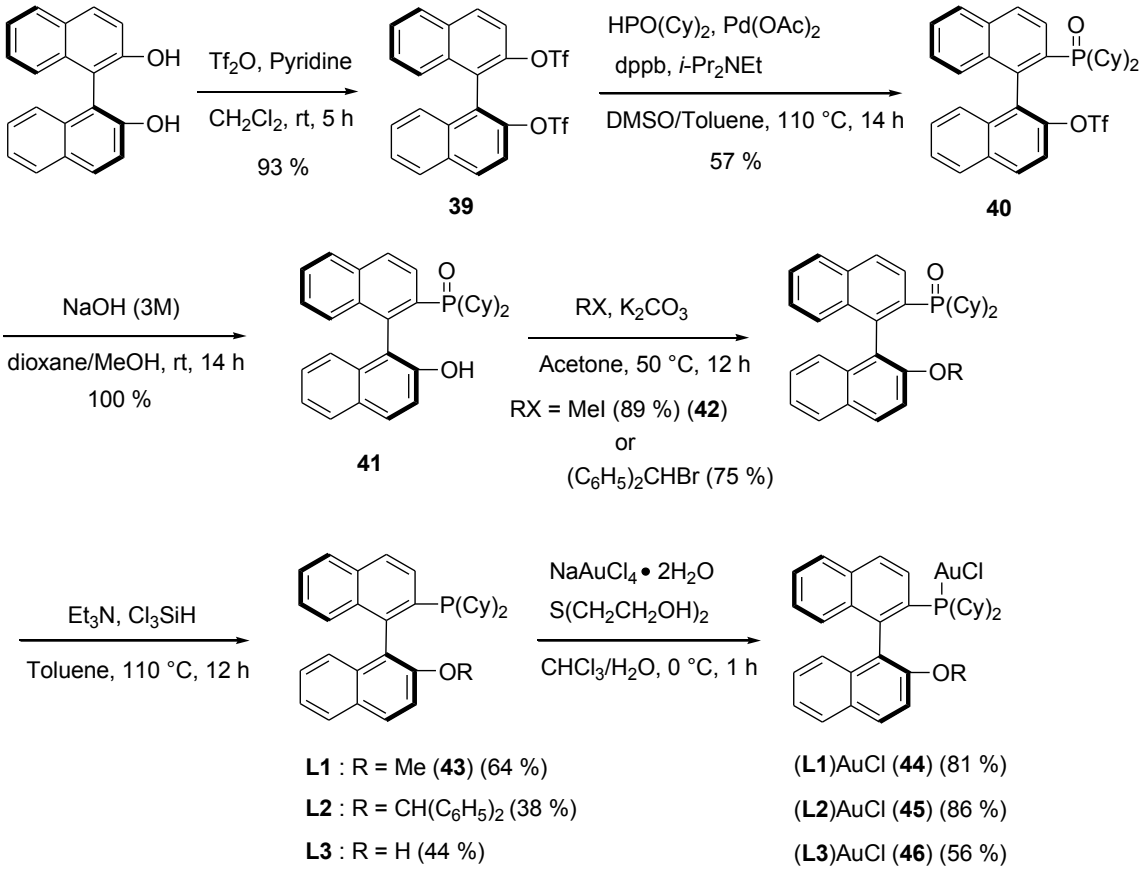

Scheme 5.

(*S*)-Dicyclohexyl(2'-methoxy-1,1'-binaphthyl-2-yloxy)phosphine-(AuCl)$_2$ [(*S*)-(L1)(AuCl)$_2$] (44). To a solution of (*S*)-(-)-1,1′-bi(2-naphthol) (2.5 g, 8.73 mmol) and pyridine (3.3 g, 41.90 mmol) in CH_2Cl_2 (36 mL) was added Tf_2O (5.9 g, 20.95 mmol) dropwise at 0 °C and the reaction mixture was stirred at rt for 3 h. The reaction mixture was diluted with Et_2O (200 mL), and washed sequentially with 5 % HCl (60 mL),

saturated $NaHCO_3$ (60 mL), and brine (60 mL). The organic phase was collected, dried over $MgSO_4$, and concentrated. The resulting mixture was chromatographed (hexanes–EtOAc = 10:1 → 1:6) to give (*S*)-1,1'-binaphthyl-2,2'-diyl bis(trifluoromethanesulfonate) (**39**) as a white solid (4.45 g, 93 %). TLC (hexanes–EtOAc = 4:1): R_f = 0.54. ^{1}H NMR: δ 8.15 (d, *J* = 9.1 Hz, 2 H), 8.01 (d, *J* = 8.2 Hz, 2 H), 7.63 (d, *J* = 9.1 Hz, 2 H), 7.58 (m, 2 H), 7.44 (m, 2 H), 7.26 (d, *J* = 8.4 Hz, 2 H).

39 (500 mg, 0.91 mmol), dicyclohexyl phosphine oxide (585 mg, 2.73 mmol), palladium(II) acetate (20 mg, 0.091 mmol), and 1,4-bis(diphenylphosphino)butane (39 mg, 0.091 mmol) in dimethyl sulfoxide (3.0 mL) and toluene (1.5 mL) was stirred for 10 min. To the reaction mixture was added *N*,*N*-diisopropylethylamine (705 mg, 5.46 mmol) lastly, and the reaction mixture was placed to an oil bath and stirred at 110 °C for 14 h. volatile material was evaporated under reduced pressure, and the resulting mixture was diluted with EtOAc (10 ml), washed with H_2O (5 mL) and brine (5 mL), dried ($MgSO_4$) and concentrated. The resulting mixture was chromatographed (hexanes–EtOAc = 2:1 → 1:1) to give (*S*)-2-(dicyclohexylphosphoryloxy)-1,1'-binaphthyl-2'-yl trifluoromethanesulfonate (**40**) as a white foam (0.32 g, 57 %). TLC (hexanes–EtOAc = 1:2): R_f = 0.28. ^{1}H NMR: δ 8.08-8.03 (m, 2 H), 7.96 (d, *J* = 8 Hz, 2 H), 7.60-7.54 (m, 3 H), 7.48 (t, *J* = 7.2 Hz, 1 H), 7.33 (t, *J* = 8.8 Hz, 1 H), 7.31-7.25 (m, 2 H), 7.15 (d, *J* = 8.4 Hz, 1 H), 2.14-2.06 (m, 1 H), 1.92-1.45 (m, 11 H), 1.29-1.0 (m, 10 H).

To a solution of **40** in 2:1 ratio of 1,4-dioxane and MeOH (4 mL) was added 3M of aqueous NaOH solution (1.9 mL), and the reaction mixture was stirred at room temperature for 14 h. The reaction mixture was acidified (pH = 1) with concentrated HCl,

and extracted with EtOAc. The organic phase was dried ($MgSO_4$) and concentrated under reduced pressure to produce 2'-hydroxy-1,1'-binaphthyl-2-yl dicyclohexylphosphinate (**41**) as a pale yellow solid. The crude product was used in the next step without further purification.

To **41** (259 mg, 0.52 mmol) and K_2CO_3 (290 mg, 2.10 mmol) in acetone (3 mL) was added MeI (298 mg, 2.10 mmol). The reaction mixture was stirred at 50 °C for 12 h. The reaction mixture was cooled to room temperature, and filtered through Celite, eluting with Et_2O. The organic phase and ether extracts were combined and concentrated in vacuo. The resulting oil was chromatographed (EtOAc only $\rightarrow$ EtOAc:MeOH=10:1) on a silica gel column to give 2'-methoxy-1,1'-binaphthyl-2-yl dicyclohexylphosphinate (**42**) as a white foam (230 mg, 89 %). TLC (EtOAc:MeOH = 10:1): R_f = 0.65. ^{1}H NMR: δ 8.09-7.99 (m, 2 H), 7.93 (d, J = 8.0 Hz, 1 H), 7.85 (d, J = 8.4 Hz, 1 H), 7.50 (t, J = 6.8 Hz, 1 H), 7.42 (d, J = 8.8 Hz, 1 H), 7.30-7.21 (m, 2 H), 7.16-7.11 (m, 2 H), 6.84 (d, J = 8.0 Hz, 1 H), 3.76 (s, 3 H), 1.66-1.21 (m, 16 H), 1.11-0.98 (m, 6 H).

To a mixture of **42** and Et_3N (1.57g, 15.47 mmol) in toluene (8 mL) was added Cl_3SiH (524 mg, 3.87 mmol) dropwise at 0 °C. The reaction mixture was stirred at 110 °C for 12 h. The reaction mixture was cooled to room temperature, diluted with Et_2O (8 mL), and quenched with saturated $NaHCO_3$ (0.8 mL). The resulting suspension was filtered through Celite eluting with Et_2O. The combined organic solution was dried over $MgSO_4$ and concentrated under reduced pressure. The resulting product was chromatographed (EtOAc:hex=1:10 $\rightarrow$ 1:4) on a silica gel column to give (*S*)-dicyclohexyl(2'-methoxy-1,1'-binaphthyl-2-yloxy)phosphine (**43**) as a white foam (142

mg, 64 %). TLC (hexanes–EtOAc = 4:1): R_f = 0.63. ^{1}H NMR: δ 7.90 (d, *J* = 9.6 Hz, 1 H), 7.81 (t, *J* = 8.8 Hz, 2 H), 7.74 (d, *J* = 8.4 Hz, 1 H), 7.69 (d, *J* = 8.8 Hz, 1 H), 7.36-7.29 (m, 2 H), 7.17 (t, *J* = 6.8 Hz, 1 H), 7.13-7.03 (m, 3 H), 6.83 (d, *J* = 8.8 Hz, 1 H), 3.64 (s, 3 H), 1.78-1.71 (m, 2 H), 1.60-1.39 (m, 11 H), 1.18-0.76 (m, 9 H).

To a solution of sodium tetrachloroaurate(III) dihydrate (116 mg, 0.291 mmol) in H_2O (2.0 mL) was added 2,2′-Thiodiethanol (107 mg, 0.873 mmol) dropwise slowly, and the reaction mixture was stirred until the solution turned from yellow to colorless at 0 °C. To this reaction mixture was added **43** (140 mg, 0.291 mmol) in CH_2Cl_2 (3 ml) dropwise, and the reaction mixture was stirred at 0 °C for 1 h. The aqueous layer was extracted with CH_2Cl_2 and the combined organic extracts were evaporated. The crude product was washed with MeOH and dried under a high vacuum to give [(*S*)-(**L1**)$(AuCl)_2$] (**44**) as a white power (168 mg, 81 %). ^{1}H NMR: δ 8.23 (d, *J* = 9.0 Hz, 1 H), 8.02 (d, *J* = 8.5 Hz, 1 H), 7.94 (t, *J* = 9.0 Hz, 2 H), 7.68 (dd, *J* = 6.5, 8.5 Hz, 1 H), 7.54 (t, *J* = 7.5 Hz, 1 H), 7.44 (d, *J* = 9.5 Hz, 1 H), 7.32 (dt, *J* = 1.0, 6.5 Hz, 1 H), 7.23-7.24 (m, 1 H), 7.17 (dt, *J* = 1.5, 7.0 Hz, 1 H), 7.08 (d, *J* = 8.0 Hz, 1 H), 6.72 (d, *J* = 8.5 Hz, 1 H), 3.78 (s, 3 H), 2.25-2.19 (m, 2 H), 2.02-2.0 (m, 1 H), 1.82-1.59 (m, 9 H), 1.50-1.08 (m, 10 H). ^{13}C{^{1}H} NMR (carbon–phosphorous couplings are not taken into consideration due to the complexity): δ 162.7, 154.7, 144.4, 144.3, 134.3, 134.27, 134.2, 133.9, 133.8, 133.2, 129.2, 128.8, 128.0, 127.9, 127.8, 127.4, 127.2, 127.1, 126.4, 125.1, 124.7, 124.6, 123.6, 119.9, 119.8, 112.7, 55.5, 55.47, 37.5, 37.3, 36.3, 36.0, 31.1, 31.06, 30.7, 30.6, 29.7, 29.6, 26.9, 26.8, 26.73, 26.70, 26.62, 26.60, 26.4, 26.3, 25.7, 25.5. ^{31}P NMR: δ 39.6. Anal. calcd (found) for $C_{33}H_{37}AuClOP$: C, 55.59 (55.50); H, 5.23 (5.23).

(2-(Benzhydryloxy)-1,4'-binaphthyl-3'-yl)dicyclohexylphosphine-$(AuCl)_2$ [(*S*)-(**L2**)$(AuCl)_2$] (**45**) and (*S*)-3'-(dicyclohexylphosphino)-1,4'-binaphthyl-2-ol-$(AuCl)_2$ [(*S*)-(**L3**)$(AuCl)_2$] (**46**) were synthesized employing a procedure similar to that used to synthesize [(*S*)-(**L1**)$(AuCl)_2$] (**44**).

(*S*)-(2-(Benzhydryloxy)-1,4'-binaphthyl-3'-yl)dicyclohexylphosphine-$(AuCl)_2$ [(*S*)-(L2)$(AuCl)_2$] (45). White power, 13 %. ^{1}H NMR: δ 8.07 (d, *J* = 9.0 Hz, 1 H), 8.03 (d, *J* = 9.0 Hz, 1 H), 8.01 (d, *J* = 8.5 Hz, 1 H), 7.88 (d, *J* = 8.0 Hz, 1 H), 7.66-7.61 (m, 2 H), 7.36-7.28 (m, 2 H), 7.20-7.16 (m, 3 H), 7.08-7.06 (m, 6 H), 7.03-7.0 (m, 2 H), 6.96-6.95 (m, 2 H), 6.84 (d, *J* = 8 Hz, 1 H), 2.15-2.08 (m, 2 H), 1.89-0.75 (m, 20 H). ^{13}C{^{1}H} NMR (carbon–phosphorous couplings are not taken into consideration due to the complexity): δ 162.7, 153.0, 149.8, 146.1, 144.4, 141.7,141.6, 130.7, 129.2, 128.8, 128.4, 128.2, 128.15, 127.8, 127.75, 127.4, 127.34, 127.30, 127.2, 126.8, 126.3, 126.2, 126.1, 125.4, 124.9, 124.8, 123.8, 144.4, 121.0, 121.96, 141.7, 141.6, 115.8, 134.3, 134.25, 133.8, 133.7, 81.6, 81.5, 36.7, 36.5, 36.4, 36.3, 30.6, 30.5, 30.1, 29.8, 26.8, 26.7, 26.6, 26.4, 26.3, 26.26, 25.6, 25.4. ^{31}P NMR: δ 39.5. Anal. calcd (found) for $C_{45}H_{45}AuClOP$: C, 62.47 (62.49); H, 5.24 (5.22).

(*S*)-3'-(Dicyclohexylphosphino)-1,4'-binaphthyl-2-ol-$(AuCl)_2$ [(*S*)-(L3)$(AuCl)_2$] (46). White powder, 13 %. ^{1}H NMR: δ 8.12 (d, *J* = 8.8 Hz, 1 H), 8.09 (d, *J* = 8.8 Hz, 1 H), 7.95 (t, *J* = 8.8 Hz, 2 H), 7.73 (dd, *J* = 6.8, 8.8 Hz, 1 H), 7.59 (t, *J* = 7.2 Hz, 1 H), 7.36-7.31 (m, 2 H), 7.28 (d, *J* = 9.2 Hz, 1 H), 7.21-7.18 (m, 2 H), 6.75 (d, *J* =

8.4 Hz, 1 H), 4.72 (br s, 1 H), 2.28-2.19 (m, 2 H), 2.08-2.03 (m, 1 H), 1.81-1.62 (m, 9 H), 1.48-1.07 (m, 10 H). $^{13}C\{^{1}H\}$ NMR (carbon–phosphorous couplings are not taken into consideration due to the complexity): δ 162.7, 151.4, 142.3, 142.2, 134.8, 134.4, 134.0, 133.96, 131.7, 129.8, 129.2, 128.8, 128.3, 128.1, 127.7, 127.69, 127.4, 126.9, 126.8, 126.5, 124.8, 124.77, 124.0, 118.1, 117.6, 117.5, 37.4, 37.1, 37.06, 36.8, 31.4, 31.1, 30.0, 29.8, 26.9, 26.6, 25.9, 25.7. ^{31}P NMR: δ 39.9. Anal. calcd (found) for $C_{32}H_{35}AuClOP$: C, 54.98 (54.79); H, 5.05 (4.95).

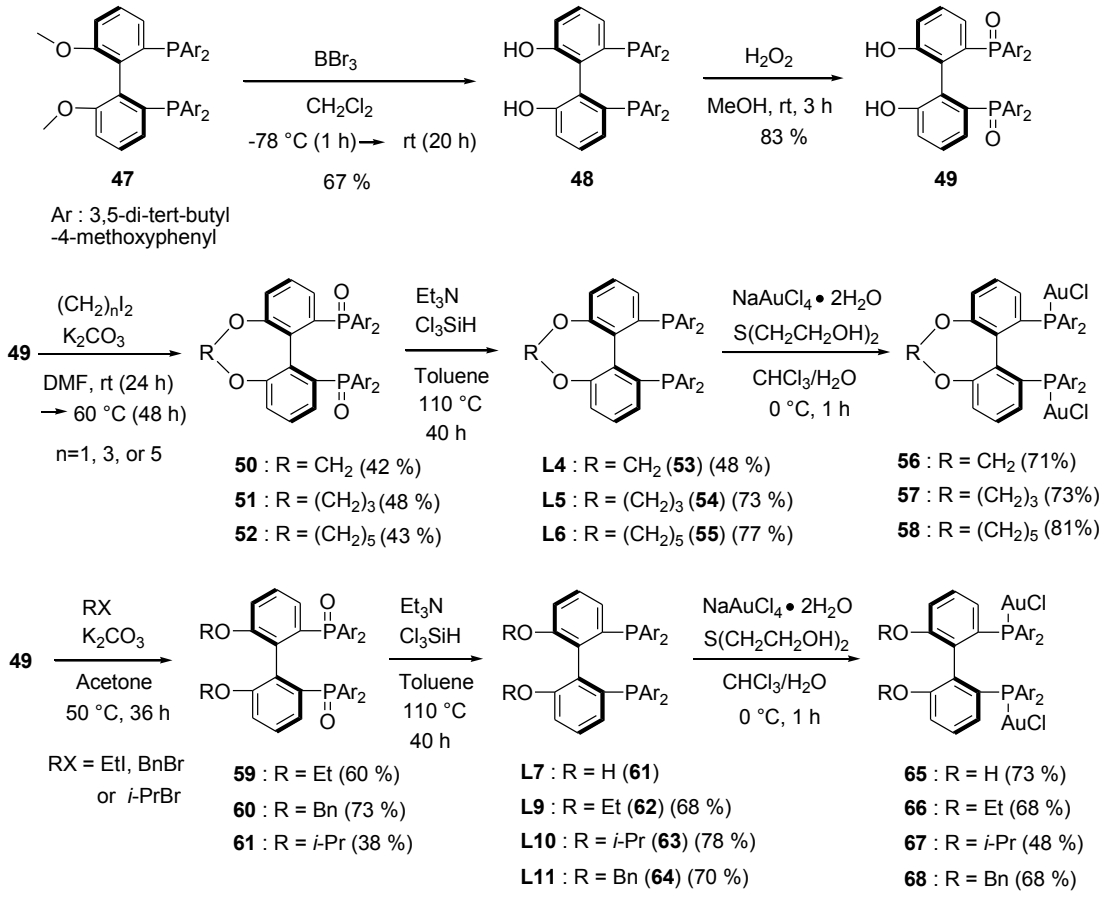

Scheme 6.

(*S*)-{15-[bis(3,5-di-tert-butyl-4-methoxyphenyl)phosphanyl]-8,10-dioxatricyclo[9.4.0.0^{2,7}]pentadeca-1(11),2,4,6,12,14-hexaen-3-yl}bis(3,5-di-tert-butyl-4-methoxyphenyl)phosphane [(*S*)-(L4)(AuCl)$_2$] (56). A solution of (*S*)-(+)-2,2'-bis[di(3,5-di-t-butyl-4-methoxyphenyl)phosphino]-6,6'-dimethoxy-1,1'-biphenyl (**47**) (500 mg, 0.434 mmol) in CH_2Cl_2 (5 mL) was cooled to – 78 °C and sparged with N_2 for 15 min. BBr_3 (1.3 mL: 1 M in CH_2Cl_2, 1.30 mmol) was added dropwise slowly via a syringe to the solution. The reaction mixture was stirred at – 78 °C for 1 h and then at room temperature for 20 h. Resulting mixture was cooled to 0 °C, and degassed H_2O (3 mL) was added slowly. After removing the aqueous layer, the organic layer was washed sequentially with degassed H_2O and brine, and dried ($MgSO_4$). The organic extract was filtered through a pad of neutral Al_2O_3, and chromatographed (hexanes–EtOAc = 20:1 → 10:1) on a silica gel column to give the product (*S*)-6,6'-bis(bis(3,5-di-tert-butyl-4-methoxyphenyl)phosphino)biphenyl-2,2'-diol (**48**) as a light yellow foam (330 mg, 67 %). TLC (hexanes–EtOAc = 6:1): R_f = 0.45. ^{1}H NMR: δ 7.36-7.35 (m, 4 H), 7.30-7.27 (m, 2 H), 7.15-7.13 (m, 4 H), 6.85 (d, J = 7.0 Hz, 2 H), 6.74 (d, J = 8.0 Hz, 2 H), 3.91 (bs, 2 H), 3.74 (s, 6 H), 3.69 (s, 6 H), 1.39 (s, 36 H), 1.35 (s, 36 H). ^{31}P NMR: δ –14.8.

To a solution of **48** (100 mg, 0.089 mmol) in MeOH (3 mL) cooled to 0 °C was added H_2O_2 (40 μL, 30 wt. % in H_2O) dropwise. The reaction mixture was stirred at room temperature for 3 h. After the reaction time, the reaction mixture was poured into water (10 mL) to generate a precipitate, and the white precipitate was filtered, washed with water, and dried under a high vacuum to give 6,6'-bis(bis(3,5-di-tert-butyl-4-

methoxyphenyl)phosphoryl)biphenyl-2,2'-diol (**49**) as a white powder (85 mg, 83 %). TLC (hexanes–EtOAc = 1 :2): R_f = 0.30. ^{31}P NMR: δ 27.9.

To **49** (66 mg, 0.057 mmol) and K_2CO_3 (39 mg, 0.28 mmol) in DMF (2 ml) was added CH_2I_2 (8 mg, 0.03 mmol; adding 0.1 ml of 0.3 M CH_2I_2 stock solution in DMF) dropwise. The reaction mixture was stirred at rt for 1 h, and additional CH_2I_2 (8 mg, 0.03 mmol; adding 0.1 ml of 0.3 M CH_2I_2 stock solution in DMF) was added to the reaction mixture. The reaction mixture was stirred at room temperature for 24h and at 60 °C for 48 h. After cooling to room temperature, the reaction mixture was diluted with Et_2O (5 mL). Water (3 mL) was added to the mixture and extracted with Et_2O (5 mL × 3). The combined organic extracts were dried ($MgSO_4$) and evaporated under a vacuum. Chromatography of the resulting mixture gave **50** as a white foam (28 mg, 42 %). TLC (hexanes–EtOAc = 1:2): R_f = 0.46. ^{1}H NMR: δ 7.76 (d, J = 12 Hz, 4 H), 7.19-7.15 (m, 4 H), 7.01-6.95 (m, 6 H), 5.30 (s, 2 H), 3.68 (s, 6 H), 3.57 (s, 6 H), 1.31 (s, 36 H), 1.21 (s, 36 H). ^{31}P NMR: δ 28.0.

To a mixture of **50** (28 mg, 0.024 mmol) and Et_3N (194 mg, 1.92 mmol) in toluene (1.5 mL) was added Cl_3SiH (65 mg, 0.48 mmol) at 0 °C. The reaction mixture was stirred at 110 °C for 40 h. The reaction mixture was cooled to room temperature, diluted with Et_2O (4 mL), and quenched with a small amount of saturated $NaHCO_3$ (0.2 mL). The resulting suspension was filtered through a pad of Celite and washed with Et_2O. The combined organic solution was concentrated and chromatographed (hexanes–EtOAc = 10:1) give **53** (13 mg, 48 %) as a white solid. TLC (hexanes–EtOAc = 6:1): R_f = 0.59. ^{1}H NMR: δ 7.57 (s, 4 H), 7.20 (t, J = 7.6 Hz), 7.0 (d, J = 7.6 Hz, 2 H), 6.95 (d, J = 7.6 Hz, 2

H), 6.73 (s, 4 H), 5.31 (s, 2 H), 3.70 (s, 6 H), 3.58 (s, 6 H), 1.33 (s, 36 H), 1.23 (s, 36 H). ^{31}P NMR: δ -15.0.

To a solution of sodium tetrachloroaurate(III) dihydrate (9 mg, 0.023 mmol) in H_2O (0.25 mL) was added 2,2′-thiodiethanol (8 mg, 0.068 mmol) dropwise slowly, and the reaction mixture was stirred 0 °C until the solution turned from yellow to colorless. To this reaction mixture was added a solution of **53** (13 mg, 0.011 mmol) in CH_2Cl_2 (0.5 mL) dropwise, and the reaction mixture was stirred at 0 °C for 1 h. The aqueous layer was extracted with CH_2Cl_2 and the combined organic extracts were evaporated. The crude product was washed with MeOH and dried to give (*S*)-C(1)-(3,5-di-tert-butyl-4-methoxyphenyl)tunephos-$(AuCl)_2$ [(*S*)-(**L4**)$(AuCl)_2$] as a white power (13 mg, 71 %). ^{1}H NMR: δ 7.77 (br s, 4 H), 7.30-7.21 (m, 4 H), 6.95 (br d, *J* = 11.5 Hz, 4 H), 6.71 (d, *J* = 7.5 Hz, 2 H), 5.01 (s, 2 H), 3.76 (s, 6 H), 3.61 (s, 6 H), 1.41 (s, 36 H), 1.20 (s, 36 H). ^{13}C{^{1}H} NMR (carbon–phosphorous couplings are not taken into consideration due to the complexity): δ 162.7, 153.0, 144.5, 144.44, 144,39, 143.6, 143.5,143.4, 134.8, 134.0, 133.5, 131.6, 129.9, 121.8, 100.4, 64.6, 64.4, 36.2, 35.7, 31.9, 31.5. ^{31}P NMR: δ 34.23. Anal. calcd (found) for $C_{73}H_{100}Au_2Cl_2O_6P_2$: C, 54.79 (54.69); H, 6.30 (6.34).

(*S*)-{17-[Bis(3,5-di-tert-butyl-4-methoxyphenyl)phosphanyl]-8,12-dioxatricyclo[11.4.0.0^{2,7}]heptadeca- 1(13),2,4,6,14,16-hexaen-3-yl}bis(3,5-di-tert- butyl-4-methoxyphenyl)phosphane [(*S*)-(**L5**)$(AuCl)_2$] (**57**) and (*S*)-{19-[bis(3,5-di-tert-butyl-4-methoxyphenyl)phosphanyl]-8,14- dioxatricyclo[13.4.0.0^{2,7}]nonadeca- 1(15),2,4,6,16,18-hexaen-3-yl}bis(3,5-di-tert- butyl-4-methoxyphenyl)phosphane [(*S*)-(**L6**)$(AuCl)_2$] (**58**)

were synthesized employing a procedure similar to that used to synthesize [(*S*)-(**L4**)$(AuCl)_2$] (**56**).

(*S*)-{17-[Bis(3,5-di-tert-butyl-4-methoxyphenyl)phosphanyl]-8,12-dioxatricyclo[11.4.0.0^{2,7}]heptadeca-1(13),2,4,6,14,16-hexaen-3-yl}bis(3,5-di-tert-butyl-4-methoxyphenyl)phosphane [(*S*)-(L5)$(AuCl)_2$] (57). white power, 26 %. ^{1}H NMR: δ 7.69 (d, *J* = 12.5 Hz, 4 H), 7.34 (t, *J* = 8.5 Hz, 2 H), 7.19-7.15 (m, 6 H), 6.70 (d, *J* = 8.0 Hz, 2 H), 3.83-3.78 (m, 2 H), 3.754 (s, 3 H), 3.752 (s, 3 H), 3.70-3.66 (m, 2 H), 3.634 (s, 3 H), 3.632 (s, 3 H), 1.48-1.45 (m, 2 H), 1.41 (s, 36 H), 1.26 (s, 36 H). ^{13}C{^{1}H} NMR (carbon–phosphorous couplings are not taken into consideration due to the complexity): δ 161.7, 161.5, 157.6, 157.5, 157.47, 143.1, 143.05, 143.0, 142.2, 142.17, 142.12, 133.3, 133.3, 133.2, 132.2, 131.7, 131.2, 129.9, 129.0, 128.3, 127.6, 122.3, 121.7, 120.7, 120.2, 71.2, 63.5, 63.4, 35.1, 34.7, 30.9, 30.7, 28.7. ^{31}P NMR: δ 30.33.

(*S*)-{19-[Bis(3,5-di-tert-butyl-4-methoxyphenyl)phosphanyl]-8,14-dioxatricyclo[13.4.0.0^{2,7}]nonadeca-1(15),2,4,6,16,18-hexaen-3-yl}bis(3,5-di-tert-butyl-4-methoxyphenyl)phosphane [(*S*)-(L6)$(AuCl)_2$] (58). white power, 15 %. ^{1}H NMR: δ 7.52-7.47 (m, 6 H), 7.23 (d, J = 13.6, 4 H), 7.03 (dd, J = 8.0, 10.4 Hz, 2 H), 6.81 (d, J = 8 Hz, 2 H), 3.81-3.76 (m, 2 H), 3.75 (s, 3 H), 3.74 (s, 3 H), 3.652 (s, 3 H), 3.648 (s, 3 H), 3.33-3.27 (m, 2 H), 1.39 (s, 36 H), 1.29 (s, 36 H), 1.27-1.24 (m, 4 H), 0.90-0.82 (m, 2 H). ^{13}C{^{1}H} NMR (carbon–phosphorous couplings are not taken into consideration due to the complexity): δ 161.7, 162.5, 162.2, 158.2, 149.1, 143.8, 143.4, 143.3, 134.4, 134.2, 134.1, 133.9, 129.2, 129.1, 127.7, 122.2, 121.8, 117.1, 67.9, 64.6,

64.5, 36.0, 35.8, 31.92, 31.87, 25.7, 21.6. ^{31}P NMR: δ 26.1. Anal. calcd (found) for $C_{77}H_{108}Au_2Cl_2O_6P_2$: C, 55.83 (55.79); H, 6.57 (6.47).

(*S*)-(6,6'-Diethoxybiphenyl-2,2'-diyl)bis(bis(3,5-di-tert-butyl-4-methoxyphenyl)phosphine)-$(AuCl)_2$ [(*S*)-(L9)$(AuCl)_2$] (66). To a suspension **49** (85 mg, 0.0735 mmol) and K_2CO_3 (122 mg, 0.883 mmol) in acetone (3 ml) was added EtI (137.7 mg, 0.883 mmol). The reaction mixture was stirred at 50 °C for 36 h. After cooling to room temperature, the reaction mixture was filtered through a pad of Celite, eluting with Et_2O. The combined organic extracts were evaporated and chromatographed (hexanes–EtOAc = 8:1→ 5:1) to give (6,6'-diethoxybiphenyl-2,2'-diyl)bis(bis(3,5-di-tert-butyl-4-methoxyphenyl)phosphine oxide) (**59**) (53 mg, 60 %) as a colorless oil. TLC (hexanes–EtOAc = 1:2): R_f = 0.49. %. ^{1}H NMR: δ 7.61-7.48 (m, 8 H), 7.24-7.19 (m, 2 H), 6.89-6.82 (m, 4 H), 3.81-3.66 (m, 2 H), 3.65 (s, 6 H), 3.64 (s, 6 H), 3.50-3.39 (m, 2 H), 1.33 (s, 36 H), 1.24 (s, 36 H), 0.65 (t, J = 6.8 Hz, 6 H). ^{31}P NMR: δ 28.3.

To a mixture of **59** and Et_3N (354.2 mg, 3.50 mmol) in toluene (2 mL) was added Cl_3SiH (118.4 mg, 0.874 mmol) at 0 °C. The reaction mixture was stirred at 110 °C for 40 h. The reaction mixture was cooled to room temperature, diluted with Et_2O (4 mL), and quenched with a small amount of saturated $NaHCO_3$ (0.2 mL). The resulting suspension was filtered through a pad of Celite and extracted with Et_2O. The combined organic extracts were concentrated and chromatographed (hexanes–EtOAc = 15:1) to give (6,6'-diethoxybiphenyl-2,2'-diyl)bis(bis(3,5-di-tert-butyl-4-methoxyphenyl)phosphine) (**62**) (35.3 mg, 68 %) as a white solid. TLC (hexanes–EtOAc = 7:1): R_f = 0.4. ^{1}H NMR: δ 7.26-7.10 (m, 10 H), 6.88 (d, J = 7.6 Hz, 2 H), 6.70 (d, J =

8.0 Hz, 2 H), 3.65-4.63 (m, 2 H), 3.63 (s, 6 H), 3.61 (s, 6 H), 3.40-3.33 (m, 2 H), 1.32 (s, 36 H), 1.23 (s, 36 H), 0.66 (t, J = 6.8 Hz, 6 H). ^{31}P NMR: δ – 13.8.

(*S*)-(6,6'-Diethoxybiphenyl-2,2'-diyl)bis(bis(3,5-di-tert-butyl-4-methoxyphenyl)phosphine)-$(AuCl)_2$ [(*S*)-(**L9**)$(AuCl)_2$] (**66**) was synthesized from **62** employing a procedure similar to that used to synthesize **56** from **53.** White power (33.2 mg, 68 %). ^{1}H NMR: δ 7.61 (dt, J = 2.4, 8.0 Hz, 2 H), 7.48 (d, J = 13.6 Hz, 4 H), 7.01-7.03 (m, 6 H), 6.93 (d, J = 8.0 Hz, 2 H), 3.70 (s, 12 H), 3.60-3.51 (m, 2 H), 3.14-3.06 (m, 2 H), 1.33 (s, 36 H), 1.32 (s, 36 H), 0.44 (t, J = 6.8 Hz, 6 H). ^{13}C{^{1}H} NMR (carbon–phosphorous couplings are not taken into consideration due to the complexity): δ 162.4, 162.3, 162.0, 161.99, 158.3, 158.2, 144.3, 144.2, 144.1, 144.0, 133.5, 133.3, 132.4, 132.2, 129.6, 129.4, 129.0, 127.8, 127.7, 124.8, 124.1, 124.0, 123.4, 114.3, 64.4, 62.9, 36.0, 35.9, 31.9, 31.8. ^{31}P NMR: δ 21.64. Anal. calcd (found) for $C_{76}H_{108}Au_2Cl_2O_6P_2$: C, 55.51 (55.54); H, 6.62 (6.69).

(*S*)-6,6'-Bis(bis(3,5-di-tert-butyl-4-methoxyphenyl)phosphino)biphenyl-2,2'-diol-$(AuCl)_2$ [(*S*)-(**L7**)$(AuCl)_2$] (**65**), **(***S*)-(6,6'-diisopropoxybiphenyl-2,2'-diyl)bis(bis(3,5-di-tert-butyl-4-methoxyphenyl)phosphine)-$(AuCl)_2$ [(*S*)-(**L10**)$(AuCl)_2$] (**67**), and (*S*)-(6,6'-bis(benzyloxy)biphenyl-2,2'-diyl)bis(bis(3,5-di-tert-butyl-4-methoxyphenyl)phosphine)-$(AuCl_2)$ [(*S*)-(**L11**)$(AuCl)_2$] (**68**) were synthesized employing a procedure similar to that used to synthesize [(*S*)-(**L9**)$(AuCl)_2$].

(*S*)-6,6'-Bis(bis(3,5-di-tert-butyl-4-methoxyphenyl)phosphino)biphenyl-2,2'-diol-$(AuCl)_2$ [(*S*)-(L7)$(AuCl)_2$] (65). Light yellow powder, 49 %. ^{1}H NMR: δ 7.66 (d, *J* = 13.2 Hz, 4 H), 7.44 (dt, *J* = 1.6, 7.6 Hz, 2 H), 7.14 (dd, *J* = 8.0, 11.2 Hz, 2 H), 6.74 (d, *J* = 8 Hz, 2 H), 3.76 (s, 6 H), 3.66 (s, 6 H), 1.40 (s, 36 H), 1.28 (s, 36 H). ^{13}C{^{1}H} NMR (carbon–phosphorous couplings are not taken into consideration due to the complexity): δ 163.1, 163.0, 155.8, 155.7, 155.5, 145.0, 144.93, 144.89, 144.4, 144.3, 144.26, 134.8,134.64, 134.56, 134.2, 133.6, 133.4, 131.1, 130.9, 128.1, 123.9, 123.3, 121.9, 120.1, 119.6, 64.6, 64.5, 36.1, 35.9, 31.8, 31.7. ^{31}P NMR: δ 28.32. Anal. calcd (found) for $C_{72}H_{100}Au_2Cl_2O_6P_2$: C, 54.44 (54.36); H, 6.35 (6.25).

(*S*)-(6,6'-Diisopropoxybiphenyl-2,2'-diyl)bis(bis(3,5-di-tert-butyl-4-methoxyphenyl)phosphine)-$(AuCl)_2$ [(*S*)-(L10)$(AuCl)_2$] (67). White powder, 8 %. ^{1}H NMR: δ 7.62 (dt, *J* = 2.5, 8.0 Hz, 2 H), 7.50 (d, *J* = 13.0 Hz, 4 H), 7.06 (dd, *J* = 7.5, 10 Hz, 2 H), 7.0 (d, *J* = 13.5 Hz, 4 H), 6.97 (d, *J* = 8.5 Hz, 2 H), 4.11 (m, 2 H), 3.72 (s, 6 H), 3.69 (s, 6 H), 1.34 (s, 36 H), 1.32 (s, 36 H), 0.74 (d, *J* = 6 Hz, 6 H), 0.34 (d, *J* = 6.5 Hz, 6 H). ^{13}C{^{1}H} NMR (carbon–phosphorous couplings are not taken into consideration due to the complexity): δ 162.5, 157.8, 157.7, 144.7, 144.6, 144.4, 144.3, 133.9, 133.7, 132.3, 132.2, 129.5, 129.4, 128.3, 125.5, 125.0, 124.3, 116.2, 70.2, 64.7, 36.3, 36.2, 32.2, 32.1, 22.1, 21.1. ^{31}P NMR: δ 20.92.

(*S*)-(6,6'-Bis(benzyloxy)biphenyl-2,2'-diyl)bis(bis(3,5-di-tert-butyl-4-methoxyphenyl)phosphine)-$(AuCl_2)$ [(*S*)-(L11)$(AuCl)_2$] (68). White powder, 19 %. ^{1}H NMR: δ 7.49 (dt, *J* = 2.0, 8.0 Hz, 2 H), 7.39 (d, *J* = 13.6 Hz, 4 H), 7.19 (d, *J* = 14 Hz, 4

H), 7.14-7.05 (m, 6 H), 7.0 (dd, J = 7.6, 10.8 Hz, 2 H), 6.89 (d, J = 7.2 Hz, 4 H), 6.78 (d, J = 8.4 Hz, 2 H), 4.34 (d, J = 15.2 Hz, 2 H), 3.73 (s, 6 H), 3.66 (d, J = 15.2 Hz, 2 H), 3.62 (s, 6 H), 1.34 (s, 36 H), 1.27 (s, 36 H). $^{13}C\{^{1}H\}$ NMR (carbon–phosphorous couplings are not taken into consideration due to the complexity): δ 162.4, 162.2, 161.3, 144.4, 144.3, 144.2, 144.1, 137.0, 133.8, 133.4, 133.3, 128.4, 127.1, 124.8, 115.22, 115.19, 68.0, 64.5, 36.0, 35.9, 31.8. ^{31}P NMR: δ 22.36 .

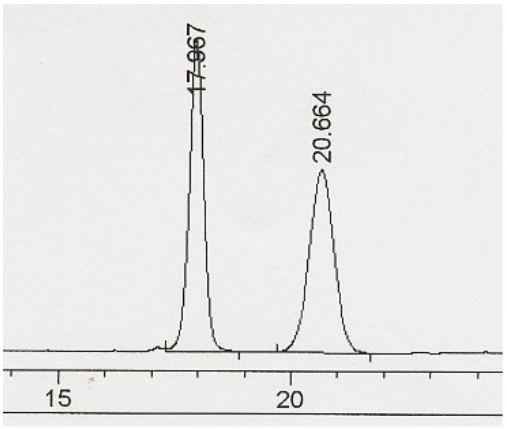

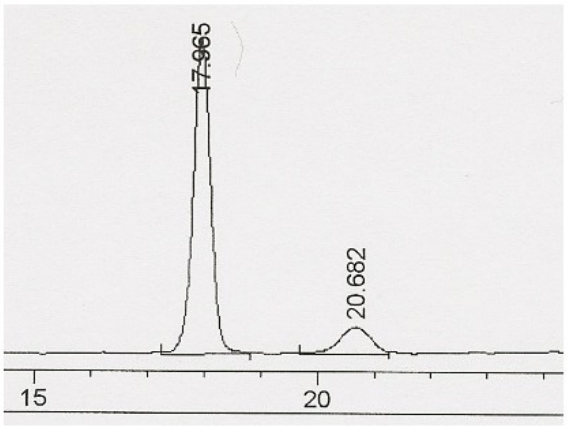

Signal 1: DAD1 A, Sig=210,4 Ref=450,80

Peak #	RetTime [min]	Type	Width [min]	Area [mAU*s]	Height [mAU]	Area %
1	17.967	VB	0.3126	1.63663e4	748.90820	49.8365
2	20.664	BP	0.4643	1.64736e4	438.11816	50.1635
Totals :				3.28399e4	1187.02637	

Signal 1: DAD1 A, Sig=210,4 Ref=450,80

Peak #	RetTime [min]	Type	Width [min]	Area [mAU*s]	Height [mAU]	Area %
1	17.965	VV	0.3197	1.29668e4	591.72272	86.0589
2	20.682	VV	0.4989	2100.55811	51.77586	13.9411
Totals :				1.50674e4	643.49857	

Figure 3. Chiral HPLC traces (85:15 hexanes/isopropanol, 0.5 mL/min) of racemic (left trace) and enantiomerically enriched (right trace, 72% ee) benzyl 2-methyl-4,4-diphenylpyrrolidine-1-carboxylate (**6**).

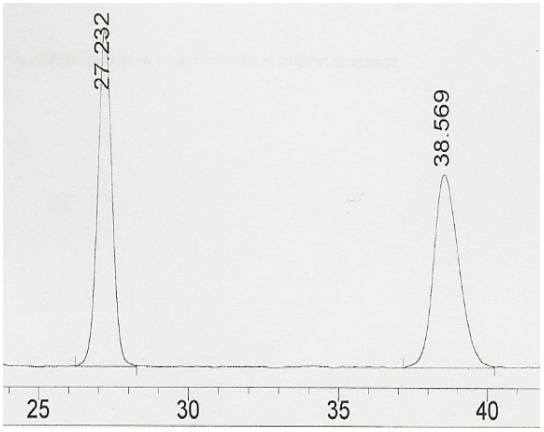

Signal 1: DAD1 A, Sig=210,4 Ref=450,80

Peak #	RetTime [min]	Type	Width [min]	Area [mAU*s]	Height [mAU]	Area %
1	27.232	BB	0.4397	2.51428e4	755.10138	49.7303
2	38.569	VB	0.7308	2.54155e4	430.22510	50.2697
Totals :				5.05582e4	1185.32648	

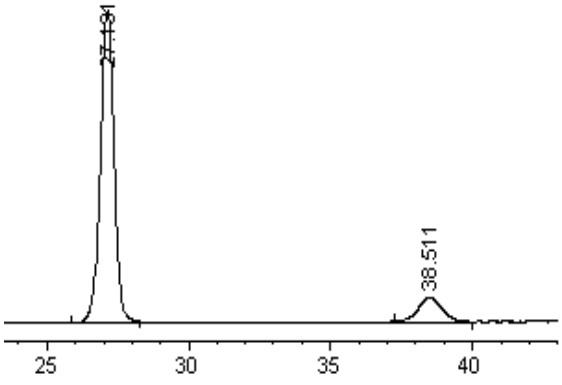

Signal 1: DAD1 A, Sig=210,4 Ref=450,80

Peak #	RetTime [min]	Type	Width [min]	Area [mAU*s]	Height [mAU]	Area %
1	27.131	PB	0.4127	6.01304e4	1768.57849	88.8762
2	38.511	VP	0.6708	7525.94141	134.73991	11.1238
Totals :				6.76564e4	1903.31841	

Figure 4. Chiral HPLC traces (90:10 hexanes/isopropanol, 0.5 mL/min) of racemic (left trace) and enantiomerically enriched (right trace, 78% ee) (9H-fluoren-9-yl)methyl 2-methyl-4,4-diphenylpyrrolidine-1-carboxylate (**2b**).

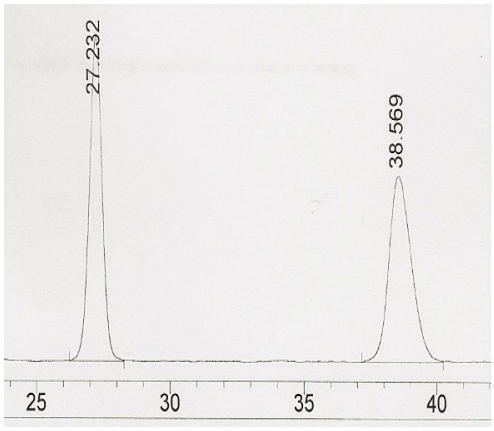

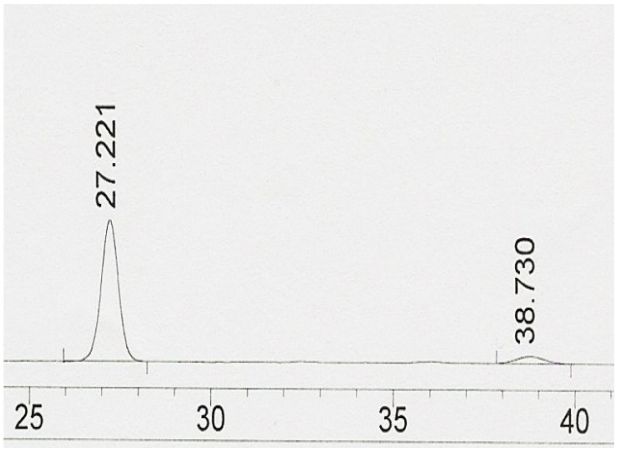

Signal 1: DAD1 A, Sig=210,4 Ref=450,80

Peak #	RetTime [min]	Type	Width [min]	Area [mAU*s]	Height [mAU]	Area %
1	27.232	BB	0.4397	2.51428e4	755.10138	49.7303
2	38.569	VB	0.7308	2.54155e4	430.22510	50.2697
Totals :				5.05582e4	1185.32648	

Signal 2: DAD1 B, Sig=220,4 Ref=450,80

Peak #	RetTime [min]	Type	Width [min]	Area [mAU*s]	Height [mAU]	Area %
1	27.221	VP	0.4625	1.70893e4	512.68567	91.8822
2	38.730	BP	0.6465	1509.83948	27.65575	8.1178
Totals :				1.85991e4	540.34142	

Figure 5. Chiral HPLC traces (90:10 hexanes/isopropanol, 0.5 mL/min) of racemic (left trace) and enantiomerically enriched (right trace, 84% ee) (9H-fluoren-9-yl)methyl 2-methyl-4,4-diphenylpyrrolidine-1-carboxylate (**2c**).

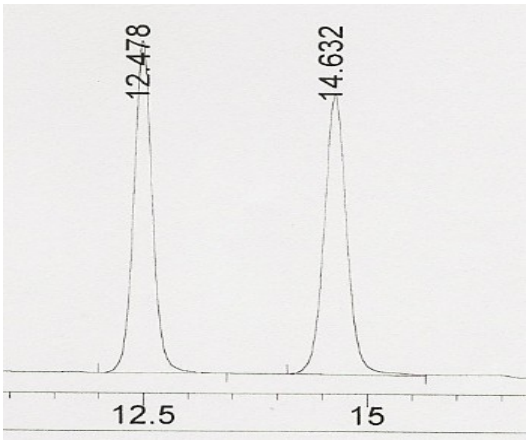

Signal 2: DAD1 B, Sig=220,4 Ref=450,80

Peak #	RetTime [min]	Type	Width [min]	Area [mAU*s]	Height [mAU]	Area %
1	12.478	VB	0.2026	2.80482e4	1954.78284	49.1949
2	14.632	BB	0.2697	2.89663e4	1642.50500	50.8051
Totals :				5.70146e4	3597.28784	

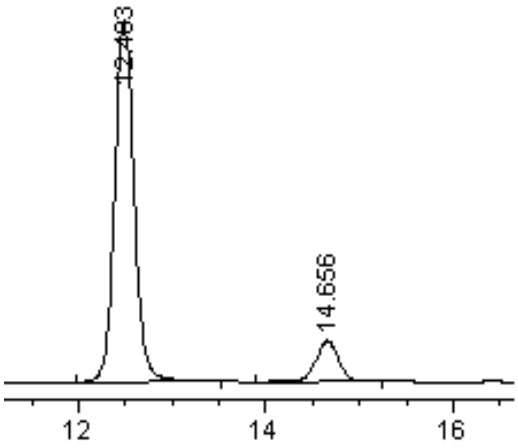

Signal 2: DAD1 B, Sig=220,4 Ref=450,80

Peak #	RetTime [min]	Type	Width [min]	Area [mAU*s]	Height [mAU]	Area %
1	12.483	PB	0.2162	1.59485e4	1127.79980	88.0499
2	14.656	PB	0.2615	2164.52563	127.84248	11.9501
Totals :				1.81131e4	1255.64228	

Figure 6. Chiral HPLC traces (90:10 hexanes/isopropanol, 0.5 mL/min) of racemic (left trace) and enantiomerically enriched (right trace, 76% ee) 2-methyl-*N*,4,4-triphenylpyrrolidine-1-carboxamide (**8**).

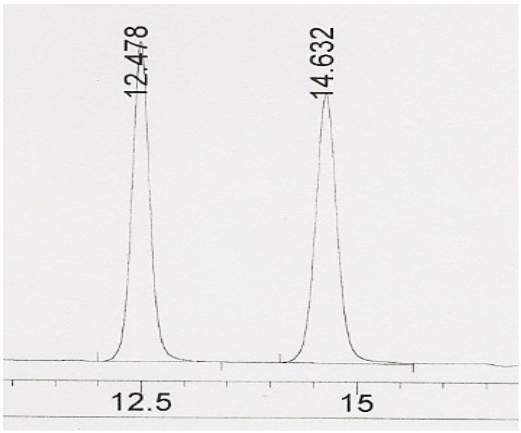

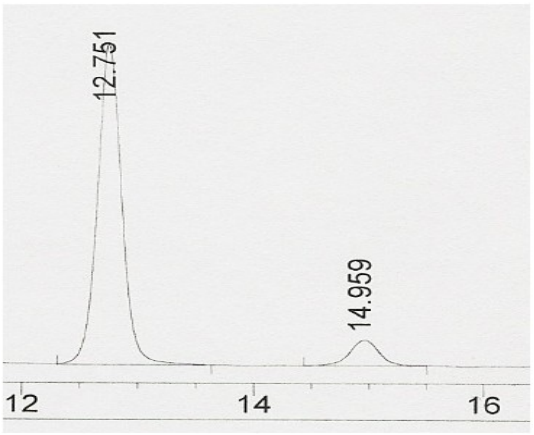

Signal 2: DAD1 B, Sig=220,4 Ref=450,80

Peak #	RetTime [min]	Type	Width [min]	Area [mAU*s]	Height [mAU]	Area %
1	12.478	VB	0.2026	2.80482e4	1954.78284	49.1949
2	14.632	BB	0.2697	2.89663e4	1642.50500	50.8051
Totals :				5.70146e4	3597.28784	

Signal 2: DAD1 B, Sig=220,4 Ref=450,80

Peak #	RetTime [min]	Type	Width [min]	Area [mAU*s]	Height [mAU]	Area %
1	12.751	BB	0.2248	9629.78320	659.13550	91.1192
2	14.959	VB	0.2502	938.55597	52.48400	8.8808
Totals :				1.05683e4	711.61950	

Figure 7. Chiral HPLC traces (90:10 hexanes/isopropanol, 0.5 mL/min) of racemic (left trace) and enantiomerically enriched (right trace, 82% ee) 2-methyl-*N*,4,4-triphenylpyrrolidine-1-carboxamide (**8b**).

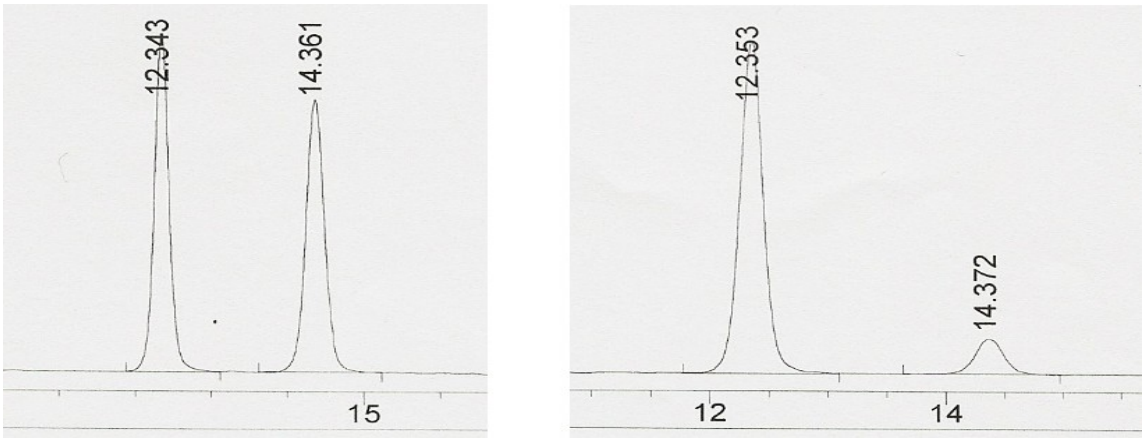

Signal 2: DAD1 B, Sig=220,4 Ref=450,80

Peak #	RetTime [min]	Type	Width [min]	Area [mAU*s]	Height [mAU]	Area %
1	12.343	BV	0.2127	1.66836e4	1204.89954	49.9458
2	14.361	VP	0.2612	1.67198e4	973.60291	50.0542
Totals :				3.34035e4	2178.50244	

Signal 1: DAD1 A, Sig=210,4 Ref=450,80

Peak #	RetTime [min]	Type	Width [min]	Area [mAU*s]	Height [mAU]	Area %
1	12.353	VB	0.2108	1.17817e4	844.05884	88.2683
2	14.372	VP	0.2535	1565.90210	88.90730	11.7317
Totals :				1.33476e4	932.96614	

Figure 8. Chiral HPLC traces (90:10 hexanes/isopropanol, 0.5 mL/min) of racemic (left trace) and enantiomerically enriched (right trace, 77% ee) propyl 2-methyl-4,4-diphenylpyrrolidine-1-carboxylate (**10**).

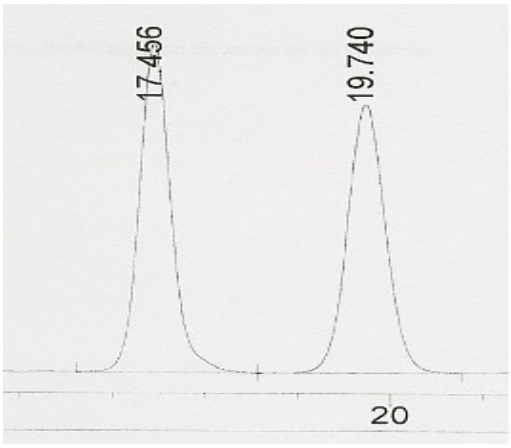

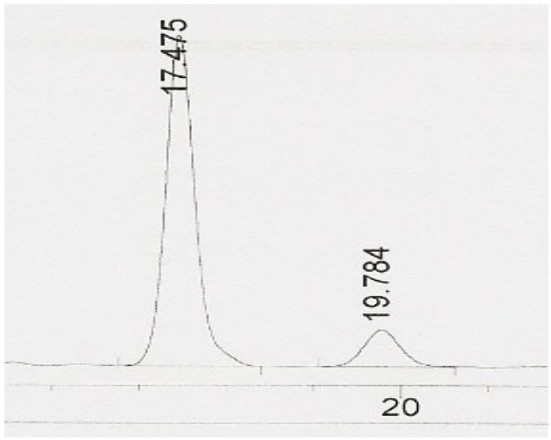

Signal 1: DAD1 A, Sig=210,4 Ref=450,80

Peak #	RetTime [min]	Type	Width [min]	Area [mAU*s]	Height [mAU]	Area %
1	17.456	VP	0.2950	3.21940e4	1361.62585	50.3774
2	19.740	VB	0.3567	3.17117e4	1106.54309	49.6226
Totals :				6.39056e4	2468.16895	

Signal 1: DAD1 A, Sig=210,4 Ref=450,80

Peak #	RetTime [min]	Type	Width [min]	Area [mAU*s]	Height [mAU]	Area %
1	17.475	VB	0.2944	2.21007e4	948.05182	87.6402
2	19.784	VB	0.3635	3116.84961	104.63859	12.3598
Totals :				2.52175e4	1052.69041	

Figure 9. Chiral HPLC traces (90:10 hexanes/isopropanol, 0.5 mL/min) of racemic (left trace) and enantiomerically enriched (right trace, 75% ee) 2-(benzyloxy)ethyl 2-methyl-4,4-diphenylpyrrolidine-1-carboxylate (**12**).

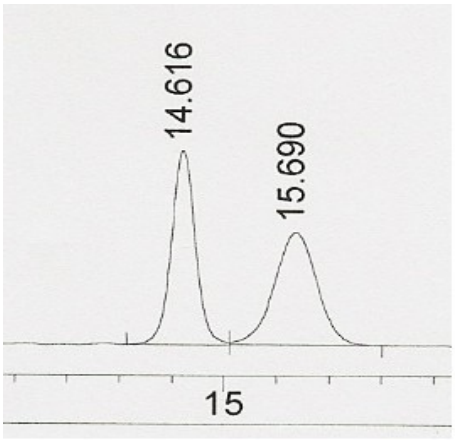

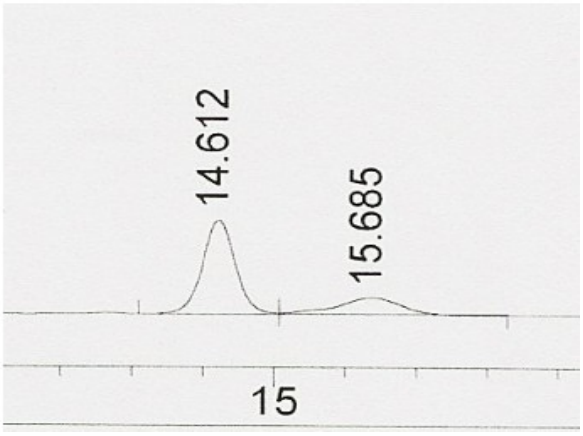

Signal 1: DAD1 A, Sig=210,4 Ref=450,80

Peak #	RetTime [min]	Type	Width [min]	Area [mAU*s]	Height [mAU]	Area %
1	14.616	VV	0.2418	4960.08545	308.86343	49.4231
2	15.690	VB	0.3745	5075.87305	179.63098	50.5769
Totals :				1.00360e4	488.49442	

Signal 2: DAD1 B, Sig=220,4 Ref=450,80

Peak #	RetTime [min]	Type	Width [min]	Area [mAU*s]	Height [mAU]	Area %
1	14.612	VV	0.2446	5854.95703	365.24945	74.2081
2	15.685	VP	0.4064	2034.96265	64.50858	25.7919
Totals :				7889.91968	429.75803	

Figure 10. Chiral HPLC traces (95:5 hexanes/isopropanol, 0.5 mL/min) of racemic (left trace) and enantiomerically enriched (right trace, 48% ee) 2,2,2-trichloroethyl 2-methyl-4,4-diphenylpyrrolidine-1-carboxylate (**14**).

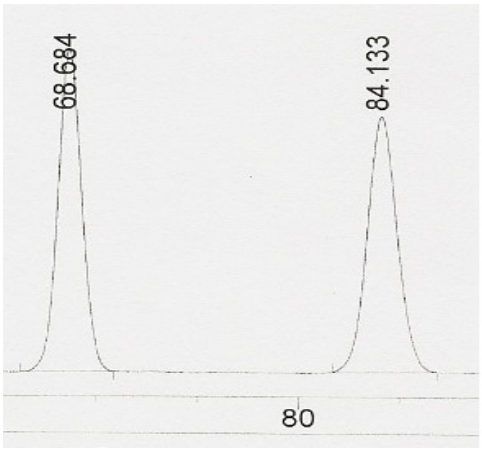

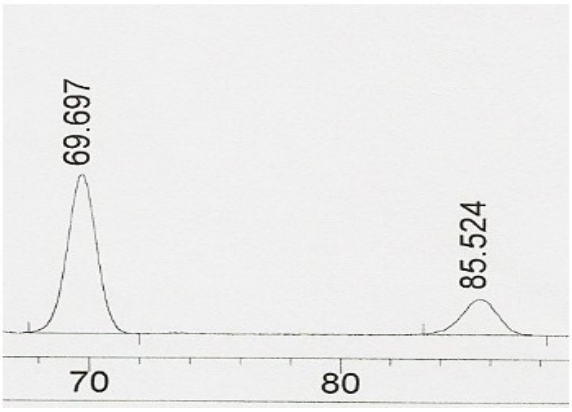

Signal 1: DAD1 A, Sig=210,4 Ref=450,80

Peak #	RetTime [min]	Type	Width [min]	Area [mAU*s]	Height [mAU]	Area %
1	68.684	VB	0.9793	6.51216e4	799.34265	49.8350
2	84.133	BB	1.2123	6.55528e4	635.86908	50.1650
Totals :				1.30674e5	1435.21173	

Signal 1: DAD1 A, Sig=210,4 Ref=450,80

Peak #	RetTime [min]	Type	Width [min]	Area [mAU*s]	Height [mAU]	Area %
1	69.697	BP	0.9632	2.30098e4	284.37802	77.7198
2	85.524	BP	1.2116	6596.30225	64.02145	22.2802
Totals :				2.96061e4	348.39947	

Figure 11. Chiral HPLC traces (99:1 hexanes/isopropanol, 0.5 mL/min) of racemic (left trace) and enantiomerically enriched (right trace, 55% ee) 9-fluorenylmethyl 2-methyl-4-cyclohexylpyrrolidine-1-carboxylate (**16**).

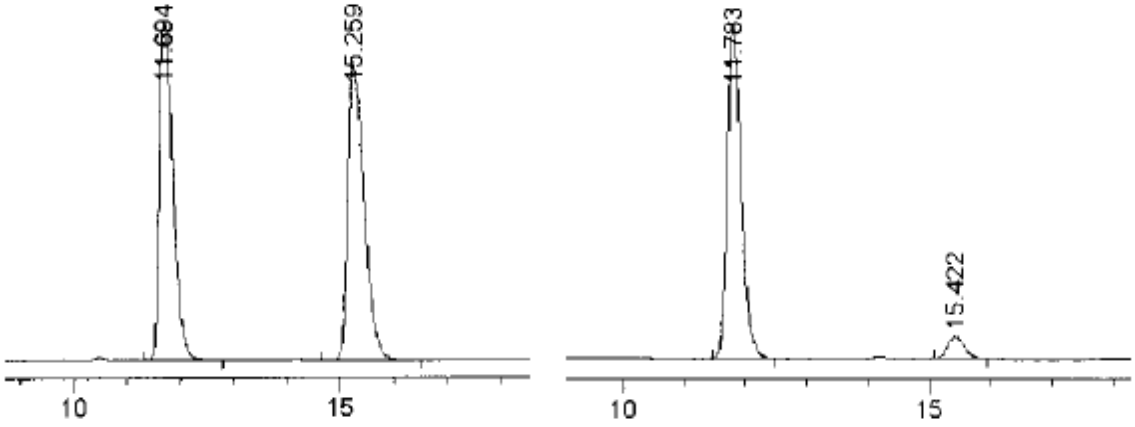

Signal 2: DAD1 B, Sig=220,4 Ref=450,80

Peak #	RetTime [min]	Type	Width [min]	Area [mAU*s]	Height [mAU]	Area %
1	11.694	VB	0.2467	4.75548e4	2662.92920	48.9535
2	15.259	BB	0.3051	4.95881e4	2307.83350	51.0465
Totals :				9.71430e4	4970.76270	

Signal 2: DAD1 B, Sig=220,4 Ref=450,80

Peak #	RetTime [min]	Type	Width [min]	Area [mAU*s]	Height [mAU]	Area %
1	11.783	PB	0.2409	3169.11792	198.21255	92.6225
2	15.422	BB	0.2528	252.42308	13.14913	7.3775
Totals :				3421.54100	211.36168	

Figure 12. Chiral HPLC traces (85:15 hexanes/isopropanol, 0.5 mL/min) of racemic (left trace) and enantiomerically enriched (right trace, 85% ee) *N*-methyl-2-methyl-4,4-diphenylpyrrolidine-1-carboxamide (**27**).

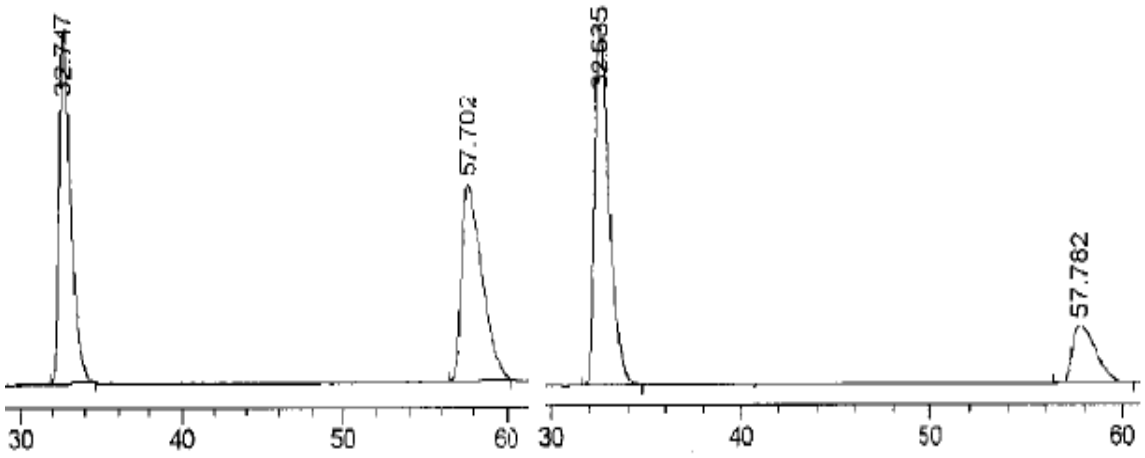

Signal 1: DAD1 A, Sig=210,4 Ref=450,80

Peak #	RetTime [min]	Type	Width [min]	Area [mAU*s]	Height [mAU]	Area %
1	32.747	BB	0.6251	1.83429e4	381.40790	50.2416
2	57.702	BB	1.0322	1.81665e4	211.21744	49.7584
Totals :				3.65093e4	592.62534	

Signal 1: DAD1 A, Sig=210,4 Ref=450,80

Peak #	RetTime [min]	Type	Width [min]	Area [mAU*s]	Height [mAU]	Area %
1	32.635	BB	0.6408	6.45922e4	1231.40991	78.9837
2	57.782	BB	1.0172	1.71869e4	199.63303	21.0163
Totals :				8.17791e4	1431.04294	

Figure 13. Chiral HPLC traces (92:8 hexanes/isopropanol, 0.5 mL/min) of racemic (left trace) and enantiomerically enriched (right trace, 58 % ee) phenyl 2-methyl-4,4-diphenyl-pyrrolidine-1-carboxamide (**19**).

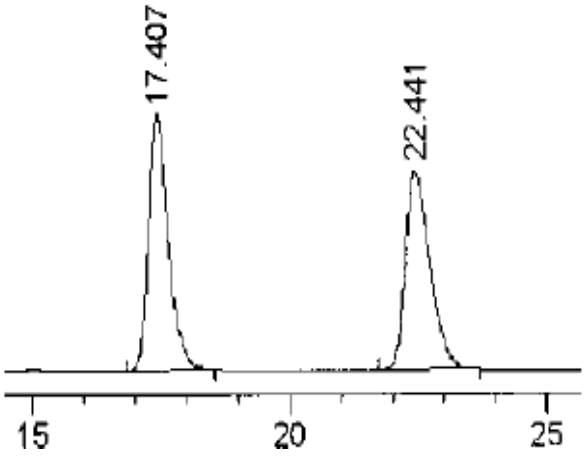

Signal 1: DAD1 A, Sig=210,4 Ref=450,80

Peak #	RetTime [min]	Type	Width [min]	Area [mAU*s]	Height [mAU]	Area %
1	17.407	BB	0.3772	8845.20215	336.30508	50.3293
2	22.441	BB	0.4665	8729.44238	261.31763	49.6707
Totals :				1.75746e4	597.62271	

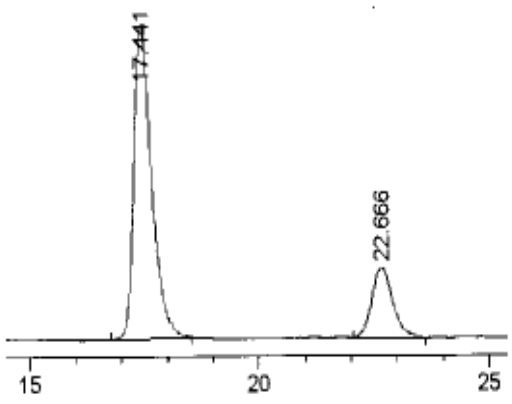

Signal 1: DAD1 A, Sig=210,4 Ref=450,80

Peak #	RetTime [min]	Type	Width [min]	Area [mAU*s]	Height [mAU]	Area %
1	17.441	BB	0.3760	4696.08838	173.84482	78.9385
2	22.666	PP	0.4171	1252.95508	38.60075	21.0615
Totals :				5949.04346	212.44556	

Figure 14. Chiral HPLC traces (80:20 hexanes/isopropanol, 0.5 mL/min) of racemic (left trace) and enantiomerically enriched (right trace, 58% ee) *N*-(4-iodophenyl)-2-methyl-4,4-diphenylpyrrolidine-1-carboxamide (**21**).

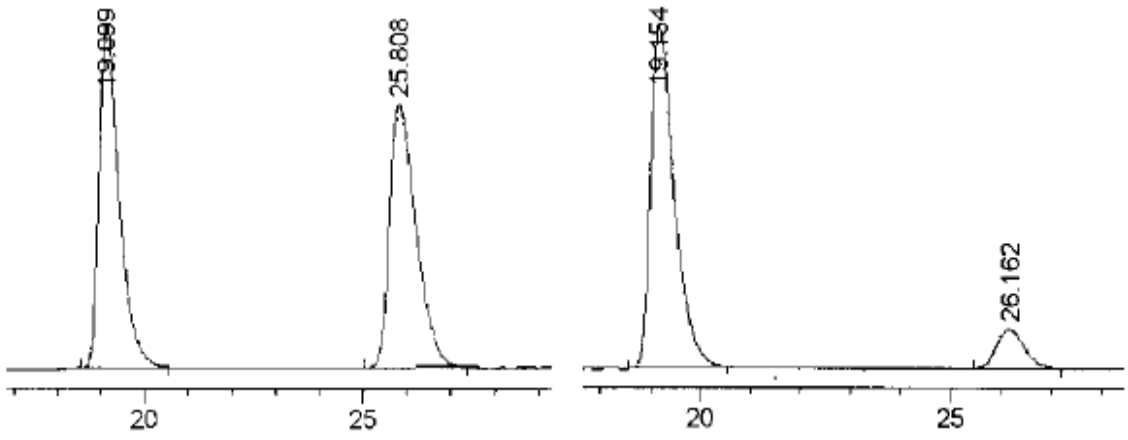

Signal 1: DAD1 A, Sig=210,4 Ref=450,80

Peak #	RetTime [min]	Type	Width [min]	Area [mAU*s]	Height [mAU]	Area %
1	19.099	BB	0.4318	1.10613e4	341.91718	50.0243
2	25.808	BB	0.5651	1.10505e4	262.28174	49.9757
Totals :				2.21118e4	604.19891	

Signal 1: DAD1 A, Sig=210,4 Ref=450,80

Peak #	RetTime [min]	Type	Width [min]	Area [mAU*s]	Height [mAU]	Area %
1	19.154	BB	0.4456	7207.12793	220.31789	88.1347
2	26.162	BB	0.4677	970.27716	25.23708	11.8653
Totals :				8177.40509	245.55497	

Figure 15. Chiral HPLC traces (80:20 hexanes/isopropanol, 0.5 mL/min) of racemic (left trace) and enantiomerically enriched (right trace, 76% ee) 2-methyl-*N*-(4-nitrophenyl)-4,4-diphenylpyrrolidine-1-carboxamide (**23**).

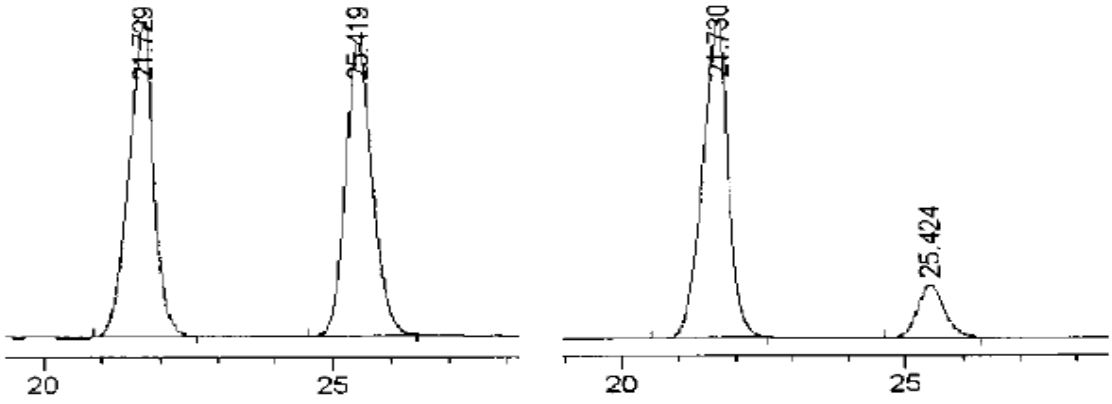

Signal 1: DAD1 A, Sig=210,4 Ref=450,80

Peak #	RetTime [min]	Type	Width [min]	Area [mAU*s]	Height [mAU]	Area %
1	21.729	BB	0.4199	6975.88818	232.83327	50.0167
2	25.419	BB	0.4311	6971.23975	215.90181	49.9833
Totals :				1.39471e4	448.73508	

Signal 1: DAD1 A, Sig=210,4 Ref=450,80

Peak #	RetTime [min]	Type	Width [min]	Area [mAU*s]	Height [mAU]	Area %
1	21.730	BB	0.4107	8488.39160	273.07071	85.6071
2	25.424	BB	0.4148	1427.12622	44.23560	14.3929
Totals :				9915.51782	317.30631	

Figure 16. Chiral HPLC traces (85:15 hexanes/isopropanol, 0.5 mL/min) of racemic (left trace) and enantiomerically enriched (right trace, 72% ee) *N*-benzyl-2-methyl-4,4-diphenylpyrrolidine-1-carboxamide (**2a**).

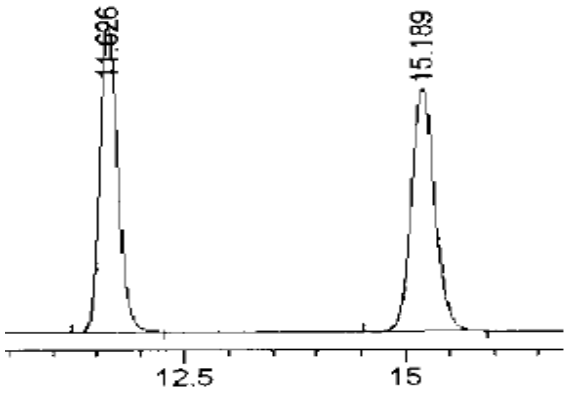

Signal 1: DAD1 A, Sig=210,4 Ref=450,80

Peak #	RetTime [min]	Type	Width [min]	Area [mAU*s]	Height [mAU]	Area %
1	11.626	BB	0.2123	7743.41553	549.81067	49.9827
2	15.189	BB	0.2747	7748.77490	429.10562	50.0173
Totals :				1.54922e4	978.91629	

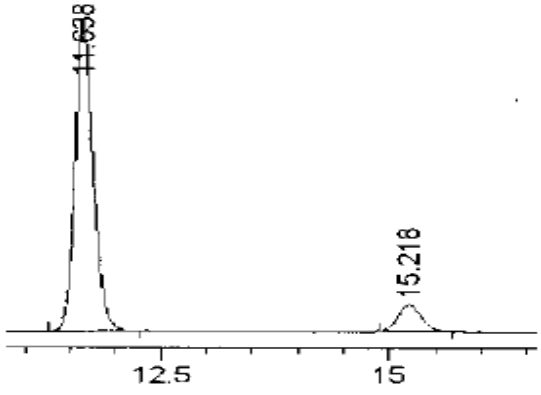

Signal 1: DAD1 A, Sig=210,4 Ref=450,80

Peak #	RetTime [min]	Type	Width [min]	Area [mAU*s]	Height [mAU]	Area %
1	11.638	BB	0.2122	3701.72656	262.95514	90.2573
2	15.218	BB	0.2551	399.57693	22.16545	9.7427
Totals :				4101.30350	285.12059	

Figure 17. Chiral HPLC traces (85:15 hexanes/isopropanol, 0.5 mL/min) of racemic (left trace) and enantiomerically enriched (right trace, 81% ee) *N*-butyl-2-methyl-4,4-diphenylpyrrolidine-1-carboxamide (**25**).

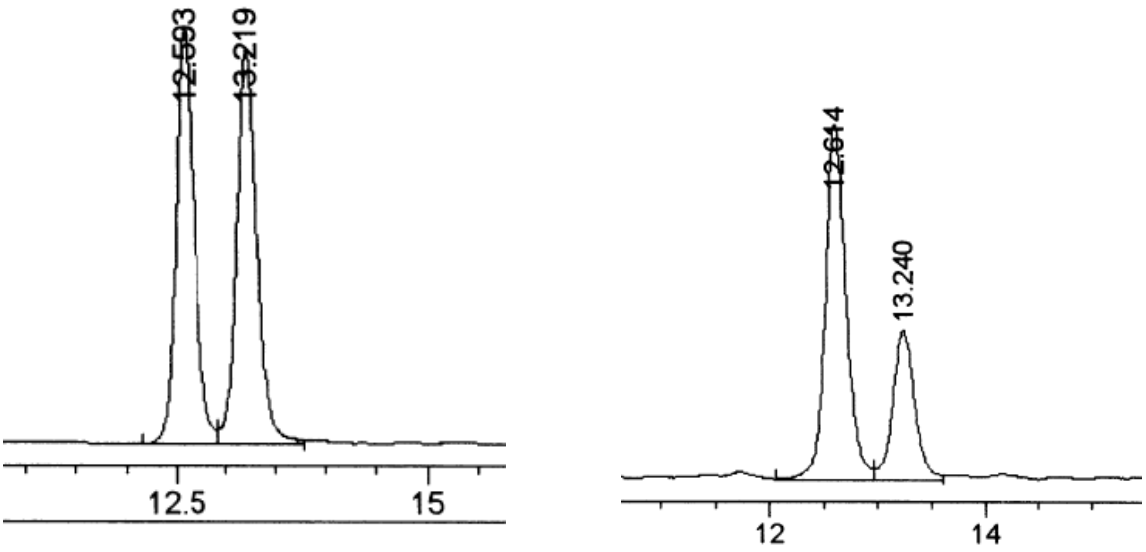

Peak #	RetTime [min]	Type	Width [min]	Area [mAU*s]	Height [mAU]	Area %
1	12.593	BV	0.1978	7538.56152	574.88110	49.4583
2	13.219	VV	0.2161	7703.70605	544.88470	50.5417
Totals :				1.52423e4	1119.76581	

Peak #	RetTime [min]	Type	Width [min]	Area [mAU*s]	Height [mAU]	Area %
1	12.614	VV	0.2009	3418.50977	255.46790	68.9647
2	13.240	VV	0.2132	1538.39075	108.62469	31.0353
Totals :				4956.90051	364.09258	

Figure 18. Chiral HPLC traces (85:15 hexanes/isopropanol, 0.5 mL/min) of racemic (left trace) and enantiomerically enriched (right trace, 38% ee) 1-(2-methylindolin-1-yl)ethanone (**29**).

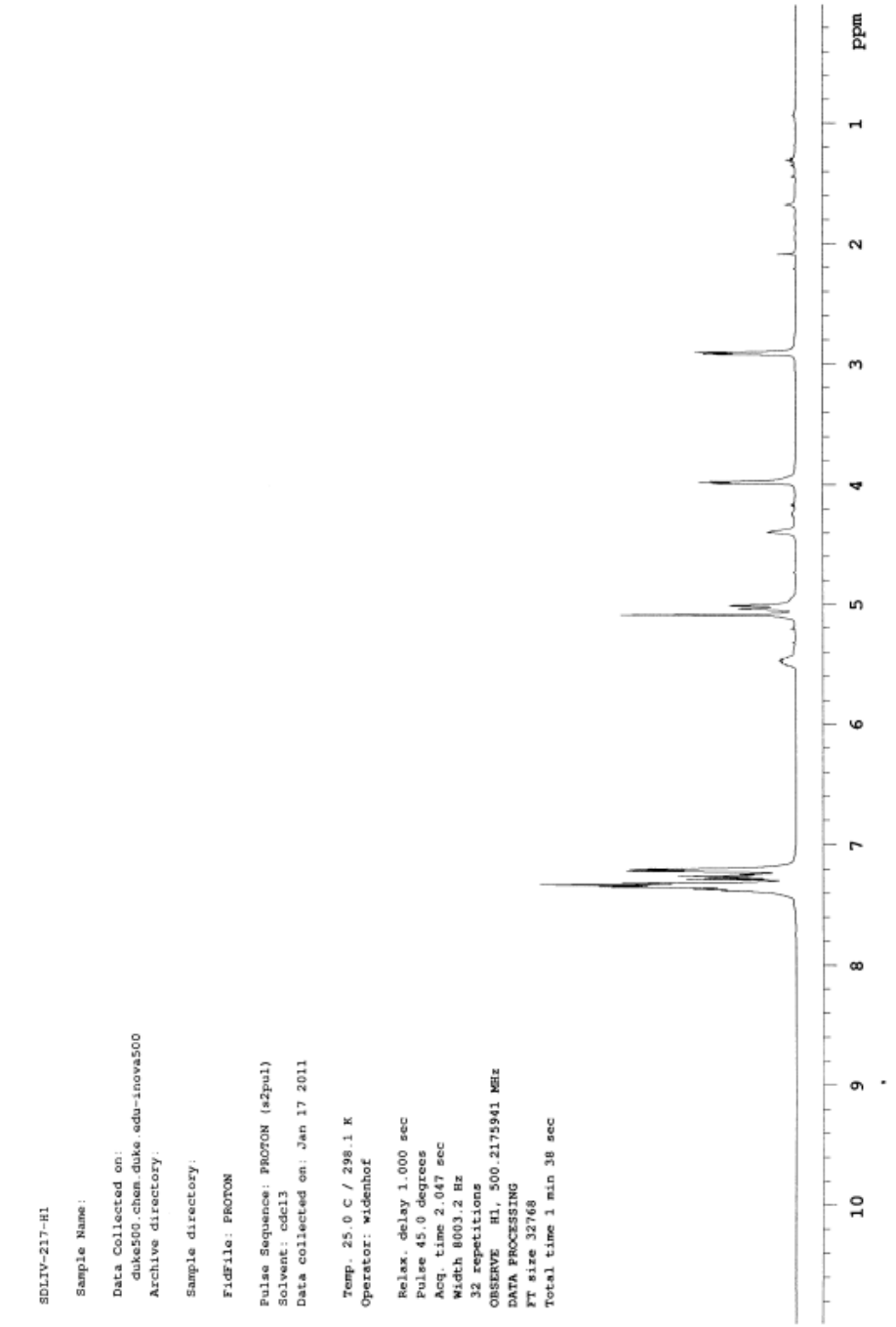

Figure 19. ^{1}H NMR spectrum of **5** in $CDCl_3$

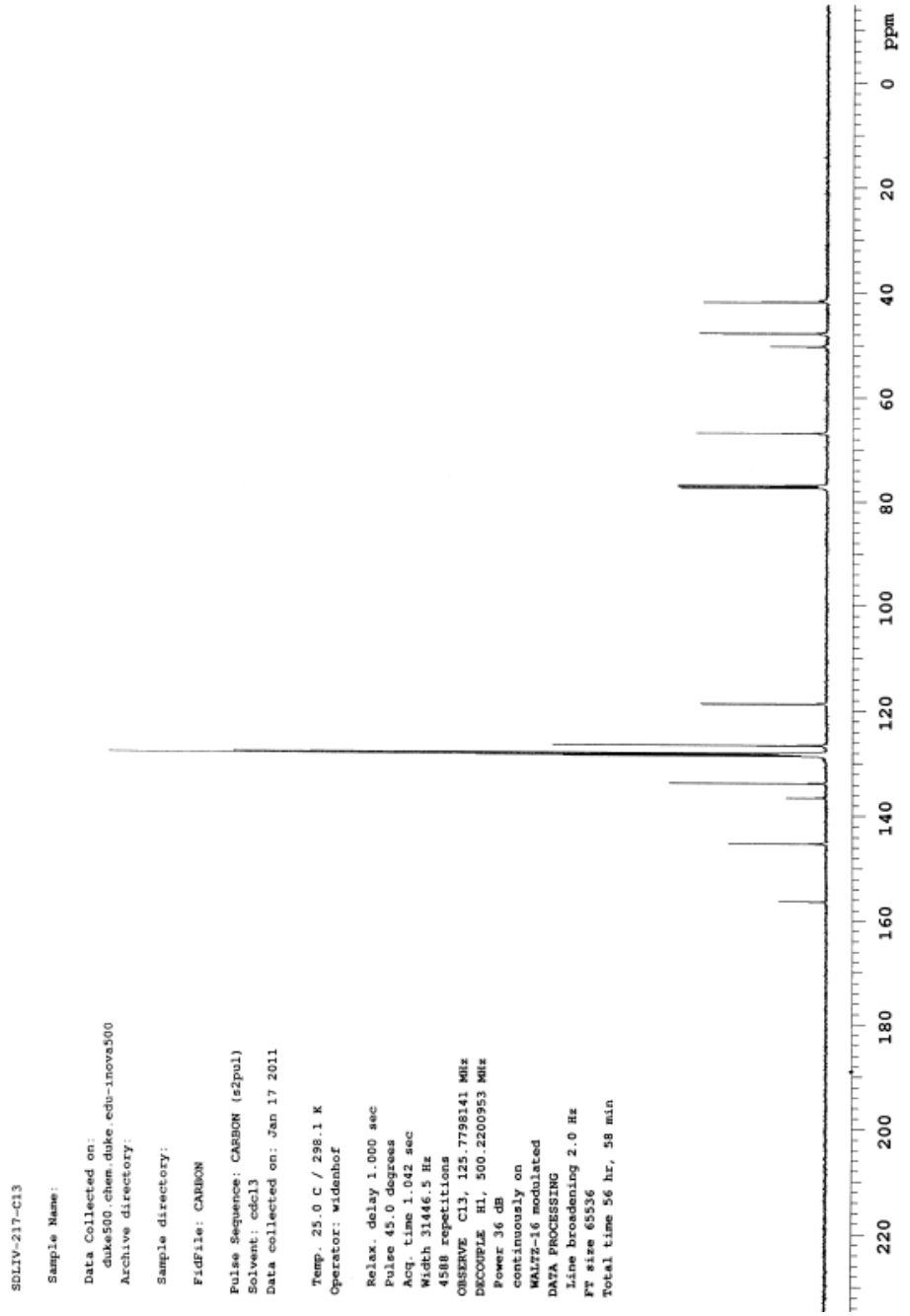

Figure 20. $^{13}C\{^{1}H\}$ NMR spectrum of **5** in $CDCl_3$.

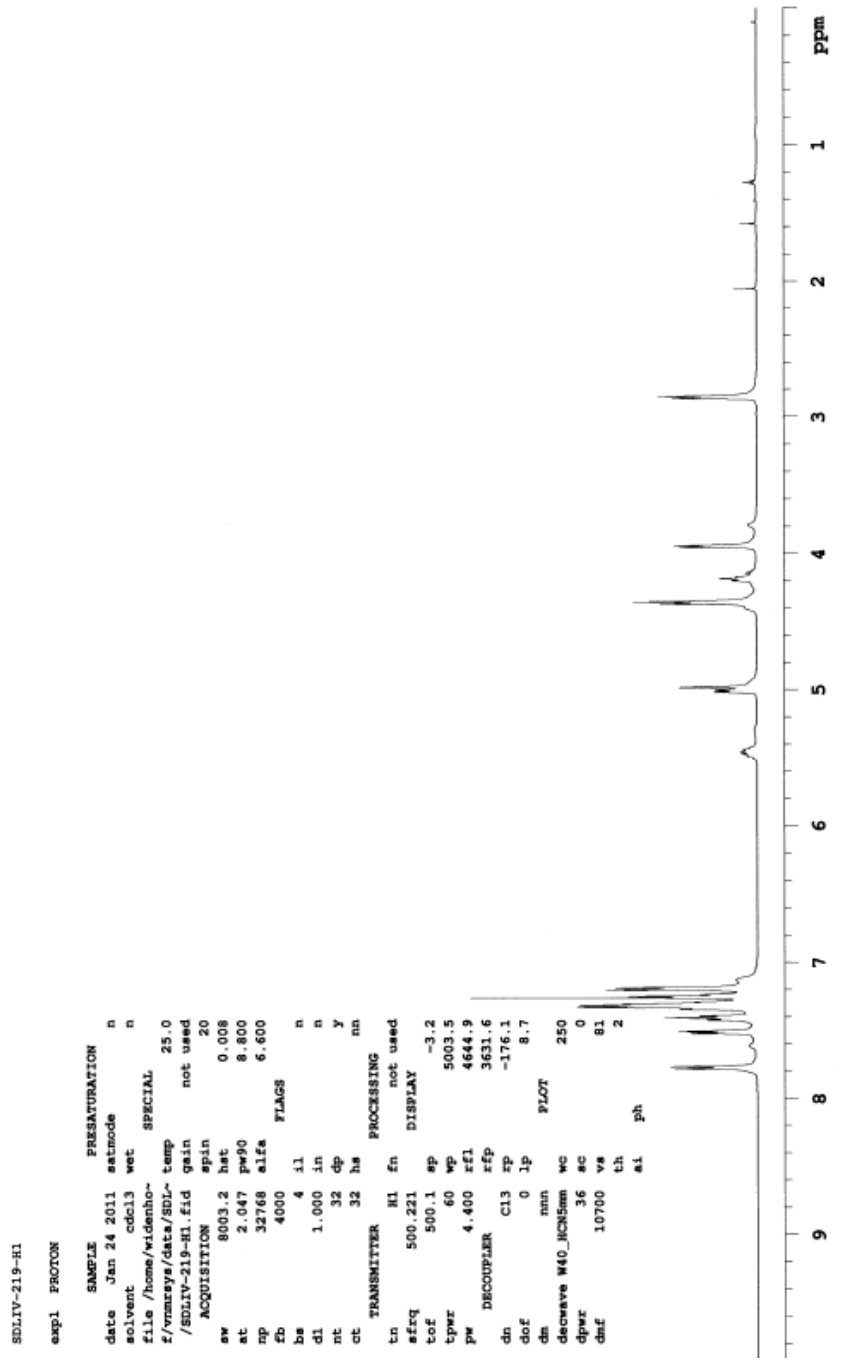

Figure 21. ^{1}H NMR spectrum of **1b** in $CDCl_3$.

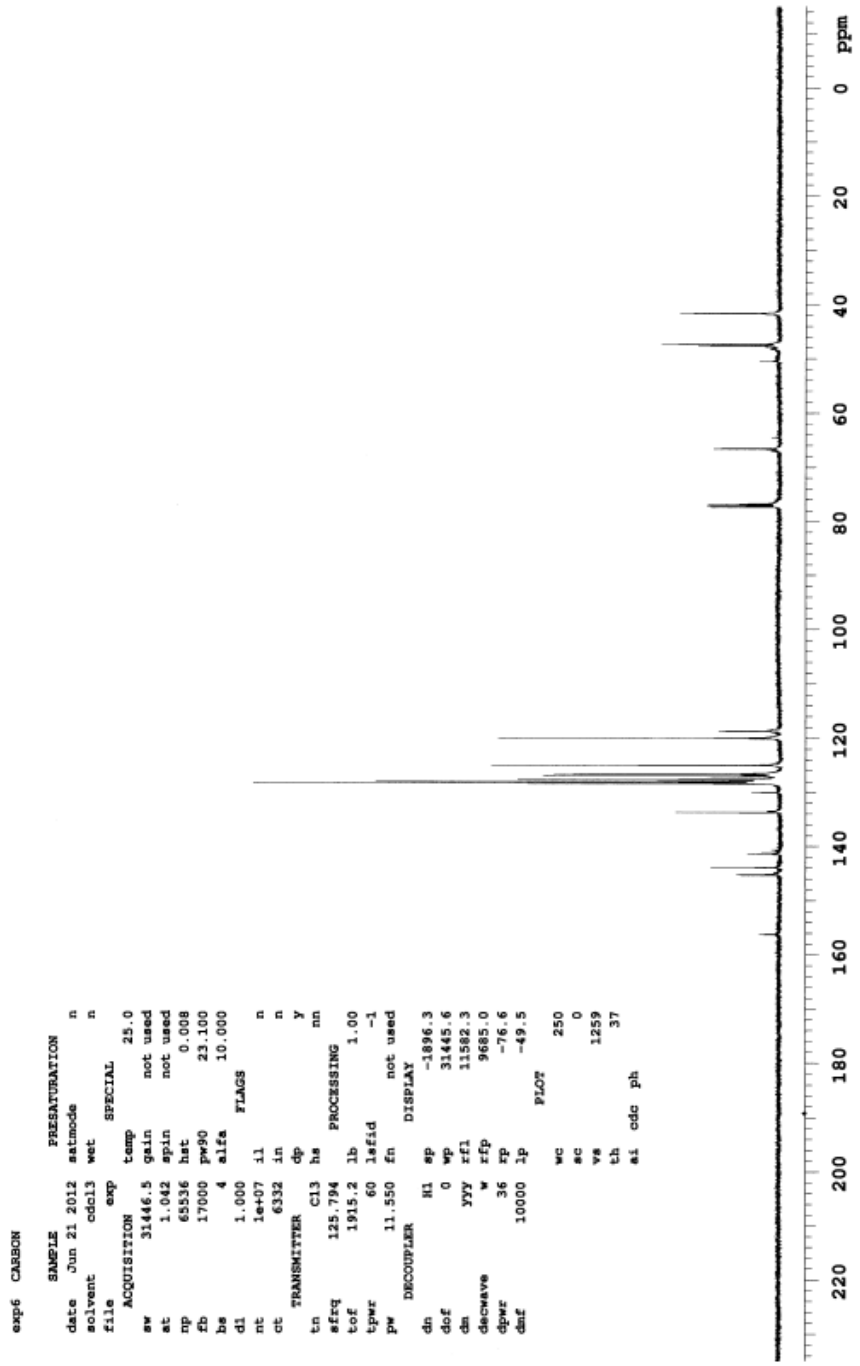

Figure 22. $^{13}C\{^{1}H\}$ NMR spectrum of **1b** in $CDCl_3$.

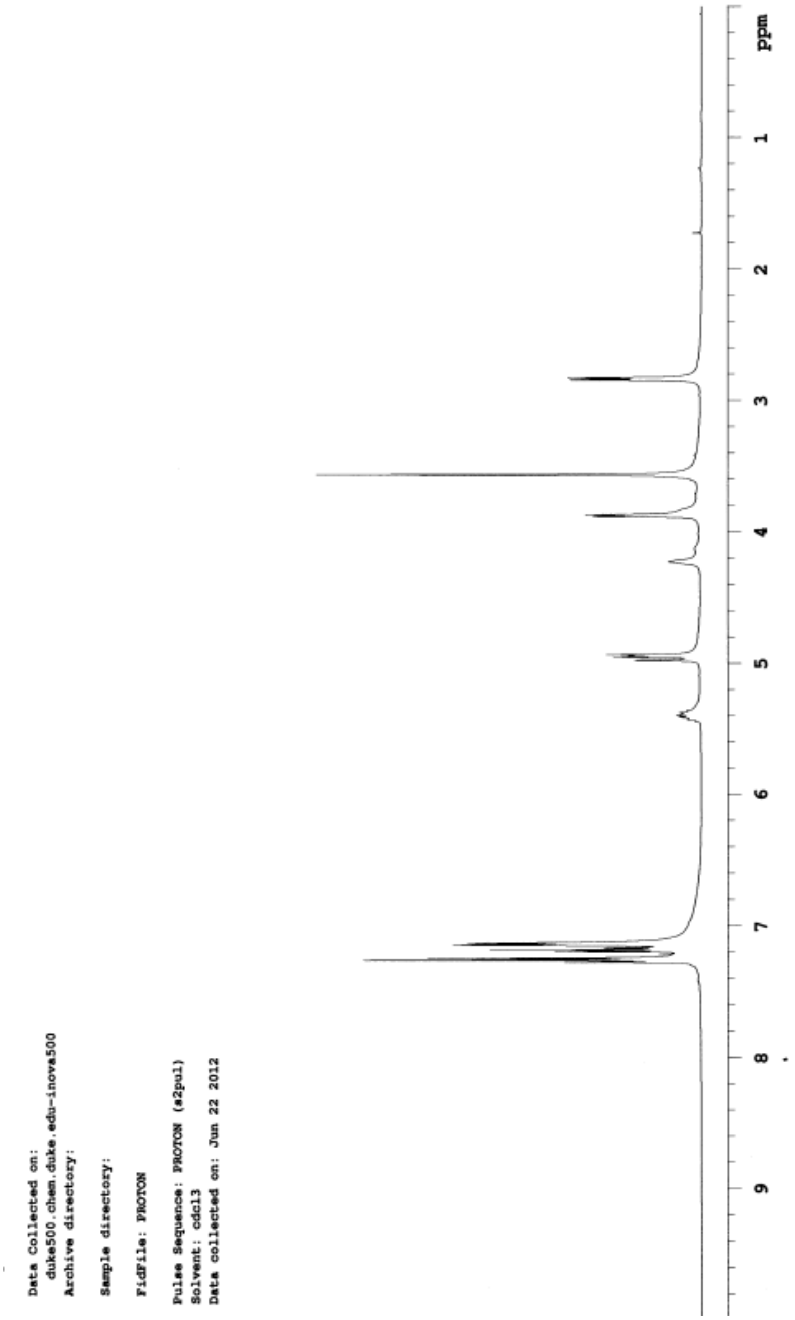

Figure 23. ^{1}H NMR spectrum of **7** in $CDCl_3$.

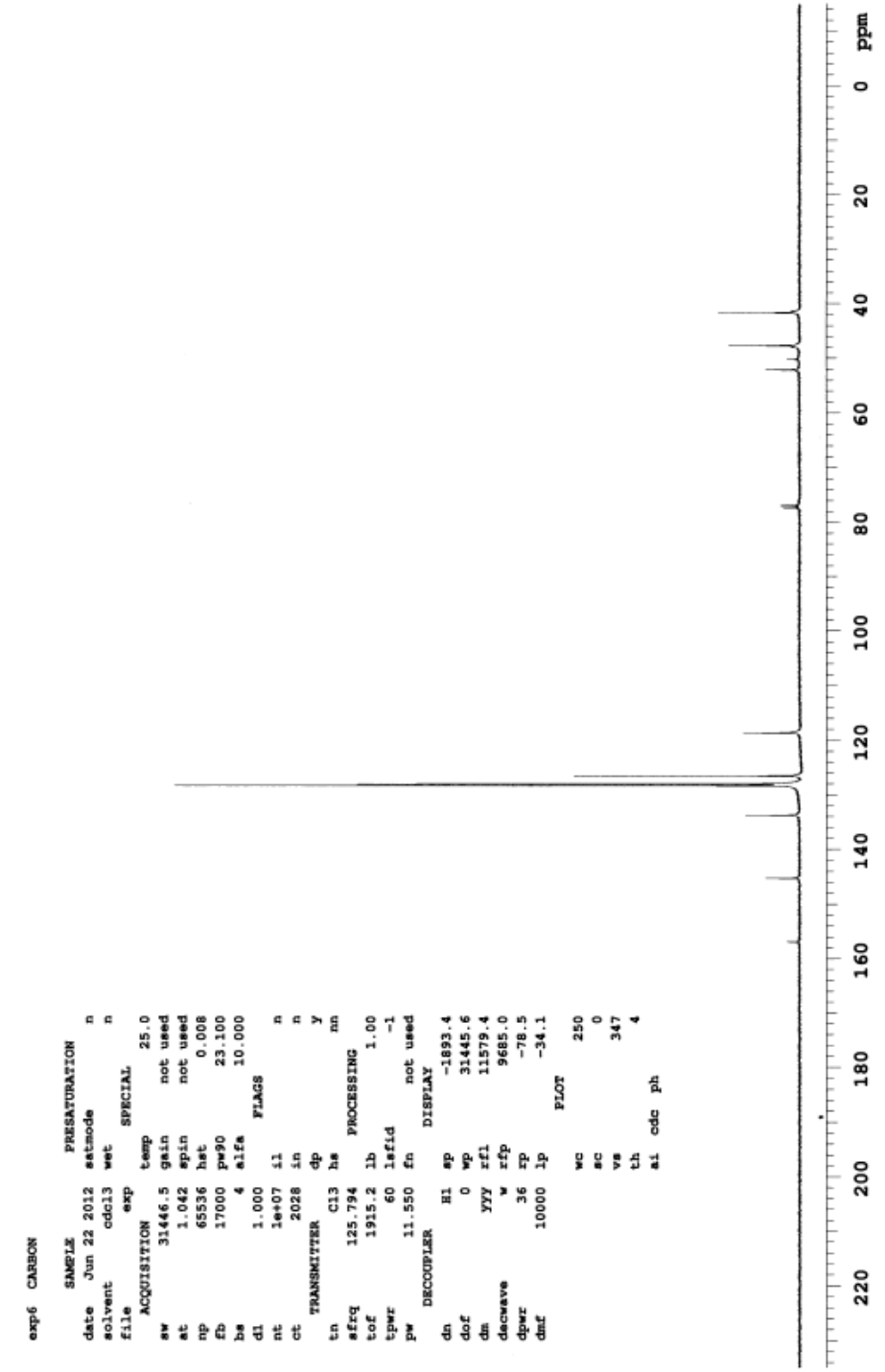

Figure 24. $^{13}C\{^{1}H\}$ NMR spectrum of **7** in $CDCl_3$.

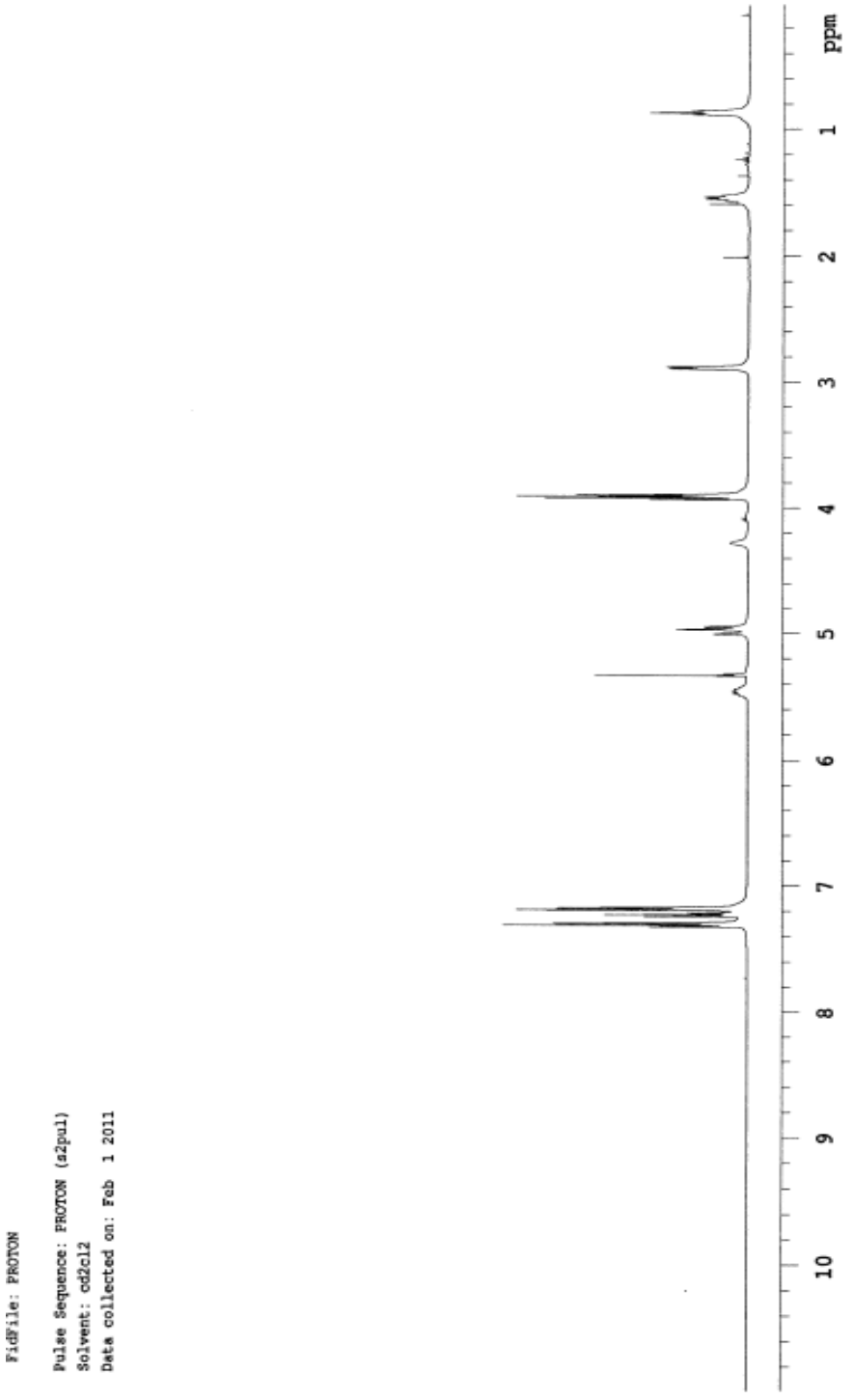

Figure 25. ^{1}H NMR spectrum of **9** in $CDCl_3$.

9

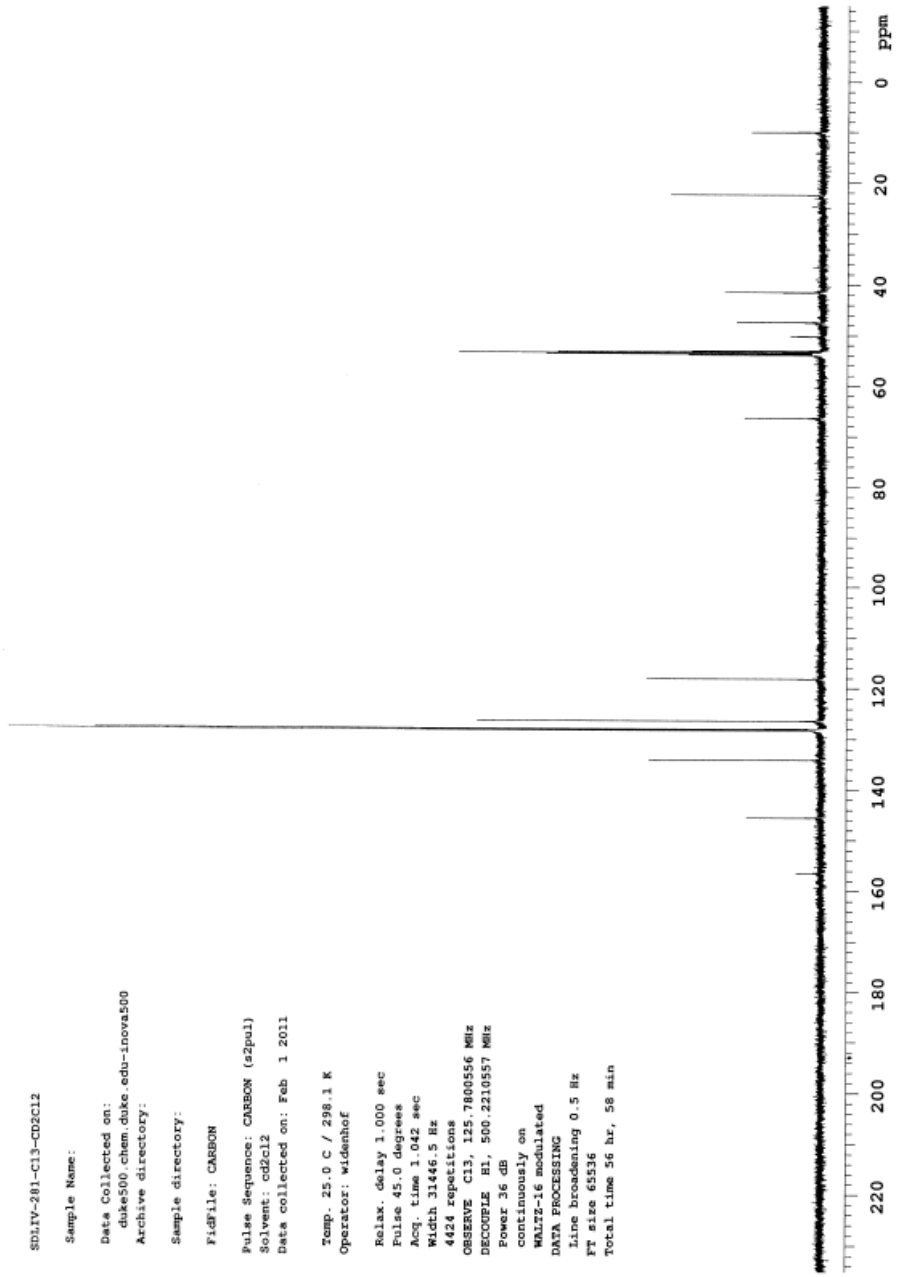

Figure 26. $^{13}C\{^{1}H\}$ NMR spectrum of **9** in $CDCl_3$.

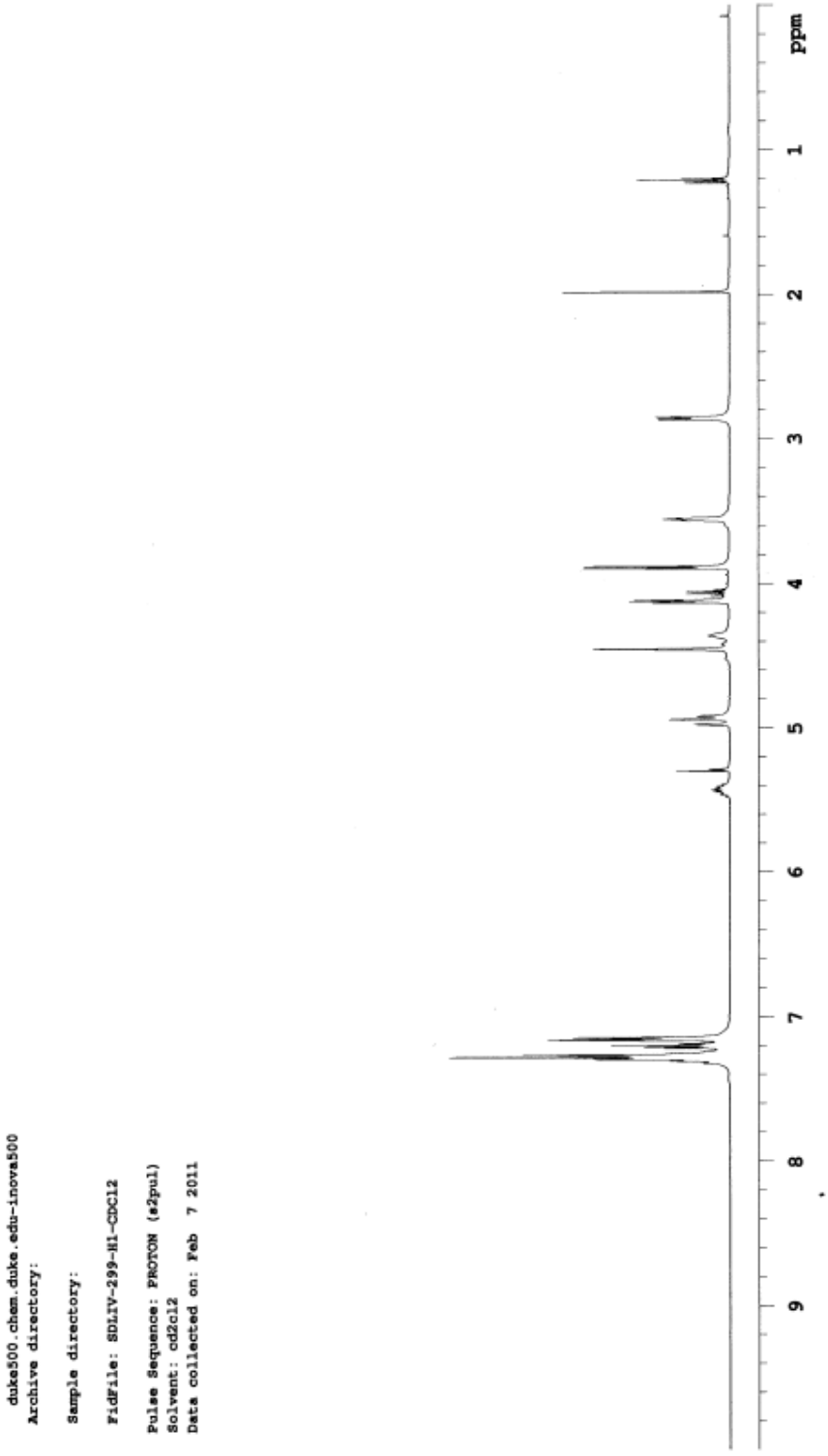

Figure 27. ^{1}H NMR spectrum of **11** in $CDCl_3$.

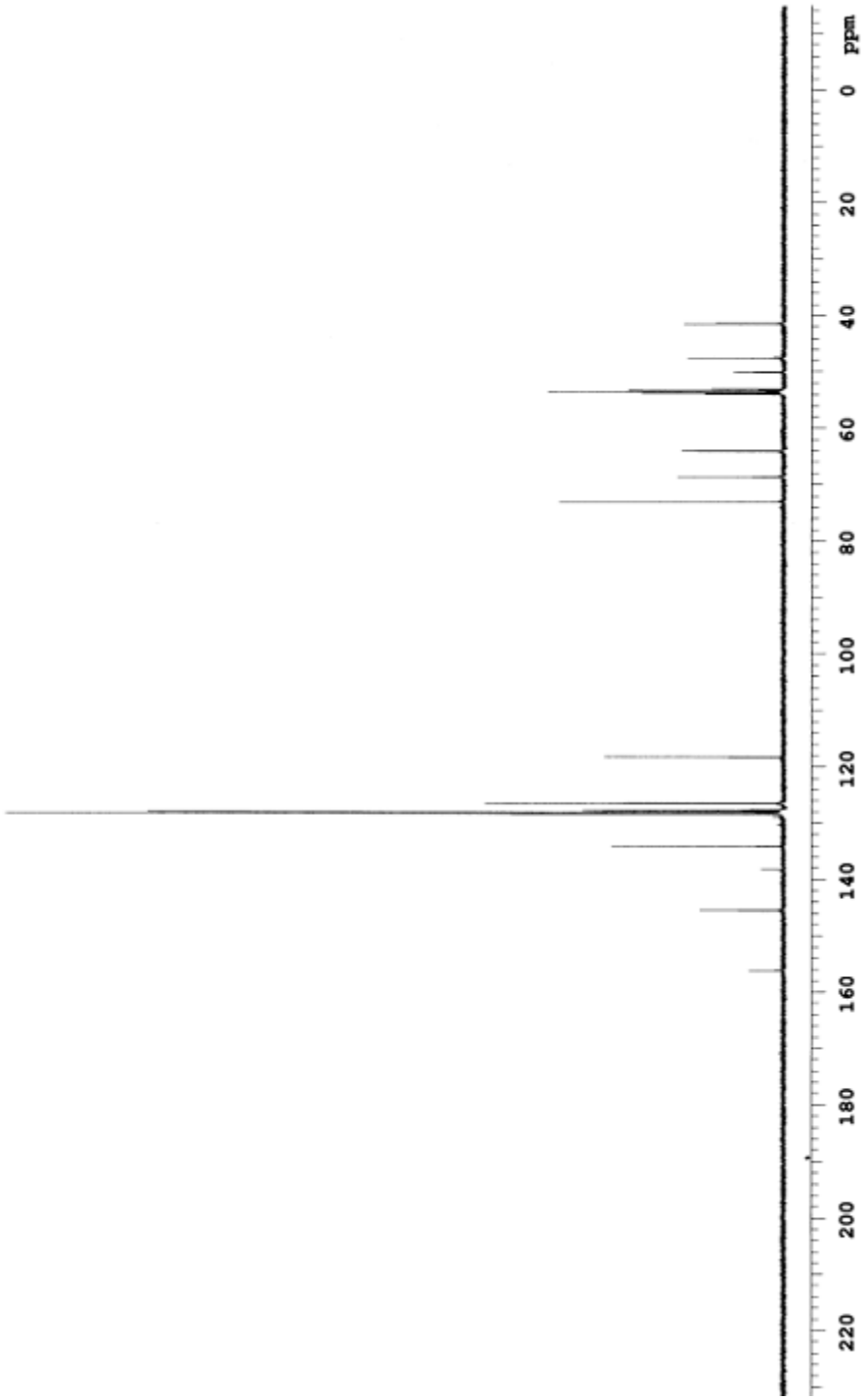

Figure 28. $^{13}C\{^{1}H\}$ NMR spectrum of **11** in $CDCl_3$.

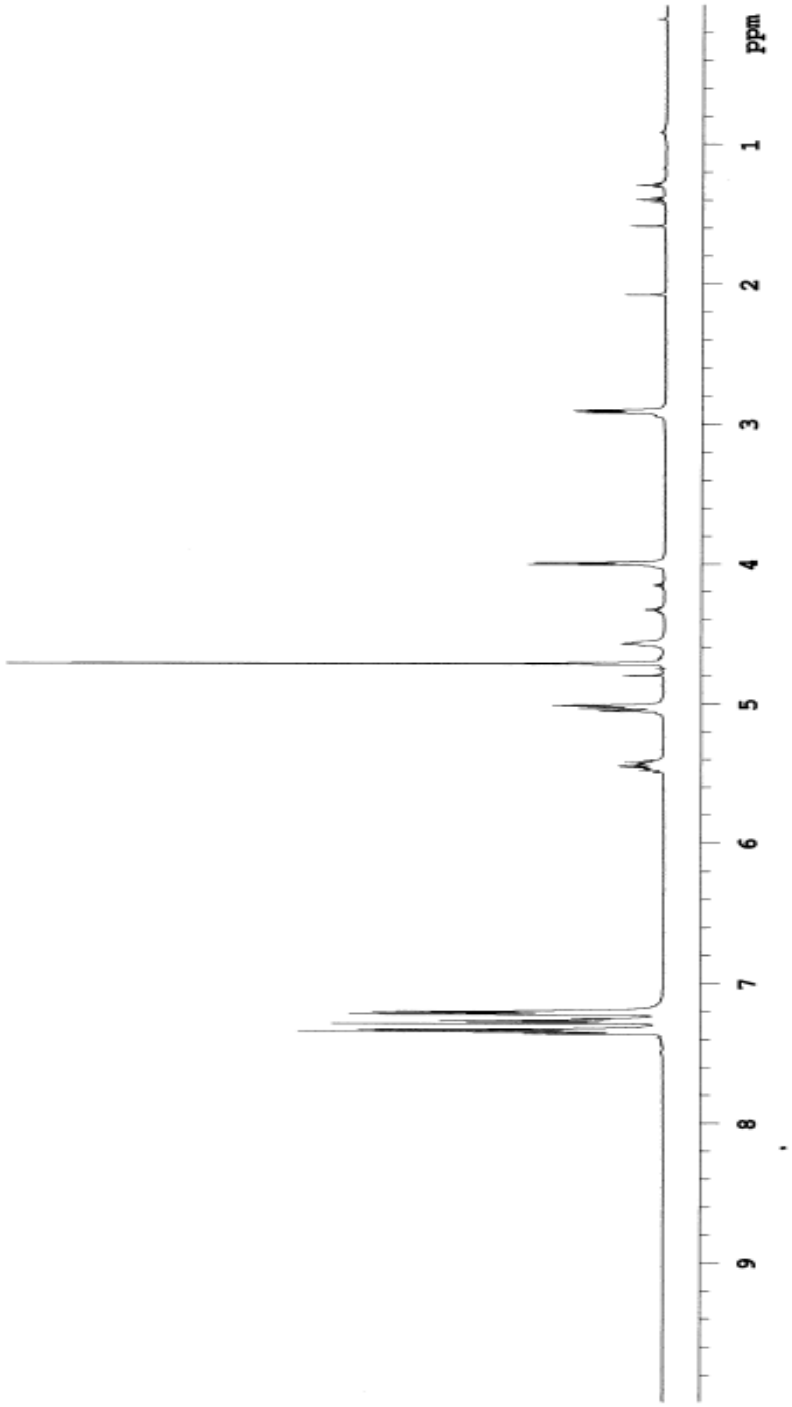

Figure 29. ^{1}H NMR spectrum of **13** in $CDCl_3$.

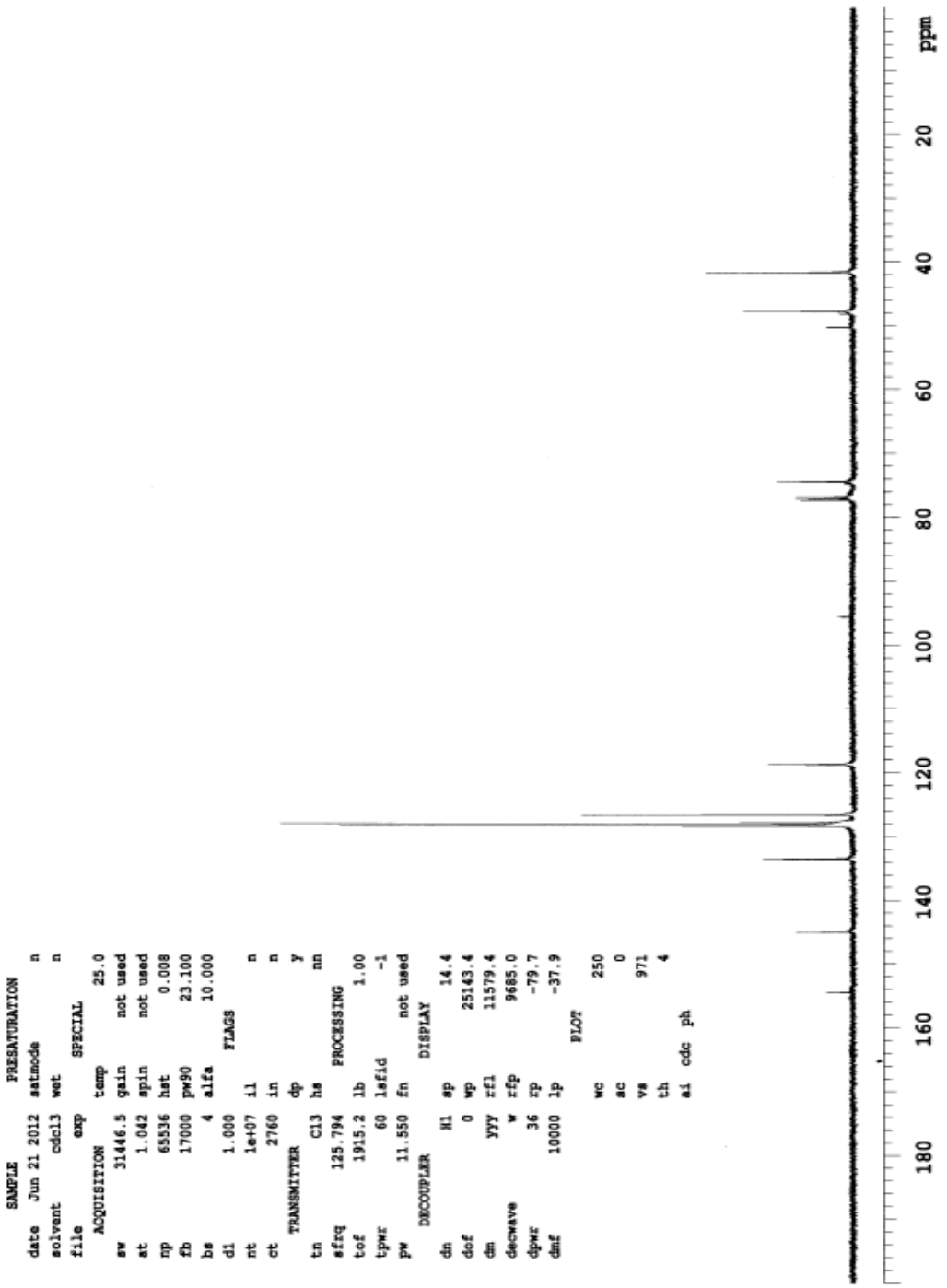

Figure 30. $^{13}C\{^{1}H\}$ NMR spectrum of **13** in $CDCl_3$.

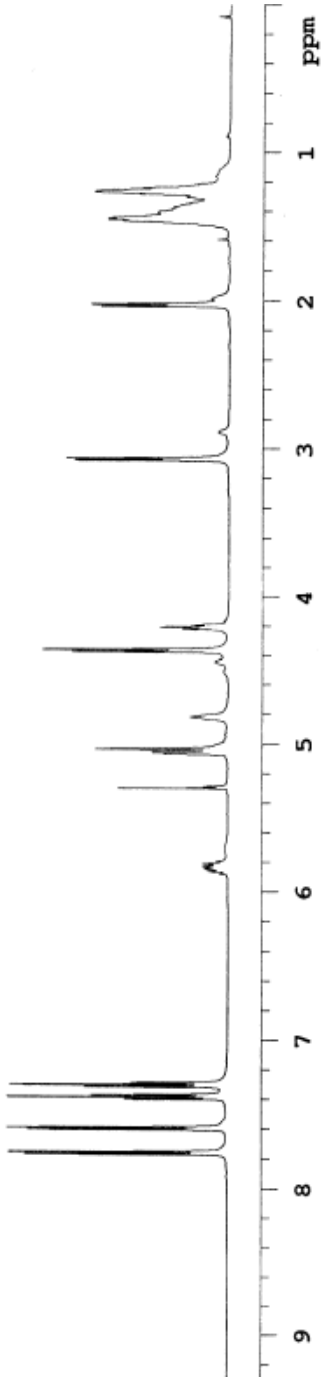

Figure 31. ^{1}H NMR spectrum of **15** in $CDCl_3$.

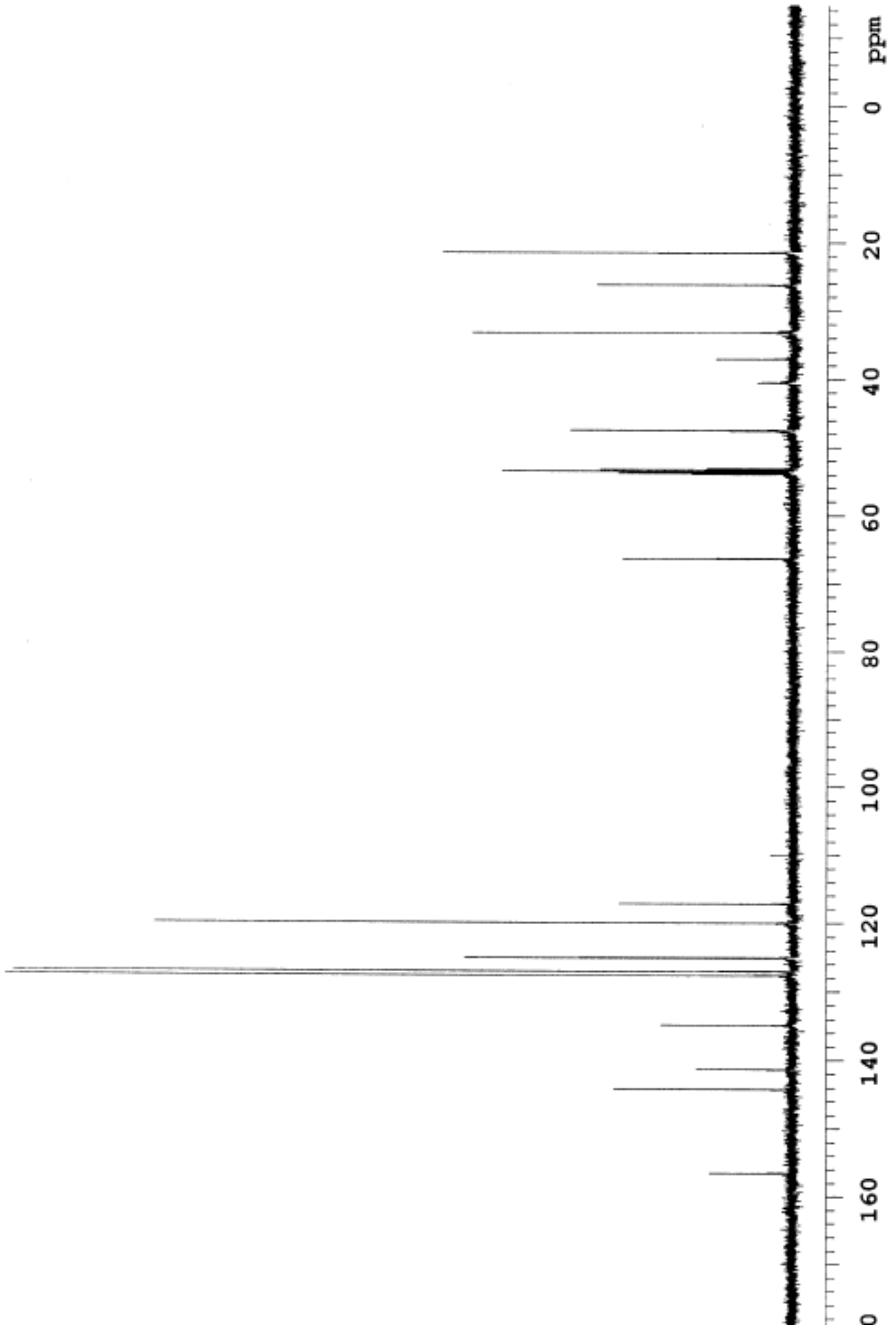

Figure 32. $^{13}C\{^{1}H\}$ NMR spectrum of **15** in $CDCl_3$.

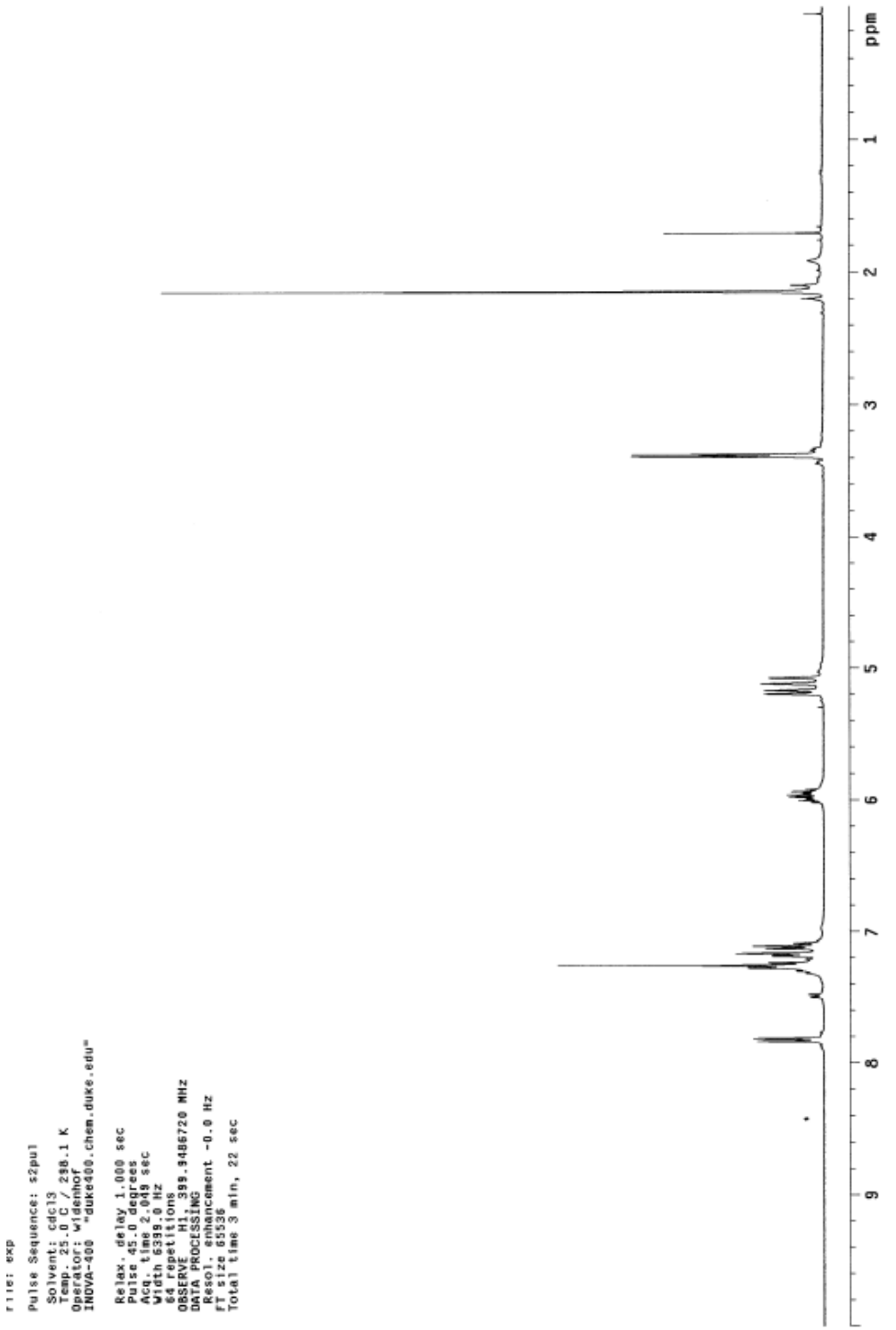

Figure 33. ^{1}H NMR spectrum of **28** in $CDCl_3$.

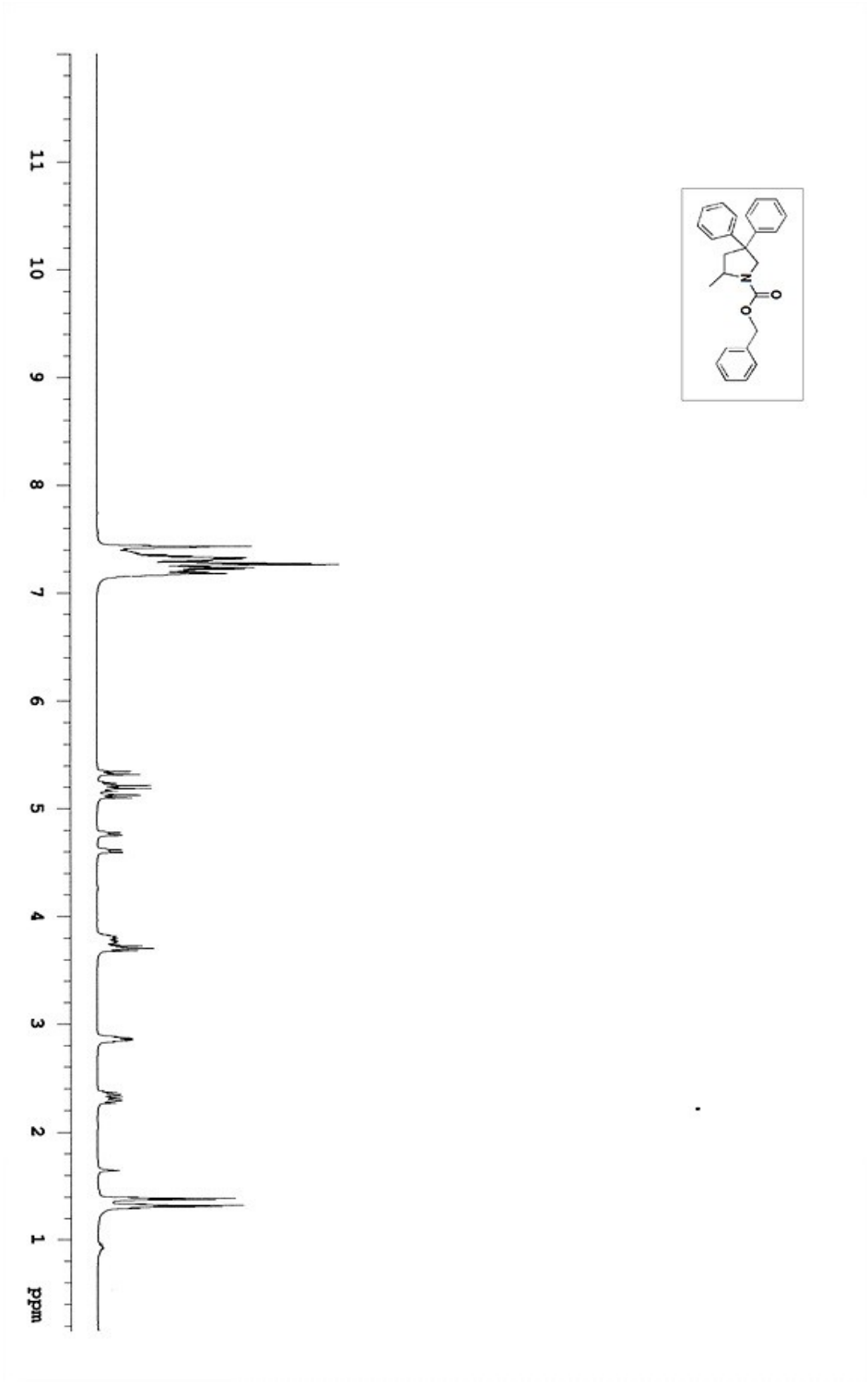

Figure 34. ^{1}H NMR spectrum of **6** in $CDCl_3$.

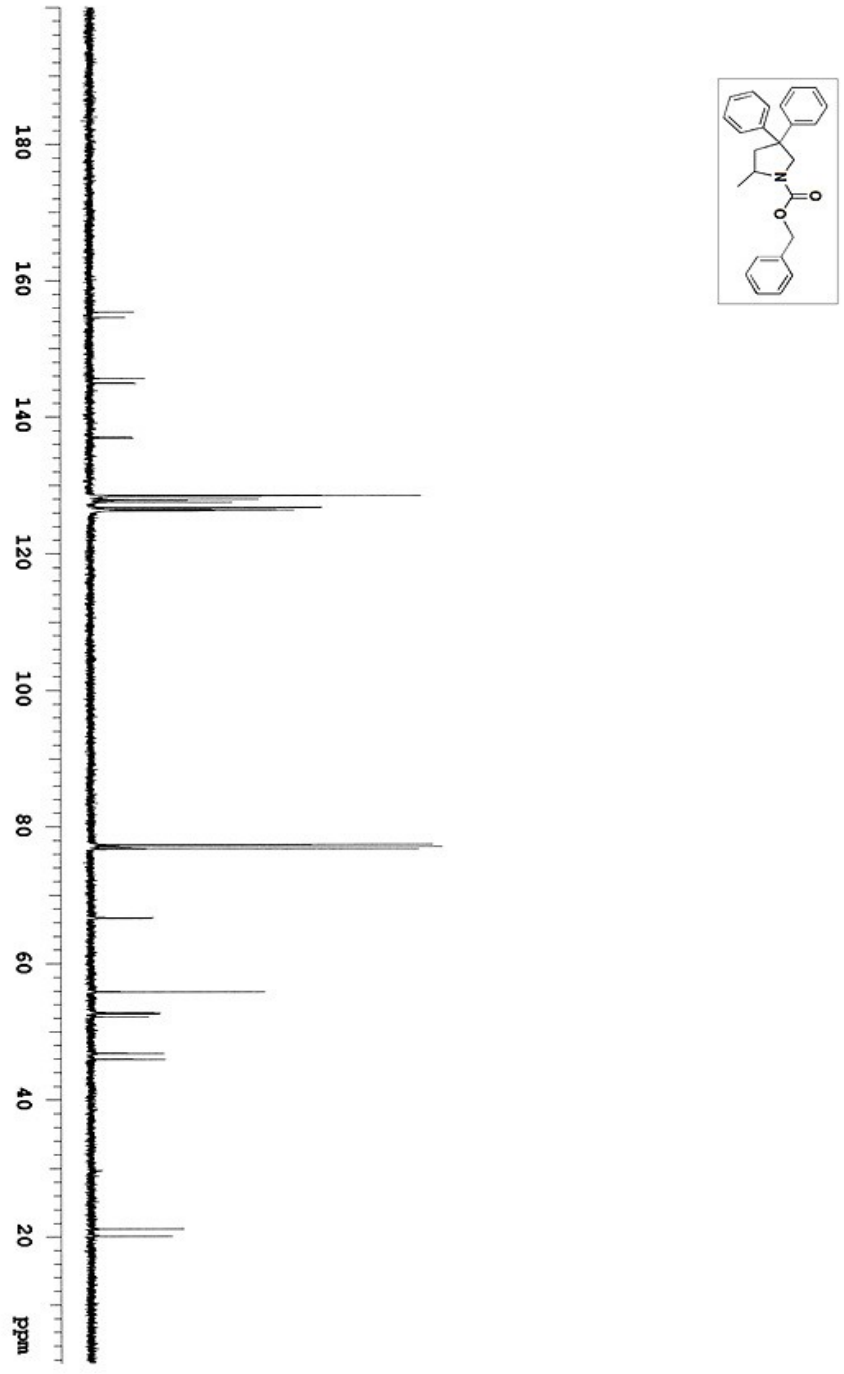

Figure 35. $^{13}C\{^{1}H\}$ NMR spectrum of **6** in $CDCl_3$.

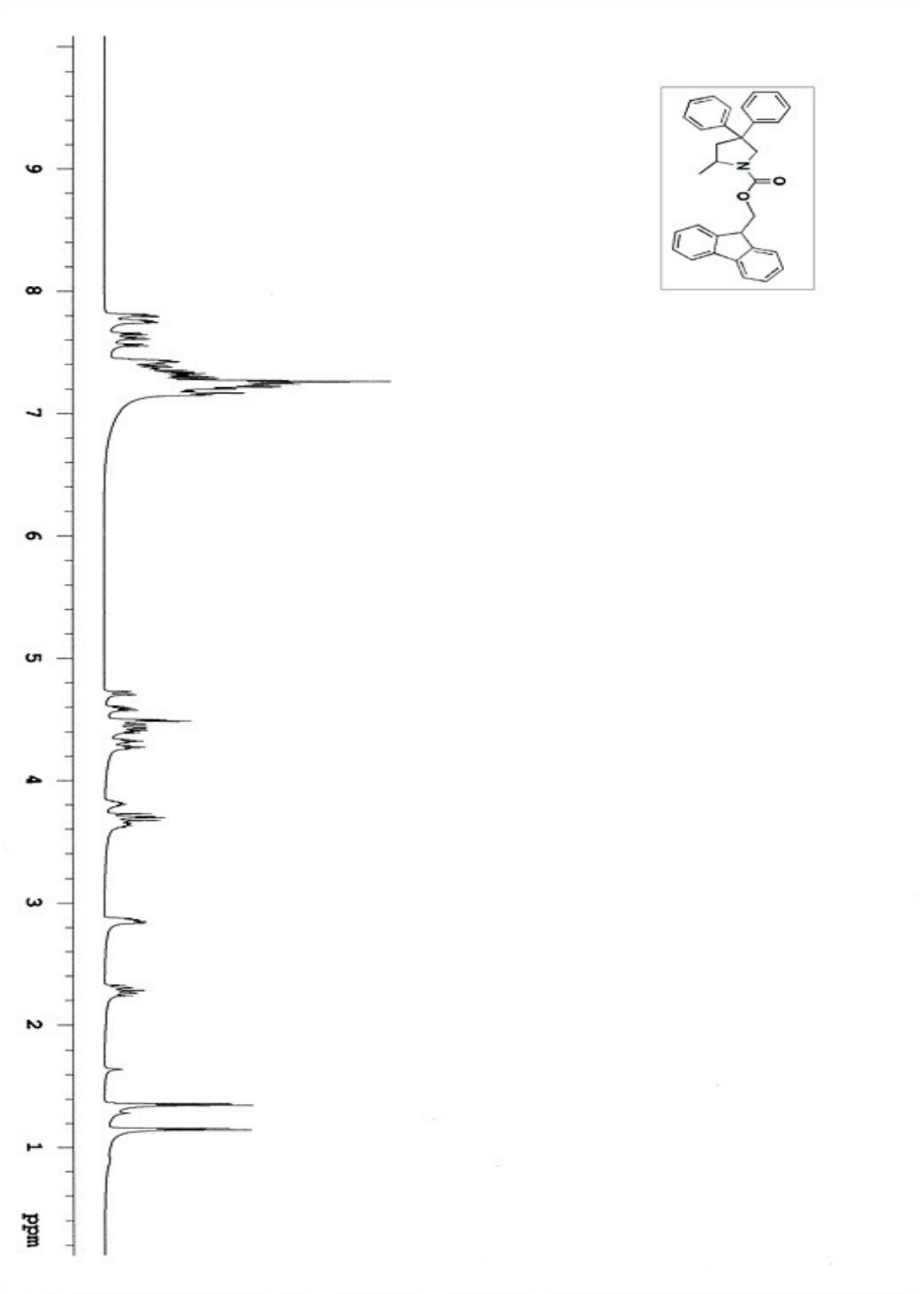

Figure 36. ^{1}H NMR spectrum of **2b** in $CDCl_3$.

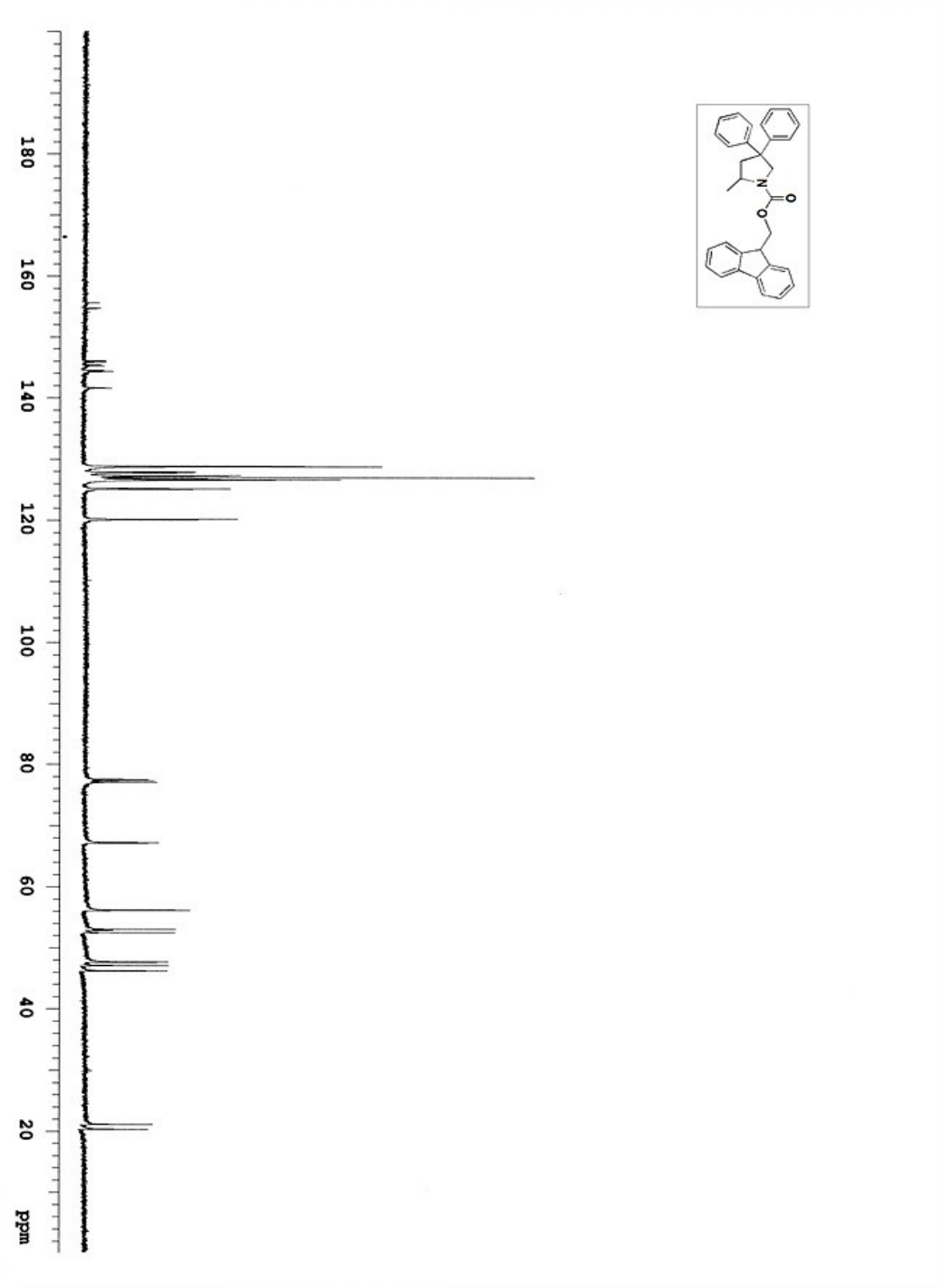

Figure 37. $^{13}C\{^{1}H\}$ NMR spectrum of **2b** in $CDCl_3$.

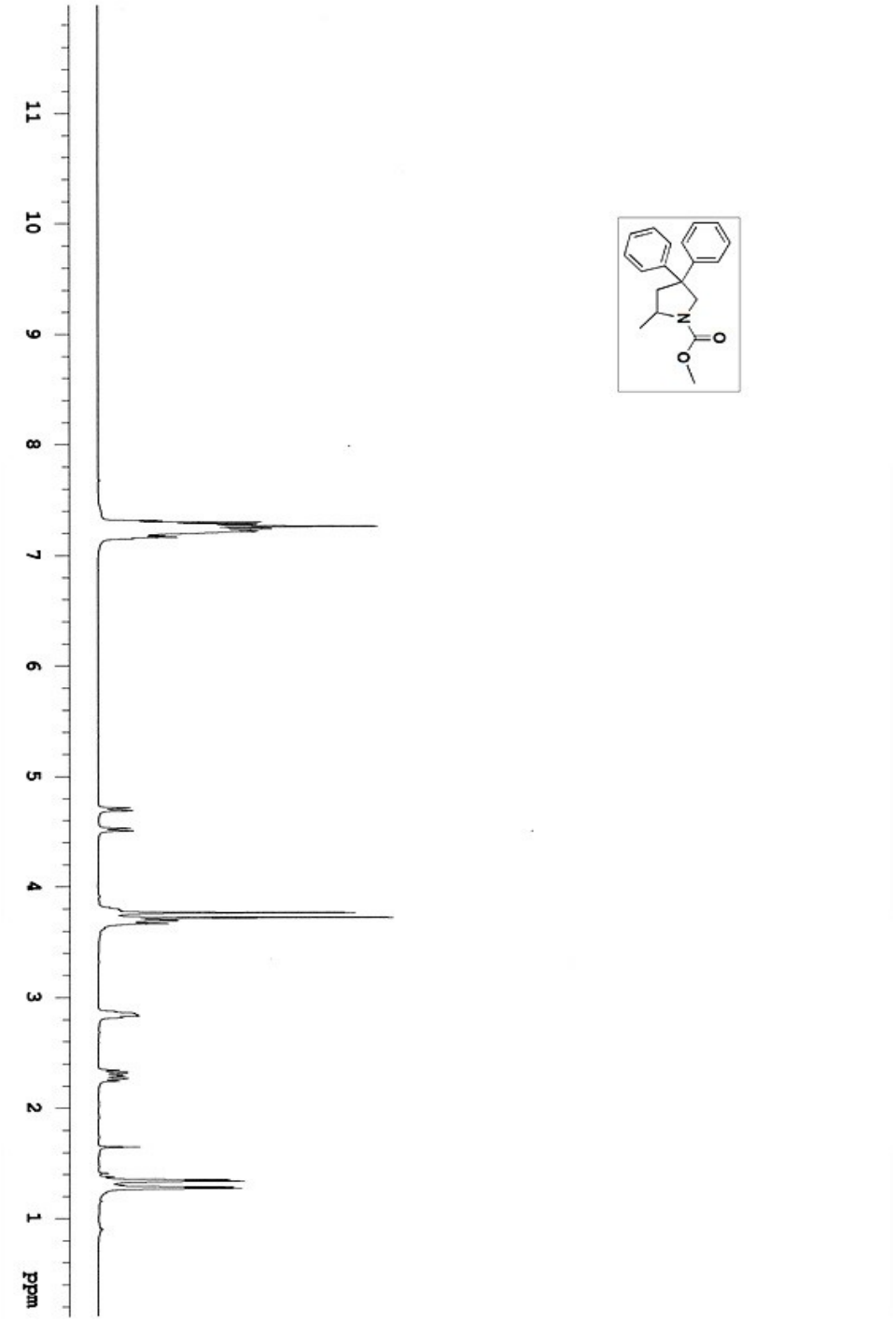

Figure 38. ^{1}H NMR spectrum of **8** in $CDCl_3$.

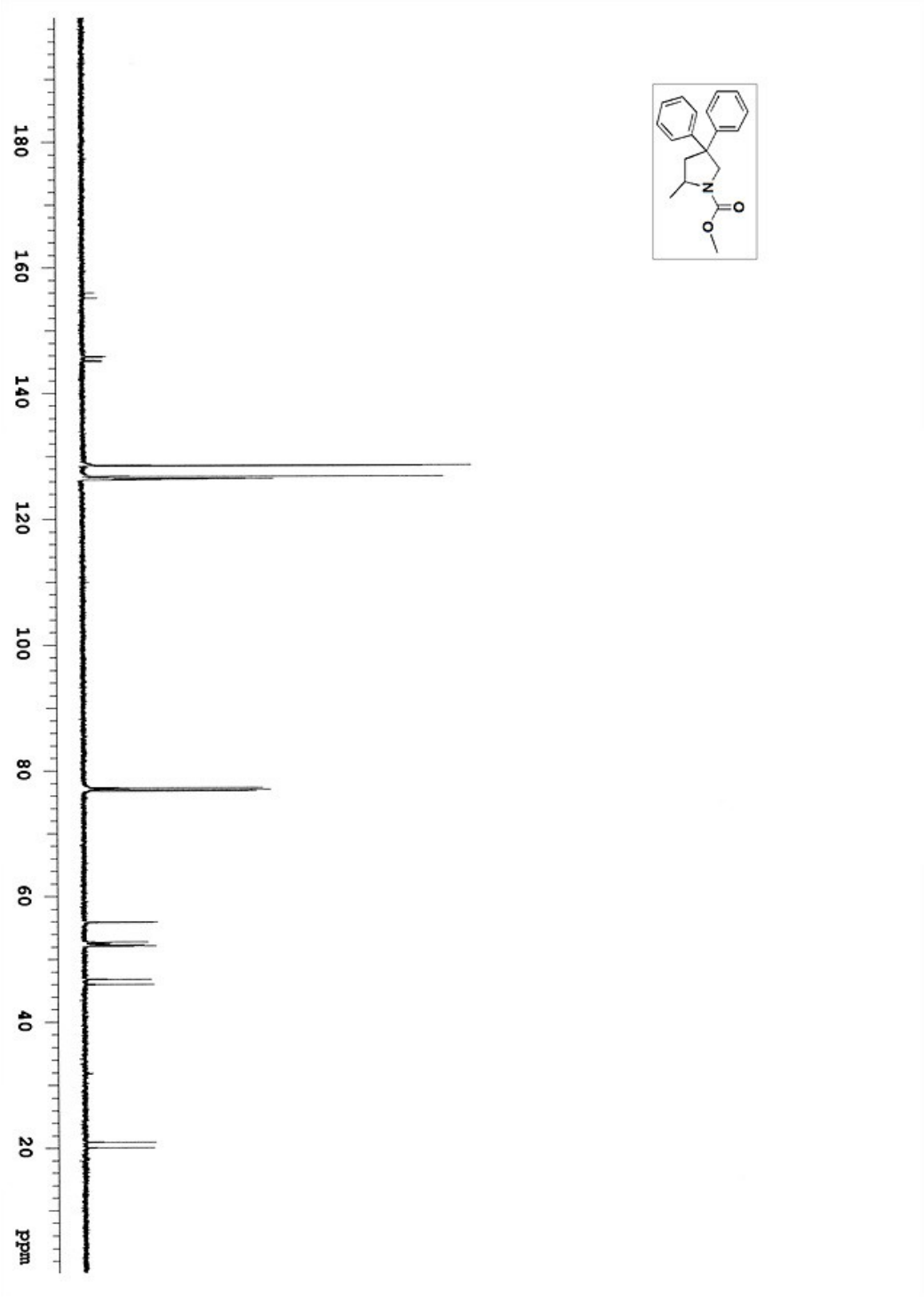

Figure 39. $^{13}C\{^{1}H\}$ NMR spectrum of **8** in $CDCl_3$.

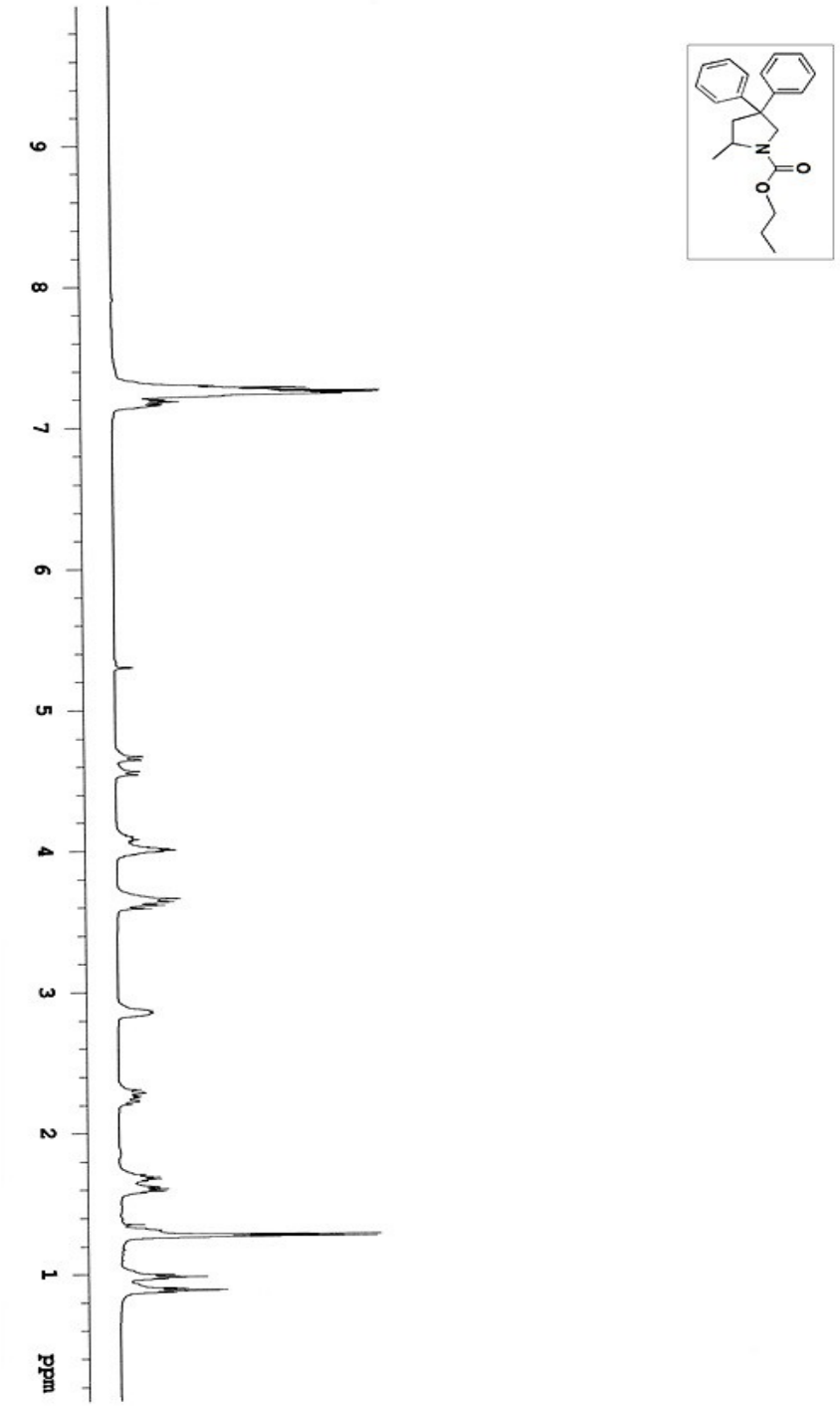

Figure 40. ^{1}H NMR spectrum of **10** in CD_2Cl_2.

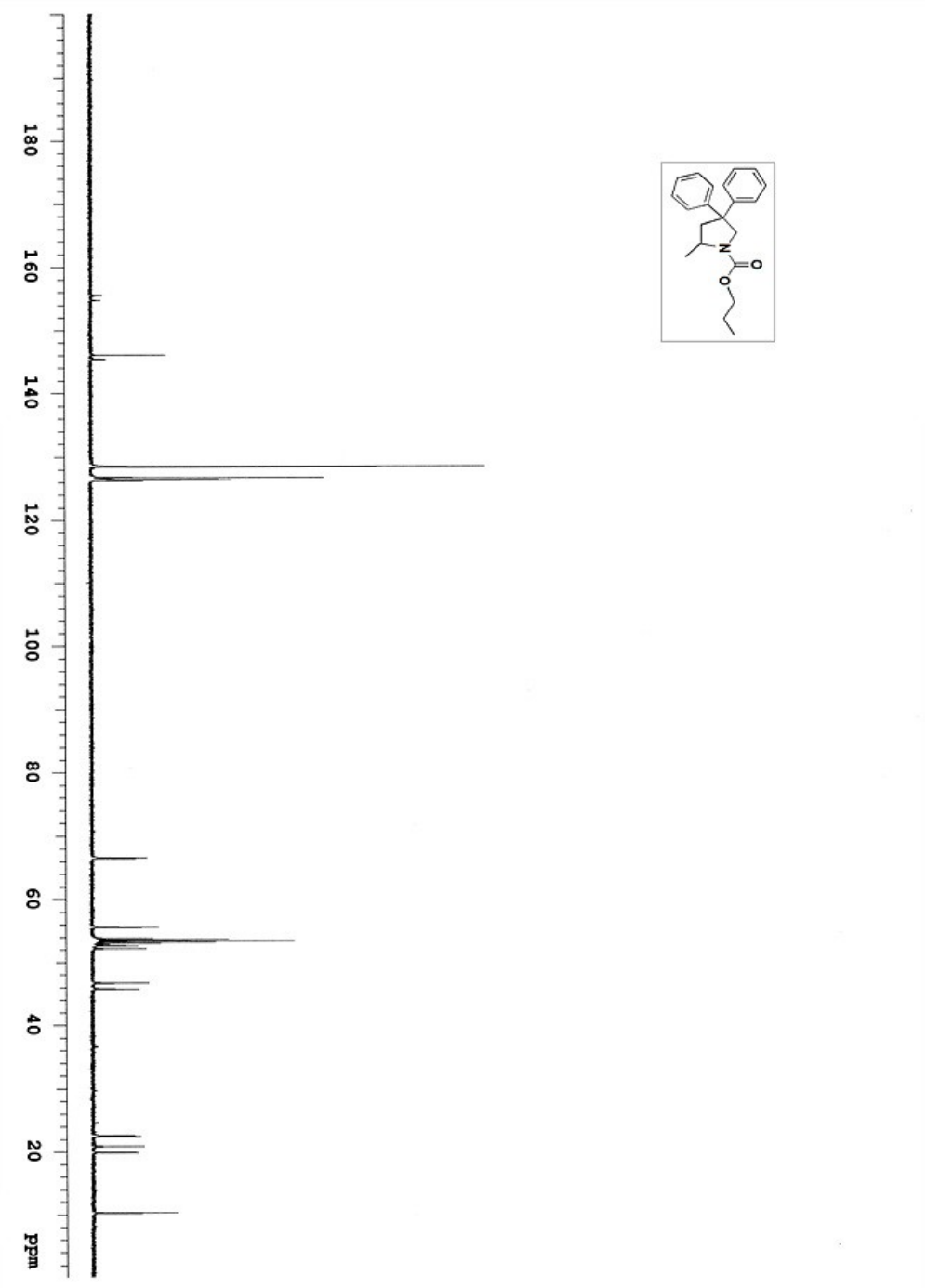

Figure 41. $^{13}C\{^{1}H\}$ NMR spectrum of **10** in $CDCl_3$**.**

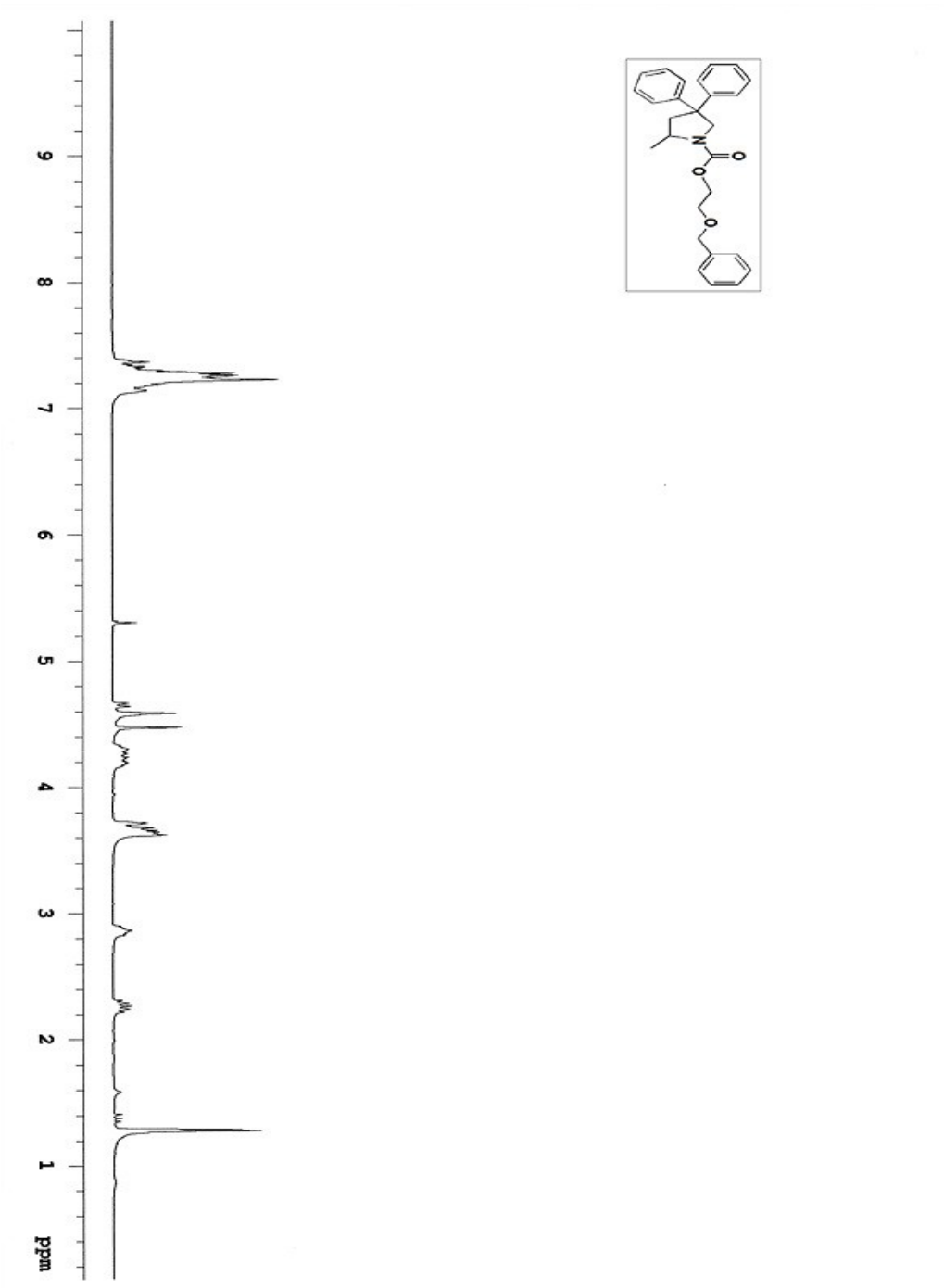

Figure 42. ^{1}H NMR spectrum of **12** in CD_2Cl_2.

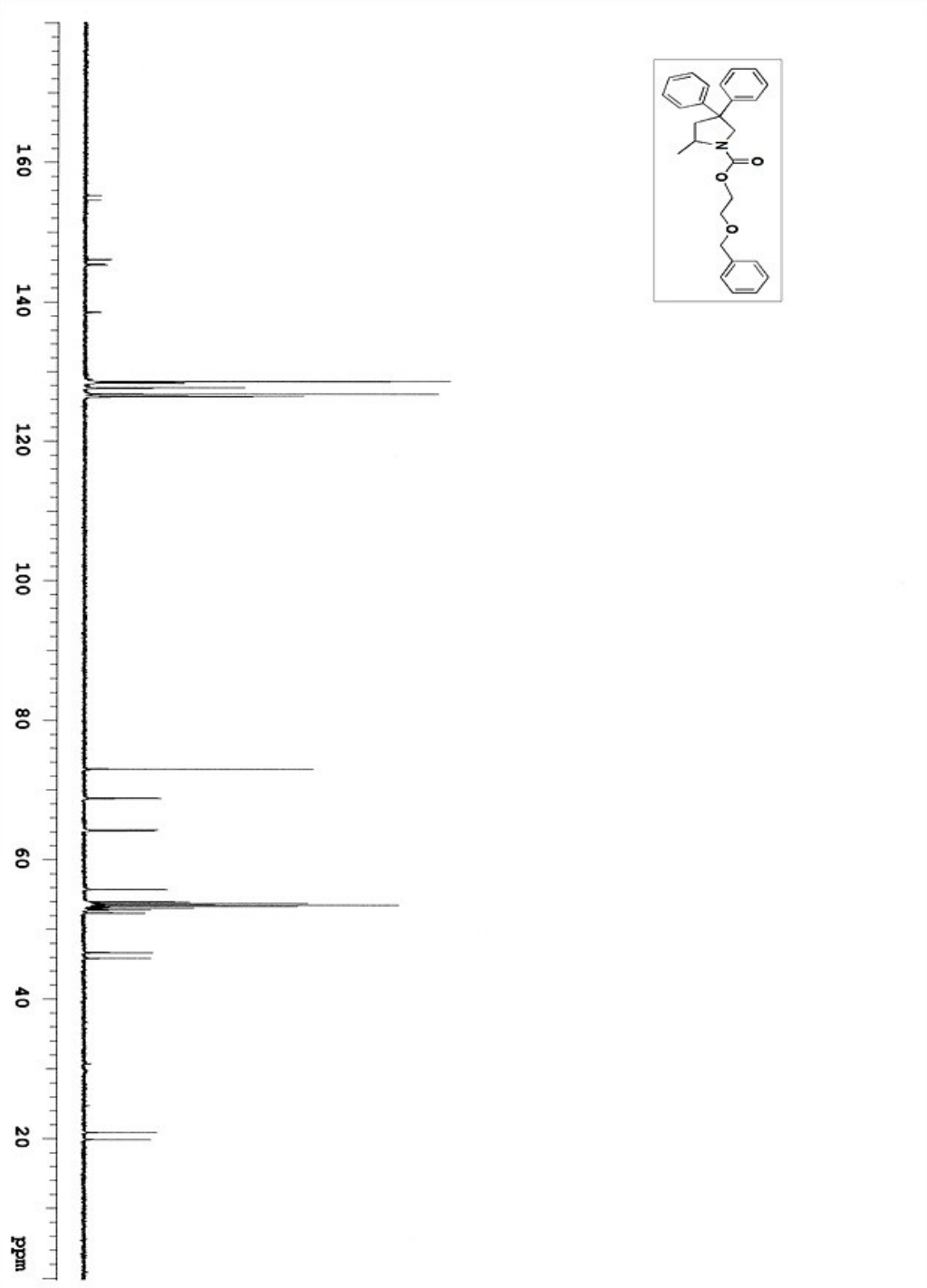

Figure 43. $^{13}C\{^{1}H\}$ NMR spectrum of **12** in $CDCl_2$.

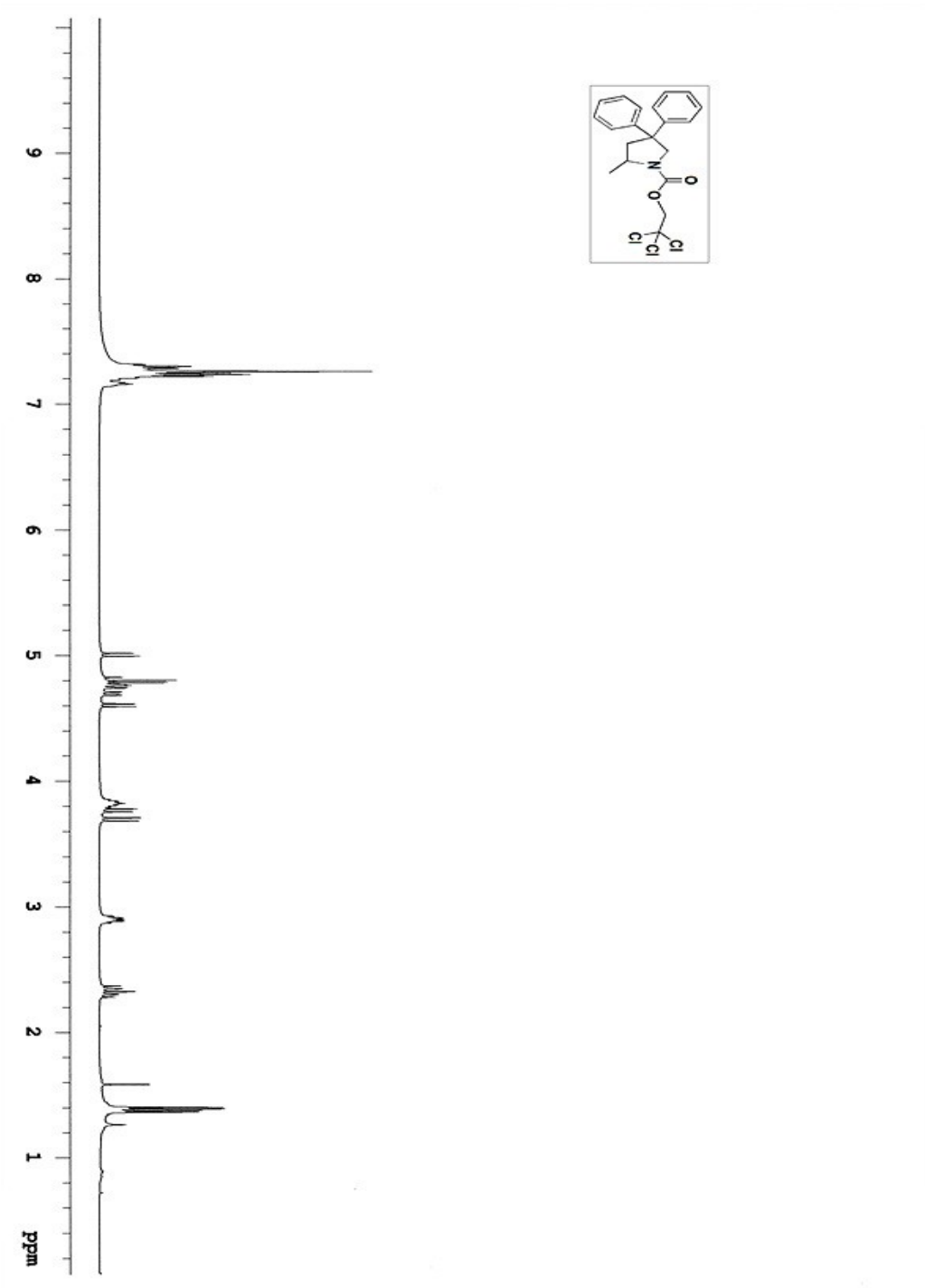

Figure 44. ^{1}H NMR spectrum of **14** in $CDCl_3$.

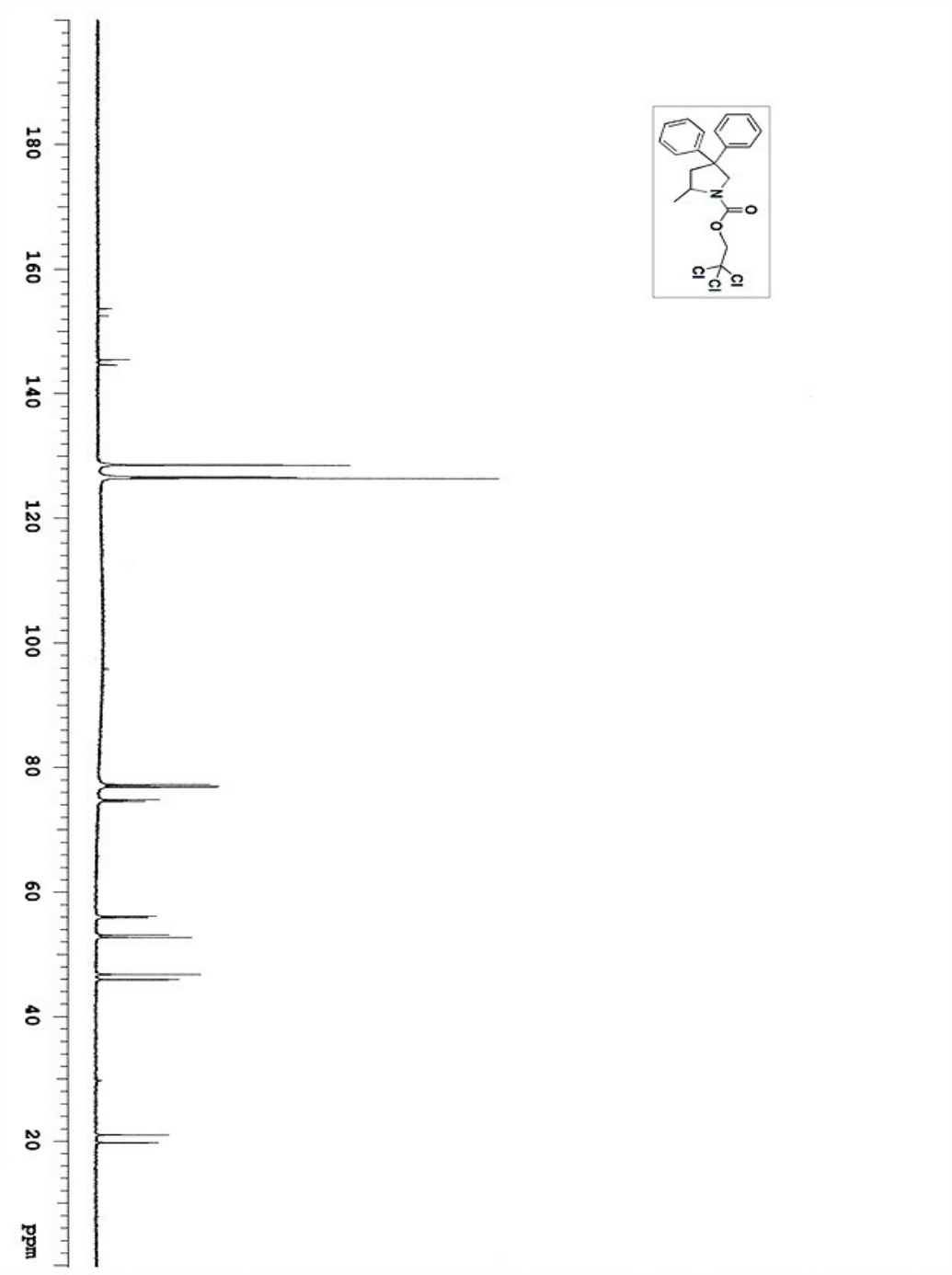

Figure 45. $^{13}C\{^{1}H\}$ NMR spectrum of **14** in $CDCl_3$.

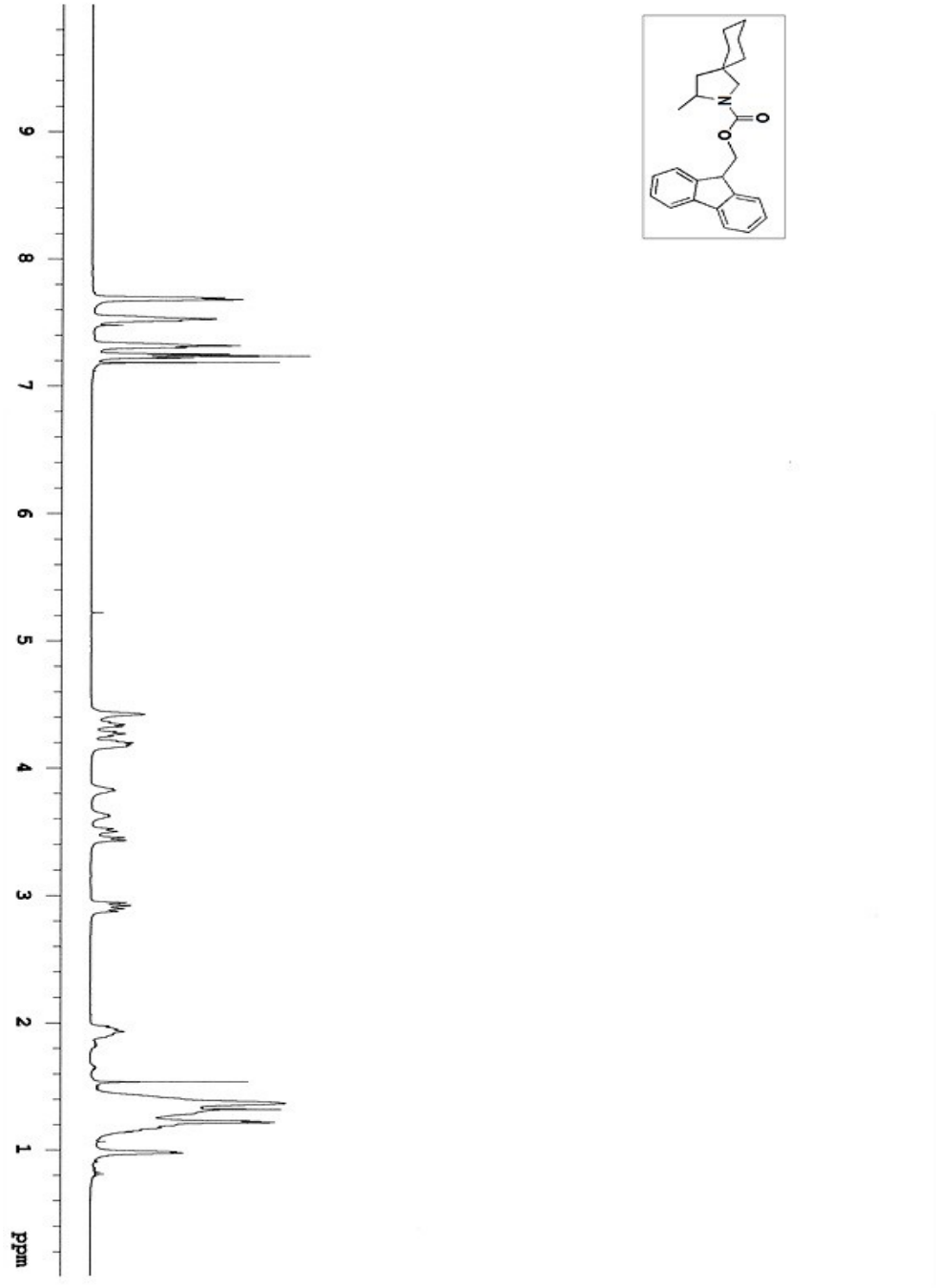

Figure 46. ^{1}H NMR spectrum of **16** in $CDCl_3$.

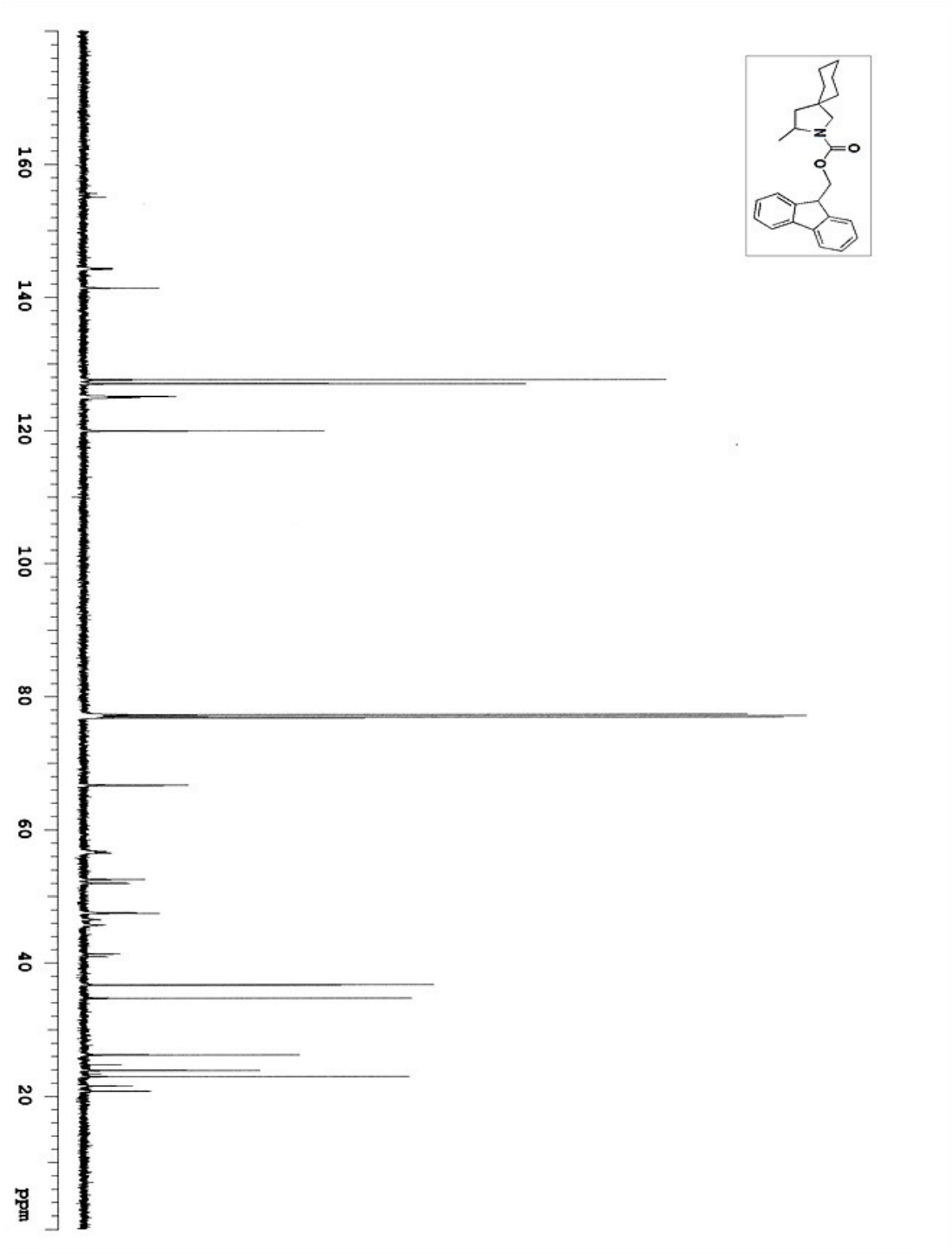

Figure 47. $^{13}C\{^{1}H\}$ NMR spectrum of **16** in $CDCl_3$.

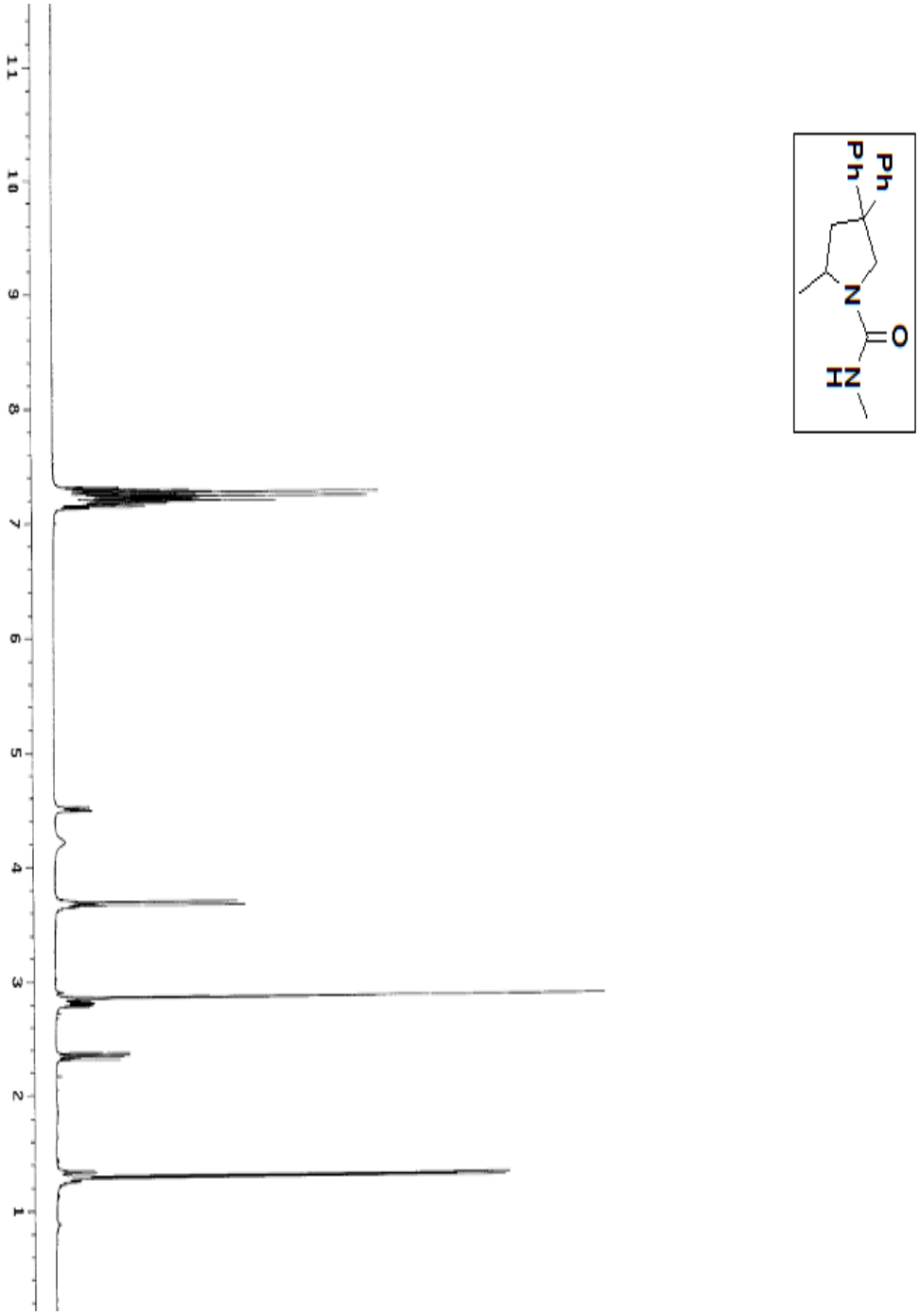

Figure 48. ^{1}H NMR spectrum of **27** in $CDCl_3$.

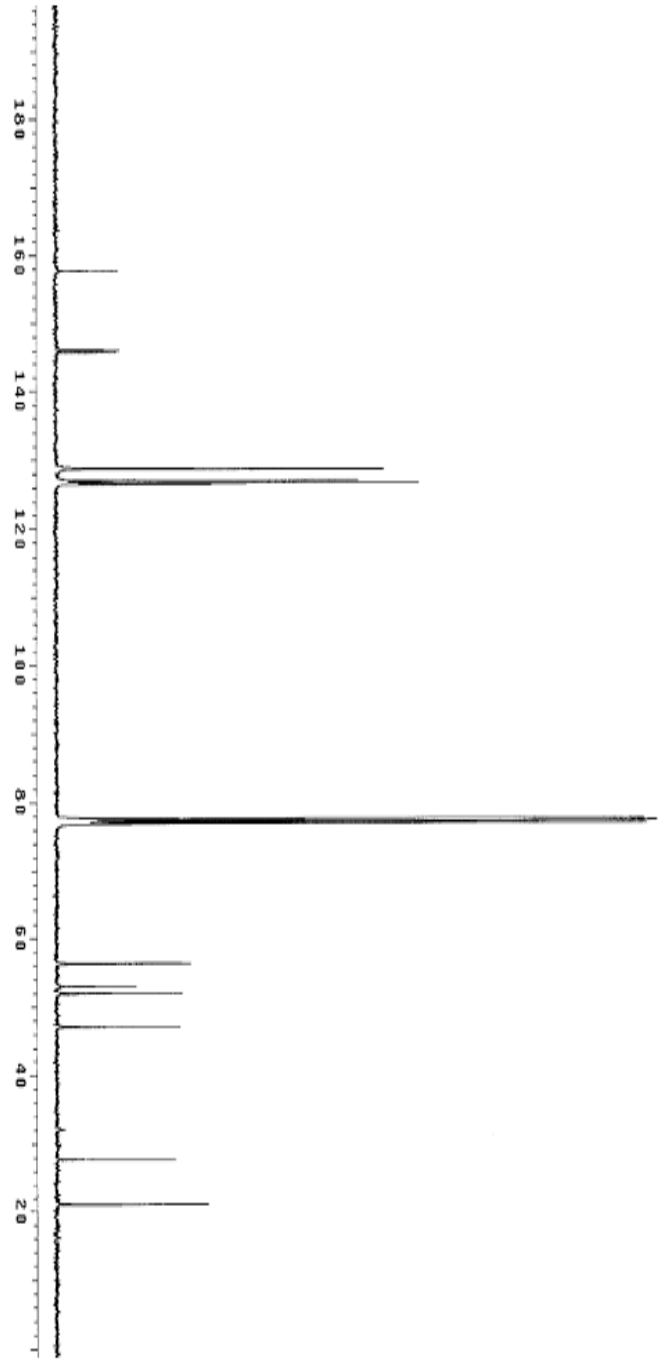

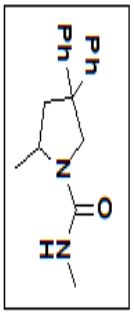

Figure 49. $^{13}C\{^{1}H\}$ NMR spectrum of **27** in $CDCl_3$.

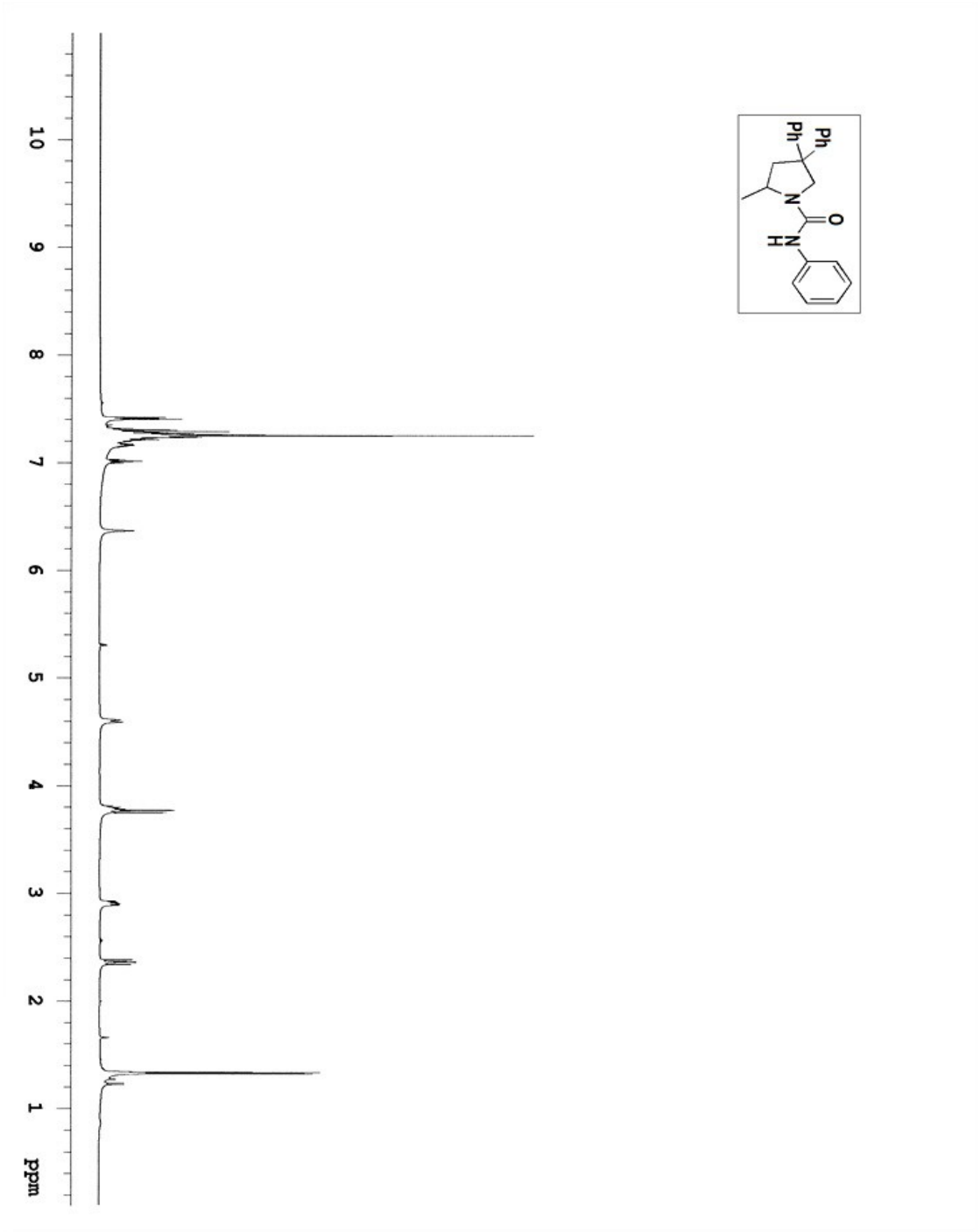

Figure 50. ^{1}H NMR spectrum of **19** in CD_2Cl_2.

Figure S28. $^{13}C\{^{1}H\}$ NMR spectrum of Phenyl 2-methyl-4,4-diphenyl-pyrrolidine-1-carboxamide in CD_2Cl_2.

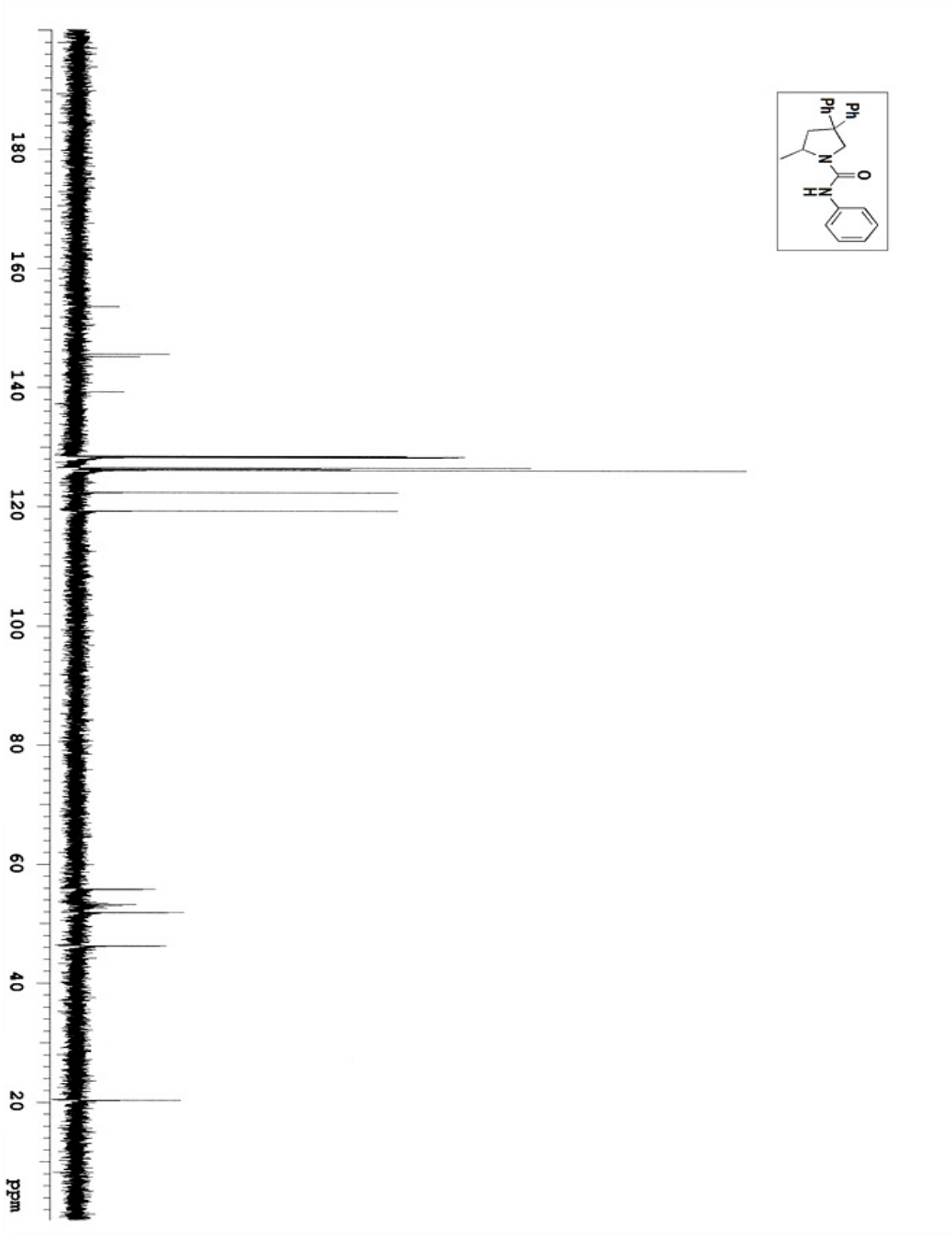

Figure 51. $^{13}C\{^{1}H\}$ NMR spectrum of **19** in CD_2Cl_2.

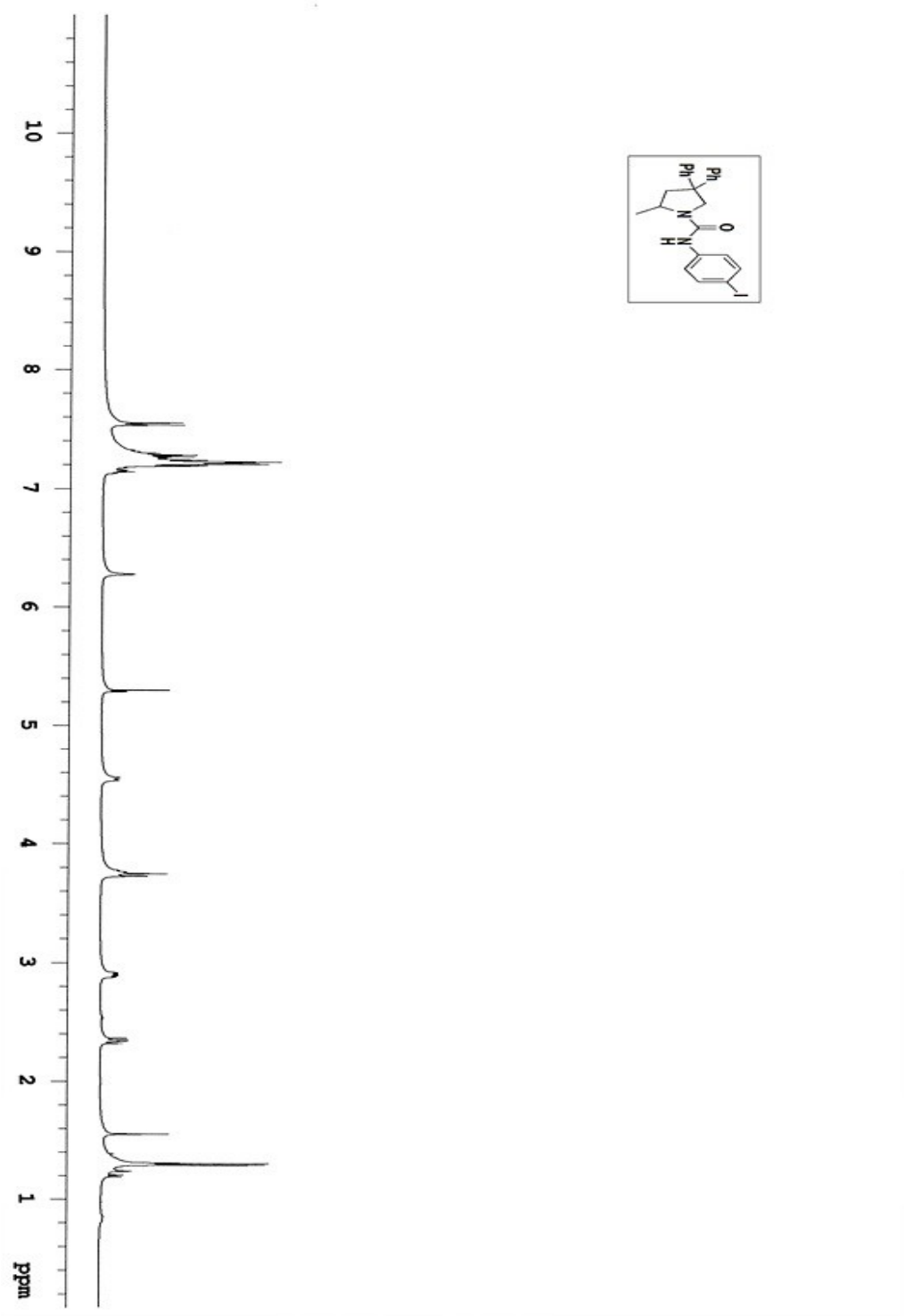

Figure 52. ^{1}H NMR spectrum of **21** in CD_2Cl_2.

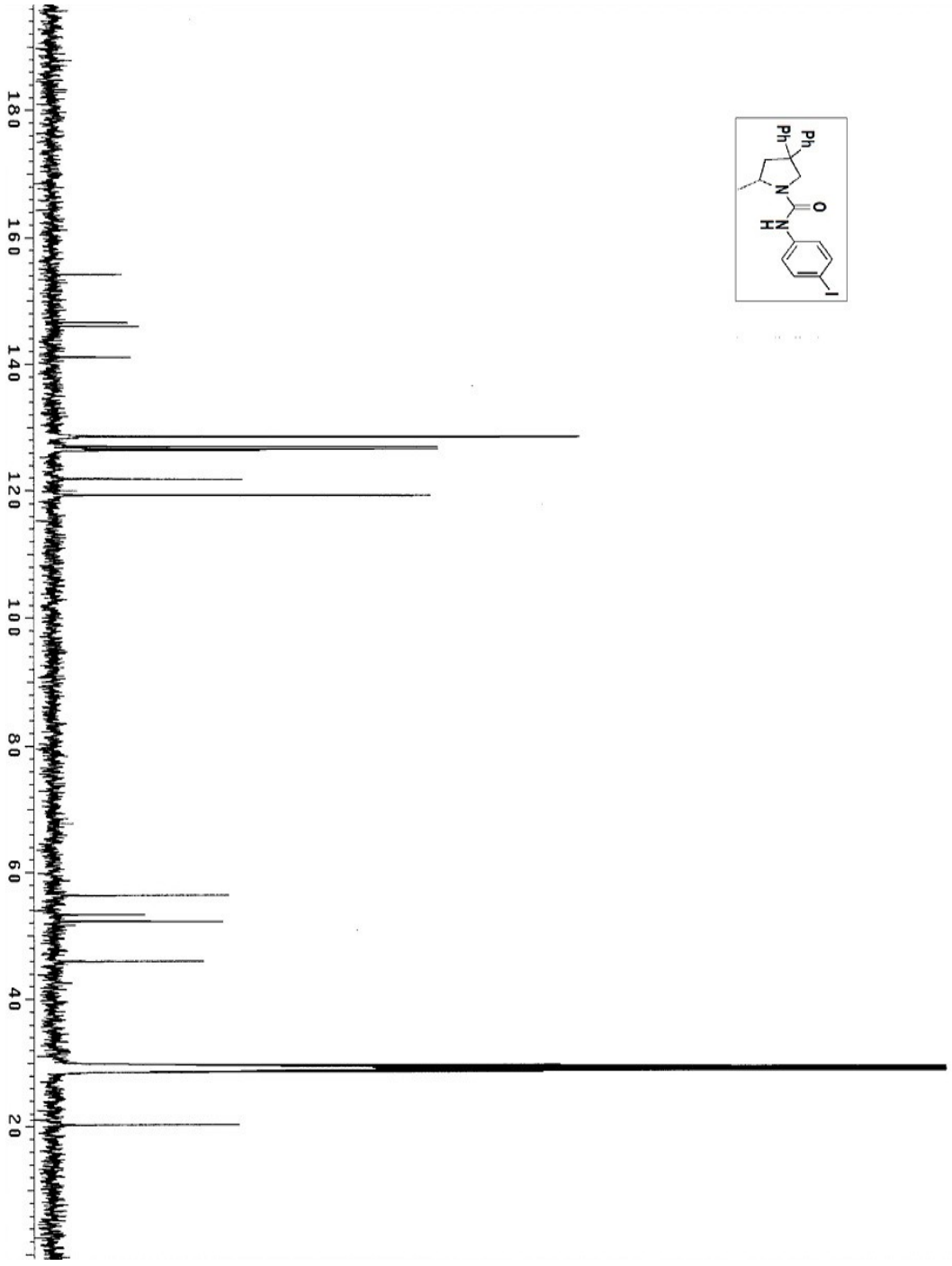

Figure 53. $^{13}C\{^{1}H\}$ NMR spectrum of **21** in $(CD_3)_2CO$.

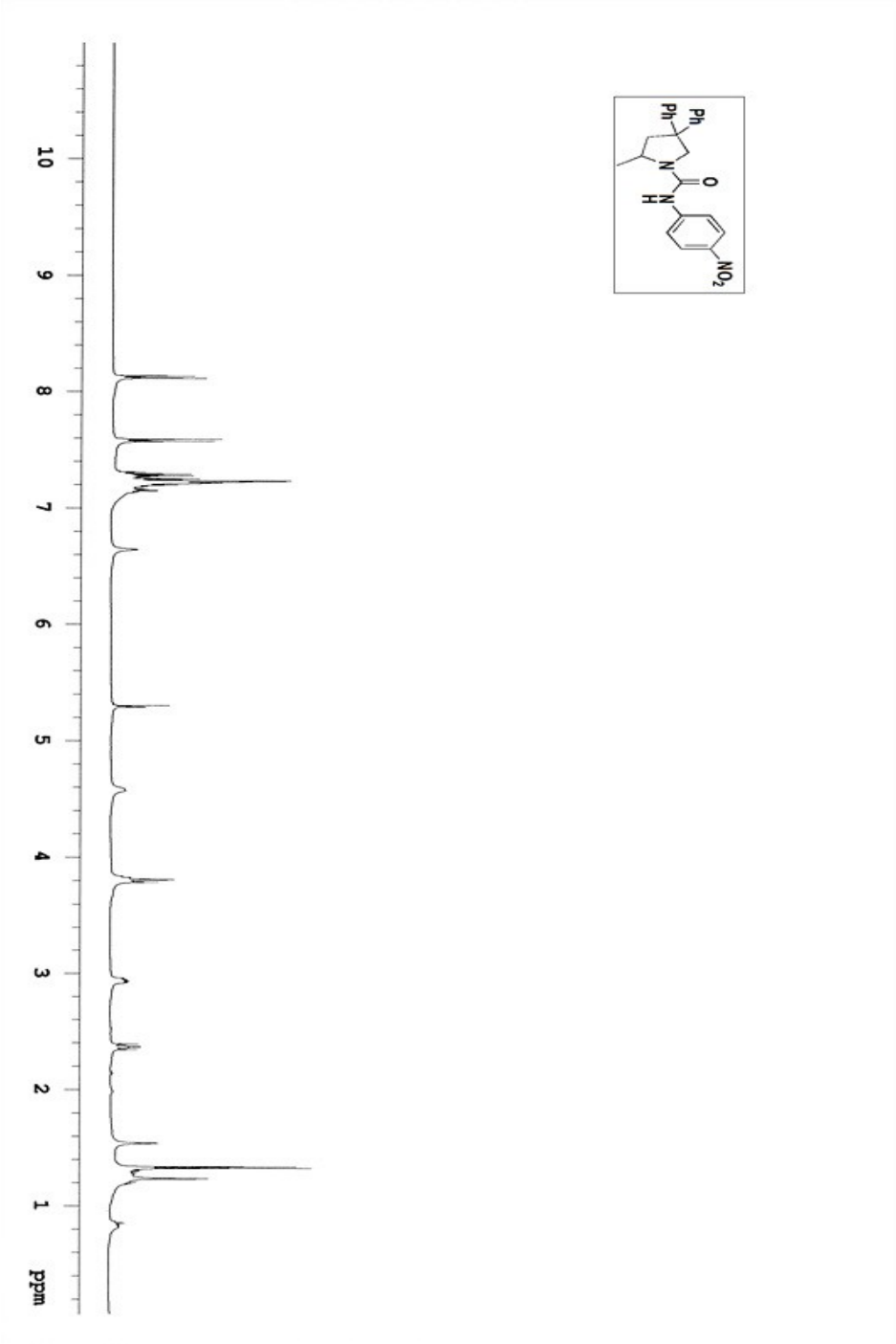

Figure 54. ^{1}H NMR spectrum of **23** in CD_2Cl_2.

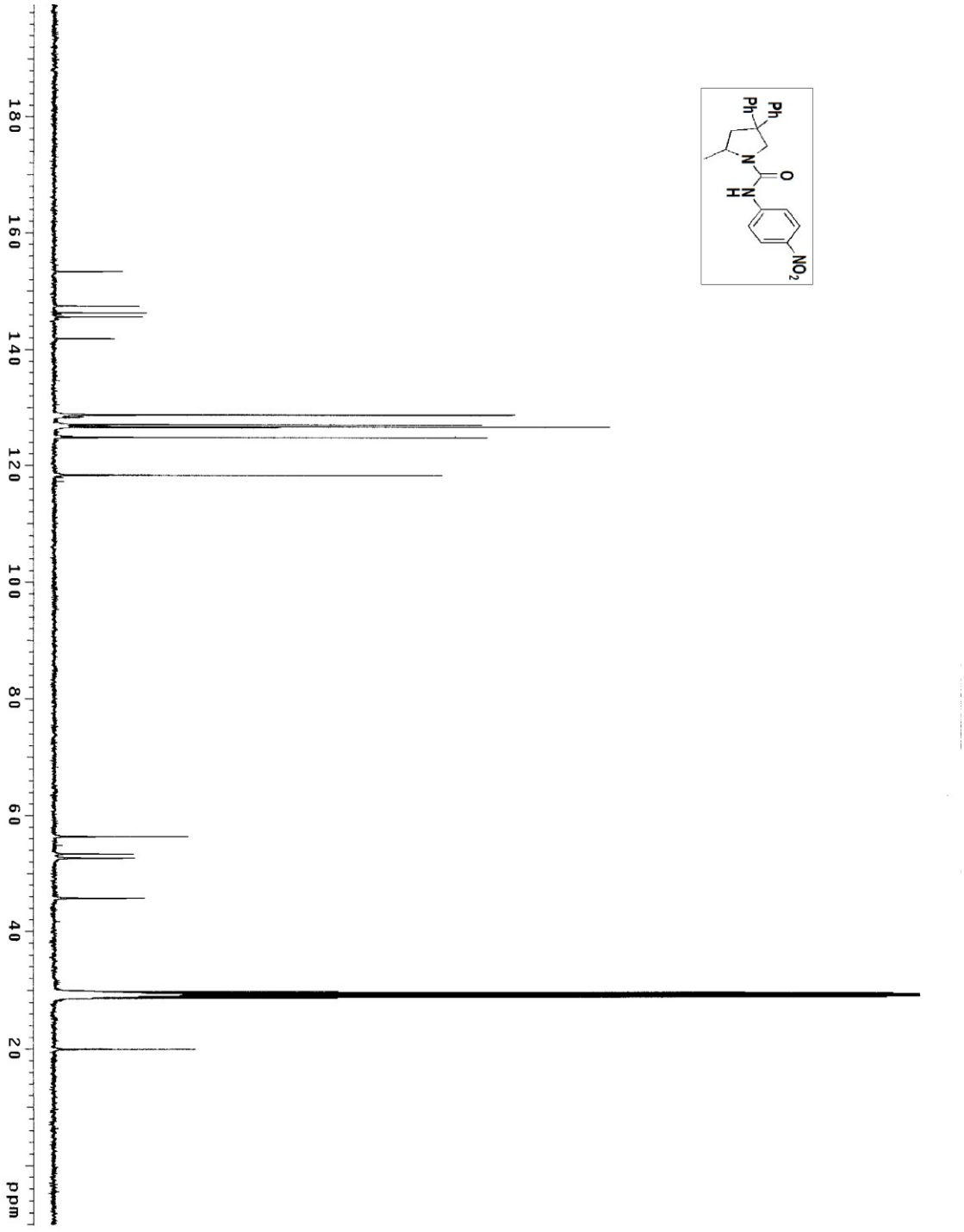

Figure 55. $^{13}C\{^{1}H\}$ NMR spectrum of **23** in $(CD_3)_2CO$.

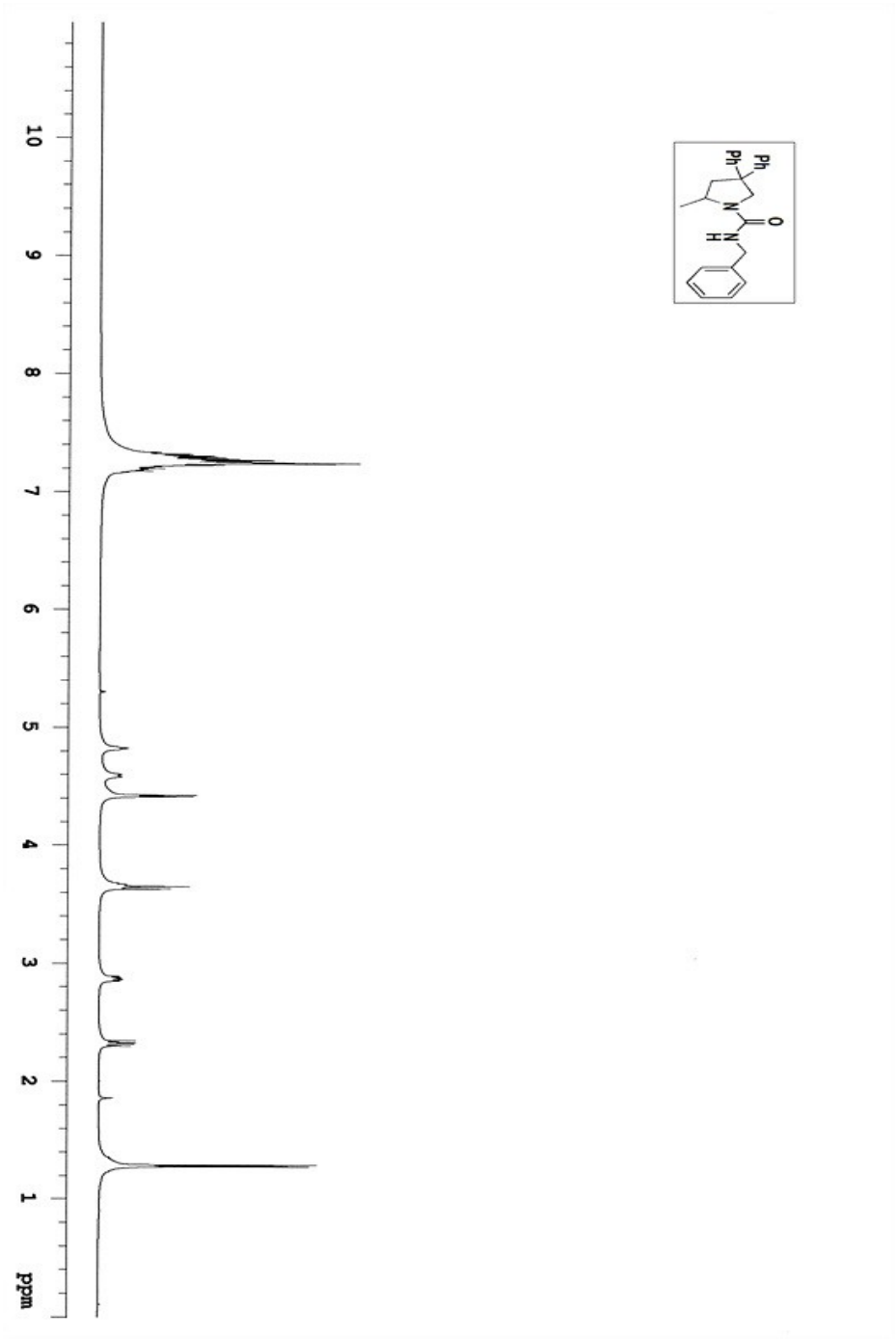

Figure 56. ^{1}H NMR spectrum of **2a** in CD_2Cl_2.

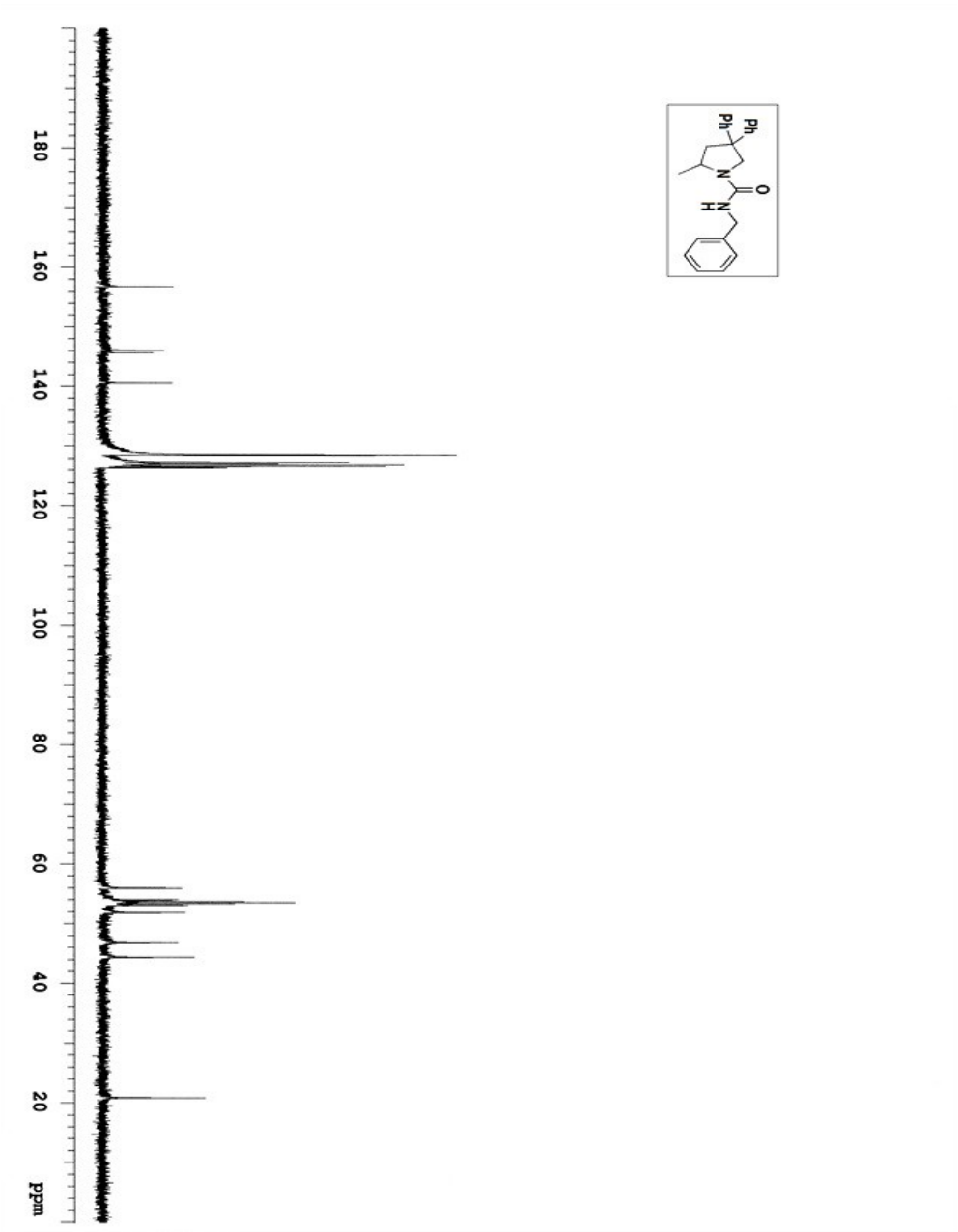

Figure 57. $^{13}C\{^{1}H\}$ NMR spectrum of **2a** in CD_2Cl_2.

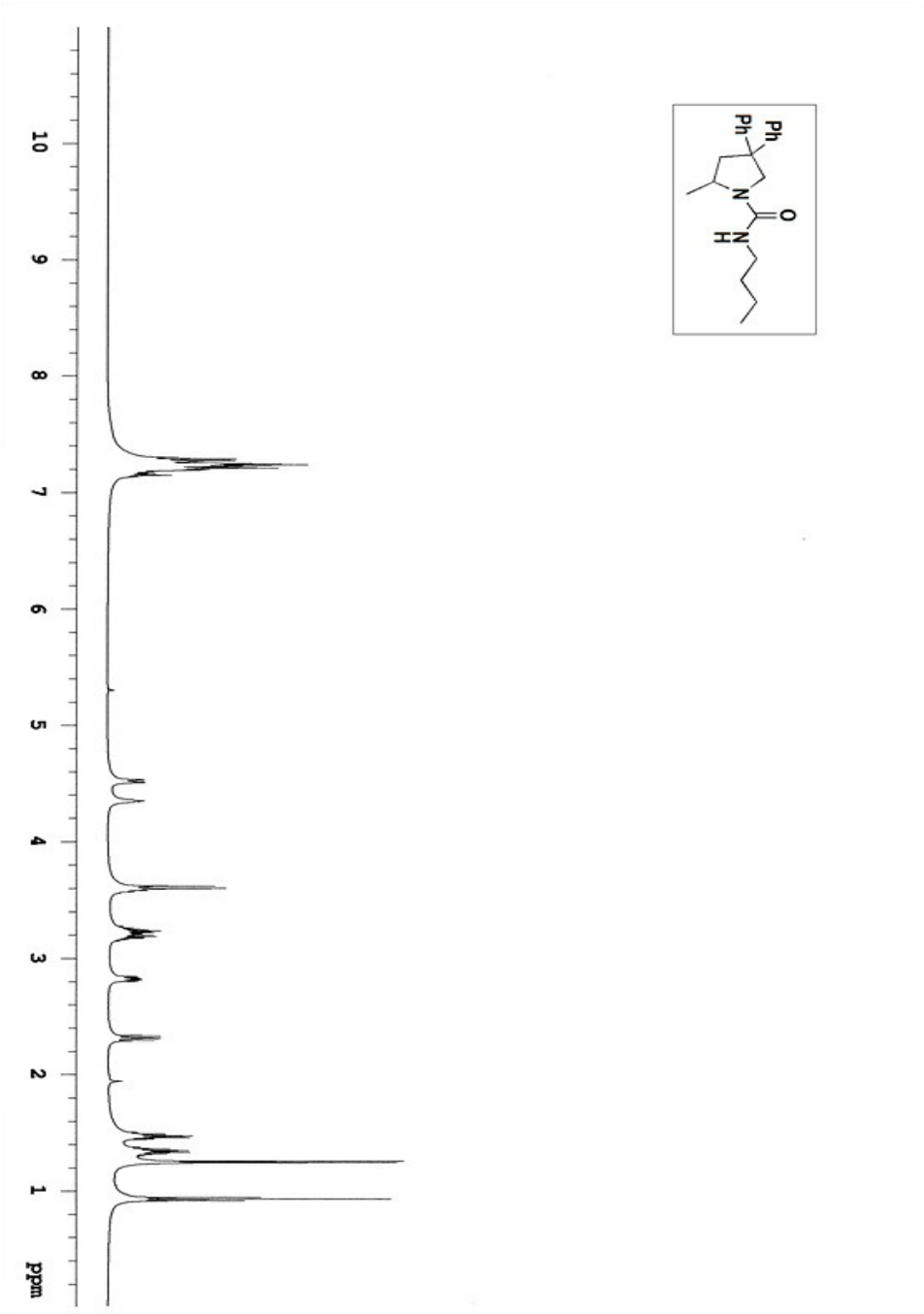

Figure 58. ^{1}H NMR spectrum of **25** in CD_2Cl_2.

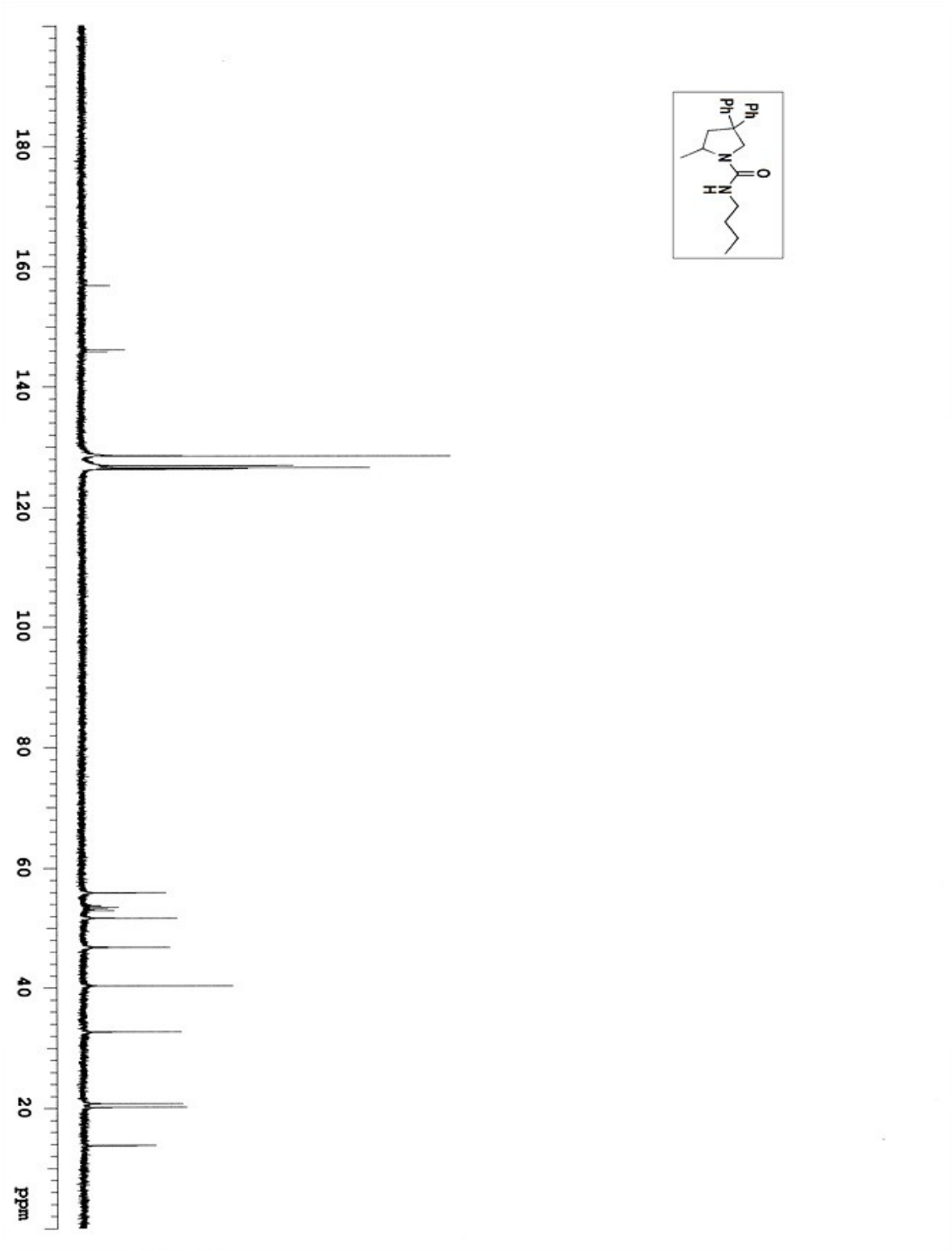

Figure 59. $^{13}C\{^{1}H\}$ NMR spectrum of **25** in CD_2Cl_2.

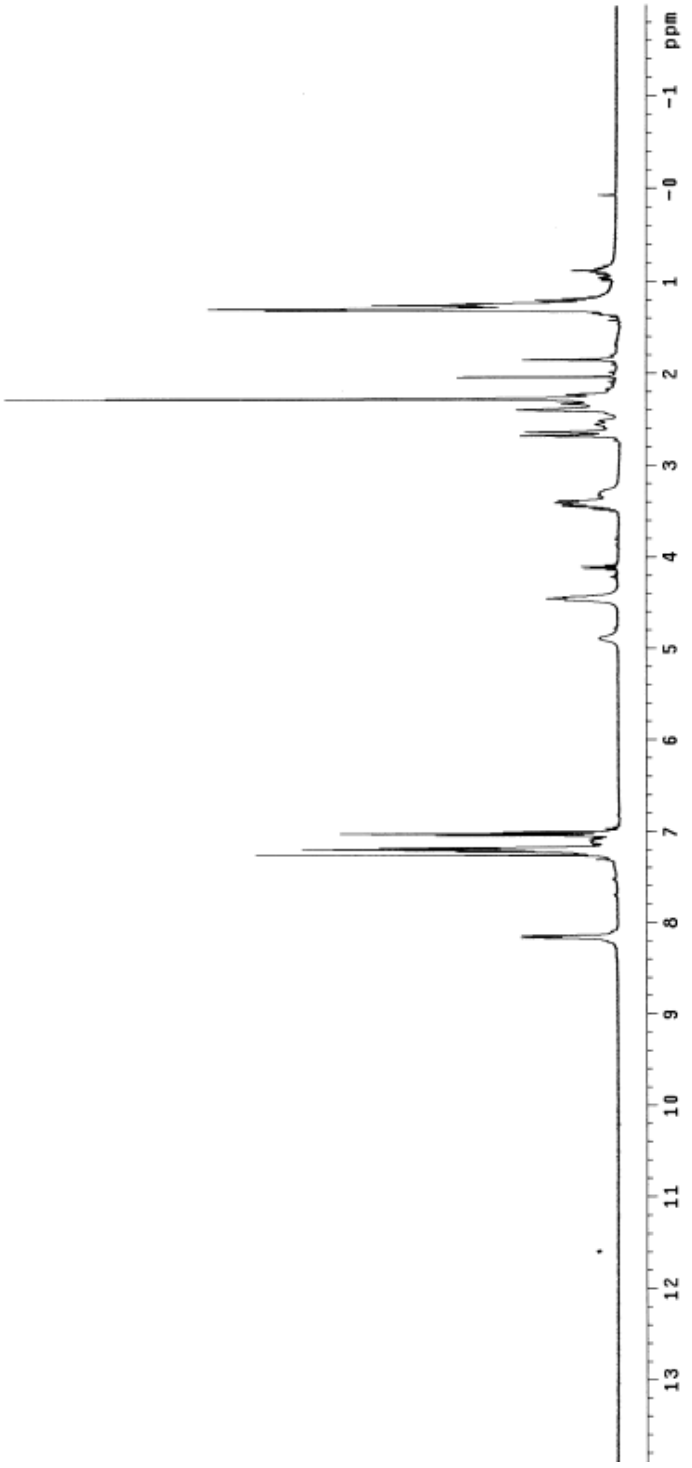

Figure 60. 1H NMR spectrum of **28** in $CDCl_3$

Chapter 2

Gold(I)-Catalyzed Enantioselective Intermolecular Hydroamination of Unactivated Alkenes

Portions of this chapter have been published: Zhang, Z.; Lee, S. D.; Widenhoefer, R. A. *Journal of the American Chemical Society* **2009**, *131*, 537

2.1 Introduction

Despite the advances regarding the enantioselective intramolecular hydroamination of unactivated alkenes, only two examples (including the work described herein) of *intermolecular* enantioselective hydroamination of unactivated alkenes have been reported.[76,89] This is because the intermolecular hydroamination of unactivated alkenes has a higher activation barrier and slower reaction rate than does intramolecular hydroamination. In addition, intermolecular hydroamination has a large negative entropy of activation relative to the intramolecular process, rendering the intermolecular transformation unfavorable at high temperatures. For these reasons, intermolecular hydroamination typically requires highly active catalysts and/or forcing conditions to achieve satisfactory rates and product yields. As a result, most of the successful reports in the area of enantioselective intermolecular hydroamination of alkenes have employed activated alkenes such as styrene,[43,44] norbornene,[45,46,90] conjugated dienes,[48] and Michael acceptors,[91,92] to compensate for the high reaction barrier while avoiding forcing conditions to attain a high level of stereoselectivity.

Intermolecular enantioselective hydroamination of activated alkenes. Hartwig has reported the enantioselective intermolecular hydroamination of vinylarenes at ambient temperature. For example, reaction of aniline with 4-(trifluoromethyl)styrene catalyzed by [((*R*)-BINAP)Pd(OSO_2CF_3)$_2$] at 25 °C produced *N*-(1-(4-(trifluoromethyl)phenyl)ethyl)benzenamine in 80 % yield with 81 % ee (eq 2.2).[43] They proposed a reaction pathway involving outer-sphere attack of the amine on a Pd(II)

coordinated alkene, followed by protonolysis of the resulting Pd–C bond. Hartwig and coworkers has also developed an iridium-catalyzed method for intermolecular enantioselective hydroamination of norbornenes with arylamines.[43] They found that inclusion of potassium bis(trimethylsilyl)amide (KHMDS) dramatically increased turnover numbers and enantioselectivity. They also found that employment of the sterically hindered SEGPHOS ligand DTBM-SEGPHOS enhanced yield while maintaining high enantioselectivity. For example, reaction of the norbornene derivative **1** with *m*-tolylamine catalyzed by a mixture of $[Ir(cyclooctene)Cl]_2$ and (*R*)-DTBM-SEGPHOS gave amine product **2** in 90 % yield with 99 % ee (eq 2.3).

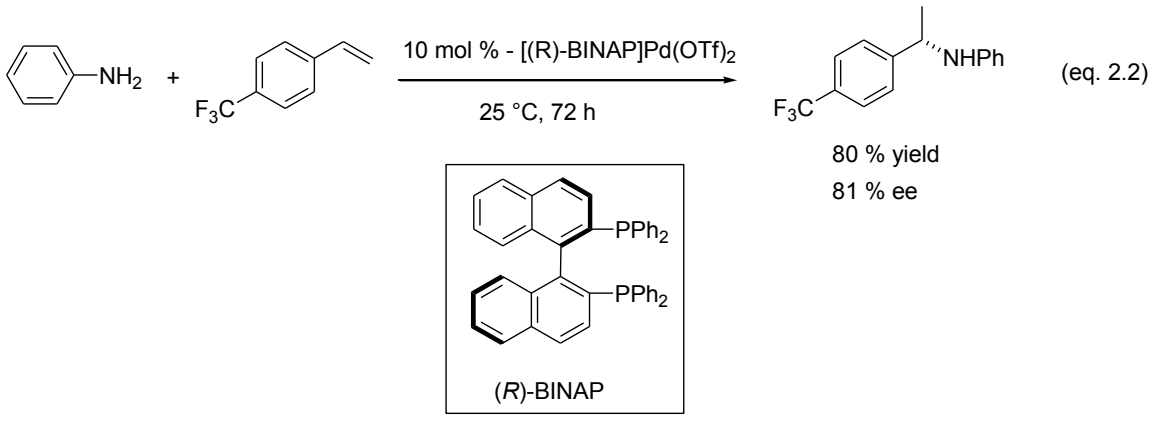

(eq. 2.2)

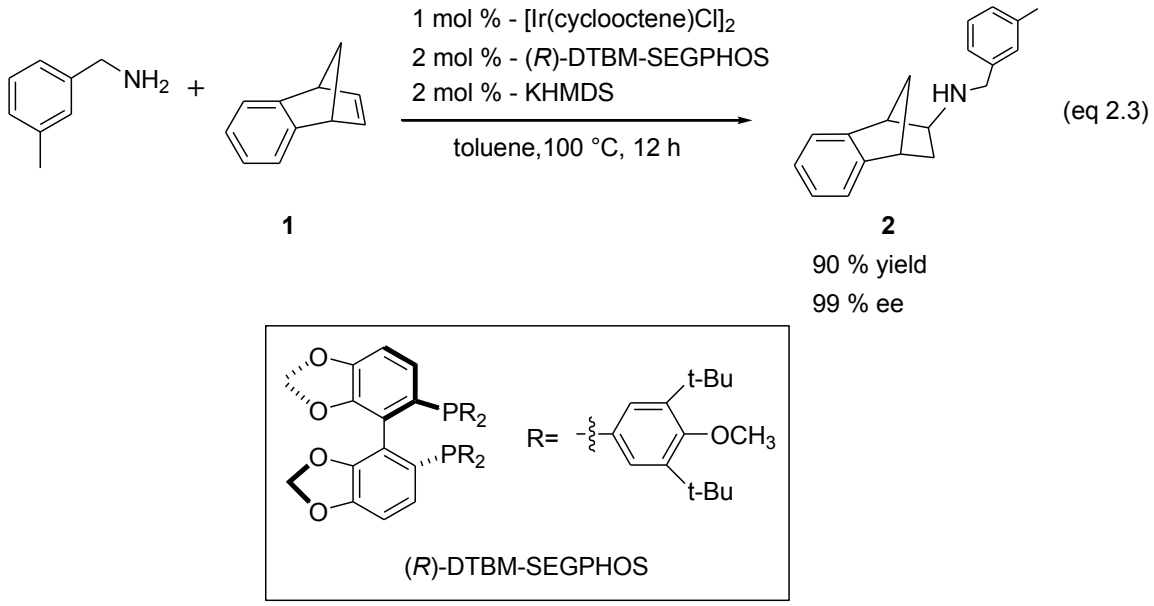

Very recently, enantioselective intermolecular hydroamination of noborbornene derivatives with aryl carboxamides and sulfonamides has been reported.[86] For example, reaction of norbornene and 4-(trifluoromethyl)benzamide catalyzed by a mixture of $[Ir(cyclooctene)Cl]_2$ and (*S*)-DTBM-SEGPHOS at 120 °C formed the hydroamination product **3** in 85 % yield and 93 % ee (eq 2.4). Palladium complexes containing the Trost ligand are effective catalysts for the intermolecular enantioselective hydroamination of dienes with aniline derivatives. For example, reaction of 1,3-cyclohexadiene with ethyl 4-aminobenzoate catalyzed by a mixture of $[Pd(\pi\text{-allyl})Cl]_2$ and Trost ligand at room temperature formed the *N*-(cyclohex-2-en-1-yl)aniline derivative **4** in 83 % yield with 95 % ee (eq 2.5).

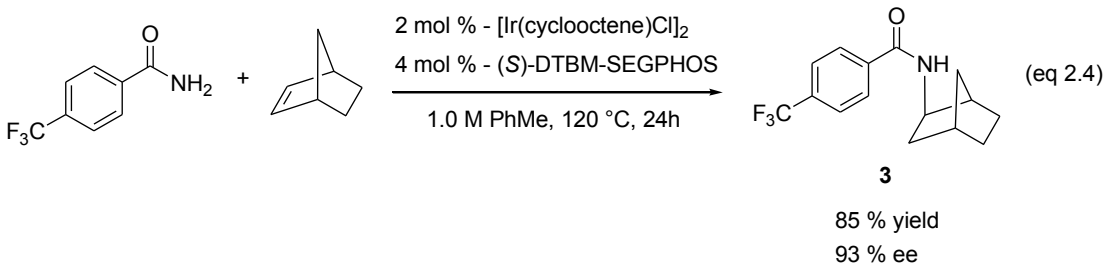

(eq 2.4)

3

85 % yield
93 % ee

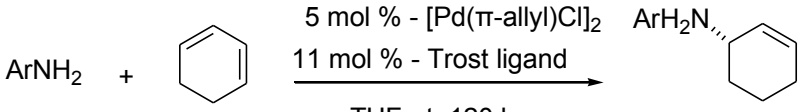

(eq 2.5)

4

Ar = p-$EtO_2CC_6H_4$

83% yield
95% ee

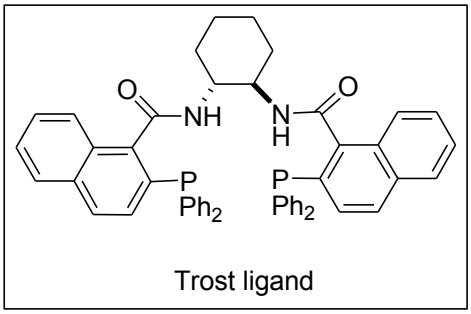

Trost ligand

Intermolecular enantioselective hydroamination of unactivated alkenes. Recently, group 4 metal complexes have been shown to catalyze the enantioselective intermolecular hydroamination of unactivated alkenes.[50] The Hultzsch group employed a binaphtholate yttrium complex as a catalyst for the intermolecular enantioselective hydroamination of unactivated 1-alkenes in good yields and modest enantioselectivity. For example, reaction of benzylamine with 1-pentene catalyzed by 5 mol % of

binaphtholate complex **6** in benzene-d_6 at 150 °C for 72 h formed *N*-benzylpentan-2-amine (**5**) in 70 % yield with 61 % ee (eq 2.6).[50]

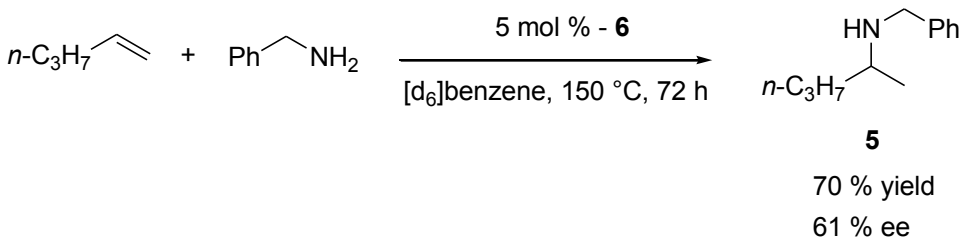

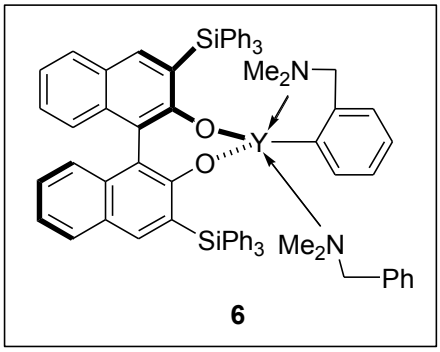

Gold-catalyzed intermolecular alkene hydroamination. Widenhoefer and coworkers have recently reported the gold(I)-catalyzed intermolecular hydroamination of unactivated 1-alkenes with imidazolidin-2-ones and related nucleophiles. The transformation was characterized by high yield and high Markovnikov regioselectivity. As an example, reaction of 1-methy-2-imidazolidinone (**7**) and 1-octene catalyzed by a 1:1 mixture of Au[P(*t*Bu)$_2$o-biphenyl]Cl (**8**) and $AgSbF_6$ at 100 °C for 24 hours formed 1-methyl-3-(2-octanyl)-2-imidazolidinone (**9**) in 96 % yield as a single regioisomer (Eq. 2.7).[76] Encouraged by this result, we aimed to establish an effective gold-catalyzed

method for the enantioselective intermolecular hydroamination of unactivated alkenes. Here we describe experiments toward this objective.

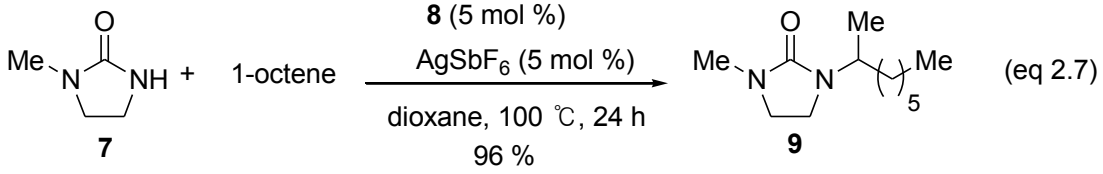

7 9 (eq 2.7)

2.2 Results and Discussion

1.2.1 Optimization and Substrate Scope

Based on the previous result depicted in eq 2.7, we targeted the reaction of 1-methyl-2-imidazolidinone (**7**) and 1-octene for gold-catalyzed enantioselective intermolecular hydroamination. In addition, the chiral bis(gold) complex [(*S*)-**L8**](AuCl)$_2$ [(*S*)-**L8** = (*S*)-3,5-t-Bu-4-MeO-MeOBIPHEP] which contained a sterically hindered axially chiral bis(phosphine) ligand was targred as the catalyzed because [(*S*)-**L8**](AuCl)$_2$ has been applied successfully in a number of enantioselective transformations.[68,77-79] In an initial experiment, reaction of **7** and 1-octene (15 equiv) with a catalytic 1:1 mixture of [(*S*)-(**L8**)(AuCl)$_2$] and $AgSbF_6$ in dioxane at 80 °C for 24 hours formed **9** with 45 % ee (eq. 2.8). We were unable to determine an accurate conversion value for this and related experiments because silica gel filtration, which was required to remove gold prior to HPLC analysis also removed the polar nucleophile **7**.

Nevertheless, based on the encouraging enantioselectivity of this experiment, further experiments were performed to improve the enantioselectivity of intermolecular hydroamination.

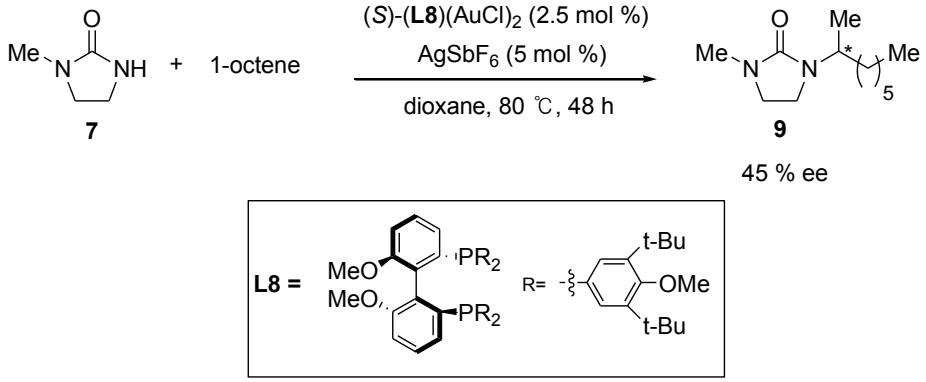

Varying the silver salt used in the hydroamination of 1-octene with **7** (Table 1, Entries 1-7) showed that AgOTf gave the highest enantioselectivity (62 %) among the silver salts tested (Table 4, entry 4). Based on this result, we employed AgOTf as a cocatalyst and examined the effect of solvent on enantioselectivity of the gold-catalyzed hydroamination of 1-octene with **7** (Table 4, entries 8-14). Concurrently, we lowered the reaction temperature from 80 °C to 60 °C and reduced the alkene loading from 15 equiv to 6 equiv under these conditions. From these experiments, we identified toluene as the most effective solvent in terms of reaction enantioselectivity (54 % ee, Table 4, entry 10). Interestingly, the enantioselectivity of gold-catalyzed hydroamination in dioxane with AgOTf under these conditions (48 % ee, Table 4, entry 11) was lower than the enantioselectivity observed in dioxane with AgOTf with the initial conditions (62 % ee,

Table 4, entry 4). Increasing the concentration of 1-octene improved the enantioselectivity of the gold-catalyzed hydroamination of 1-octene with **7** (Table 4, entries 11 and 16). Not surprisingly, the reaction of 15 equiv 1-octene and **7** in toluene showed improved enantioselectivity of 66 % relative to the 54 % ee obtained by employing 6 equiv of 1-octene (Table 4, entries 10 and 15).

Table 4. Effect of silver salt and solvent on the gold(I)-catalyzed enantioselective hydroamination of 1-Octene with **7**.

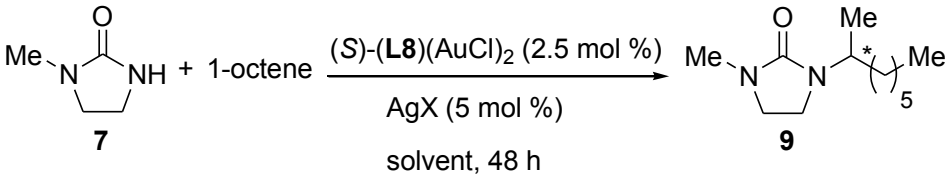

7 **9**

entry	X	sovent	1-octene amt	temp.(℃)	ee(%)[a]
1	BF_4	dioxane	15 eq.	80	46
2	OTs	dioxane	15 eq.	80	-
3	PF_6	dioxane	15 eq.	80	47
4	OTf	dioxane	15 eq.	80	62
5	ClO_4	dioxane	15 eq.	80	47
6	AsF_6	dioxane	15 eq.	80	45
7	SbF_6	dioxane	6 eq.	60	38
8	OTf	MeOH	6 eq.	60	38
9	OTf	DMSO	6 eq.	60	-
10	OTf	toluene	6 eq.	60	54
11	OTf	dioxane	6 eq.	60	48
12	OTf	CH_3NO_2	6 eq.	60	-
13	OTf	MeCN	6 eq.	60	34
14	OTf	THF	6 eq.	60	46
15	OTf	toluene	15 eq.	60	66
16	OTf	dioxane	15 eq.	60	61

[a] Enantiopurity determined by HPLC analysis on a chiral stationary phase.

Employing AgOTf as a co-catalyst, the effect of ligand and solvent on the gold-catalyzed enantioselective intermolecular hydroamination of 1-octene with **7** was further investigated. While the reactions of **7** and 1-octene employing (*S*)-DTBM-SEGPHOS ligand **12** (Figure 61) as a chiral ligand produced modest enantioselectivity (50% ee in toluene, 56% ee in dioxane; Table 5, entries 1 and 2), reactions using (*S*)-DM-SEGPHOS ligand **13**, which has the same dioxole biaryl framework as **12**, showed no reaction and/or very poor enantioselectivity (Table 5, entries 3 and 4). Gold-catalyzed hydroamination of 1-octene with **7** employing ligand **11**, which possessed a dimethyl amine substituent on the aryl group, did not form **9** (Table 5, entries 5 and 6). Gold-catalyzed hydroamination of 1-octene with **7** employing ligand **10**, which contained P-bound isopropyl groups, gave enantioselectivity up to 70 % ee (Table 5, entries 7-10). In addition, increasing the amount of 1-octene to 30 equiv from 15 equiv and changing the solvent to *m*-xylene from toluene further improved the enantioselectivity (Table 5, entries 9-12). While increasing the reaction temperature showed almost no effect on enantioselectivity of hydroamination (Table 5, entries 12, 13, and 15, and 14 and 16), increasing concentration of 1-octene led to higher enantioselectivity (Table 5, entries 3 and 5).

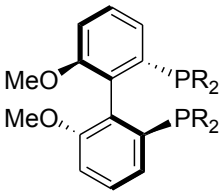	R= 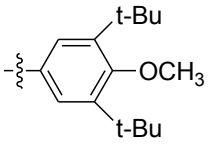	(S)-3,5-t-Bu-4-MeO-MeOBIPHEP **L8**
	R= 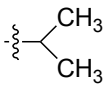	(S)-iPr-MeOBIPHEP **10**
	R= 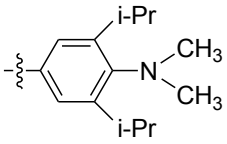	(S)-3,5-iPr-NMe_2-MeOBIPHEP **11**
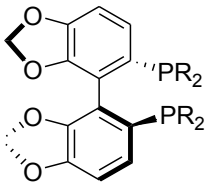	R= 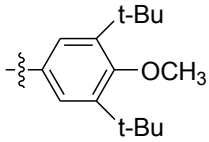	(S)-DTBM-SEGPHOS **12**
	R= 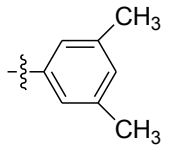	(S)-DM-SEGPHOS **13**

Figure 61. Chiral bisphosphine ligands utilized for the gold-catalyzed intermolecular enantioselective hydroamination of 1-alkenes.

Table 5. Effect of ligand and solvent on the gold(I)-catalyzed enantioselective hydroamination of 1-octene with **7**.

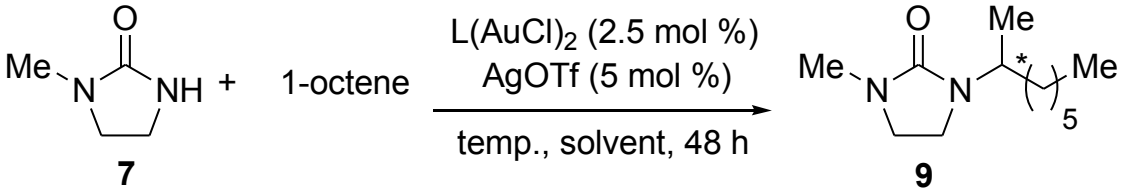

7 **9**

entry	L	solvent	temp.(℃)	1-octene amt	ee(%)[a]
1	**12**	toluene	60	15 eq.	50
2	**12**	dioxane	60	15 eq.	56
3	**13**	toluene	60	15 eq.	-
4	**13**	dioxane	60	15 eq.	7
5	**11**	toluene	60	15 eq.	-
6	**11**	dioxane	60	15 eq.	-
7	**10**	toluene	60	15 eq.	68
8	**10**	dioxane	60	30 eq.	57
9	**10**	toluene	60	30 eq.	69
10	**10**	m-xylene	60	30 eq.	70
11	**L8**	toluene	60	30 eq.	71
12	**L8**	m-xylene	60	30 eq.	74
13	**L8**	m-xylene	100	30 eq.	73
14	**L8**	m-xylene	100	60 eq.	76
15	**L8**	m-xylene	120	30 eq.	73
16	**L8**	m-xylene	120	60 eq.	75

[a] ee values determined by HPLC analysis on a chiral stationary phase. entry 12: 38 % isolated yield, entries 13-16: 100 % conversion (determined by ^{1}H NMR analysis of the crude reaction mixture)

In a preparative-scale experiment employing the optimized reaction conditions, reaction of **7** and 1-octene (60 equiv) catalyzed by [(*S*)-**L8**](AuCl)$_2$ (2.5 mol %) and AgOTf (5 mol %) in *m*-xylene at 100 °C for 48 h led to isolation of **9** in 86% yield with 76% ee (Table 6, entry 1). This catalyst system was effective for the addition of 1-alkyl or 1-aryl-imidazolidin-2-ones to unactivated and unfunctionalized 1-alkenes in good yield and with modest enantioselectivity (Table 6). Increasing the length of the alkyl chain on alkene substrates had a small effect on enantioselectivity of intermolecular hydroamination but deteriorated the reaction yield (Table 6, entries 1, 5 and 6). Alkyl substituted imidazolidin-2-ones gave better enantioselectivity than did aryl substituted imidazolidin-2-ones, and sterically hindered *t*-butyl substituted cyclic urea **21** produced the highest enantioselectivity of 78 % (Table 6, entry 4).

Table 6. Enatioselective intermolecular hydroamination of 1-alkenes with imidazolidin-2-ones catalyzed by a mixture of [(*S*)-**L8**]$(AuCl)_2$ (2.5 mol %) and AgOTf (5 mol %) in *m*-xylene at 100 °C for 48 h.

entry	cyclic urea	alkene[a]	product	yield(%)[b]	ee(%)[c]
	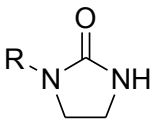	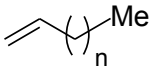	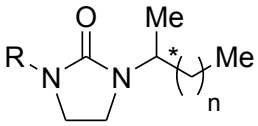		
1	R = Me	n = 5	**9**	86	76
2	R = Ph	n = 5	**14**	80	71
3	R = 4-FC_6H_4	n = 5	**15**	81	74
4	R = *t*-Bu (**21**)	n = 5	**16**	89	78
5	R = Me	n = 7	**17**	83	73
6	R = Me	n = 9	**18**	76	75
		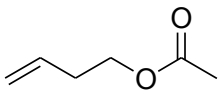	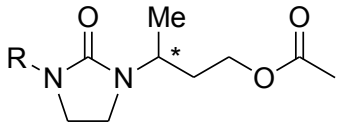		
7[d]	R = Me	**20**	**19**	17[e]	19

[a]Amount of alkene : 60 eq. [b] isolated yield of >95% purity. [c] enantiopurity determined by HPLC analysis on a chiral stationary phase. [d]Amount of alkene : 20 eq.
[e] % conversion.

Unfortunately, functionalized alkenes or nucleophiles other than imidazolidin-2-one failed to undergo effective gold-catalyzed intermolecular hydroamination employing these conditions (Figure 63 and Table 6, entry 7). The failures of hydroamination with fuctionalized alkenes (**24** and **25**) was attributed to solvent effect as the large excess of polar 1-alkene leads to significant perturbation of the solvent system. There is often a pronounced dependence on the basicity of the nucleophile in the late transition metal catalyzed intermolecular hydroamination of alkenes, which typically require weakly basic

amine derivatives as nucleophiles.[93,94] The pK_a of the conjugate acid of imidazolidin-2-one is ~14.2, which is higher than that of the conjugate acid of 1-(4-methoxyphenyl)imidazolidine-2,4-dione **23** (pK_a = ~9.1) and oxazolidin-2-one **22** (pK_a = ~13.0) and is similar to that of the conjugate acid of 1-methylimidazolidine-2-thione **26** (pK_a = ~14.4). This observation suggests that the inability of nucleophiles **22**, **23**, and **26** to undergo gold-catalyzed intermolecular hydroamination under our optimized conditions is not readily explained by the normal pK_a dependence of transition metal-catalyzed hydroamination. Also, sterically hindered 1- *t*-butyl imidazolidin-2-one (**21**) underwent facile gold-catalyzed hydroamination with 1-octene (Table 6, entry 4), indicating that the effect of steric hindrance at this site is minimal and, therefore, does not explain the lack of reactivity of **23**.

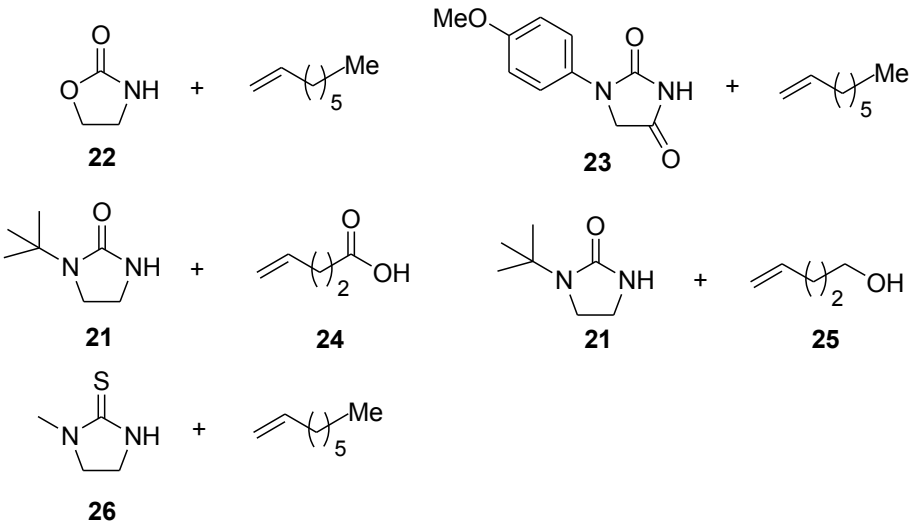

Figure 62. Substrate combinations that failed to undergo gold-catalyzed enantioslective intermolecular hydroamination under our optimized conditions.

2.2.2 Mechanism

As described in Chapter 1 for the gold-catalyzed intramolecular hydroamination of unactivated alkenes, gold-catalyzed intermolecular hydroamination of alkenes is thought to proceed via outer-sphere attack of the amine nucleophile on a coordinated alkene, followed by protolytic cleavage of the Au–C bond to produce the alkylamine product (Scheme 2.1). We observed that excess alkene was essential to achieve high reactivity, which can be explained based on the mechanism. Increasing the concentration of alkene relative to amine would favor formation of the Au(I)-alkene complex (**I**) rather than the Au(I)-amine complex (**II**) preventing catalyst poisoning by the amine substrate.[91-93] As a result, higher yield of hydroamination product can be expected by employing excess alkene. However, it remains unclear what influence the excess alkene has on the improved enantioselectivity observed under these conditions.

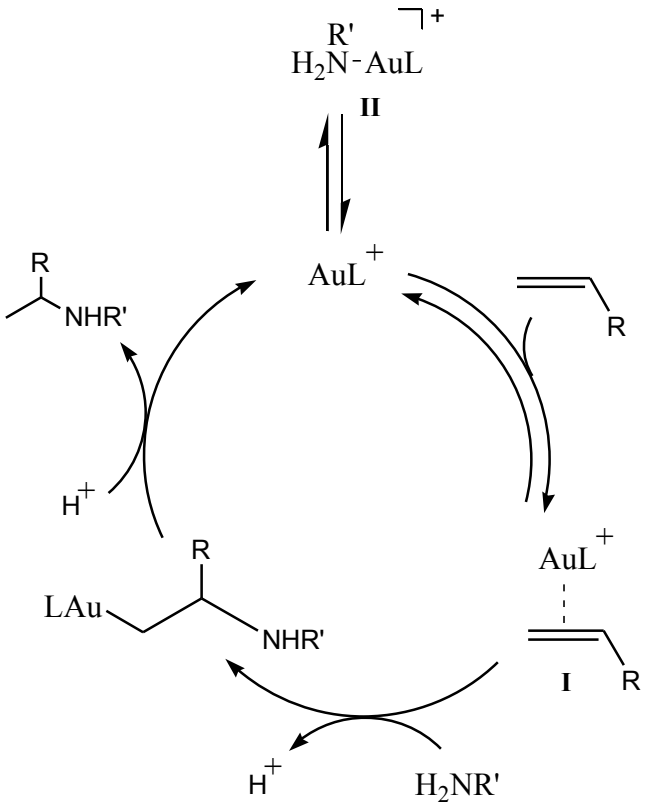

Scheme 2.1

2.3 Experimental Section

2.3.1 General Methods

Reactions were performed under a nitrogen atmosphere employing standard Schlenk and/or drybox techniques unless specified otherwise. Catalytic reactions were performed in sealed heavy-walled pressure tubes under an atmosphere of dry nitrogen unless noted otherwise. NMR spectra were obtained on Varian spectrometers operating at 400 MHz for ^{1}H NMR and 101 MHz for ^{13}C NMR in $CDCl_3$ at 25 °C unless noted

otherwise. IR spectra were obtained on a Nicolet Avatar 360-FT IR spectrometer. Gas chromatography was performed on a Hewlett-Packard 5890 gas chromatography equipped with a 15 m or 25 m polydimethylsiloxane capillary column and FID detector. Chiral HPLC was performed on a Hewlett-Parkard chromatograph equipped with a 0.46 cm x 25 cm Chiralpak AD-H column. Column chromatography was performed employing 230-400 mesh silica gel (Silicycle). Thin layer chromatography (TLC) was performed on silica gel 60 F_{254} (EMD Chemicals Inc.). All solvents were purchased from Aldrich or Acros in anhydrous form and used as received. All reagents were purchased from major suppliers and used as received.

2.3.2 Gold(I)-Catalyzed Enantioselective Intermolecular Hydroamination of 1-Alkenes.

1-Methyl-3-(octan-2-yl)imidazolidin-2-one (9; Table 6, entry 1). A suspension of **7** (20 mg, 0.20 mmol), 1-octene (1.3 g, 12 mmol), [(*S*)-**L8**]$(AuCl)_2$ (8.0 mg, 5.0×10^{-3} mmol), and AgOTf (2.6 mg, 1.0×10^{-2} mmol) in *m*-xylene (0.5 mL) was stirred at 100 °C for 48 h. The crude mixture was filtered through a plug of silica gel, concentrated, and chromatographed (hexanes–EtOAc = 5:1 $\rightarrow$ 1:1) to give **9** (37 mg, 86%) as a colorless oil. The enantiopurity of **9** (76% ee) was determined by HPLC analysis employing a chiral solid support (95:5 hexanes/isopropanol, 0.5 mL/min; Figure 20).

All remaining enantiomericially enriched cyclic ureas were synthesized employing a procedure similar to that used to synthesize enantiomerically enriched **9**.

1-(Octan-2-yl)-3-phenylimidazolidin-2-one (14; Table 6, entry 2). Colorless oil, 80% yield. TLC (hexanes–EtOAc = 5:1): R_f = 0.43. ^{1}H NMR : δ 7.57-7.55 (m, 2 H), 7.34-7.30 (m, 2 H), 7.01 (t, *J* = 7.6 Hz, 1 H), 4.08 (qt, *J* = 6.4, 8.8 Hz, 1 H), 3.82-3.78 (m, 2 H), 3.50-3.33 (m, 2 H), 1.52-1.21 (m, 10 H), 1.15 (d, *J* = 7.2 Hz, 3 H), 0.87 (t, *J* = 7.2 Hz, 3 H). ^{13}C{^{1}H} NMR: δ 157.38, 140.76, 128.70, 122.0, 117.17, 47.67, 42.53, 36.37, 34.0, 31.73, 29.12, 26.46, 22.59, 17.87, 14.05. IR (neat, cm^{-1}): 2924, 2855, 1697, 1600, 1503, 1481, 1456, 1417, 1391, 1259, 1145, 1095, 752. HRMS calcd (found) for $C_{17}H_{26}N_2O$ (M^+): 274.2045 (274.2050). Enantiopurity (71% ee) was determined by HPLC analysis (99:1 hexanes/isopropanol, 0.5 mL/min; Figure 21).

1-(4-Fluorophenyl)-3-(octan-2-yl)imidazolidin-2-one (15; Table 6, entry 3). Colorless oil, 81% yield. TLC (hexanes–EtOAc = 5:1): R_f = 0.37. ^{1}H NMR: δ 7.45-7.41 (m, 2 H), 6.97-6.92 (m, 2 H), 4.06 (qt. *J* = 7.2, 8.4 Hz, 1H), 3.73-3.68 (m, 2 H), 3.38-3.26 (m, 2 H), 1.49-1.33 (m, 2 H), 1.32-1.14 (m, 8 H), 1.08 (d, *J* = 6.8 Hz, 3 H), 0.80 (t, *J* = 6.4 Hz, 3 H). ^{13}C{^{1}H} NMR: δ 159.4, 157.4, 136.9, 118.8, 118.7, 115.4, 115.1, 47.8, 42.8, 36.4, 34.0, 31.7, 29.1, 26.5, 22.6, 17.8, 14.0. IR (neat, cm^{-1}): 2926, 2856, 1693, 1510, 1482, 1424, 1392, 1259, 1224, 1160, 1144, 828, 750. HRMS calcd (found) for $C_{17}H_{25}FN_2O$ (M^+): 292.1951 (292.1954). Enantiopurity (74% ee) was determined by HPLC analysis (95:5 hexanes/isopropanol, 0.5 mL/min; Figure 22).

1-*tert*-Butyl-3-(octan-2-yl)imidazolidin-2-one (16; Table 6, entry 4). Colorless oil, 89% yield. TLC (hexanes–EtOAc = 2:1): $R_f = 0.70$. ^{1}H NMR: δ 3.90 (sextet, $J = 6.8$ Hz, 1 H), 3.30-3.21 (m, 2 H), 3.14-3.03 (m, 2H), 1.33 (s, 9 H), 1.32-1.19 (m, 10 H), 1.04 (d, $J = 6.8$ Hz, 3 H), 0.85 (t, $J = 7.2$ Hz, 3 H). ^{13}C{^{1}H} NMR: δ 161.4, 53.09, 47.44, 41.16, 36.92, 34.28, 32.0, 29.4, 27.6, 26.7, 22.8, 17.8, 14.3. IR (neat, cm^{-1}): 2958, 2925, 2855, 1683, 1482, 1455, 1414, 1392, 1361, 1267, 1249, 1227, 1144, 1102, 765, 745. HRMS calcd (found) for $C_{15}H_{30}N_2O$ (M^+): 254.2358 (254.2357). Enantiopurity (78% ee) was determined by HPLC analysis (97:3 hexanes/isopropanol, 0.5 mL/min; Figure 23).

1-(Decan-2-yl)-3-methylimidazolidin-2-one (17; Table 6, entry 5). Colorless oil. 83% yield. TLC (hexanes–EtOAc = 1:1): $R_f = 0.33$. ^{1}H NMR: δ 3.92 (qt, $J = 6.4$, 8.8 Hz, 1 H), 3.24-3.10 (m, 4 H), 2.73 (s, 3 H), 1.45-1.33 (m, 2 H), 1.32-1.17 (m, 12 H), 1.03 (d, $J = 6.8$ Hz, 3 H), 0.83 (t, $J = 7.2$ Hz, 3 H). ^{13}C{^{1}H} NMR: δ 161.9, 48.3, 46.0, 37.5, 34.6, 32.4, 32.0, 30.0, 29.9, 29.8, 27.0, 23.1, 18.3, 14.6. IR (neat, cm^{-1}): 2923, 2853, 1690, 1493, 1433, 1401, 1277, 1253, 1048, 760. HRMS calcd (found) for $C_{14}H_{28}N_2O$ (M^+): 240.2202 (240.2207). Enantiopurity (73% ee) was determined by HPLC analysis (98:2 hexanes/isopropanol, 0.5 mL/min; Figure 24).

1-(Dodecan-2-yl)-3-methylimidazolidin-2-one (18; Table 6, entry 6). Colorless oil, 76% yield. TLC (hexanes–EtOAc = 1:1): $R_f = 0.36$. ^{1}H NMR: δ 3.87 (qt, $J = 7$, 8.5 Hz, 1 H), 3.21-3.08 (m, 4 H), 2.71 (s, 3 H), 1.39-1.27 (m, 2 H), 1.26-1.13 (m, 16 H), 1.05 (d, $J = 7.0$ Hz, 3 H), 0.81 (t, $J = 7.0$ Hz, 3 H). ^{13}C{^{1}H} NMR: δ 161.7, 48.0, 45.8, 37.3,

34.3, 32.1, 31.8, 29.8, 29.8, 29.8, 29.6, 26.7, 22.9, 18.0, 14.3. IR (neat, cm^{-1}): 2922, 2852, 2922, 2852, 1693, 1493, 1433, 1401, 1277, 1254, 1046, 760. HRMS calcd (found) for $C_{16}H_{32}N_2O$ (M^+): 268.2515 (268.2511). Enantiopurity (75% ee) was determined by HPLC analysis (97:3 hexanes/isopropanol, 0.5 mL/min; Figure 25).

2.3.3 Control Reactions

(1) Silver/ligand only. A suspension of **7** (20.0 mg, 0.20 mmol), 1-octene (1.92 mL, 12.0 mmol), AgOTf (5.1 mg, 0.020 mmol), and (*S*)-**L8** (23.0 mg, 0.020 mmol) in *m*-xylene (0.5 mL) in a pressure tube was stirred at 100 °C for 48 h. The crude mixture was then filtered through a silica gel plug and concentrated. NMR analysis of the crude reaction mixture revealed no detectable formation of **9**.

(2) HOTf/ligand only. A suspension of **7** (20.0 mg, 0.20 mmol), 1-octene (1.92 mL, 12.0 mmol), HOTf (3.0 mg, 0.020 mmol), and (*S*)-**L8** (23.0 mg, 0.020 mmol) in *m*-xylene (0.5 mL) in a pressure tube was stirred at 100 °C for 48 h. The crude mixture was then filtered through a silica gel plug and concentrated. NMR analysis of the crude reaction mixture revealed no detectable formation of **9**.

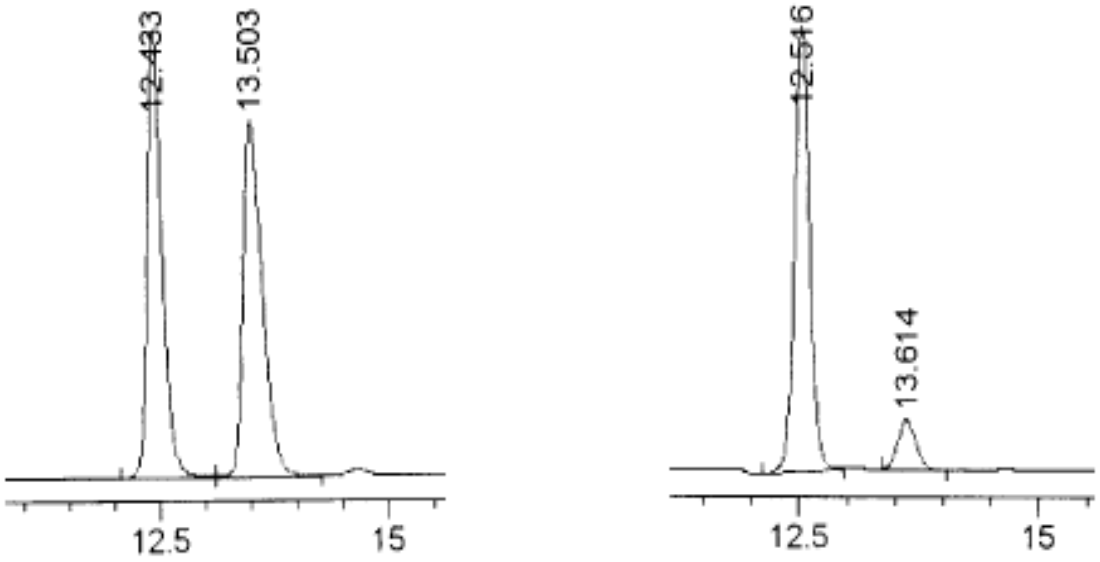

Figure 63. Chiral HPLC traces of racemic (left trace) and enantiomerically enriched (right trace, 76 % ee) methyl-3-(octan-2-yl)imidazolidin-2-one (**9**).

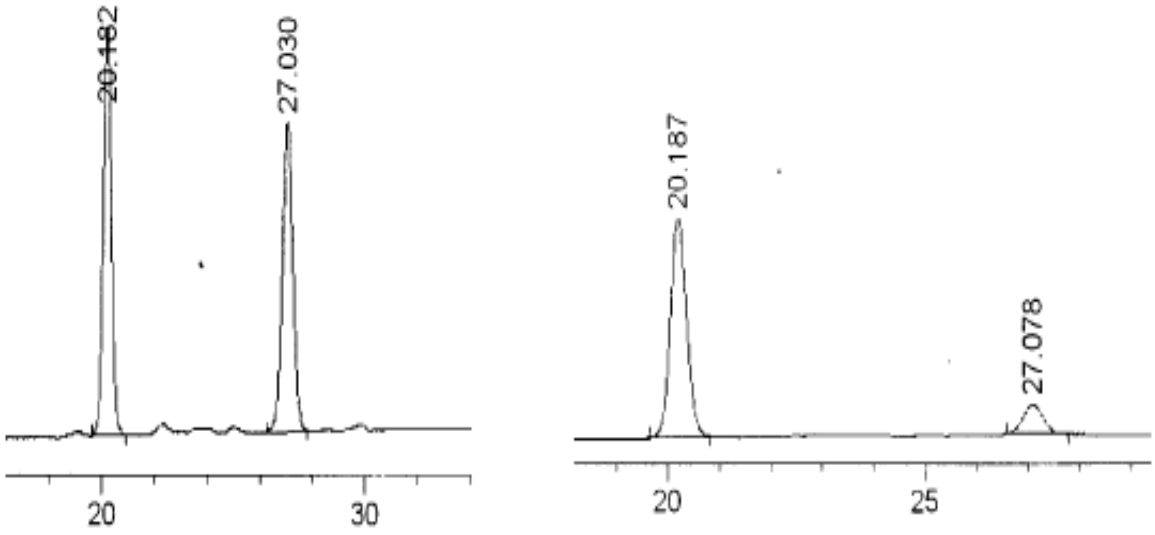

Figure 64. Chiral HPLC traces of racemic (left trace) and enantiomerically enriched (right trace, 71 % ee) 1-(octan-2-yl)-3-phenylimidazolidin-2-one (**14**).

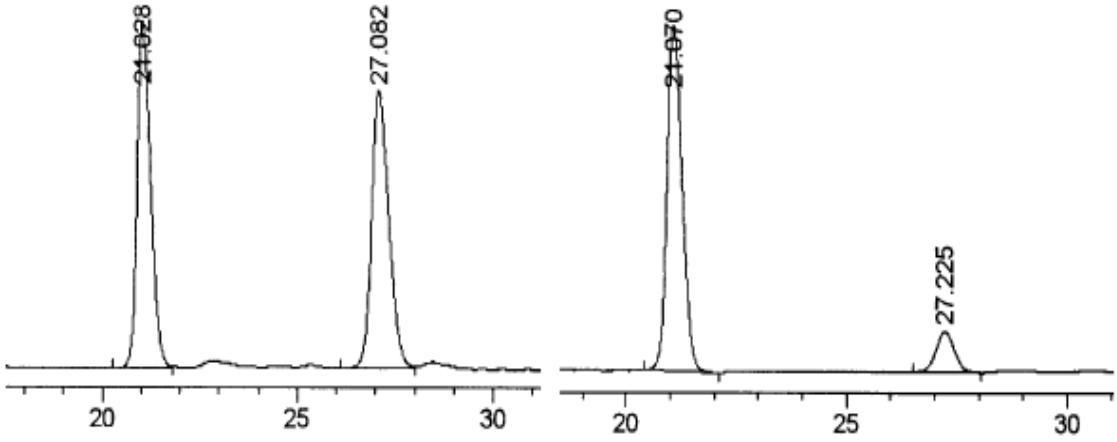

Figure 65. Chiral HPLC traces of racemic (left trace) and enantiomerically enriched (right trace, 74 % ee) 1-(4-fluorophenyl)-3-(octan-2-yl)imidazolidin-2-one (**15**).

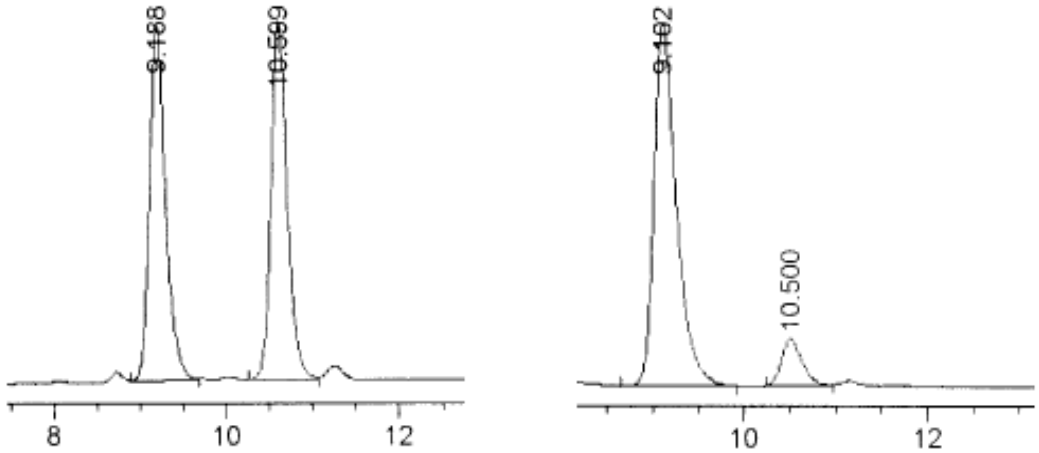

Figure 66. Chiral HPLC traces of racemic (left trace) and enantiomerically enriched (right trace, 78 % ee) 1-tert-butyl-3-(octan-2-yl)imidazolidin-2-one (**16**).

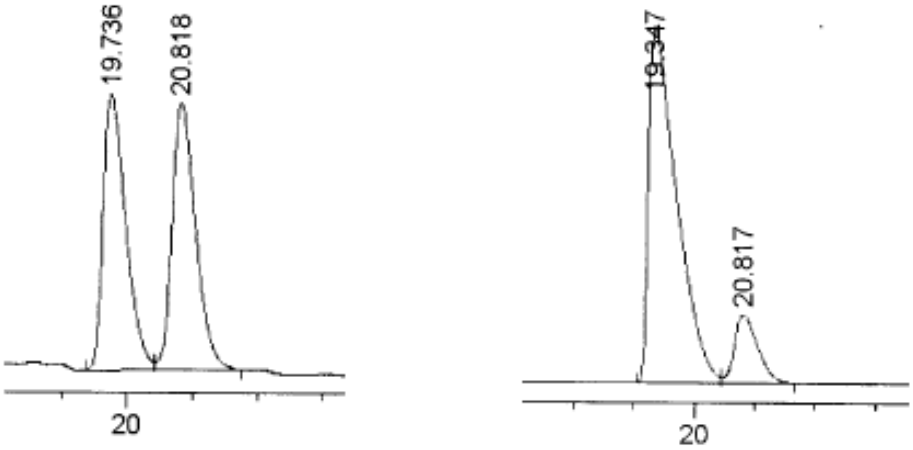

Figure 67. Chiral HPLC traces of racemic (left trace) and enantiomerically enriched (right trace, 73 % ee) 1-(decan-2-yl)-3-methylimidazolidin-2-one (**17**).

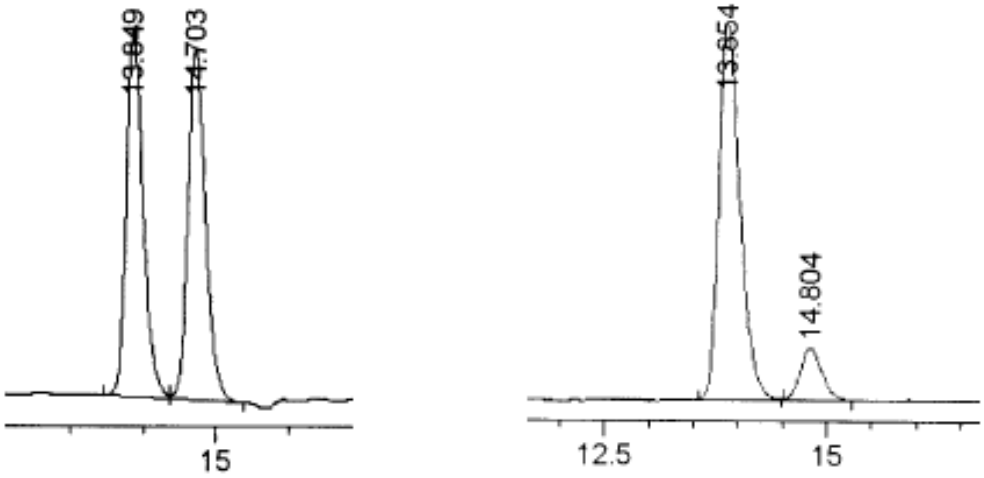

Figure 68. Chiral HPLC traces of racemic (left trace) and enantiomerically enriched (right trace, 75 % ee) 1-(dodecan-2-yl)-3-methylimidazolidin-2-one (**18**).

Chapter 3

Synthesis and Application of Polymer Embedded Bis(phosphine) Ligands for Mechanocatalysis

Polymerization reactions to produce **PS-1a**, **PS-2a**, **SAN-1a**, and **SAN-2a** from **XII** and operation of the rheometer for reactions listed in Table 8 were performed by Zachary S. Kean from Craig group at Duke University.

3.1 Introduction

3.1.1 Mechanocatalysis

Utilization of mechanical forces to engineer synthetic pathways is an intriguing approach as it offers altered reaction pathways that are not accessible thermally. Some groups have utilized mechanical forces to activate catalytic complexes, called mechanocatalysis.[95-97] Mechanical forces can be effectively applied to catalysts when polymeric substituents are tethered to the catalysts, and the mechanical forces are transmitted in a directional fashion via the polymer chain. The first example of mechanocatalysis was reported by Klibanov *et. al.*, where they used a nylon-fiber bound enzyme to apply mechanical forces (stretch or unstretch) and observed changes in activity of the enzymes.[98] Recently, Sijbesma has reported mechanocatalysis via sonochemical activation of latent coordination complexes.[99] In this system, applied ultrasound generates shear forces from collapsing cavitation bubbles in solution, breaking a metal-ligand bond and activating the catalyst. The polymeric coordination complexes of bis *N*-heterocyclic carbenes becomes activated via force induced ligand displacement, resulting in active catalysis for ring closing metathesis or transesterification. This is a well regarded example for on-off switching of catalyst activity by a mechanical force that is potentially applicable to many practical uses such as mechanical signal sensors and self-healing materials (Figure 70).

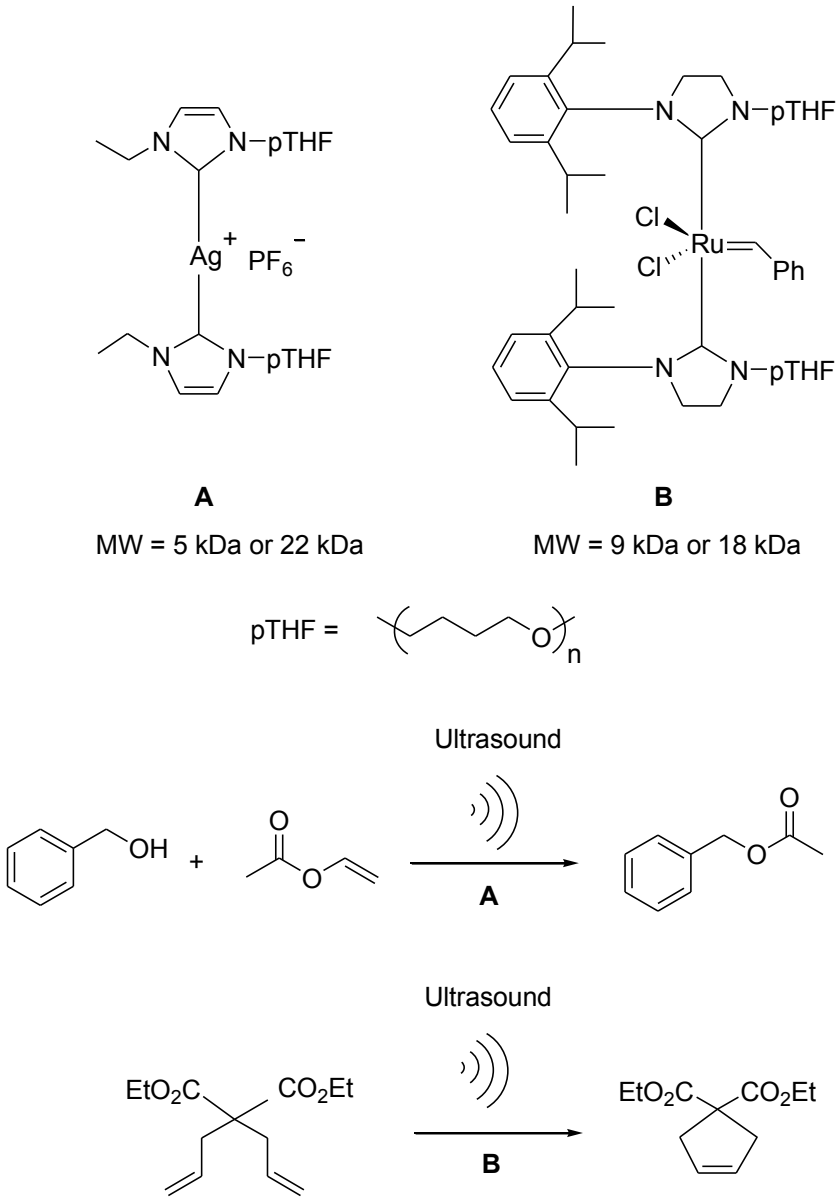

Figure 69. Examples of mechanocatalysis.

3.1.2 Asymmetric Allylic Alkylation and Dihedral Angle Effect

The formation of carbon-carbon bonds through palladium catalysis is widely used in organic synthesis. Among the many palladium catalyzed C-C bond forming reactions, asymmetric allylic alkylation (AAA) is one of the most widely used reactions for introducing asymmetry in organic molecules.[100-107] AAA employs various activated allylic electrophiles with different leaving groups such as carboxylate or carbonate, and is compatible with a wide range of carbon and heteroatom nucleophiles. Also, this reaction generally shows a high level of stereoselectivity. The reaction mechanism of allylic alkylation is depicted Scheme 3.1. The allylic electrophile undergoes oxidative addition to a Pd(0) complex with expulsion of the leaving group (X^-) to and generating a cationic π-allyl complex (Scheme 3.1, **I**). Outer-sphere attack of a nucleophile on the π-allyl moiety and subsequent decomplexation forms the alkylated nucleophile with regeneration of the Pd(0) catalyst.

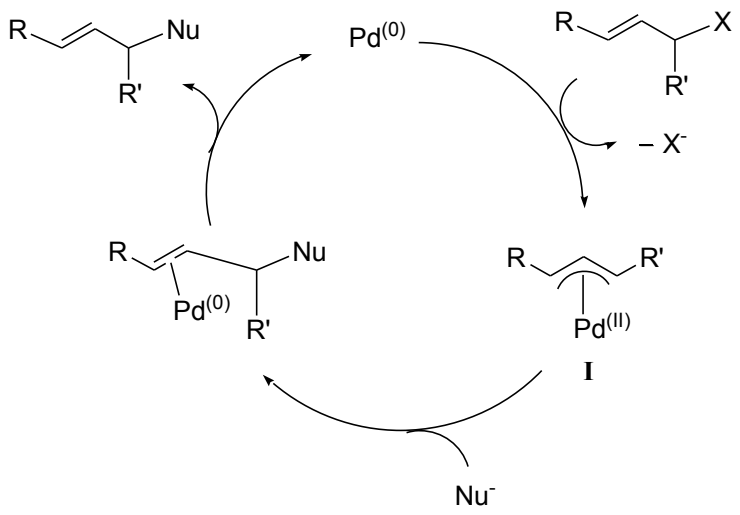

Scheme 3.1. Proposed mechanism for palladium catalyzed allylic alkylation.

To achieve high reactivity and stereoselectivity in metal catalyzed transformations, many new types of ligands with varied electronic and steric properties have been introduced. Among the many ligand types, axially chiral atropisomeric biaryl bisphosphines such as BINAP, BIPHEP, and MeOBIPHEP are one of the most effective ligand types in many asymmetric catalytic reactions. For chiral atopisomeric bisphosphines, the asymmetric spatial environment can be rationalized by the concept of "quadrants", where the steric hindrance around the metal is created by the phosphorus substituents in pseudoequatorial positions (Figure 71). The dihedral angle (θ) of the biaryl backbone is geometrically related to the bite angle (β), which determines the proximity of the pseudoequatorial aryl groups and the chelating substrate around the metal. Based on this model, the smaller dihedral angle would provide the higher interaction between ligand and substrate, and *vice versa*.

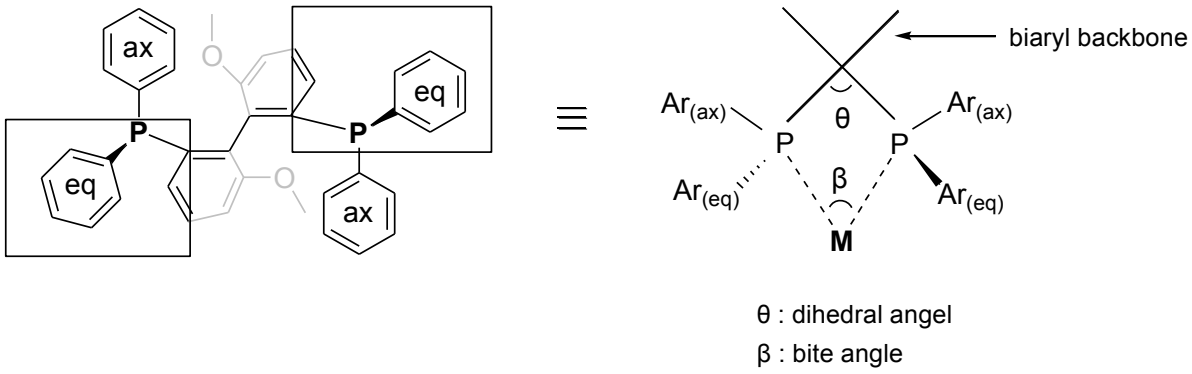

Figure 70. Schematic representation of MeO-BIPHEP for quadrants rule and relationship between dihedral and bite angle.

Zhang *et. al.* reported an interesting correlation study between ligand dihedral angle and enantioselectivity in the Pd catalyzed AAA reaction.[76] For the correlation study, they synthesized a series of tunable phosphine ligands (Tunephos), which have variable number of carbon atoms as a linker to connect 6,6'-positions of biaryl backbone. As the number of carbon atoms in the linker increased, the dihedral angle of the ligand increased (Figure 71). They chose the AAA reaction of 1,3-diphenylpropenyl acetate with dimethyl malonate to form (*E*)-dimethyl 2-(1,3-diphenylallyl)malonate. Under the condition of 2.5 mol % $[Pd(allyl)Cl]_2$, 5 mol % ligand, *N,O*-bis(trimethylsilyl)acetamide (BSA), and catalytic amounts of KOAc (5 mol %) in THF, (*E*)-dimethyl 2-(1,3-diphenylallyl)malonate was produced in good yield with up to 95 % (Table 7). Interestingly, AAA reaction with larger dihedral angle C6-Tunephos ligand afforded the

highest enantioselectivity of 95 % ee (Table 7, entry 6). This study demonstrated a clear relationship between dihedral angle and enantioselectivity in palladium-catalyzed AAA.

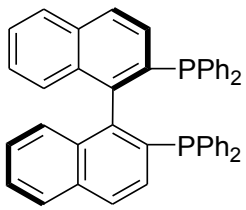

(*R*)-BINAP

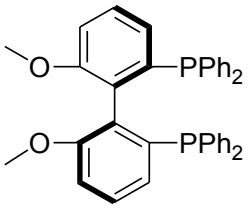

(*R*)-MeO-MIPHEP

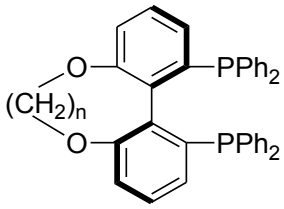

(*R*)-Cn-Tunephos : Cn (n = 1-6)

ligand	(*R*)-BINAP	(*R*)-MeO-MIPHEP	C1	C2	C3	C4	C5	C6
dihedral angle(deg.)	87	87	60	74	77	88	94	106

Figure 71. Dihedral angle of axially chiral bisphosphine ligands.

Table 6. Effect of ligand dihedral angle on the yield and enantioselectivity the palladium-catalyzed AAA reaction of 1,3-diphenylpropenyl acetate with dimethyl malonate to form (*E*)-dimethyl 2-(1,3-diphenylallyl)malonate employing Cn-Tunephos ligands.

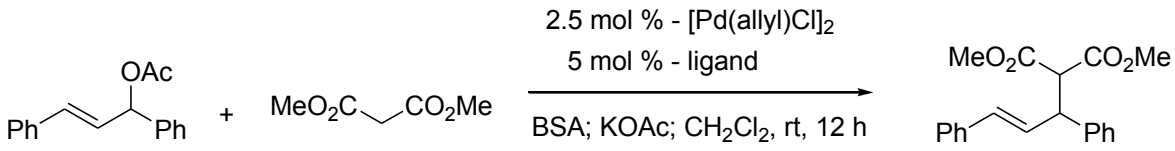

entry	ligand	yield(%)[a]	ee(%)[b]
1	C1-Tunephos	89	77
2	C2-Tunephos	86	82
3	C3-Tunephos	90	84
4	C4-Tunephos	91	87
5	C5-Tunephos	91	92
6	C6-Tunephos	90	95

[a] Isolated yield. [b]determined by chiral HPLC.

3.1.3 Project Goals

Chiral atropisomeric biaryl bisphosphines are effective ligands in many asymmetric catalytic reactions, and extensive studies on modifying these ligands have been performed to achieve high levels of reactivity and stereoselectivity in asymmetric catalytic reactions for decades. However, since subtle changes in ligand properties such

as the electronic, steric, and geometic character of the ligand can produce large variations in reactivity and enantioselectivity, searching for an optimal ligand for a particular reaction demands great amount of time and effort.

Our approach for designing a mechanocatalytic chiral bisphosphine ligand involves introducing a chiral bisphosphine ligand into a polymeric substituent so that mechanical forces can be applied to a geometry sensitive catalyst via the polymer chain. More specifically, we aim to generate tension on a polymer-embedded ligand in a cup in bob rheometer. By doing this, the polymer-embedded ligand would deform to increase its dihedral angle (θ), which would be evidenced by a change in enantioselectivity in a palladium-catalyzed AAA reaction. This process is coined as "fluxional mechanocatalysis", where the outcome is influenced by the stress state of the catalyst (Figure 73). Our primary goal is to demonstrate proof of concept for fluxional mechanocatalysis by introducing polymer embedded ligands to Pd-catalyzed AAA system, and after successful realization of the first goal, we will expand our fluxional mechanocatalysis to another systems.

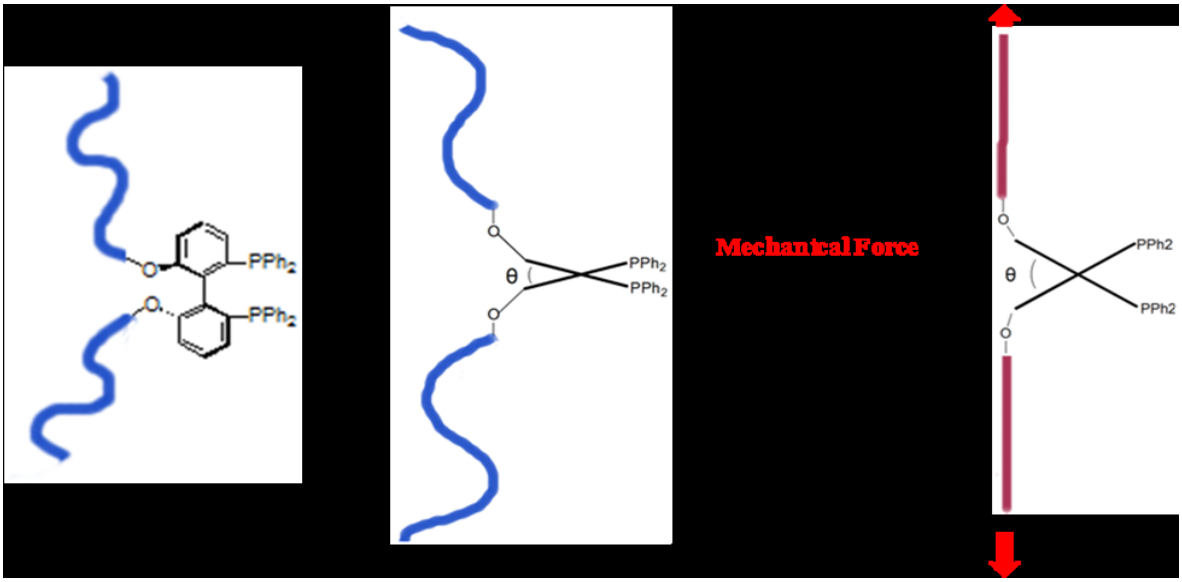

Figure 72. Schematic representation of fluxional mechanocatalysis.

3.2 Results and Discussion

3.2.1 Synthesis of Polymer-Embedded Ligands for Fluxional Mechanocatalysis

For an effective generation of the mechanical force, a high molecular weight polymer needs to be tethered to the catalyst. Our basic strategy to generate polymer tethered chiral catalysts was to synthesize a ligand possessing a controlled radical polymerization initiator, so that a polymer could be grown from the ligand through various polymerization reactions. Initial attempts were made to generate a radical initiator, benzyl bromide, directly on a biaryl backbone (Scheme. 3.2). To this end, copper catalyzed Ullmann homocoupling reaction of 2-iodo-3-nitrotoluene gave biaryl compound **II**. Reduction of the aromatic nitro groups using Pd/C generated the biaryl

amine complex **III** that was converted via a Sandmeyer reaction to form **IV** via nucleophilic displacement of diazonium ion intermediate with iodide. Treatment of **IV** with *n*-BuLi and diphenylphosphinic chloride produced the bis(phosphine oxide) compound **V**. Unfortunately, attempts to generate the brominated product under various reaction conditions utilizing *N*-bromosuccinimide (NBS) or 1,3-dibromo-5,5-dimethylhydantoin and 2,2′-azobis(2-methylpropionitrile) **(**AIBN) or benzoyl peroxide in CCl_4 at various reaction temperatures did not yield the desired halogenated product, but rather produced decomposed products of mono-aryl moieties and some unidentified side products.

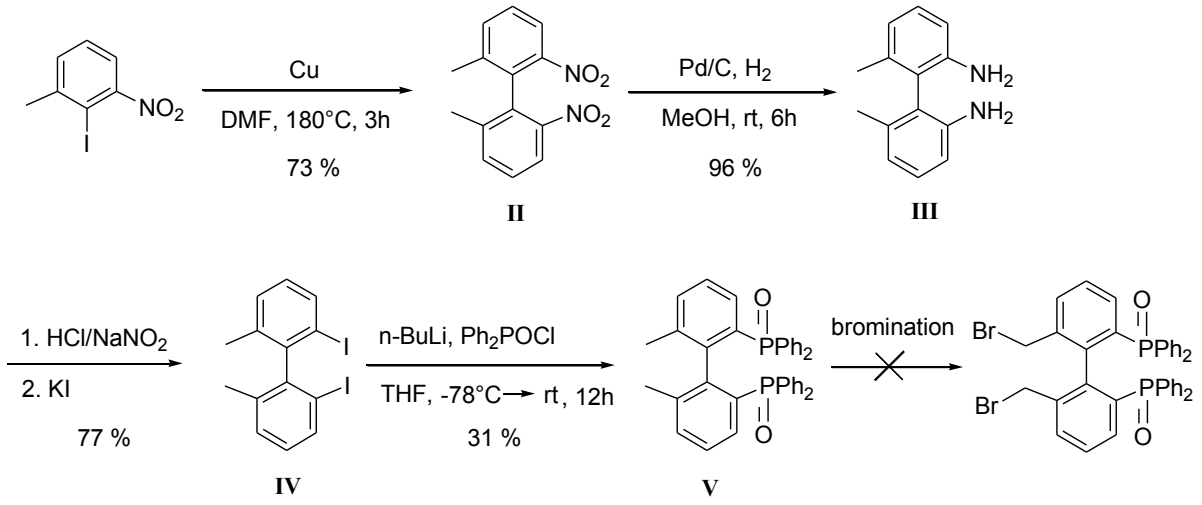

Scheme 3.2. Reaction scheme for the generation of a radical initiator on a biaryl bisphosphine ligand.

Another approach was made to introduce a different radical initiator, 2-bromo-isobutyryl moiety, onto a biaryl backbone (Scheme 3.3). Demethylation of (*S*)-MeO-

BIPHEP using BBr_3 and following esterification with 2-bromo-isobutyryl bromide produced the coupled product **VII**. However, during the subsequent polymerization to produce the polymer-embedded ligand, the undesirable phosphine oxide species **VIII** was produced in addition to the desired bis(phosphine) species. Unfortunately, attempts to reduce the phosphine oxide to phosphine failed, presumably due to the cleavage of the ester bond between the aryl ring and radical initiator under reducing conditions.

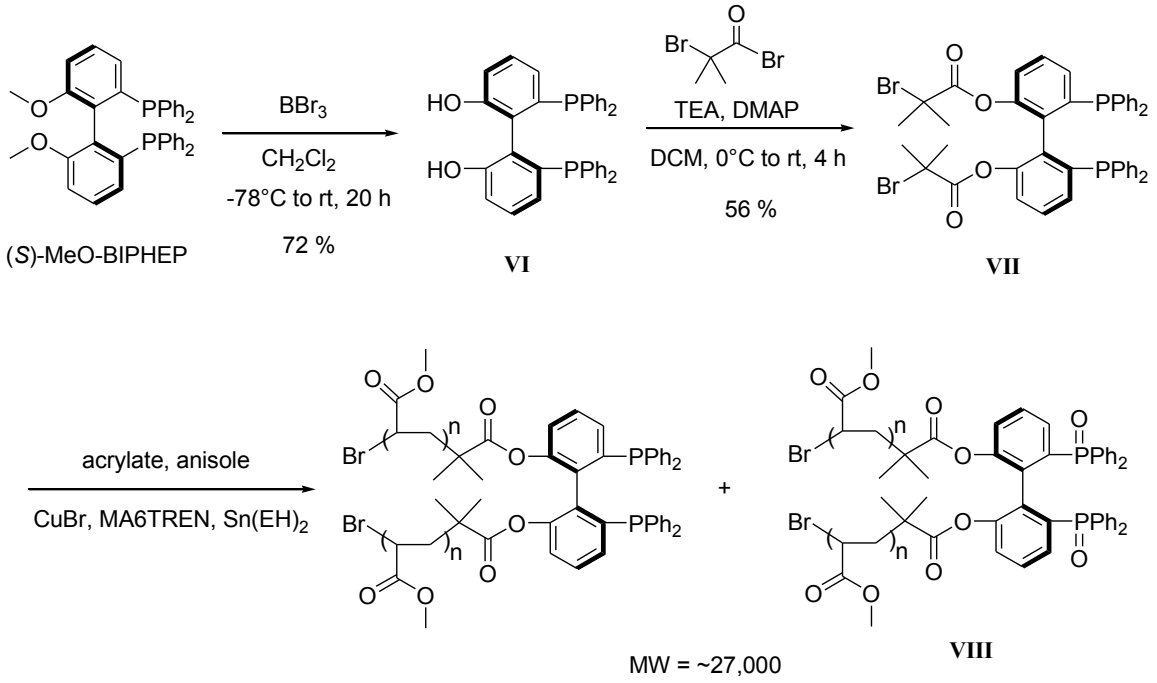

Scheme 3.3. Reaction scheme for the synthesis of polyacrylate-embedded bis(phosphine) ligand.

Taking into account the need to reduce the phosphine oxide after polymerization, our next approach to the synthesis of a polymer-embedded bis(phosphine) ligand aimed

to introduce (1-bromoethyl)benzene as a radical initiator via an ether linkage and to employ either polystyrene (PS) or styrene acrylonitile (SAN) as a polymer (Scheme 3.4). To this end, demethylation of the methoxy groups of (*S*)-MeO-BIPHEP using tribromoborane generated the bis(phenol) **VI**, followed by oxidation with hydrogen peroxide in methanol to give **IX**. Alkylation of **IX** with 1-(4-(bromomethyl)phenyl)ethanone (**S1**) in the presence of potassium carbonate in refluxing acetone formed bis(ether) **X**. Reduction of the aromatic ester with sodium borohydride formed bis(benylic alcohol) complex **XI** followed by bromination acetyl bromide to form **XII** with the desired radical initiator of 1-phenyl ethylbromide on the biaryl backbone. Copper catalyzed polymerization[108] of **XII** produced the polystyrene-embedded bis(phosphine oxide) ligands **PS-1a** and **PS-2a** (method A) or the styrene acrylonitrile-embedded bis(phosphine oxide) ligands **SAN-1a** and **SAN-2a** (method B). Treatment of polymer-embedded ligands **PS-1a**, **PS-2a**, **SAN-1a**, and **SAN-2a** with trichlorosilane of in the presence of triethylamine led to reduction of the phosphine oxide to generate the desired polymer-embedded bis(phosphine) ligands **PS-1** and **PS-2,** and **SAN-1** and **SAN-2**, respectively. Initially however, we observed that this reduction protocol generated a cross-linked polymer, which became a gel type compound. We reasoned that the production of the cross-linked polymer was caused by radical formation under the elevated temperatures used for the reduction. Adding a catalytic amount of the radical inhibitor, 2,6-Di-*tert*-butyl-4-methylphenol (BHT) to the reduction sequence allowed us to obtain soluble polymer after reduction, and polymer-embedded ligands (**PS-1** and **PS-2,** and **SAN-1** and **SAN-2**) for fluxional mechanocatalysis were attained.

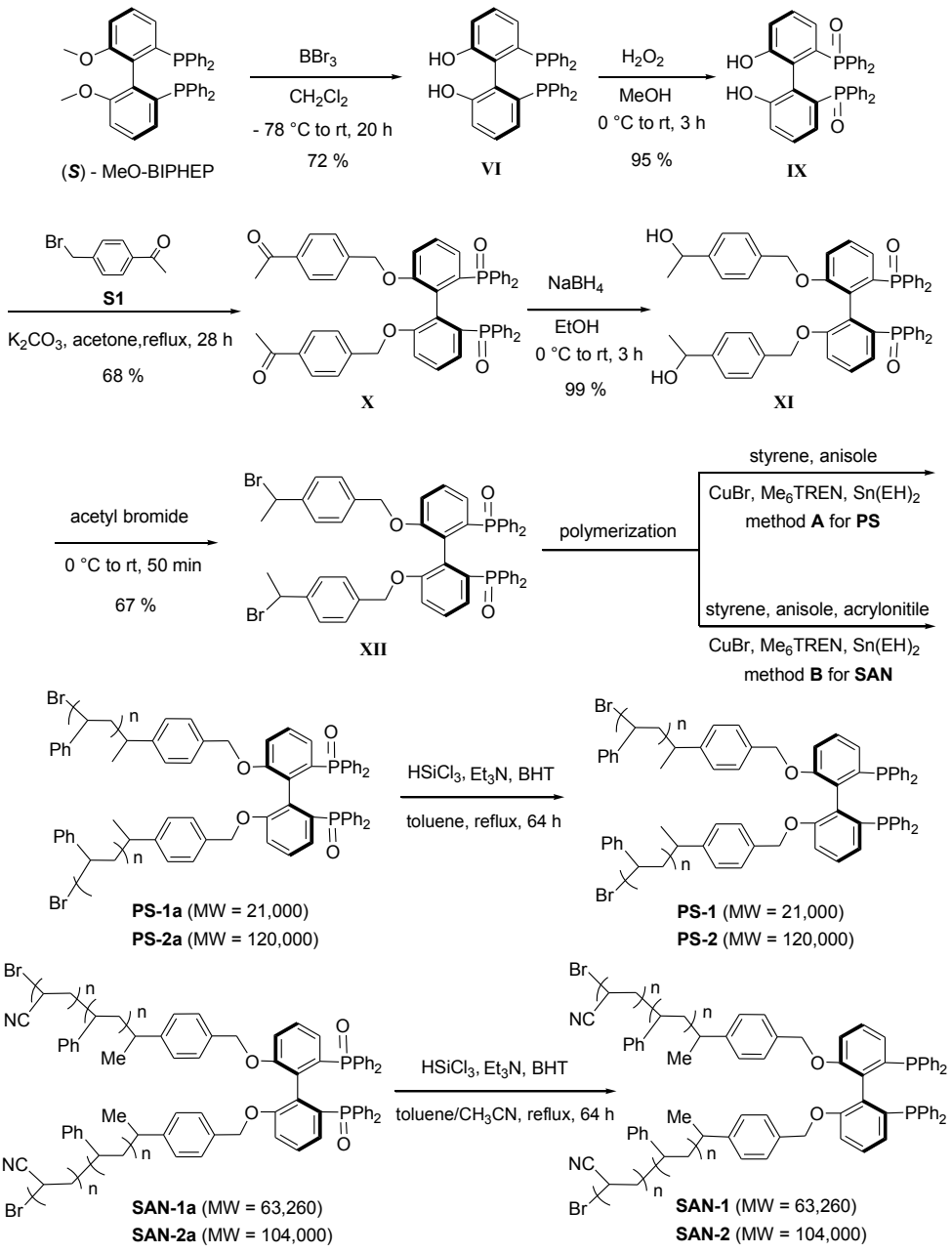

Scheme 3.4. Scheme for the synthesis of polymer-embedded ligands **PS-1**, **PS-2, SAN-1**, and **SAN-2**.

3.2.2 Pd-Catalyzed Asymmetric Allylic Alkylation under a Shear Force

A correlation study between ligand dihedral angle and enantioselectivity in Pd-catalyzed asymmetric allylic alkylation (AAA) was reported, showing that increasing ligand dihedral angle resulted in increasing enantioselectivity.[76] Based on the results, we chose the Pd-catalyzed AAA reaction of 1,3-diphenylpropenyl acetate with dimethyl malonate to form (*E*)-dimethyl 2-(1,3-diphenylallyl)malonate in an effort to demonstrate fluxional mechanocatalysis. Our first task was to determine if the large molecular weight of polymer-tethered ligand would function as a ligand in palladium-catalyzed AAA. However, prior to the application of polymer-embedded ligand to AAA, we performed reaction optimization of the palladium-catalyzed AAA of 1,3-diphenylpropenyl acetate with dimethyl malonate employing (*S*)-MeO-BIPHEP as the ligand (Table 8), which has the same biaryl backbone and the polymer-embedded bis(phosphine) ligands **PS-1**, **PS-2,** **SAN-1**, and **SAN-2**. Among the reagents, combination of tris(dibenzylideneacetone)dipalladium [$(dba)_3Pd_2$] and *N,O*-Bis(trimethylsilyl)acetamide (BSA) showed moderate reactivity (78%) and enantioselectivity (71 % ee) (Table 8, entry 2). Employing these conditions, we evaluated the AAA reaction of 1,3-diphenylpropenyl acetate with dimethyl malonate employing $(dba)_3Pd_2$ and BSA with ligand **PS-1** to gauge the efficacy of the polymer-embedded ligand. Indeed, the polystyrene-embedded ligand **PS-1** produced (*E*)-dimethyl 2-(1,3-diphenylallyl)malonate in 65% yield with 57% ee (eq 3.1). However, further examination revealed the background reaction, presumably catalyzed by unligated $(dba)_3Pd_2$ that decreased the enantiopurity of the product over time from 86% ee at 4 h to 50% ee at 28 h. For consistent results, another Pd source was

necessary, and among the Pd sources tested, $[Pd(allyl)Cl]_2$ functioned as an effective palladium source with no detectable background reaction, good reactivity, and high enantioselectivity in AAA.

Table 7. Effect of reaction conditions on the AAA reaction 1,3-diphenylpropenyl acetate with dimethyl malonate employing (*S*)-MeO-BIPHEP as the ligand.

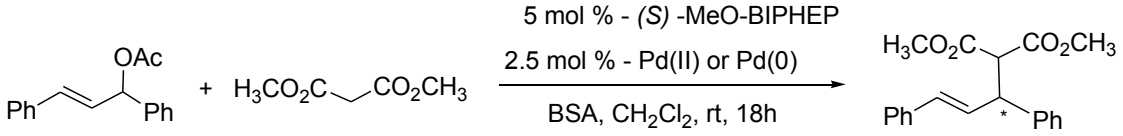

entry	Pd	yield (%)[a]	*ee* (%)[b]
1	$[Pd(allyl)Cl]_2$	91	92
2	$(dba)_3Pd_2$	78	71
3	$(dba)_2Pd$	84	46
4	$Pd(OAc)_2$	82	35

[a] Isolated yield. [b] enantiopurity determined by HPLC analysis on a chiral stationary phase.

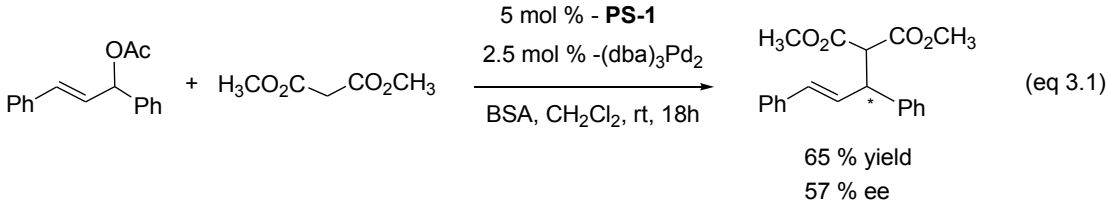

(eq 3.1)

Another important factor for realization of fluxional mechanocatalysis was the solubility of the polymer-embedded ligand in the reaction medium. Solubility test of the

polymer-embedded ligands showed an amount of the ligand corresponding 1.7 mol % catalyst loading was completely dissolved in 1 mL of CH_2Cl_2. Considering the results of our optimization studies, we employed the following reaction conditions for mechanocatalytic palladium-catalyzed AAA: 1,3-diphenylallyl acetate (0.2 mmol), dimethyl malonate (3 equiv), BSA (3 equiv), polymer-embedded ligand (1.7 mol %), and $[Pd(allyl)Cl]_2$ (0.85 mol %) in 1 mL of CH_2Cl_2 at room temperature for 18 h. Employing these reaction conditions, control AAA reactions with polymer-embedded ligands in a normal reaction vessel were performed prior to application of shear force in a rheometer (Table 8, entries 1-3). Different types and molecular weights of polymer-embedded ligands underwent successful AAA in moderate conversion with high enantioselectivity indicating the reaction condition was feasible for next step to apply steady shear flow in a cup and bob rheometer (Figure 74).

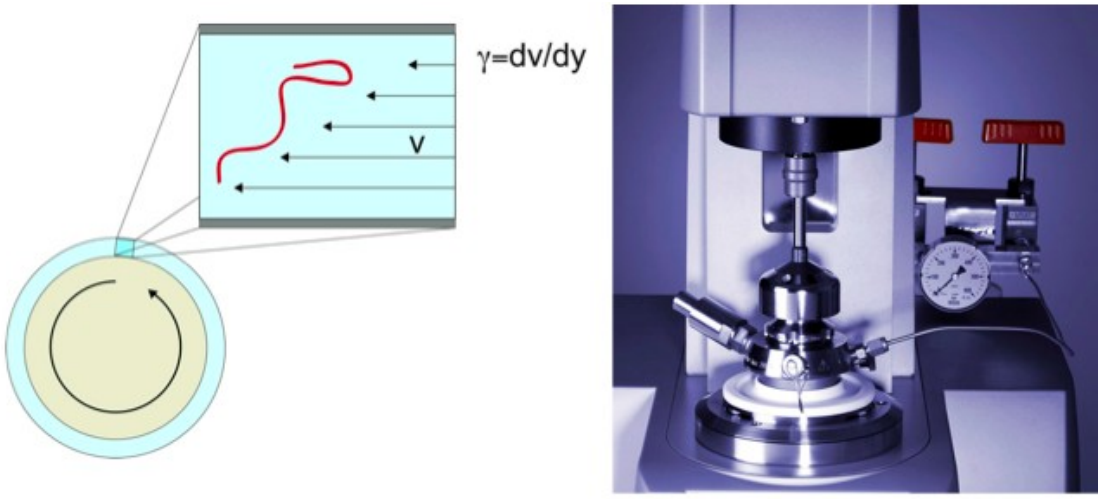

Figure 73. Illustration of applied steady shear flow to a sample of polymer in the 0.25 mm gap (left) and a cup and bob rheometer (right).

$$P_e = \frac{6\pi a^3}{k_B T}\sigma = \frac{6\pi a^3}{k_B T}\dot{\gamma}\eta \qquad \text{(eq 3.2)}$$

a : radius of the polymer
σ : shear stress
η : viscosity
$\dot{\gamma}$: shear rate

Applied force onto the polymer-embedded ligand was estimated using Péclet number (P_e), which is a dimensionless quantity that gauges whether solution flow or Brownian fluctuations dominate the behavior of an object in solution. For example, if $P_e > 1$, shear flow dominates and if $P_e < 1$, Brownian motion dominates. Based on the equation 3.2,

increasing polymer MW (polymer radius), shear rate, and/or viscosity will create P_e >1 environment and polymer chain deformation and stretching may occur. We set our first AAA reaction under a shear stress using **SAN-2** ligand at 6000 s^{-1} of shear rate, and the reaction showed 51% conversion and 91% ee, which was similar to that obtained with the control reaction in the absence of sheer (Table 9, entries 1 and 4), leading us to assume there was no effective polymer chain deformation and stretching under the reaction condition. Other trials were made by adding different amount of polystyrene additive to change the viscosity of the reaction medium. However, increasing viscosity did not provide observable changes in enantioselectivity (Table 9, entries 5-7). At this point, we suspected degradation of the polymer chain under a high shear stress, resulting in the ineffective transmission of shear stress. Checking the molecular weight of the polymer and polydispersity index (PDI) value after the reactions, however, showed the same values as intact ligands, indicating no degradation of the polymer chains occurred under the levels of the shear stress.

Table 8. AAA reactions under shear stress.

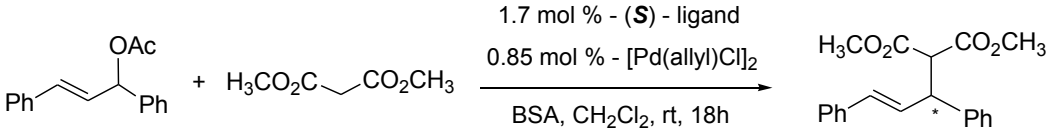

entry	ligand	conv.(%)[a]	*ee* (%)[b]
1	**SAN-2**	53	92
2[c]	**SAN-1**	53	92
3	**PS-2**	62	89

entry	ligand	shear rate (sec^{-1})	conv.(%)[a]	*ee* (%)[b]
4	**SAN-2**	6000	51	91
5[c]	**SAN-1**	6000	51	92
6[d]	**SAN-1**	6000	46	92
7[e]	**SAN-1**	6000	45	92
8	**PS-2**	6000	58	89
9	**PS-2**	2000	61	89
10	**PS-2**	3000	64	89

entry 1-3: control reactions in a vial, entry 4-10: a shear force applied in a rheometer. [a]conversion determined by GC. [b]enantiopurity determined by HPLC on a chiral stationary phase. [c]adding 300mg of polystyrene.[d]adding 600mg of polystyrene. [e]adding 1g of polystyrene.

We further tested reactions at varying shear rate with **PS-2** ligand, and the results showed identical enantioselectivity to the corresponding control reaction (Table 8, entries 3 and 8-10). Close examinations revealed that high viscosity of the reaction solution at high shear rate of the rheometer necessitates high level of torque, which exceeded the instrumental torque limit, resulting in instability of the spinning of the rheometer and disruption of the constant applied shear force. We tried a series of experiments by setting different reaction conditions (shear rate and viscosity) to avoid exceeding a torque limit of the rheometer, and at the same time acquiring % ee change. However, it turned out that a high shear stress demanded a change the geometry of the polymer-embedded ligand, and the high shear stress can only be achieved through a combination of when high

viscosity and high shear rate, which caused a high level of torque that exceeded the instrumental limit (eq 3.3).

$$\sigma = \eta\dot{\gamma}$$
$$M = k\eta \qquad \text{(eq 3.3)}$$

σ : shear stress
η : viscosity
$\dot{\gamma}$: shear rate
M : torque

3.2.3 Future Directions.

Another approach to realize fluxional mechanocatalysis will involve incorporating similar polymer-embedded bis(phosphine) ligands such as **PS-1**, **PS-2**, **SAN-2**, and **SAN-2** as crosslinkers in elastomeric materials. This should allow us to apply consistent stress to the system, as well as tune the amount of stress localized at the ligand crosslink points by choosing co-crosslinkers with long spacer lengths.[109] Additionally, we can embed spiropyran crosslinkers as a colorimetric stress sensor to ensure we are applying sufficient force to cause bond deformation. Synthesis of a gel-type cross-linked polymer possessing proper physical properties for an applied mechanical force would be a key step for the success of this approach.

3.3 Experimental Section

3.3.1 General Methods

Reactions were performed under a nitrogen atmosphere employing standard Schlenk and/or drybox techniques unless specified otherwise. NMR spectra were obtained on Varian spectrometers operating at 400 MHz for ^{1}H NMR, 100 MHz for ^{13}C and 160 MHz for ^{31}P NMR for in $CDCl_3$ at 25 °C unless noted otherwise. Gas chromatography was performed on a Hewlett-Packard 5890 gas chromatography equipped with a 25 m polydimethylsiloxane capillary column and FID detector. Chiral HPLC was performed on a Shimadzu LC-2010A chromatograph equipped with a 0.46 cm × 25 cm Chiralpak AD-H column. Gel permeation chromatography (GPC) was performed on two in series columns (Agilent Technology PL gel 10^4Å, 10^3Å) with THF as the mobile phase at 0.5 mL min^{-1}. An Anton Paar Physica MCR 301 rheometer was used for applying a shear stress. Column chromatography was performed employing 230-400 mesh silica gel (Silicycle). Thin layer chromatography (TLC) was performed on silica gel 60 F_{254} (EMD Chemicals Inc.). Room temperature is 23 °C. All solvents were purchased from Aldrich or Acros in anhydrous form and used as received. All reagents were purchased from major suppliers and used as received.

3.3.2 Ligand Synthesis

(6,6'-Dimethylbiphenyl-2,2'-diyl)bis(diphenylphosphineoxide) (Scheme 3.2, **V**). To 2-iodo-3-nitrotoluene (5.0 g, 19 mmol) in DMF (30 mL) was added copper (2.0 g, 31.3 mmol) and the reaction mixture was refluxed at 180 °C for 3 h. The hot mixture was filtered through a Celite pad and eluted with Et_2O (60 mL). The combined Et_2O and DMF extracts were evaporated under reduced pressure until only DMF remained. The resulting DMF suspension was poured into water (200 mL) and the resulting milky precipitate coagulated on standing overnight. The resulting solid was recrystallized from EtOH to produce 2,2'-dimethyl-6,6'-dinitrobiphenyl (**II)** as a yellow powder (1.88 g, 73 %). TLC (hexanes–EtOAc = 1:1): R_f = 0.68. ^{1}H NMR: δ 7.99 (d, J = 8.4 Hz, 2 H), 7.58 (d, J = 7.6 Hz, 2 H), 7.46 (t, J = 8.0 Hz, 2 H), 1.98 (s, 6 H).

2,2'-Dimethyl-6,6'-dinitrobiphenyl (1.8 g, 6.6 mmol) and Pd/C (100 mg, 5 wt. %) in MeOH (30 mL) was stirred under H_2 (1 atm) at room temperture for 6 h. The reaction mixture was filtered through a Celite pad and the filtrate was evaporated to produce 6,6'-dimethylbiphenyl-2,2'-diamine (**III**) as a yellow powder (1.35 g, 96 %). TLC (hexanes–EtOAc = 1:1): R_f = 0.58. ^{1}H NMR: δ 7.10 (t, J = 8.0 Hz, 2 H), 6.73 (d, J = 7.8 Hz, 2 H), 6.64 (d, J = 8.0 Hz, 2 H), 3.51 (bs, 2 H), 2.0 (s, 6 H).

Concentrated HCl (17 mL) was added slowly to 6,6'-dimethylbiphenyl-2,2'-diamine (1.18 g, 5.56 mmol) in an ice bath. To this mixture was added a solution of $NaNO_2$ (920 mg, 13.3 mmol) in deionized water (5 mL) at ~10 °C and this mixture was stirred for 30 min. The resulting dark solution was poured into a solution of KI (3.7 g, 22.2 mmol) in deionized water (16 mL). $NaHSO_3$ solution (20 mL) was added to this

reaction mixture, and resulting solid was filtered and washed with water (40 mL x 5) to give 2,2'-diiodo-6,6'-dimethylbiphenyl (**IV**) as a light brown powder (1.85g, 77%). TLC (hexanes only): R_f = 0.38. ^{1}H NMR: δ 7.80 (d, J = 8.0 Hz, 2 H), 7.26 (t, J = 8.0 Hz, 2 H), 7.0 (d, J = 8.0 Hz, 2 H), 2.01 (s, 6 H).

To 2,2'-diiodo-6,6'-dimethylbiphenyl (1.5g, 3.46 mmol) in THF (17 mL) was added *n*-BuLi (3.3 mL, 2.5 M in hexane) at –78 °C and the reaction mixture was stirred for 1 h. To the reaction mixture was added a solution of diphenylphosphinic chloride (1.64 g, 6.92 mmol) in THF (8.5 mL) dropwise and the reaction mixture was slowly warmed to room temperature and stirred for 12 h. The resulting mixture was quenched with EtOH (10 mL) and the solvent was evaporated under vacuum. The resulting mixture was dissolved in CH_2Cl_2 to form a white precipitate that was filtered and discarded. The filtrate was concentrated and chromatographed on silica gel to give **V** as a white solid (620 mg, 31 %). TLC (CH_2Cl_2–MeOH = 10:1): R_f = 0.47. ^{1}H NMR: δ 7.84-7.09 (m, 26 H), 1.41 (s, 6 H). ^{31}P NMR: δ 30.68.

(*S*)-6,6'-Bis(diphenylphosphino)biphenyl-2,2'-diylbis(2-bromo-2-methylpropanoate) (Scheme 3.3, **VII**). A solution of (*S*)-MeO-BIPHEP (500 mg, 0.434 mmol) in CH_2Cl_2 (5 mL) was cooled at – 78 °C and sparged with N_2 for 15 min. BBr_3 (1.3 mL: 1 M in CH_2Cl_2, 1.30 mmol) was added dropwise slowly via a syringe to the solution. The reaction mixture was stirred at –78 °C for 1 h, and at room temperature for 20 h. The reaction mixture was warmed to 0 °C, and degassed H_2O (3 mL) was added slowly. After removing the aqueous layer, the organic layer was washed sequentially with degassed H_2O and brine, and dried over $MgSO_4$. The combined organic extracts were

filtered through a pad of neutral Al_2O_3, and chromatographed on silica gel to give (S)-6,6'-bis(diphenylphosphino)biphenyl-2,2'-diol (**VI**) as a light yellow foam (343 mg, 72 %). TLC (hexanes–EtOAc = 3 :1): R_f = 0.28. ^{1}H NMR: δ 7.34-7.15 (m, 22 H), 6.80-6.76 (m, 4 H), 4.26 (bs, 2 H). ^{31}P NMR: δ −13.81.

To (*S*)-6,6'-bis(diphenylphosphino)biphenyl-2,2'-diol (**VI**) (50 mg, 0.090 mmol), triethyl amine (27 mg, 0.270 mmol), and 4-dimethylaminopyridine (2.2 mg, 0.018 mmol) in CH_2Cl_2 (3 mL) was added dropwise 2-bromo-2-methylpropanoyl bromide (50 mg, 0.216 mmol) at 0 °C and the reaction mixture was stirred for 4 h at room temperature. The reaction mixture was cooled to 0 °C and deionized water (6 mL) was added dropwise with vigorous stirring for 15 min. The mixture was extracted with CH_2Cl_2 and the organic extract was concentratee and chromatographed on silica gel to give (*S*)-6,6'-bis(diphenylphosphino)biphenyl-2,2'-diyl bis(2-bromo-2-methylpropanoate) (**VII**) as a white foam (41 mg, 56 %). TLC (hexanes–EtOAc = 5 :1): R_f = 0.60. ^{1}H NMR: δ 7.33-7.23 (m, 11 H), 7.15-7.03 (m, 15 H), 1.58 (s, 6 H), 1.16 (s, 6 H). ^{31}P NMR: δ −15.62. HRMS calcd (found) for $C_{44}H_{38}Br_2O_4P_2$ (M^+): 851.0685 (851.0680).

1-(4-(Bromomethyl)phenyl)ethanone (Scheme 3.4, **S1**). To a solution of 1-*p*-tolylethanone in CH_3CN (40 mL) was added *N*-bromosuccinimide (7.3 g, 41.0 mmol) and 2,2′-azobis(2-methylpropionitrile) (615 mg, 3.75 mmol) and the reaction mixture was stirred for 2 h at 90 °C. The solvent was evaporated under a reduced pressure and toluene (50 mL) was added to the residue. The solution was filtered, and the filtrate was concentrated and chromatographed on silica gel to give 1-(4-(bromomethyl)phenyl)ethanone as a colorless oil (5.4 g, 68 %). TLC (hexanes–EtOAc =

7 :1): R_f = 0.21. ^{1}H NMR: δ 7.90 (d, J = 7.8 Hz, 2 H) 11 H), 7.46 (d, J = 7.6 Hz, 2 H), 4.48 (s, 2 H), 2.57 (s, 2 H).

((S)-6,6'-Bis(4-(1-bromoethyl)benzyloxy)biphenyl-2,2'-diyl)bis(diphenylphosphineoxide) (Scheme 3.4, XII). To a solution of (*S*)-6,6'-bis(diphenylphosphino)biphenyl-2,2'-diol (**VI**) (517 mg, 0.932 mmol) in MeOH (10 mL) cooled to 0 °C was added H_2O_2 (140 μL, 30 wt. % in H_2O) dropwise. The reaction mixture was stirred at room temperature for 3 h. After the reaction time, the reaction mixture was poured into H_2O (40 mL) and the resulting white precipitate was filtered, washed with H_2O, and dried under a high vacuum to give 6,6'-bis(bis(3,5-di-tert-butyl-4-methoxyphenyl)phosphoryl)biphenyl-2,2'-diol (**IX**) as a white powder (522 mg, 95 %). ^{31}P NMR: δ 32.24.

To 6,6'-Bis(bis(3,5-di-tert-butyl-4-methoxyphenyl)phosphoryl)biphenyl-2,2'-diol (**IX**) (300 mg, 0.512 mmol) and K_2CO_3 (566 mg, 4.096 mmol) in acetone (12 mL) was added 1-(4-(bromomethyl)phenyl)ethanone (**S1**) and the reaction mixture was refluxed at 60 °C for 20 h. After the reaction time, the reaction mixture was cooled to room temperature and deionized water (15 mL) was added dropwise. After 5 min of stirring, additional deionized water (30 mL) was added to the reaction mixture. The reaction mixture was extracted with Et_2O (60 mL) and the aqueous phase extracted with CH_2Cl_2 (60 mL). The combined organic extracts were concentrated and chromatographed on silica gel to give (*S*)-1,1'-(4,4'-(6,6'-bis(diphenylphosphoryl)biphenyl-2,2'-diyl)bis(oxy)bis(methylene)bis(4,1-phenylene))diethanone (**X**) as a white foam (296 mg, 68 %). TLC (CH_2Cl_2–MeOH = 16:1): R_f = 0.32. ^{1}H NMR : δ 7.65-7.56 (m, 8 H), 7.54-

7.49 (m, 4 H), 7.40-7.36 (m, 2 H), 7.30-7.22 (m, 8 H), 7.15-7.11 (m, 4 H), 6.89-6.83 (m, 8 H), 4.76 (d, J = 14.0 Hz, 2 H), 4.45 (d, J = 14.0 Hz, 2 H), 2.47 (s, 6 H). ^{31}P NMR: δ 29.21.

To (*S*)-1,1'-(4,4'-(6,6'-bis(diphenylphosphoryl)biphenyl-2,2'-diyl)bis(oxy)bis(methylene)bis(4,1-phenylene))diethanone (**X**) (180 mg, 0.212 mmol) in EtOH (4 mL) was added $NaBH_4$ (16 mg, 0.424 mmol) in EtOH (4 mL) at 0 °C. The reaction mixture was stirred at 0 °C for 30 min and at room temperature for 3 h. After the reaction time, saturated NH_4Cl solution (10 mL) was added, and the reaction mixture was extracted with CH_2Cl_2 (30 mL). The extract was washed with deionized water (10 mL) and the organic phase was dried over $MgSO_4$. The solvent was evaporated under vacuum to produce 1,1'-(4,4'-((*S*)-6,6'-bis(diphenylphosphoryl)biphenyl-2,2'-diyl)bis(oxy)bis(methylene)bis(4,1-phenylene))diethanol (**XI**) as a white foam (180 mg, 99%). (CH_2Cl_2–MeOH = 16:1): R_f = 0.18.

To 1,1'-(4,4'-((S)-6,6'-bis(diphenylphosphoryl)biphenyl-2,2'-diyl)bis(oxy)bis(methylene)bis(4,1-phenylene))diethanol (**XI**) (180 mg, 0.211 mmol) was added acetyl bromide (1.0 g, 6.8 mmol) at 0 °C. The reaction mixture was vigorously stirred at 0 °C for 10 min, and then slowly warmed to room temperature and stirred for 40 min. Excess acetyl bromide was evaporated under vacuum and the resulting light yellow foam was dissolved in CH_2Cl_2 (15 mL). The resulting solution was cooled at 0 °C, and deionized water (10 mL) was added dropwise. The resulting mixture was extracted with CH_2Cl_2 and the organic phase was dried over $MgSO_4$. The solution was concentrated and chromatographed on silica gel to give ((*S*)-6,6'-bis(4-(1-bromoethyl)benzyloxy)biphenyl-

2,2'-diyl)bis(diphenylphosphineoxide) (**XII**) as a white foam (139 mg, 67 %). (CH_2Cl_2–MeOH = 16:1): R_f = 0.45. ^{1}H NMR : δ 7.66-7.53 (m, 4 H), 7.51-7.41 (m, 4 H), 7.42-7.39 (m, 2 H), 7.33-7.29 (m, 6 H), 7.27-7.23 (m, 2 H), 7.23-7.12 (m, 8 H), 6.88-6.80 (m, 8 H), 5.13 (q, J = 6.8, 14.0 Hz, 2 H), 4.72 (d, J = 13.2 Hz, 2 H), 4.42 (d, J = 13.6 Hz, 2 H), 1.97 (t, J = 6.8 Hz, 6 H). ^{31}P NMR: δ 29.94. HRMS calcd (found) for $C_{54}H_{46}Br_2O_4P_2$ (M^+): 979.1311 (979.1310).

SAN-2 (Scheme 3.4). XII (68 mg, 0.070 mmol), styrene (9.6 mL, 84 mmol), acrylonitrile (3.2 mL, 49 mmol), and anisole (3.1 mL) were combined in a 25 mL pear shaped Schlenk flask with a stirbar. $CuCl_2$ (0.0042 mmol) and Me_6TREN (0.0042 mmol) were added as a 200 μL portion of a stock solution in Anisole (4.2 mL) and DMF (0.8 mL). The reaction flask was subjected to 5 freeze-pump-thaw cycles and backfilled with Argon at room temperature. $Sn(EH)_2$ (0.070 mmol) and Me_6TREN (0.070 mmol) were added as 500 μL of a degassed stock solution in Anisole, turning the reaction mixture from a pale green to yellow. The reaction mixture was heated at 80 °C for 21 hours at which time the solution was purged with air to terminate the reaction. Upon cooling, the solution was diluted with DCM and twice precipitated from DCM into MeOH, filtered and dried under vacuum overnight to yield 4.6 g of **SAN-2a** as a white power (M_n = 104 kDa, PDI = 1.17).

To a mixture of **SAN-2a** (1.5 g, 14.42 x 10^{-3} mmol), Et_3N (525 mg, 5.19 mmol) and butylated hydroxytoluene (BHT) (32 mg, 0.144 mmol) in mixture of toluene (40 mL) and CH_3CN (25 mL) was added Cl_3SiH (156 mg, 1.154 mmol) at 0 °C. The reaction mixture was stirred at 100 °C for 64 h. The reaction mixture was cooled to room

temperature and diluted with Et_2O (60 mL). The resulting suspension was filtered through a fritted glass funnel. The filtrate was added dropwise to MeOH (600 mL) to generate a white precipitate. The collected precipitate was washed with MeOH and dried under a high vacuum to produce **SAN-2** as a white solid (1.42 g, 95 %). M_n = 104 kDa, PDI = 1.17. ^{31}P NMR (CD_2Cl_2): δ -13.69.

SAN-1 was synthesized employing a procedure similar to that used to synthesize **SAN-2**.

PS-2 (Scheme 3.4). XII (30 mg, 0.031 mmol), styrene (17.5 mL, 153 mmol), and anisole (13.1 mL) were combined in a 25 mL pear shaped Schlenk flask with a stirbar. CuBr (0.0015 mmol) and Me_6TREN (0.0015 mmol) were added as a 200 μL portion of a stock solution in Anisole (4.2 mL) and DMF (0.8 mL). The reaction flask was subjected to 5 freeze-pump-thaw cycles and backfilled with Argon at room temperature. $Sn(EH)_2$ (0.061 mmol) and Me_6TREN (0.061 mmol) were added as 500 μL of a degassed stock solution in anisole, turning the reaction mixture from a pale green to yellow. The reaction mixture was heated at 110 °C for 36 hours at which time the solution was purged with air to terminate the reaction. Upon cooling, the solution was diluted with CH_2Cl_2 and twice precipitated from CH_2Cl_2 into MeOH, filtered and dried under vacuum overnight to yield 6.0 g of **PS-2a** as a white power (M_n = 120 kDa, PDI = 1.59).

To a mixture of **PS-2a** (6 g, 50.0 x 10^{-3} mmol), Et_3N (1.82 g, 12.0 mmol) and BHT (110 mg, 0.50 mmol) in mixture of toluene (200 mL) was added Cl_3SiH (1.63 g, 12.0 mmol) at 0 °C. The reaction mixture was stirred at 100 °C for 64 h. The reaction mixture was cooled to room temperature. The resulting suspension was filtered through a

fritted glass funnel. The filtrate was added dropwise to MeOH (800 mL) to generate a white precipitate. The collected precipitate was washed with MeOH and dried under a high vacuum to produce **PS-2** as a white solid (5.10 g, 85 %). M_n = 120 kDa, PDI = 1.59. ^{31}P NMR (CD_2Cl_2): δ –13.99.

PS-1 was synthesized employing a procedure similar to that used to synthesize **PS-2**.

3.3.3 Asymmetric Allylic Alkylation

3.3.3.1 Asymmetric Allylic Alkylation using (*S*)-MeO-BIPHEP

Dimethyl 2-(1,3-diphenylallyl)malonate (Table 7, entry 1). The mixture of (*S*)-MeO-BIPHEP (5.8 mg, 0.01 mmol) and allylpalladium(II) chloride dimer (1.8 mg, 50 x 10^{-3} mmol) in CH_2Cl_2 (1 ml) was stirred for 1h at room temperature in a glove box. *trans*-1,3-diphenylallyl acetate (50 mg, 0.2 mmol) was added to the reaction mixture and the resulting solution was stirred for 5 min. Dimethyl malonate (79 mg, 0.6 mmol) and *N*, *O*-bis(trimethylsilyl)acetamide (122 mg, 0.6 mmol) were then added to the resulting solution and stirred for 18 h. The reaction mixture was diluted with Et_2O and washed sequentially with saturated NH_4Cl, saturated $NaHCO_3$, and brine. The combined organic extracts were dried over $MgSO_4$, filtered, and concentrated *in vacuo*. The resulting product was chromatographed on a silica gel column to give dimethyl 2-(1,3-diphenylallyl)malonate as a colorless oil (59 mg, 91 %). TLC (hexanes–EtOAc = 3:1): R_f = 0.53. ^{1}H NMR: δ 7.38-7.22 (m, 10 H), 6.53 (d, J = 15.0 Hz, 1 H), 6.38 (dd, J = 10.0,

15.0 Hz, 1 H), 4.31 (dd, *J* = 8.0, 10.0 Hz, 1 H), 4.0 (d, *J* = 10.5 Hz, 1 H), 3.74 (s, 3 H), 3.55 (s, 3 H). $^{13}C\{^{1}H\}$ NMR : δ 168.2, 167.7, 140.0, 136.8, 131.8, 129.0, 128.7, 128.4, 127.8, 127.5, 127.1, 126.3, 57.6, 52.6, 52.4, 49.2. Enantiopurity (92% ee) was determined by HPLC analysis (98:2 hexanes/isopropanol, 1.0 mL/min).

3.3.3.2 Asymmetric Allylic Alkylation using Polymer-Embedded Ligands

Dimethyl 2-(1,3-diphenylallyl)malonate (Table 8, entry 8). The mixture of polymer-embedded ligand **PS-2** (408 mg, 3.4 x 10^{-3} mmol) and allylpalladium(II) chloride dimer (0.6 mg, 1.7 x 10^{-3} mmol; 0.1 mL of a 17 x 10^{-3} M stock solution in CH_2Cl_2) in CH_2Cl_2 (1 ml) was stirred for 1 h at room temperature. *trans*-1,3-diphenylallyl acetate (50 mg, 0.2 mmol) was added to the reaction mixture and stirred for 5 min, and then dimethyl malonate (79 mg, 0.6 mmol) and *N*, *O*-bis(trimethylsilyl)acetamide (122 mg, 0.6 mmol) were added to the reaction mixture. The reaction mixture was transferred to a rheometer via syringe, and the solution was maintained at a shear rate of 6000 sec^{-1} for 18 h. The resulting mixture was added dropwise to hexane (10 mL) and the resulting suspension was filtered through a silca gel pad eluting with Et_2O/EtOAc (1:1). The combined organic extracts were evaporated under reduced pressure. The resulting oily residue was dissolved in 3 mL of hexane/isopropanol (10:1) and the solution was filtered through a syringe filter (PTFE 0.45 μm). The resulting solution was analyzed by GC and HPLC: 58% conversion (GC), 89% ee (98:2 hexanes/isopropanol, 1.0 mL/min, Figure 42).

The AAA reactions listed in Table 8 (entries 4-7 and 9, 10) were performed employing a similar procedure utilizing the conditions outlined in Table 8. Control reactions (Table 8, entries 1-3) were performed in a vial without applying a shear employing a procedure similar to that used to produce dimethyl 2-(1,3-diphenylallyl)malonate (Table 8, entry 8) utilizing the conditions outlined in Table 8.

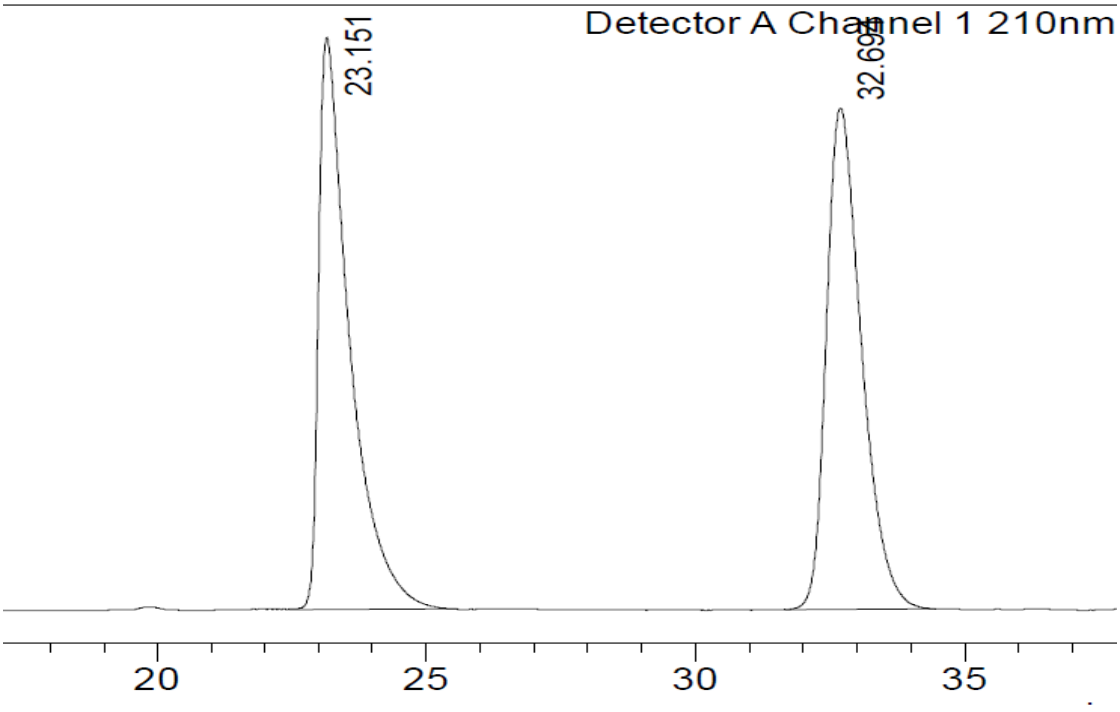

Peak#	Ret. Time	Area	Height	Conc.	Unit	Mark	Name
1	23.151	23673283	589668	50.126			
2	32.694	23554473	517390	49.874			
Total		47227757	1107058				

Figure 74. Chiral HPLC traces (98:2 hexanes/isopropanol, 1.0 mL/min) of racemic dimethyl 2-(1,3-diphenylallyl)malonate.

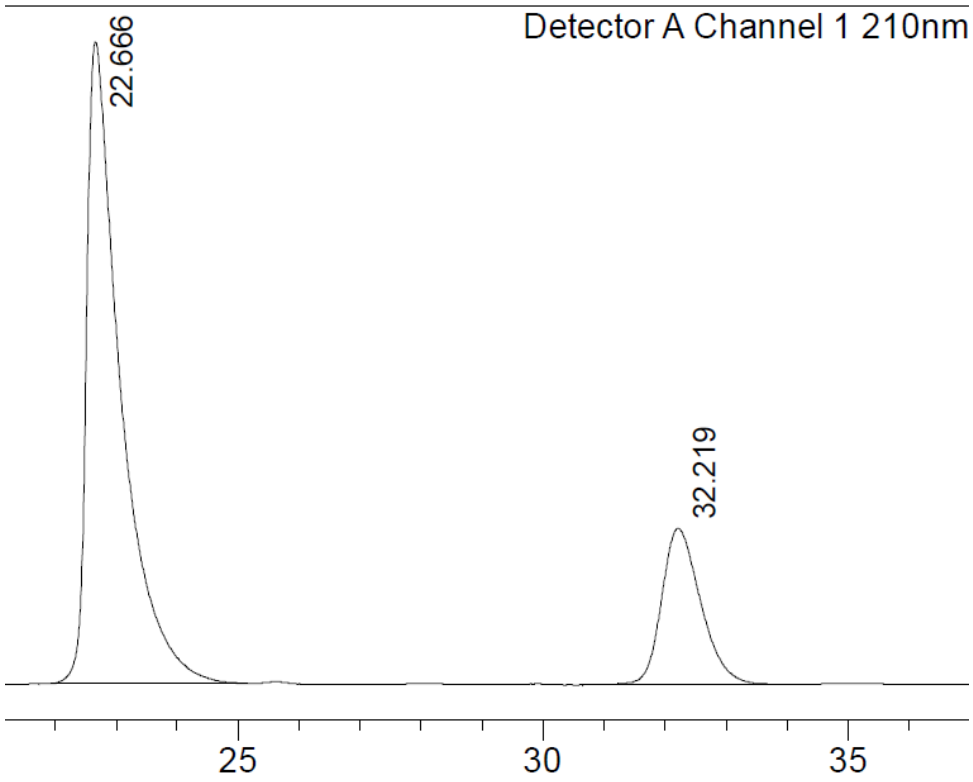

Peak#	Ret. Time	Area	Height	Conc.	Unit	Mark	Name
1	22.666	27140790	694531	78.379			
2	32.219	7486833	168915	21.621			
Total		34627623	863446				

Figure 75. Chiral HPLC traces (98:2 hexanes/isopropanol, 1.0 mL/min) of enatiomerically enriched dimethyl 2-(1,3-diphenylallyl)malonate (eq 3.1), 57 % ee .

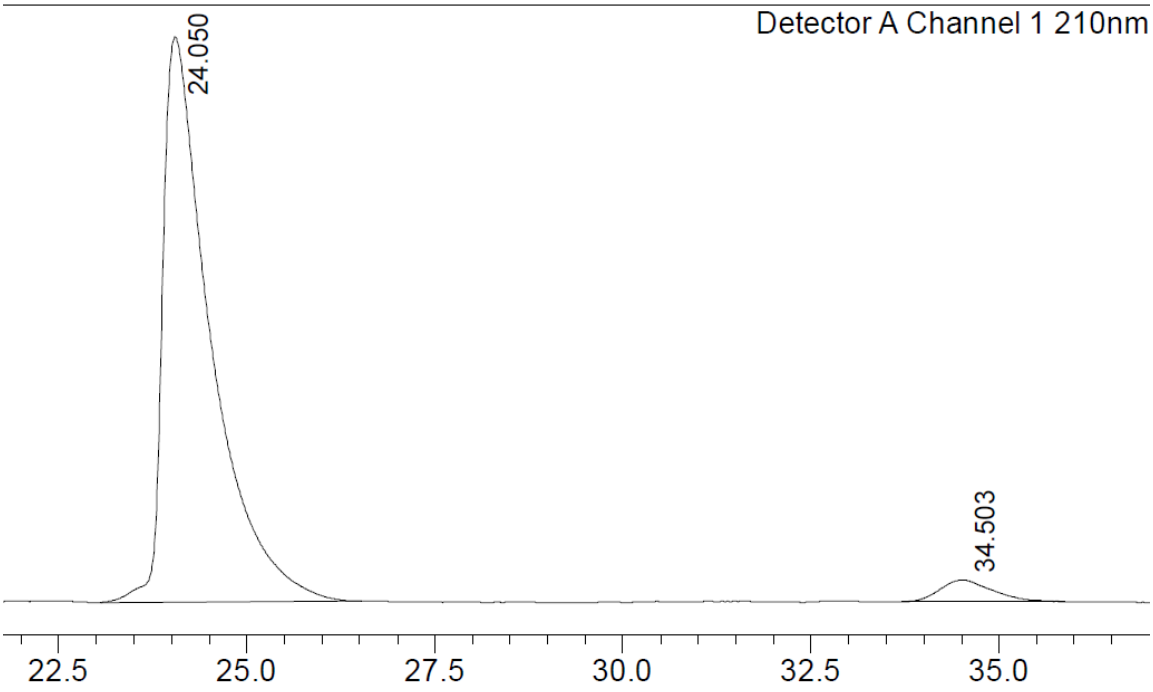

Peak#	Ret. Time	Area	Height	Conc.	Unit	Mark	Name
1	24.050	40947307	917896	95.923			
2	34.503	1740236	35303	4.077			
Total		42687544	953198				

Figure 76. Chiral HPLC traces (98:2 hexanes/isopropanol, 1.0 mL/min) of enatiomerically enriched dimethyl 2-(1,3-diphenylallyl)malonate (Table 8, entry 1), 92 % ee .

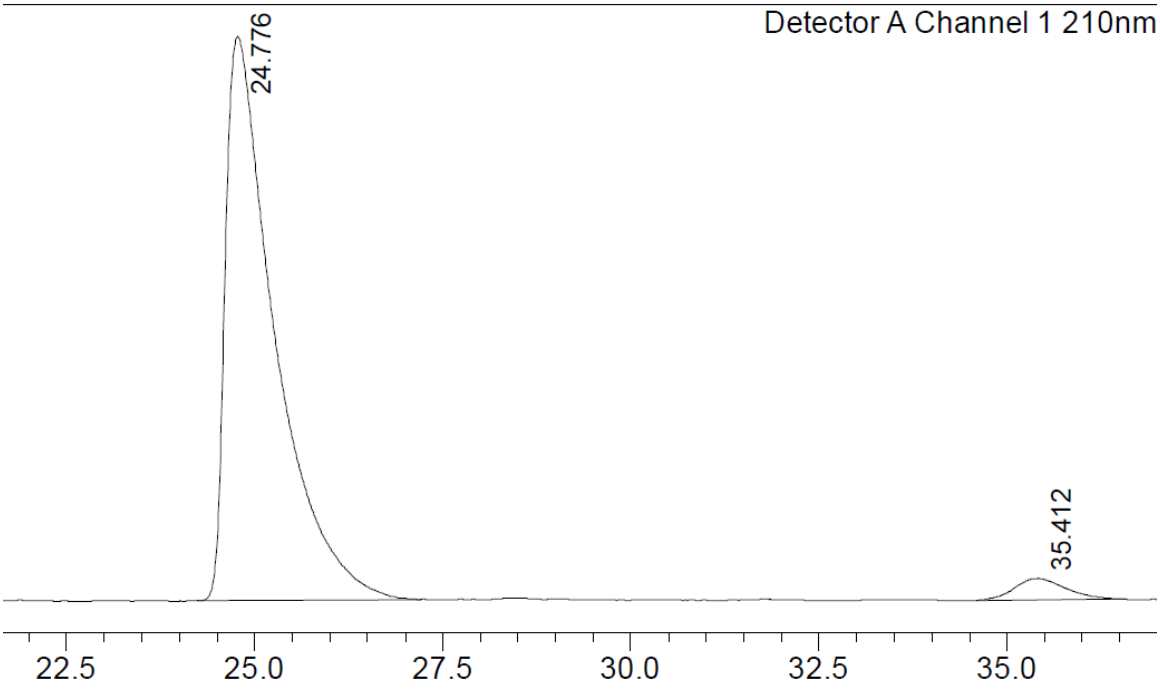

Peak#	Ret. Time	Area	Height	Unit	Mark	Name	Area%
1	24.776	22184568	484152				96.194
2	35.412	877869	18376				3.806
Total		23062437	502528				100.000

Figure 77. Chiral HPLC traces (98:2 hexanes/isopropanol, 1.0 mL/min) of enatiomerically enriched dimethyl 2-(1,3-diphenylallyl)malonate (Table 8, entry 2), 92 % ee .

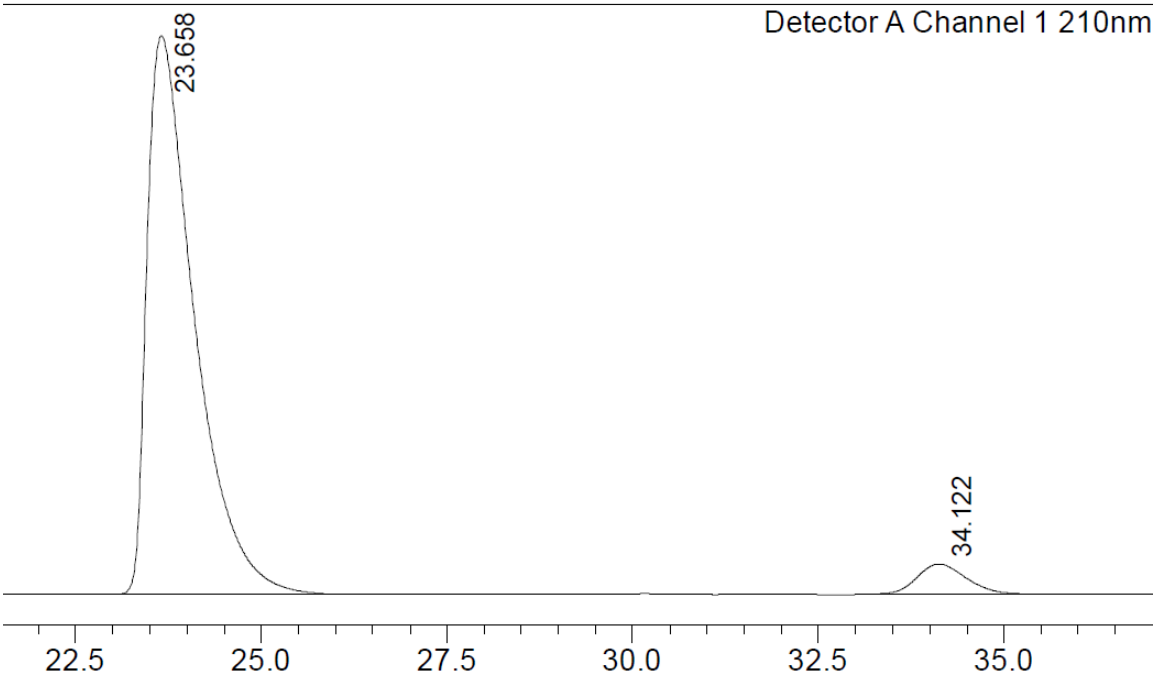

Peak#	Ret. Time	Area	Height	Conc.	Unit	Mark	Name
1	23.658	109884598	2471476	94.674			
2	34.122	6182129	133415	5.326			
Total		116066727	2604891				

Figure 78. Chiral HPLC traces (98:2 hexanes/isopropanol, 1.0 mL/min) of enatiomerically enriched dimethyl 2-(1,3-diphenylallyl)malonate (Table 8, entry 3), 89 % ee.

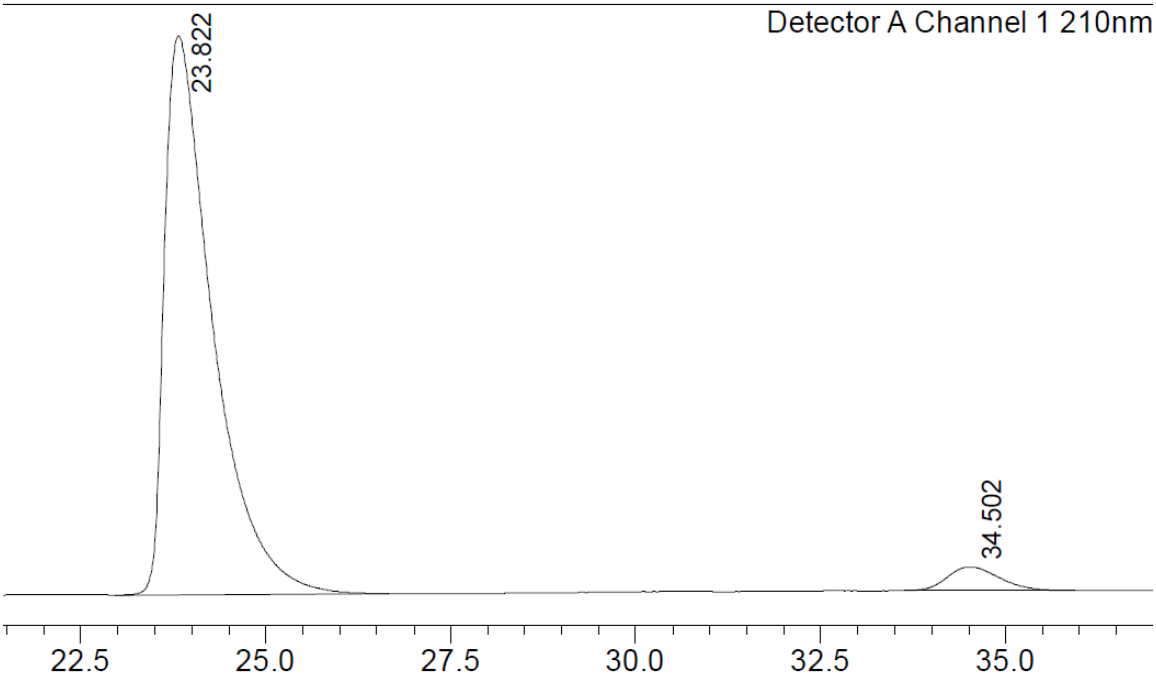

Peak#	Ret. Time	Area	Height	Conc.	Unit	Mark	Name
1	23.822	95715499	2098198	95.676			
2	34.502	4325867	88341	4.324			
Total		100041367	2186539				

Figure 79. Chiral HPLC traces (98:2 hexanes/isopropanol, 1.0 mL/min) of enatiomerically enriched dimethyl 2-(1,3-diphenylallyl)malonate (Table 8, entry 4), 91 % ee.

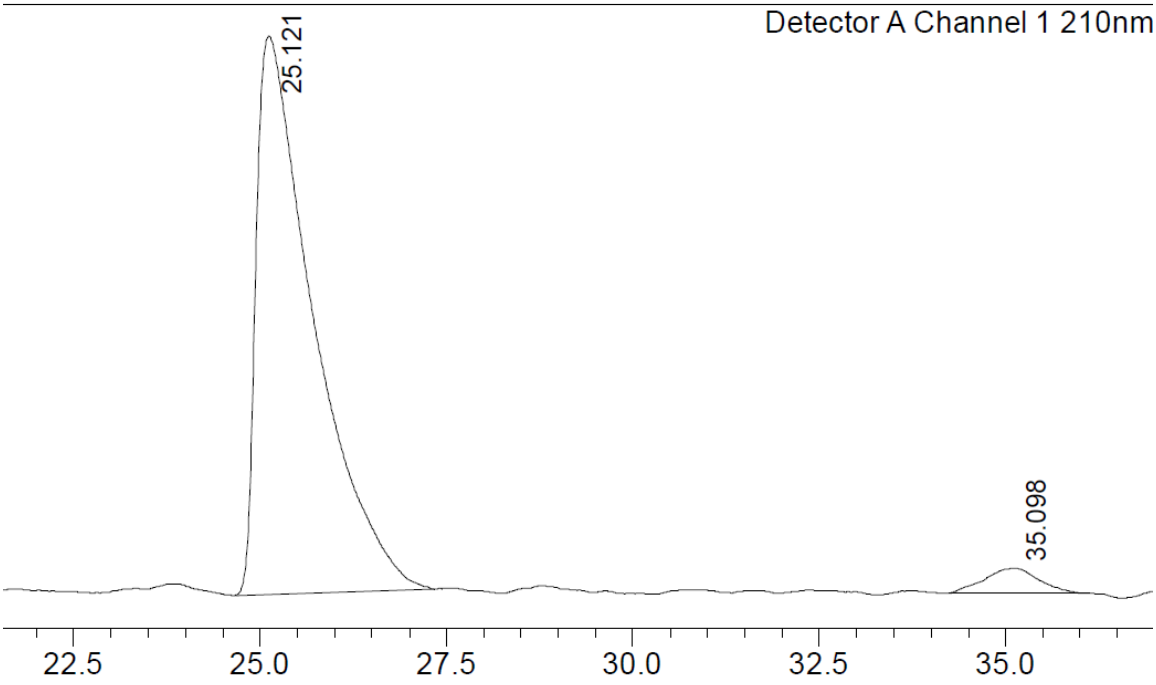

Peak#	Ret. Time	Area	Height	Conc.	Unit	Mark	Name
1	25.121	13028610	243454	95.841			
2	35.098	565331	11048	4.159			
Total		13593941	254502				

Figure 80. Chiral HPLC traces (98:2 hexanes/isopropanol, 1.0 mL/min) of enatiomerically enriched dimethyl 2-(1,3-diphenylallyl)malonate (Table 8, entry 5), 92 % ee.

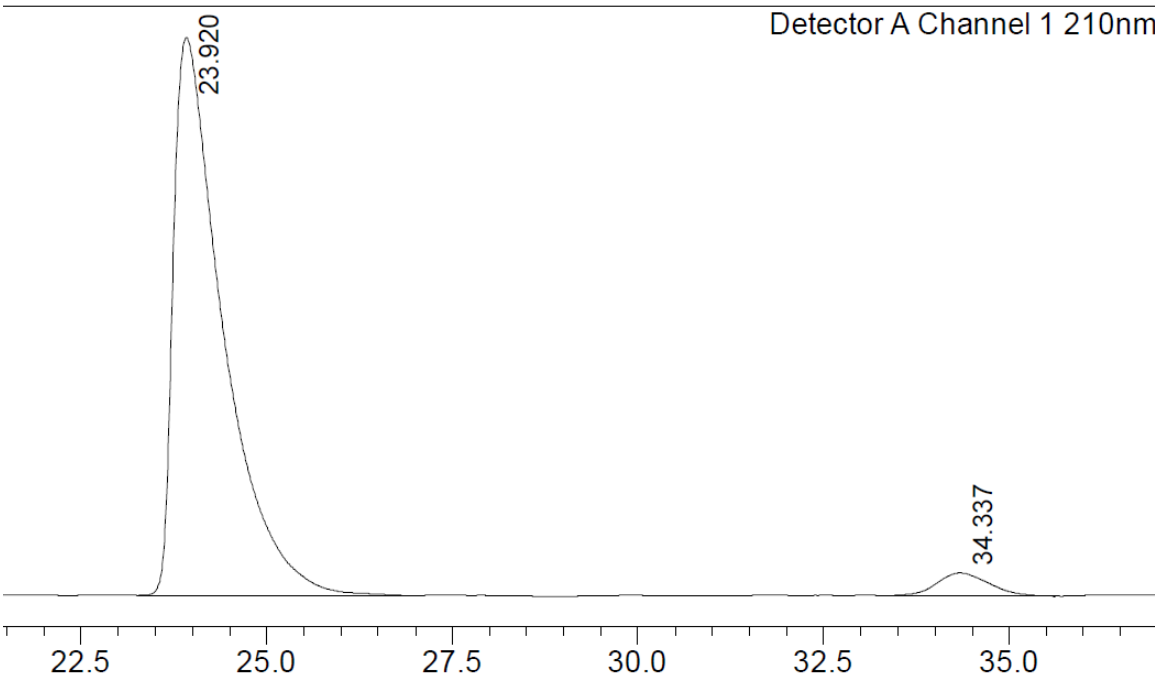

Peak#	Ret. Time	Area	Height	Conc.	Unit	Mark	Name
1	23.920	49334664	1056336	95.912			
2	34.337	2102670	43179	4.088			
Total		51437333	1099515				

Figure 81. Chiral HPLC traces (98:2 hexanes/isopropanol, 1.0 mL/min) of enatiomerically enriched dimethyl 2-(1,3-diphenylallyl)malonate (Table 8, entry 6), 92 % ee.

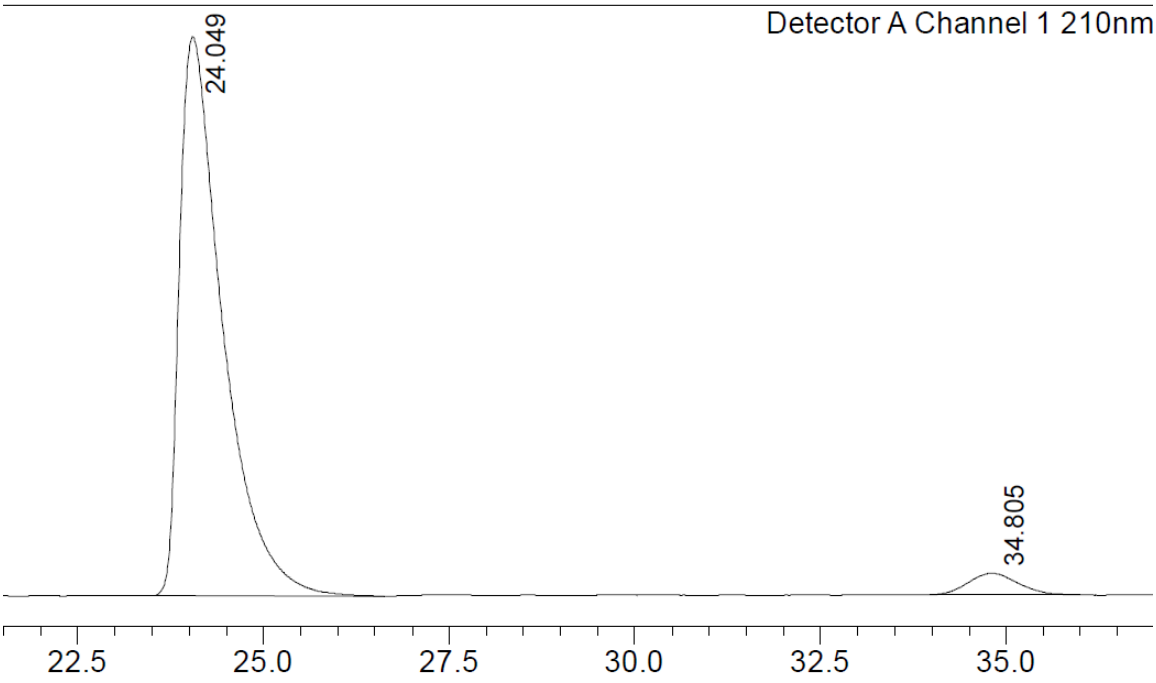

Peak#	Ret. Time	Area	Height	Conc.	Unit	Mark	Name
1	24.049	46821047	1148048	95.803			
2	34.805	2051258	43926	4.197			
Total		48872305	1191974				

Figure 82. Chiral HPLC traces (98:2 hexanes/isopropanol, 1.0 mL/min) of enatiomerically enriched dimethyl 2-(1,3-diphenylallyl)malonate (Table 8, entry 7), 92 % ee.

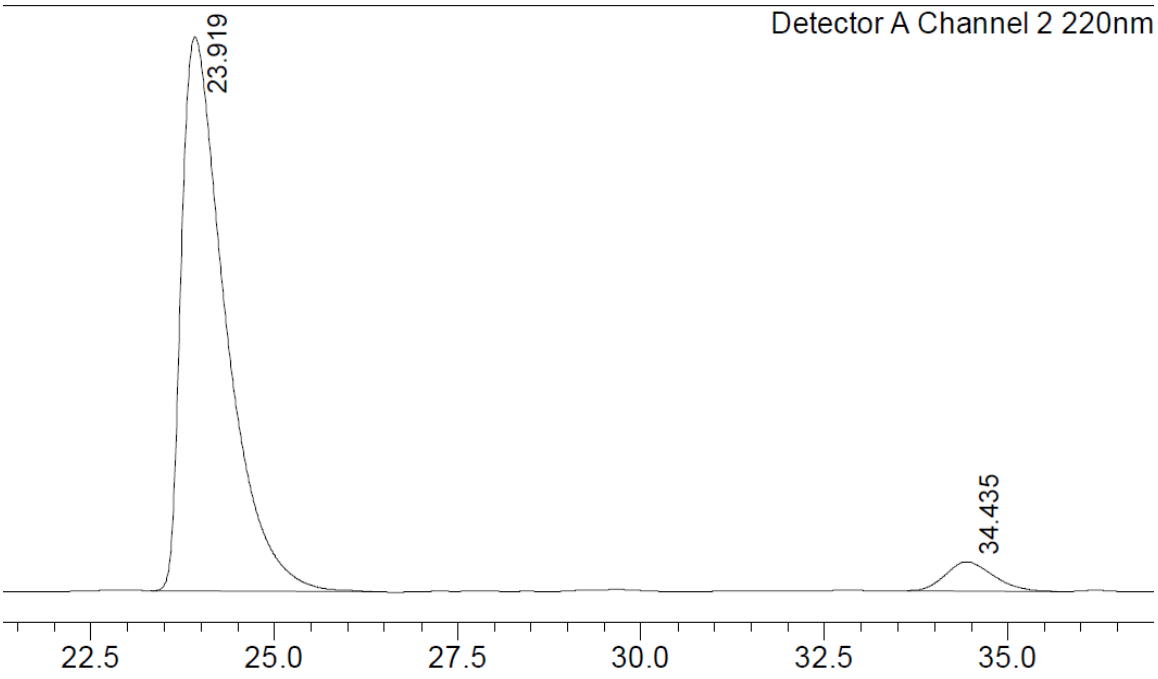

Peak#	Ret. Time	Area	Height	Unit	Name	Area%
1	23.919	25951228	617814			94.658
2	34.435	1464604	32461			5.342
Total		27415832	650275			100.000

Figure 83. Chiral HPLC traces (98:2 hexanes/isopropanol, 1.0 mL/min) of enatiomerically enriched dimethyl 2-(1,3-diphenylallyl)malonate (Table 8, entry 8), 89 % ee.

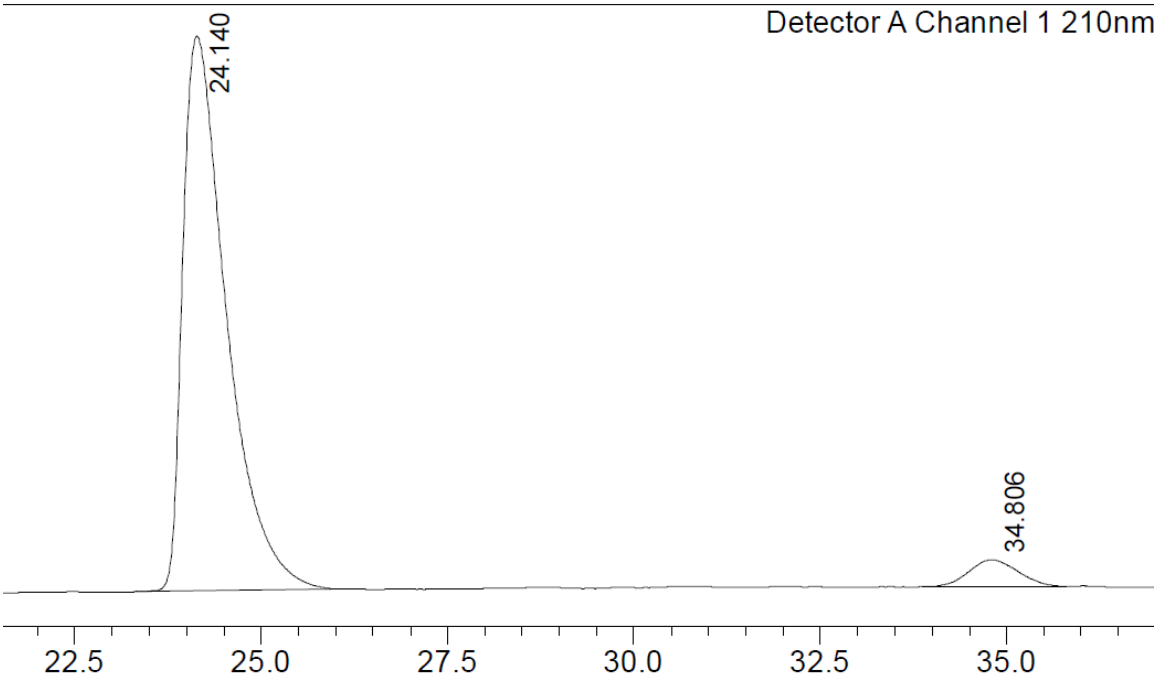

Peak#	Ret. Time	Area	Height	Conc.	Unit	Mark	Name
1	24.140	46560301	1133762	94.886			
2	34.806	2509598	54650	5.114			
Total		49069899	1188412				

Figure 84. Chiral HPLC traces (98:2 hexanes/isopropanol, 1.0 mL/min) of enatiomerically enriched dimethyl 2-(1,3-diphenylallyl)malonate (Table 8, entry 9), 89 % ee.

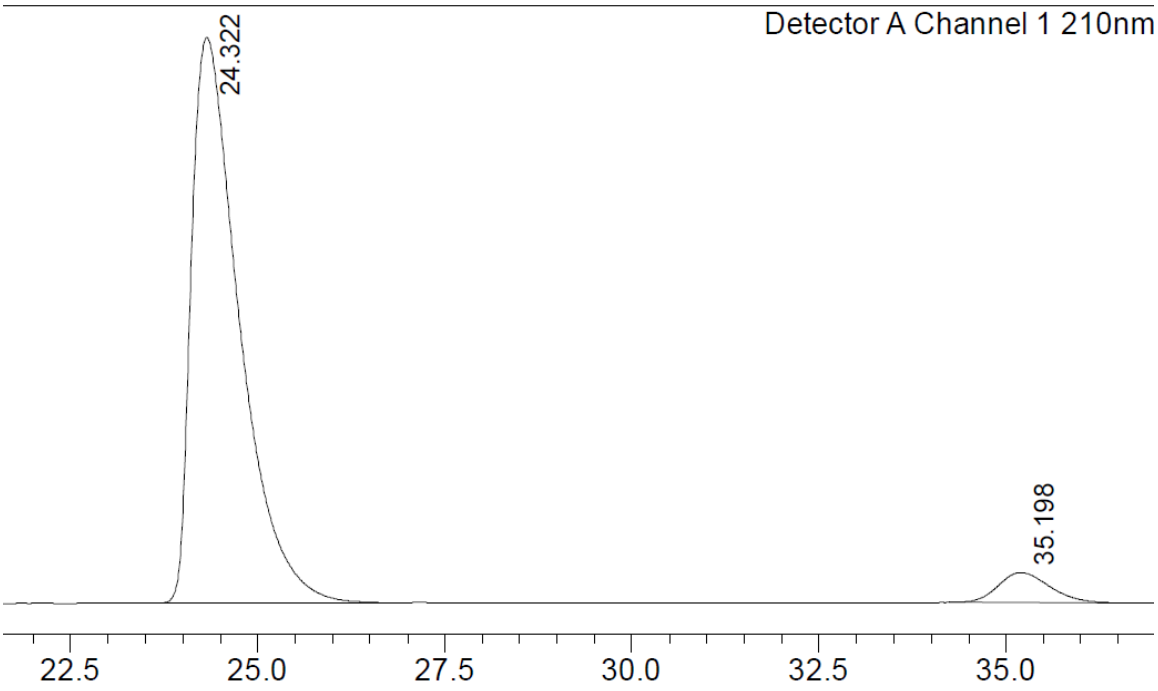

Peak#	Ret. Time	Area	Height	Conc.	Unit	Mark	Name
1	24.322	91557533	2053621	94.629			
2	35.198	5196891	108431	5.371			
Total		96754424	2162052				

Figure 85. Chiral HPLC traces (98:2 hexanes/isopropanol, 1.0 mL/min) of enatiomerically enriched dimethyl 2-(1,3-diphenylallyl)malonate (Table 8, entry 10), 89 % ee.

References

(1) Hultzsch, K. C. *Adv. Synth. Catal.* **2005**, *347*, 367.

(2) Müller, T. E.; Hultzsch, K. C.; Yus, M.; Foubelo, F.; Tada, M. *Chem. Rev.* **2008**, *108*, 3795.

(3) Su, R. Q.; Müller, T. E. *Tetrahedron* **2001**, *57*, 6027.

(4) Kang, J. E.; Kim, H. B.; Lee, J. W.; Shin, S. *Org. Lett.* **2006**, *8*, 3537.

(5) Field, L. D.; Messerle, B. A.; Vuong, K. Q.; Turner, P. *Organometallics* **2005**, *24*, 4241.

(6) Burling, S.; Field, L. D.; Messerle, B. A.; Turner, P. *Organometallics* **2004**, *23*, 1714.

(7) Shi, Y.; Hall, C.; Ciszewski, J. T.; Cao, C.; Odom, A. L. *Chem. Commun.* **2003**, 586.

(8) Esteruelas, M. A.; xf; pez, A. M.; Mateo, A. C.; Oate, E. *Organometallics* **2005**, *24*, 5084.

(9) Tillack, A.; Castro, I. G.; Hartung, C. G.; Beller, M. *Angew. Chem., Int. Ed.* **2002**, *41*, 2541.

(10) Haak, E.; Bytschkov, I.; Doye, S. *Angew. Chem., Int. Ed.* **1999**, *38*, 3389.

(11) Zulys, A.; Panda, T. K.; Gamer, M. T.; Roesky, P. W. *Chem. Commun.* **2004**, 2584.

(12) Bürgstein, M. R.; Berberich, H.; Roesky, P. W. *Chem. Eur. J.* **2001**, *7*, 3078.

(13) Bürgstein, M. R.; Berberich, H.; Roesky, P. W. *Organometallics* **1998**, *17*, 1452.

(14) Panda, T. K.; Zulys, A.; Gamer, M. T.; Roesky, P. W. *Organometallics* **2005**, *24*, 2197.

(15) Panda, T. K.; Zulys, A.; Gamer, M. T.; Roesky, P. W. *J. Organomet. Chem.* **2005**, *690*, 5078.

(16) Stubbert, B. D.; Marks, T. J. *J. Am. Chem. Soc.* **2007**, *129*, 4253.

(17) Li, Y.; Marks, T. J. *J. Am. Chem. Soc.* **1996**, *118*, 9295.

(18) Li, Y.; Fu, P. F.; Marks, T. J. *Organometallics* **1994**, *13*, 439.

(19) Hultzsch, K. C.; Hampel, F.; Wagner, T. *Organometallics* **2004**, *23*, 2601.

(20) Li, H.; Du Lee, S.; Widenhoefer, R. A. *J. Organomet. Chem.* **2011**, *696*, 316.

(21) Benedetti, E.; Lemière, G.; Chapellet, L. L.; Penoni, A.; Palmisano, G.; Malacria, M.; Goddard, J. P.; Fensterbank, L. *Org. Lett.* **2010**, *12*, 4396.

(22) Winter, C.; Krause, N. *Angew. Chem.* **2009**, *121*, 6457.

(23) Li, H.; Widenhoefer, R. A. *Org. Lett.* **2009**, *11*, 2671.

(24) Chemler, S. R. *Org. Biomol. Chem.* **2009**, *7*, 3009.

(25) Aikawa, K.; Kojima, M.; Mikami, K. *Angew. Chem.* **2009**, *121*, 6189.

(26) Zhang, Z.; Bender, C. F.; Widenhoefer, R. A. *Org. Lett.* **2007**, *9*, 2887.

(27) Widenhoefer, R. A.; Han, X. *Eur. J. Org. Chem.* **2006**, 4555.

(28) Morita, N.; Krause, N. *Eur. J. Org. Chem.* **2006**, 4634.

(29) Kaden, S.; Reissig, H. U.; Brüdgam, I.; Hartl, H. *Synthesis* **2006**, 1351.

(30) Lee, P. H.; Kim, H.; Lee, K.; Kim, M.; Noh, K.; Seomoon, D. *Angew. Chem.* **2005**, *117*, 1874.

(31) Morita, N.; Krause, N. *Org. Lett.* **2004**, *6*, 4121.

(32) Larock, R. C.; He, Y.; Leong, W. W.; Han, X.; Refvik, M. D.; Zenner, J. M. *J. Org. Chem.* **1998**, *63*, 2154.

(33) Gardiner, M.; Grigg, R.; Sridharan, V.; Vicker, N. *Tetrahedron Lett.* **1998**, *39*, 435.

(34) Al-Masum, M.; Meguro, M.; Yamamoto, Y. *Tetrahedron Lett.* **1997**, *38*, 6071.

(35) Grigg, R.; Sridharan, V.; Terrier, C. *Tetrahedron Lett.* **1996**, *37*, 4221.

(36) Grigg, R.; Savic, V. *Tetrahedron Lett.* **1996**, *37*, 6565.

(37) Grigg, R.; Sridharan, V.; Xu, L. H. *J. Chem. Soc., Chem. Commun.* **1995**, 1903.

(38) Besson, L.; Gor; xe; J.; Cazes, B. *Tetrahedron Lett.* **1995**, *36*, 3853.

(39) Larock, R. C.; Berrios, P.; xf; a, N. G.; Fried, C. A. *J. Org. Chem.* **1991**, *56*, 2615.

(40) Schore, N. E. *Chem. Rev.* **1988**, *88*, 1081.

(41) Coulson, D. R. *J. Org. Chem.* **1973**, *38*, 1483.

(42) Hu, A.; Ogasawara, M.; Sakamoto, T.; Okada, A.; Nakajima, K.; Takahashi, T.; Lin, W. *Adv. Synth. Catal.* **2006**, *348*, 2051.

(43) Utsunomiya, M.; Hartwig, J. F. *J. Am. Chem. Soc.* **2003**, *125*, 14286.

(44) Kawatsura, M.; Hartwig, J. F. *J. Am. Chem. Soc.* **2000**, *122*, 9546.

(45) Zhou, J.; Hartwig, J. F. *J. Am. Chem. Soc.* **2008**, *130*, 12220.

(46) Dorta, R.; Egli, P.; Zürcher, F.; Togni, A. *J. Am. Chem. Soc.* **1997**, *119*, 10857.

(47) Kanno, O.; Kuriyama, W.; Wang, Z. J.; Toste, F. D. *Ang. Chem. Int. Ed.* **2011**, *50*, 9919.

(48) Löber, O.; Kawatsura, M.; Hartwig, J. F. *J. Am. Chem. Soc.* **2001**, *123*, 4366.

(49) Gagne, M. R.; Brard, L.; Conticello, V. P.; Giardello, M. A.; Stern, C. L.; Marks, T. J. *Organometallics* **1992**, *11*, 2003.

(50) Gagne, M. R.; Stern, C. L.; Marks, T. J. *J. Am. Chem. Soc.* **1992**, *114*, 275.

(51) Motta, A.; Lanza, G.; Fragalà, I. L.; Marks, T. J. *Organometallics* **2004**, *23*, 4097.

(52) Giardello, M. A.; Conticello, V. P.; Brard, L.; Gagne, M. R.; Marks, T. J. *J. Am. Chem. Soc.* **1994**, *116*, 10241.

(53) Douglass, M. R.; Ogasawara, M.; Hong, S.; Metz, M. V.; Marks, T. J. *Organometallics* **2001**, *21*, 283.

(54) Aillaud, I.; Collin, J.; Duhayon, C.; Guillot, R.; Lyubov, D.; Schulz, E.; Trifonov, A. *Chem. Eur. J.* **2008**, *14*, 2189.

(55) Kim, J. Y.; Livinghouse, T. *Org. Lett.* **2005**, *7*, 1737.

(56) Gribkov, D. V.; Hultzsch, K. C.; Hampel, F. *J. Am. Chem. Soc.* **2006**, *128*, 3748.
(57) Yu, X.; Marks, T. J. *Organometallics* **2006**, *26*, 365.

(58) Pfaltz, A. *Acc. Chem. Res.* **1993**, *26*, 339.

(59) Johnson, J. S.; Evans, D. A. *Acc. Chem. Res.* **2000**, *33*, 325.

(60) Hong, S.; Tian, S.; Metz, M. V.; Marks, T. J. *J. Am. Chem. Soc.* **2003**, *125*, 14768.

(61) Knight, P. D.; Munslow, I.; O'Shaughnessy, P. N.; Scott, P. *Chem. Commun.* **2004**, 894.

(62) Watson, D. A.; Chiu, M.; Bergman, R. G. *Organometallics* **2006**, *25*, 4731.

(63) Wood, M. C.; Leitch, D. C.; Yeung, C. S.; Kozak, J. A.; Schafer, L. L. *Ang. Chem. Int. Ed.* **2007**, *46*, 354.

(64) Aillaud, I.; Collin, J.; Hannedouche, J.; Schulz, E. *Dalton Trans.* **2007**, 5105.

(65) Shen, X.; Buchwald, S. L. *Ang. Chem. Int. Ed.* **2010**, *49*, 564.

(66) Kojima, M.; Mikami, K. *Synlett* **2012**, *2012*, 57.

(67) Gorin, D. J.; Sherry, B. D.; Toste, F. D. *Chem. Rev.* **2008**, *108*, 3351.

(68) Widenhoefer, R. A. *Chem. Eur. J.* **2008**, *14*, 5382.

(69) Corma, A.; Leyva-Pérez, A.; Sabater, M. J. *Chem. Rev.* **2011**, *111*, 1657.

(70) Rudolph, M.; Hashmi, A. S. K. *Chem. Commun.* **2011**, *47*, 6536.

(71) Krause, N.; Winter, C. *Chem. Rev.* **2011**, *111*, 1994.

(72) Furstner, A. *Chem. Soc. Rev.* **2009**, *38*, 3208.

(73) Arcadi, A. *Chem. Rev.* **2008**, *108*, 3266.

(74) Pyykkö, P. *Ang. Chem. Int. Ed.* **2004**, *43*, 4412.

(75) Bender, C. F.; Widenhoefer, R. A. *Org. Lett.* **2006**, *8*, 5303.

(76) Zhang, Z.; Lee, S. D.; Widenhoefer, R. A. *J. Am. Chem. Soc.* **2009**, *131*, 5372.

(77) Zhang, Z.; Bender, C. F.; Widenhoefer, R. A. *Org. Lett.* **2007**, *9*, 2887.

(78) Zhang, Z.; Widenhoefer, R. A. *Ang. Chem. Int. Ed.* **2007**, *46*, 283.

(79) Han, X.; Widenhoefer, R. A. *Org. Lett.* **2006**, *8*, 3801.

(80) Raghunath, M.; Zhang, X. *Tetrahedron Lett.* **2005**, *46*, 8213.

(81) LaLonde, R. L.; Brenzovich, J. W. E.; Benitez, D.; Tkatchouk, E.; Kelley, K.; Goddard, I. I. I. W. A.; Toste, F. D. *Chem. Sci.* **2010**, *1*, 226.

(82) Shapiro, N. D.; Toste, F. D. *Proc. Natl. Acad. Sci. USA* **2008**, *105*, 2779.

(83) Hooper, T. N.; Green, M.; McGrady, J. E.; Patel, J. R.; Russell, C. A. *Chem. Commun.* **2009**, 3877.

(84) Hooper, T. N.; Butts, C. P.; Green, M.; Haddow, M. F.; McGrady, J. E.; Russell, C. A. *Chem. Eur. J.* **2009**, *15*, 12196.

(85) Brown, T. J.; Dickens, M. G.; Widenhoefer, R. A. *J. Am. Chem. Soc.* **2009**, *131*, 6350.

(86) Brown, T. J.; Dickens, M. G.; Widenhoefer, R. A. *Chem. Commun.* **2009**, 6451.

(87) Bandini, M.; Eichholzer, A. *Ang. Chem. Int. Ed.* **2009**, *48*, 9533.

(88) Hamada, T.; Chieffi, A.; Åhman, J.; Buchwald, S. L. *J. Am. Chem. Soc.* **2002**, *124*, 1261.

(89) Reznichenko, A. L.; Nguyen, H. N.; Hultzsch, K. C. *Ang. Chem. Int. Ed.* **2010**, *49*, 8984.

(90) Sevov, C. S.; Zhou, J.; Hartwig, J. F. *J. Am. Chem. Soc.* **2012**, *134*, 11960.

(91) Li, K.; Hii, K. K. *Chem. Commun.* **2003**, 1132.

(92) Li, K.; Phua, P. H.; Hii, K. K. *Tetrahedron* **2005**, *61*, 6237.

(93) McBee, J. L.; Bell, A. T.; Tilley, T. D. *J. Am. Chem. Soc.* **2008**, *130*, 16562.

(94) Karshtedt, D.; Bell, A. T.; Tilley, T. D. *J. Am. Chem. Soc.* **2005**, *127*, 12640.

(95) den Boer, D.; Shklyarevskii, O. I.; Coenen, M. J. J.; van der Maas, M.; Peters, T. P. J.; Elemans, J. A. A. W.; Speller, S. *J. Phys. Chem. C* **2011**, *115*, 8295.

(96) Ikeda, S.; Takata, T.; Komoda, M.; Hara, M.; N. Kondo, J.; Domen, K.; Tanaka, A.; Hosono, H.; Kawazoe, H. *Phys. Chem. Chem. Phys.* **1999**, *1*, 4485.

(97) Hick, S. M.; Griebel, C.; Restrepo, D. T.; Truitt, J. H.; Buker, E. J.; Bylda, C.; Blair, R. G. *Green Chem.* **2010**, *12*, 468.

(98) Berezin, I. V.; Klibanov, A. M.; Samokhin, G. P.; Martinek, K.; Klaus, M., Ed.; *Methods in Enzymology* Academic Press: 1976; Vol. Volume 44, p 558.

(99) Piermattei, A.; Karthikeyan, S.; Sijbesma, R. P. *Nat Chem* **2009**, *1*, 133.

(100) Trost, B. M.; Fullerton, T. J. *J. Am. Chem. Soc.* **1973**, *95*, 292.

(101) Trost, B. M.; Van Vranken, D. L. *Chemical Reviews* **1996**, *96*, 395.

(102) Trost, B. M.; Dietsch, T. J. *J. Am. Chem. Soc.* **1973**, *95*, 8200.

(103) Trost, B. M.; Strege, P. E. *J. Am. Chem. Soc.* **1977**, *99*, 1649.

(104) Trost, B. M.; Crawley, M. L. *Chemical Reviews* **2003**, *103*, 2921.

(105) Trost, B. M.; Tang, W.; Toste, F. D. *J. Am. Chem. Soc.* **2005**, *127*, 14785.

(106) Goldfuss, B.; Löschmann, T.; Kop-Weiershausen, T.; Neudörfl, J.; Rominger, F. *Beilstein J. Org. Chem.* **2006**, *2*, 7.

(107) Trost, B. M.; Xie, J. *J. Am. Chem. Soc.* **2006**, *128*, 6044.

(108) Pietrasik, J.; Dong, H.; Matyjaszewski, K. *Macromolecules* **2006**, *39*, 6384.

(109) Kingsbury, C. M.; May, P. A.; Davis, D. A.; White, S. R.; Moore, J. S.; Sottos, N. R. *J. Mater. Chem.* **2011**, *21*, 8381.

Biography

Date of Birth

May 24, 1976.

Place of Birth

Seoul, South Korea

Education

2007-2012 Ph.D., Organometallic Chemistry
Department of Chemistry, Duke University, Durham, NC, USA
Advisor: Professor Ross A. Widenhoefer
Thesis: Gold(I)-Catalyzed Enantioselective Hydroamination of Unactivated Alkenes

2003-2005 M.S., Organic Chemistry
Department of Chemistry, Seoul National University, Seoul, South Korea
Advisor: Professor Junghun Suh
Thesis: Peptide-Cleaving Catalyst Selective for Peptide Deformylase

1995-2003 B.S., Chemistry
Department of Applied Chemistry, Kyung Hee University, South Korea
Advisor: Professor Young-Sook Paik
Thesis: Synthesis of Blue Pigment from Geniposide of Gardenia Fructus

Publications

6. Lee, S. D.; Widenhoefer, R. A. "Room temperature Au(I)-catalyzed enantioselective intramolecular hydroamination of unactivated alkenes," In publication preparation.

5. Li, H.; Lee, S. D.; Widenhoefer, R. A. "Gold(I)-Catalyzed Enantioselective Intramolecular Hydroamination of Allenes with Ureas," *J. Organomet. Chem.* 2011, *696*, 316-320.

4. Zhang, Z.; Lee, S. D.; Widenhoefer, R. A. "Intermolecular Hydroamination of Ethylene and 1-Alkenes with Cyclic Ureas Catalyzed by Achiral and Chiral Gold(I) Complexes," *J. Am. Chem. Soc.* 2009, *131*, 5372-5373.

3. Zhang, Z.; Lee, S. D.; Fisher, A. S.; Widenhoefer, R. A. "Gold(I)-Catalyzed Hydration of Allenes," *Tetrahedron* 2009, *65*, 1794-1798.

2. Kim, M. G.; Kim, M.; Lee, S. D.; Suh, J. "Peptide-cleaving catalyst selective for melanin-concentrating hormone : oxidative decarboxylation of N-terminal aspartate catalyzed by Co(III)cyclen," *J. Biol. Inorg. Chem.* 2006, *11*, 867-875.

1. Chae, P. S.;Kim, M.; Jeung, C.-S.; Lee, S. D.; Park, H.; Lee, S.; Suh, J.; "Peptide-Cleaving Catalyst Selective for Peptide Deformylase," *J. Am. Chem. Soc.* 2005*, 127*, 2396-2397.

Presentations

6. Lee, S. D.; Widenhoefer, R. A. "Room temperature Au(I)-catalyzed enantioselective intramolecular hydroamination of unactivated alkenes," *The Southeastern Regional Meeting of the American Chemical Society*, Raleigh, NC, **2012**.

5. Lee, S. D.; Widenhoefer, R. A. "Gold(I)-Catalyzed Intermolecular Enantioselective Hydroamination of 1-Alkenes with Cyclic Ureas," *National Meeting of the American Chemical Society*, Denver, CO, **2011**.

4. Lee, S. D.; Zhang, Z.; Fisher, A. S.; Widenhoefer, R. A. "Gold(I)-Catalyzed Hydration of Allenes," *32nd Reaction Mechanisms Conference*, University of North Carolina-Chapel Hill, Chapel Hill, NC, **2008**.

3. Lee, S. D.; Kim, M.; Suh, J. "Peptide-Cleaving Catalyst Selective for Melanin-Concentrating Hormone," *Asian Chemical Congress*, Seoul, South Korea, **2005**.

2. Chae, P. S.;Kim, M.; Lee, S. D.; Suh, J. "Peptide-Cleaving Catalyst Selective for Peptide Deformylase," *Asian Chemical Congress* , Seoul, South Korea, **2005**.

1. Chae, P. S.; Lee, S. D.; Suh, J. "Library of Candidates of Protein-Cleaving Catalysts Accessed by Ugi Four Component Reaction," *National Meeting of the Korean Chemical Society*, Seoul, South Korea, **2004**.